

Warning!!!**This document only contains the notes form the lecture.****The text was not language corrected.**

Some symbols and abbreviations	3
Introduction	4
1. Continuous-time signals and systems	5
1.1 Continuous-time signals	5
1.1.1 Exponential signal	5
1.1.2 Complex exponential signal	7
1.1.3 Sinusoidal signal	14
1.1.4 Damped sinusoidal signal.....	17
1.1.5 Delta function.....	18
1.2 Continuous-time systems	19
1.2.1 LTI systems	20
1.2.2 Frequency response of LTI systems.....	23
1.2.3 Linear Constant-Coefficient Differential Equation.....	23
1.3 Fourier analysis	24
1.3.1 The Fourier Series	26
1.3.2 The Fourier Integral	32
1.4 Continuous-time filters.....	41
1.4.1 The Laplace transform	41
1.4.2 Butterworth filter.....	53
1.4.3 Chebyshev type I and type II filters	56
1.4.4 Elliptic filter	61
1.4.5 Bessel filter.....	62
1.4.6 Comparison of analog filters	62
1.4.7 Frequency transformation: LP, HP, BP, BS filters	65
2. Digital signal processing	67
2.1 Discrete-time signals and systems.....	67
2.1.1 Exponential signal	68
2.1.2 Complex exponential signal	68
2.1.3 Sinusoidal signal	69
2.1.4 Damped sinusoidal signal.....	72
2.1.5 Unite impulse	73
2.2 Discrete-time systems	74
2.2.1 LTI systems	75
2.2.2 Linear Constant-Coefficient Difference Equation	79
2.3 Fourier analysis	80
2.3.1 The Discrete Time Fourier Transform	80
2.3.2 The Discrete Fourier Transform.....	89
2.4 Discrete-time filters.....	97
2.4.1 The z-Transform.....	97
2.4.2 IIR recursive filters.....	109
2.4.3 FIR non recursive filters.....	113
2.4.4 Structures for discrete-time systems	137
2.5 Sampling of signals	140
2.5.1 Sampling of lowpass signals	141
2.5.2 Sampling of bandpass signals	146
2.5.3 Reconstruction of continuous-time signal from samples	148

2.5.4	Changing the sampling rate of discrete-time signals	149
2.5.5	Multirate signal processing	154
2.5.6	Impulse invariance	157
2.6	Analysis of signals using DFT	159
2.6.1	Analysis of sinusoidal signals	160
2.6.2	Time-dependent frequency analysis: the spectrogram	165
2.6.3	Fourier analysis of stationary random signals: the periodogram.....	171
	References	172

Some symbols and abbreviations

<i>const</i>	Constant value.
DFT	The Discrete Fourier Transform; Fourier transform of discrete-time periodic signal.
DTFT	The Discrete Time Fourier Transform; Fourier transform of discrete-time aperiodic signal.
F_0	Frequency of continuous-time signal in Hertz.
FIR	Finite Impulse Response discrete-time system.
FS	The Fourier series for continuous-time periodic signals.
$F_s=1/T$	Sampling frequency in Hz, T - sampling period in seconds.
FT	The Fourier transform (Fourier integral) of continuous-time aperiodic signals.
$H(\Omega), H(j\Omega)$	Complex frequency characteristic of continuous-time signal or system.
IIR	Infinite Impulse Response (Recursive) discrete-time system.
Imag	Imaginary part of complex number.
LP, HP, BP, BS	Lowpass, highpass, bandpass, and bandstop filters.
M	The half of signal samples that is $N=2M$ or $N=2M+1$
N	The number of samples. The signal contains N samples if it is defined for $n=0,1,2,\dots,N-1$ or $N+1$ samples if it is defined for $n=0,1,2,\dots,N$.
Real	Real part of complex number.
STFT	Short-Time Fourier Transform.
T_0	The fundamental period of continuous-time signal in seconds.
$x(t), y(t)$	Continuous-time functions of t .
$x[n], y[n]$	Discrete-time signals (sequences) indexed by n .
ϕ	Phase of sinusoidal signal in radians.
Ω, Ω_0	Angular frequency of continuous-time signal in radians per second. Ω is variable, Ω_0 is specific value.
ω, ω_0	Frequency (angular frequency, pulsation) of discrete-time signal in radians. ω is variable, ω_0 is specific value.

Introduction

This lecture is about signals and systems.

It is about continuous-time signals that are most often measured in practice.

It is about discrete-time signals that are processed by computers.

It is about continuous-time and discrete-time systems that are used to process signals.

It is about how to draw useful information from observed signals and how to place information in communication signals.

Fig. 1 depicts typical signal flow in the processing of continuous-time signals by discrete-time system.

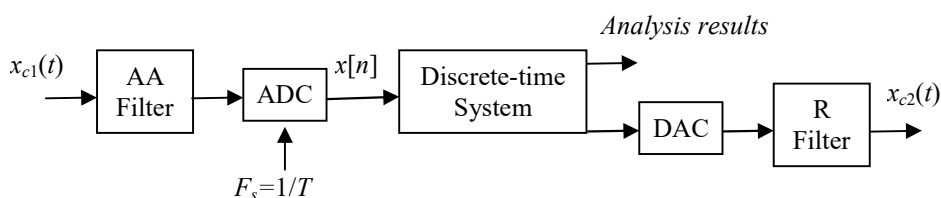


Fig. 1 Processing of continuous-time signals in discrete-time system

$x_{c1}(t)$ Continuous-time input signal
(e.g. voltage, current, temperature, position, pressure, etc.),

AA Filter Continuous-time anti-aliasing filter,

ADC Analog to Digital Converter,

$x[n]$ Discrete-time signal,

DAC Digital to Analog Converter,

$x_{c2}(t)$ Continuous-time output signal,

R Filter Continuous-time reconstruction filter,

$F_s=1/T$ Sampling frequency in Hz, T - sampling period in seconds.

1. Continuous-time signals and systems

1.1 Continuous-time signals

Signals are represented mathematically as functions of one or more independent variables. Most often the symbol t stands for this independent variable, and lower case letter denote the function itself, e.g. $x(t)$, $y(t)$, $z(t)$, etc. are continuous functions of t .

Independent variable t may represent time in seconds or any other physical quantity e.g. position in meters, temperature in Celsius, etc..

Continuous-time signal $x(t)$ is periodic with period T if there is a positive value of T such that

$$x(t) = x(t + T) \quad \text{for all } t. \quad (1.1)$$

If continuous-time signal $x(t)$ is periodic with period T , then it is also periodic with the period $2T, 3T, 4T, \dots$

$$x(t) = x(t + T) = x(t + mT) \quad m = 0, 1, 2, 3, \dots. \quad (1.2)$$

Constant signal $x(t) = \text{const}$ is not periodic.

A signal $x(t)$ that is not periodic is called aperiodic.

1.1.1 Exponential signal

$$x(t) = Ce^{at} \quad (1.3)$$

If a in (1.3) is positive and $C > 0$, then $x(t)$ increases (grows) exponentially with increasing t . This describes unstable process e.g. chain reactions in atomic explosions.

If a in (1.3) is negative and $C > 0$, then $x(t)$ decreases (decay) exponentially with increasing t . This describes stable process e.g. the response of RC circuits, or damped mechanical systems.

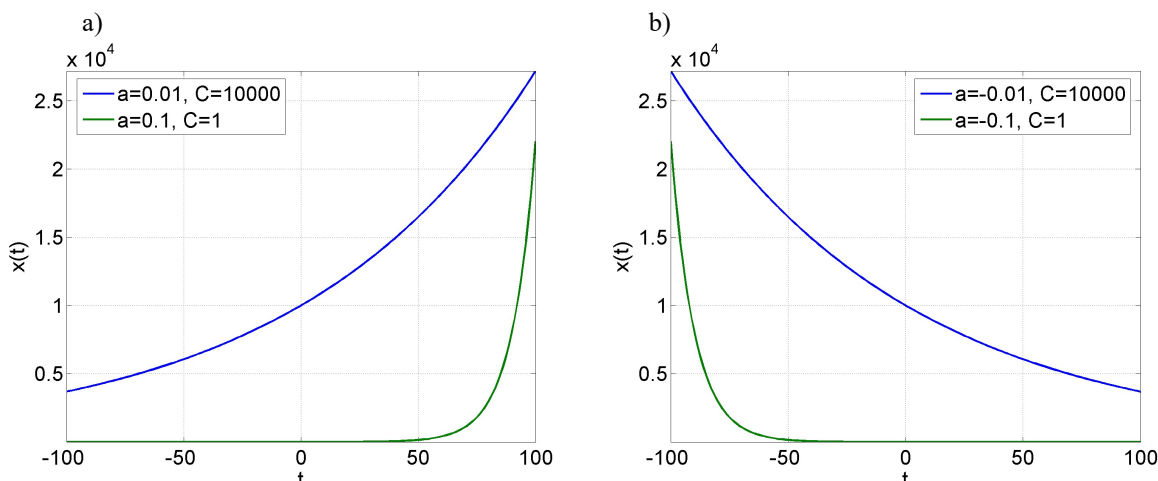


Fig. 1.1 Continuous-time exponential signals (1.3): a) $a > 0$, b) $a < 0$.

Matlab ref. book p. 126

Arithmetic Operators + - * / \ ^ '

Matrix Operations		Array Operations	
x	1 2 3	y	4 5 6
x'	1 2 3	y'	4 5 6
x+y	5 7 9	x-y	-3 -3 -3
x + 2	3 4 5	x-2	-1 0 1
x * y	Error	x.*y	4 10 18
x' * y	32	x' .* y	Error
x*y'	4 5 6 8 10 12 12 15 18	x.*y'	Error
x*2	2 4 6	x.*2	2 4 6
x\y	16/7	x.\y	4 5/2 2
2\x	1/2 1 3/2	2./x	2 1 2/3
x/y	0 0 1/6 0 0 1/3 0 0 1/2	x./y	1/4 2/5 1/2
x/2	1/2 1 3/2	x./2	1/2 1 3/2
x^y	Error	x.^y	1 32 729
x^2	Error	x.^2	1 4 9
2^x	Error	2.^x	2 4 8
(x+i*y)'	1 - 4i 2 - 5i 3 - 6i		
(x+i*y).'	1 + 4i 2 + 5i 3 + 6i		

1.1.2 Complex exponential signal

$$x(t) = e^{j\Omega_0 t}, \quad (1.4)$$

where t is time in seconds, and Ω_0 is angular frequency in radians per second.

Complex exponential signal (complex sinusoid) is periodic with the period T_0

$$x(t) = e^{j\Omega_0(t+T_0)} = e^{j\Omega_0 t} e^{j\Omega_0 T_0} = e^{j\Omega_0 t}. \quad (1.5)$$

The fundamental (i.e. the smallest positive) period computed from

$$e^{j\Omega_0 T_0} = 1 \Rightarrow \Omega_0 T_0 = 2\pi k, \quad k = \dots -2, -1, 0, 1, 2, \dots \quad (1.6)$$

is

$$T_0 = \frac{2\pi}{|\Omega_0|}, \quad (1.7)$$

thus the signals $e^{j\Omega_0 t}$ and $e^{-j\Omega_0 t}$ both have the same period (1.7).

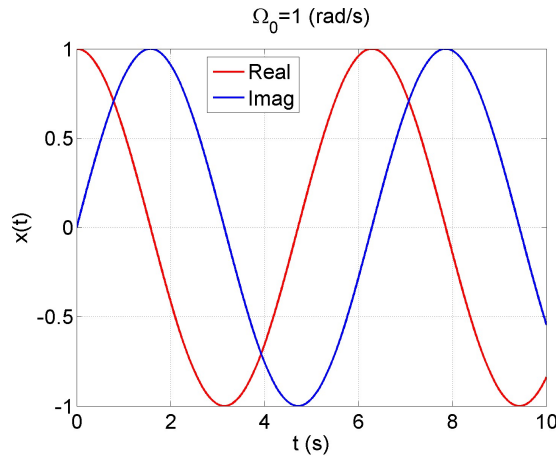
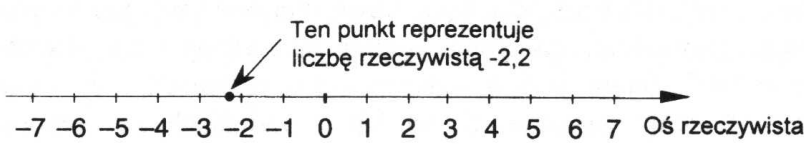
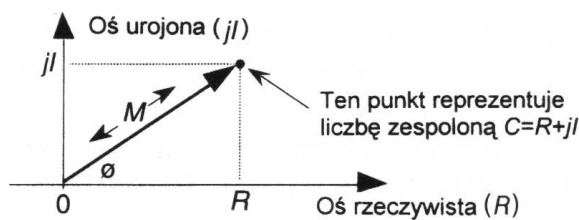


Fig. 1.2 Continuous-time complex exponential signal (1.4).



Rys. A.1.

Reprezentacja liczby rzeczywistej jako punktu na jednowymiarowej osi rzeczywistej



Rys. A.2.

Wskazowa reprezentacja liczby zespolonej $C = R + jI$ na płaszczyźnie zespolonej

A.2. Arytmetyczna reprezentacja liczb zespolonych

Liczba zespolona C jest w literaturze reprezentowana na wiele sposobów, takich jak

$$\text{Postać we współrzędnych prostokątnych} \quad C = R + jI \quad (\text{A.1})$$

$$\text{Postać trygonometryczna:} \quad C = M[\cos \phi + j \sin(\phi)] \quad (\text{A.1}')$$

$$\text{Postać we współrzędnych biegunowych (wykładnicza):} \quad C = Me^{j\phi} \quad (\text{A.1}'')$$

$$\text{Postać modułu i kąta fazowego:} \quad C = M \angle \phi \quad (\text{A.1}''')$$

Równania (A.1'') i (A.1''') przypominają nam, że liczba zespolona C może być również traktowana jako koniec wskazu na płaszczyźnie zespolonej, o długości M i kierunku ϕ stopni względem części dodatniej osi rzeczywistej, jak to pokazano na rys. A.2. (Unikamy nazywania wskazu *M wektorem*, ponieważ termin *wektor* oznacza różne rzeczy w różnych kontekstach. W algebrze liniowej *wektor* jest terminem używanym na oznaczenie macierzy jednowymiarowej. Z drugiej strony, w mechanice i w teorii pola wektory są używane na oznaczenie długości i kątów, lecz istnieją operacje na wektorach (*iloczyn skalarny* lub *iloczyn wektorowy*), które nie stosują się do naszej definicji wskazu.) Związek pomiędzy wielkościami na tym rysunku wynika ze standardowych zależności, obowiązujących w geometrii trójkątów prostokątnych. Miejmy na uwadze, że C jest liczbą zespoloną, wielkości zaś R , I , M i ϕ są wszystkie liczbami rzeczywistymi. Wartość bezwzględną liczby C , czasem zwaną *modułem* liczby C , stanowi

$$M = |C| = \sqrt{R^2 + I^2} \quad (\text{A.2})$$

a, z definicji, kątem fazowym lub *argumentem* liczby C jest arcus tangens ilorazu I/R lub

$$\phi = \operatorname{arctg} \left(\frac{I}{R} \right) \quad (\text{A.3})$$

Wielkość ϕ we wzorze (A.3) jest wartością kąta. Może ona mieć wymiar stopni lub radianów. Możemy, oczywiście, zamieniać stopnie na radiany i na odwrotnie, używając π radianów = 180° . Zatem, jeśli ϕ_r oznacza kąt w radianach, a ϕ_d – kąt w stopniach, wówczas możemy zamienić ϕ_r na kąt w radianach za pomocą wyrażenia

$$\phi_d = \frac{180\phi_r}{\pi} \quad (\text{A.4})$$

Podobnie, możemy zamienić ϕ_d na kąt w radianach za pomocą wyrażenia

$$\phi_r = \frac{\pi\phi_d}{180} \quad (\text{A.5})$$

Postać wykładnicza (tj. we współrzędnych biegunkowych) liczby zespolonej ma ciekawą cechę charakterystyczną, którą powinniśmy mieć na uwadze. O ile pojedyncze wyrażenie we współrzędnych prostokątnych może przedstawiać tylko jedną liczbę zespoloną, o tyle liczba zespolona C w postaci wykładniczej, reprezentowana jako $C = Me^{j\phi}$, odpowiada nieskończonym wielu liczbom zespolonym, gdyż

$$C = Me^{j\phi} = Me^{j(\phi + 2\pi n)} \quad (\text{A.6})$$

gdzie $n = \pm 1, \pm 2, \pm 3, \dots$ i kąt ϕ jest wyrażony w radianach. Jeśli kąt ϕ jest wyrażony w stopniach, wzór (A.6) przyjmuje postać

$$C = Me^{j\phi} = Me^{j(\phi + n360^\circ)} \quad (\text{A.7})$$

Wzory (A.6) i (A.7) są prawie oczywiste. Wskazują one, że punkt płaszczyzny zespolonej, reprezentowany przez koniec wskazu liczby C pozostaje niezmieniony, jeśli obracamy wskaz o pewną całkowitą wielokrotność 2π radianów lub o całkowitą wielokrotność 360° . Jeśli zatem, na przykład, $C = Me^{j(20^\circ)}$, to wówczas

$$C = Me^{j(20^\circ)} = Me^{j(380^\circ)} = Me^{j(740^\circ)} \quad (\text{A.8})$$

Wielkość ϕ , czyli kąt wskazu na rys. A.2 nie musi być stałą. Często napotkamy wyrażenia zawierające sinusoidę zespoloną, które przyjmują postać

$$C = Me^{j\omega t} \quad (\text{A.9})$$

Równanie (A.9) reprezentuje wskaz o amplitudzie M , którego kąt na rys. A.2 zwiększa się liniowo w czasie, z szybkością ω radianów w każdej sekundzie. Jeśli $\omega = 2\pi$, to wskaz przedstawiony równaniem (A.9) obraca się w kierunku przeciwnym do ruchu wskazówek zegara z szybkością 2π radianów na sekundę – jedna ewolucja na sekundę – i oto dlaczego ω jest zwana pulsacją. Wyrażając to częstotliwościowo, wskaz z równania (A.9) obraca się w kierunku przeciwnym do ruchu wskazówek zegara z szybkością $\omega = 2\pi f$ radianów na sekundę, gdzie f jest

częstotliwością w okresach na sekundę (Hz). Jeśli częstotliwość ta wynosi 10 Hz, to wskaz obraca się 20π radianów na sekundę. Podobnie, wyrażenie

$$C = Me^{-j\omega t} \quad (\text{A.9}')$$

reprezentuje wskaz o amplitudzie M , który obraca się zgodnie z kierunkiem ruchu wskazówek zegara wokół początku układu współrzędnych płaszczyzny zespolonej z ujemną pulsacją — ω radianów na sekundę.

A.3. Operacje arytmetyczne na liczbach zespolonych

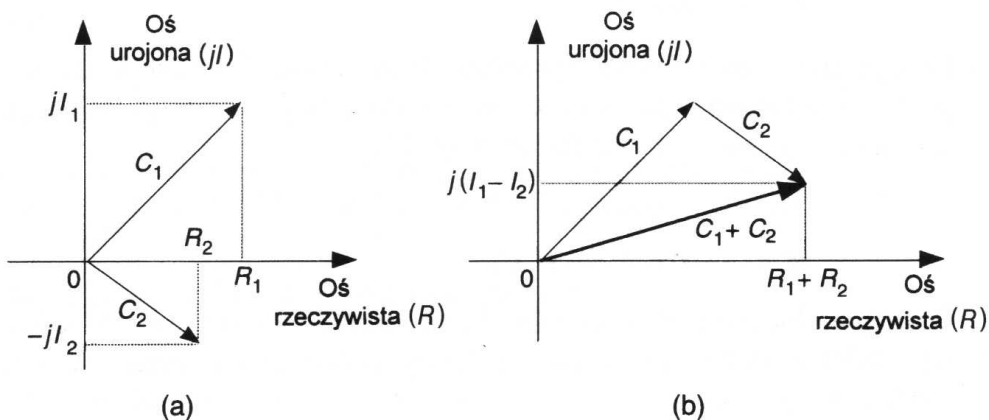
A.3.1. Dodawanie i odejmowanie liczb zespolonych

Której z podanych postaci liczby zespolonej C we wzorach (A.1) najlepiej jest używać? Zależy to od operacji arytmetycznej, jaką chcemy przeprowadzić. Na przykład, jeśli dodajemy dwie liczby zespolone, najłatwiejsza w użyciu jest postać wyrażona w równaniu (A.1) we współrzędnych prostokątnych. Wynik dodawania dwóch liczb zespolonych $C_1 = R_1 + jI_1$ i $C_2 = R_2 + jI_2$ jest sumą ich części rzeczywistych oraz przemnożoną przez j sumą ich części urojonych, czyli po prostu

$$C_1 + C_2 = R_1 + jI_1 + R_2 + jI_2 = R_1 + R_2 + j(I_1 + I_2) \quad (\text{A.10})$$

Na rysunku A.3 graficznie przedstawiono sumę dwóch liczb zespolonych, używając koncepcji wskazów. Wskaz sumy $C_1 + C_2$ z rys. A.3(a) jest nowym wskazem, o punkcie początkowym w początku wskazu C_1 i punkcie końcowym w końcu wskazu C_2 , co pokazano na rys. A.3(b). Pamiętajmy, że części rzeczywiste R i części urojone I mogą być liczbami zarówno dodatnimi, jak też ujemnymi. Odejmowanie jednej liczby zespolonej od drugiej sprowadza się do obliczenia różnic ich części rzeczywistych i urojonych. Zatem

$$C_1 - C_2 = (R_1 + jI_1) - (R_2 + jI_2) = R_1 - R_2 + j(I_1 - I_2) \quad (\text{A.11})$$



Rys. A.3. Reprezentacja geometryczna sumy dwóch liczb zespolonych

Przykład dodawania liczb zespolonych jest omówiony w punkcie 8.3, gdzie rozpatrzyliśmy zadanie uśredniania wartości wyjściowych szybkich transformat Fouriera.

A.3.2. Mnożenie liczb zespolonych

Mnożenie dwóch liczb zespolonych zapisanych we współrzędnych prostokątnych można zapisać jako

$$C_1 C_2 = (R_1 + jI_1)(R_2 + jI_2) = (R_1 R_2 - I_1 I_2) + j(R_1 I_2 - R_2 I_1) \quad (\text{A.12})$$

Jednakowoż, jeśli wykorzystujemy zapis obydwu liczb zespolonych w postaci wykładniczej, ich iloczyn przyjmuje postać prostszą

$$C_1 C_2 = M_1 e^{j\phi_1} M_2 e^{j\phi_2} = M_1 M_2 e^{j(\phi_1 + \phi_2)} \quad (\text{A.13})$$

ponieważ przy mnożeniu dodaje się wykładniki.

Skalowanie, jako szczególny przypadek mnożenia dwóch liczb zespolonych, jest mnożeniem danej liczby zespolonej przez liczbę zespoloną, której część urojona jest równa zeru. Możemy tutaj użyć również dobrze zapisu we współrzędnych prostokątnych, a więc

$$kC = k(R + jI) = kR + jkI \quad (\text{A.14})$$

lub też we współrzędnych biegunowych, czyli

$$kC = k(Me^{j\phi}) = kMe^{j\phi} \quad (\text{A.15})$$

A.3.3. Sprzężenie liczby zespolonej

Aby otrzymać liczbę zespoloną sprzężoną, wystarczy jedynie zmienić znak części urojonej danej liczby. Zatem, jeśli przez C^* oznaczymy liczbę zespoloną sprzężoną z liczbą $C = R + jI = Me^{j\phi}$, to C^* wyraża się jako

$$C^* = R - jI = Me^{-j\phi} \quad (\text{A.16})$$

Istnieją dwie właściwości sprzężeń, które czasami okazują się wygodne. Po pierwsze, sprzężenie iloczynu jest równe iloczynowi sprzężeń. Oznacza to, że jeśli $C = C_1 C_2$, to wówczas z zależności (A.13)

$$\begin{aligned} C^* &= (C_1 C_2)^* = (M_1 M_2 e^{j(\phi_1 + \phi_2)})^* = M_1 M_2 e^{-j(\phi_1 + \phi_2)} = \\ &= M_1 e^{-j\phi_1} M_2 e^{-j\phi_2} = C_1^* C_2^* \end{aligned} \quad (\text{A.17})$$

Po drugie, iloczyn liczby zespolonej i jej sprzężenia jest równy kwadratowi modułu tej liczby zespolonej. Można to łatwo pokazać, używając zapisu w postaci wykładniczej, gdyż

$$CC^* = Me^{j\phi} \cdot Me^{-j\phi} = M^2 e^{j0} = M^2 \quad (\text{A.18})$$

(Właściwość ta jest często używana w cyfrowym przetwarzaniu sygnałów w celu określenia mocy zespolonego wskazu sinusoidalnego, reprezentowanego przez $Me^{j\omega t}$.)

A.3.4. Dzielenie liczb zespolonych

Wygodnie jest przeprowadzać dzielenie dwóch liczb zespolonych zapisanych zarówno w postaci wykładniczej

$$\frac{C_1}{C_2} = \frac{M_1 e^{j\phi_1}}{M_2 e^{j\phi_2}} = \cancel{\frac{M_1}{M_2}} e^{\cancel{j\phi_2}} \frac{M_1}{M_2} e^{j(\phi_1 - \phi_2)} \quad (\text{A.19})$$

jak również z wykorzystaniem modułu i kąta

$$\frac{C_1}{C_2} = \frac{M_1}{M_2} \angle \phi_1 - \phi_2 \quad (\text{A.19}')$$

Wprawdzie nie w tak wygodny sposób, niemniej możemy przeprowadzić dzielenie liczb zespolonych zapisanych we współrzędnych prostokątnych, przemnażając licznik i mianownik przez zespolone sprzężenie mianownika, czyli

$$\begin{aligned} \frac{C_1}{C_2} &= \frac{R_1 + jI_1}{R_2 + jI_2} = \frac{R_1 + jI_1}{R_2 + jI_2} \cdot \frac{R_2 - jI_2}{R_2 - jI_2} = \\ &= \frac{(R_1 R_2 + jI_1 I_2) + j(R_2 I_1 - R_1 I_2)}{R_2^2 + I_2^2} \end{aligned} \quad (\text{A.20})$$

A.3.5. Odwrotność liczby zespolonej

Szczególną postacią dzielenia jest odwrotność danej liczby zespolonej. Jeśli $C = Me^{j\phi}$, to jej odwrotność wyraża się jako

$$\frac{1}{C} = \frac{1}{Me^{j\phi}} = \frac{1}{M} e^{-j\phi} \quad (\text{A.21})$$

Używając zapisu we współrzędnych prostokątnych, odwrotność liczby $C = R + jI$ jest dana przez

$$\frac{1}{C} = \frac{1}{R + jI} = \frac{R - jI}{R^2 + I^2} \quad (\text{A.22})$$

Wzór (A.22) otrzymujemy, podstawiając w zależności (A.20) $R_1 = 1$, $I_1 = 0$, $R_2 = R$ i $I_2 = I$.

A.3.6. Potęgowanie liczb zespolonych

Podniesienie liczby zespolonej do pewnej potęgi jest łatwo wykonalne w postaci wykładniczej. Jeśli $C = Me^{j\phi}$, wówczas

$$C^k = M^k (e^{j\phi})^k = M^k e^{jk\phi} \quad (\text{A.23})$$

Przykładowo, jeśli $C = 3e^{j125^\circ}$, to C podniesione do trzeciej potęgi wynosi

$$(C)^3 = 3^3(e^{j3 \cdot 125^\circ}) = 27e^{j375^\circ} = 25e^{j15^\circ} \quad (\text{A.24})$$

Podsumowujemy ten dodatek, wprowadzając cztery pozostałe zespolone operacje arytmetyczne, które nie są zbyt powszechnie używane w cyfrowym przetwarzaniu sygnałów – ale możemy ich kiedyś potrzebować.

A.3.7. Pierwiastki liczby zespolonej

Pierwiastek k -tego stopnia liczby zespolonej C , to taka liczba, która mnożona przez siebie k krotnie, daje w wyniku liczbę C . Aby przebadać tę operację, najwygodniej jest użyć postaci wykładniczej liczby zespolonej. Kiedy liczba zespolona jest zapisana jako $C = Me^{j\phi}$, pamiętajmy, że może ona być reprezentowana również przez

$$C = Me^{j(\phi + n360^\circ)} \quad (\text{A.25})$$

W tym przypadku wielkość ϕ w zależności (A.25) jest wyrażona w stopniach. Wyznaczając pierwiastek k -tego stopnia liczby C , można stwierdzić, iż istnieje k różnych pierwiastków tej liczby. Przez różne rozumiemy takie pierwiastki, których wykładniki są mniejsze, niż 360° . Znajdujemy te pierwiastki wykorzystując poniższą zależność:

$$\sqrt[k]{C} = \sqrt[k]{Me^{j(\phi + n360^\circ)}} = \sqrt[k]{M} e^{j(\phi + n360^\circ)/k} \quad (\text{A.26})$$

Następnie, przypisujemy zmiennej n we wzorze (A.26) wartości $0, 1, 2, 3, \dots, k-1$, aby otrzymać k pierwiastków liczby C . Rozważmy więc przykład! Powiedzmy, że poszukujemy pierwiastka trzeciego stopnia liczby $C = 125e^{j(75^\circ)}$. Postępujemy następująco:

$$\sqrt[3]{C} = \sqrt[3]{125e^{j(75^\circ)}} = \sqrt[3]{125e^{j(75^\circ + n360^\circ)}} = \sqrt[3]{125e^{j(75^\circ + n360^\circ)/3}} \quad (\text{A.27})$$

Następnie przypisujemy wartości $n = 0, n = 1$ i $n = 2$ w równaniu (A.27), aby otrzymać trzy pierwiastki liczby C . A więc tymi trzema pierwiastkami są:

$$1. \text{ pierwiastek } \rightarrow \sqrt[3]{C} = \sqrt[3]{125e^{j(75^\circ + 0 \cdot 360^\circ)/3}} = 5e^{j(25^\circ)}$$

$$2. \text{ pierwiastek } \rightarrow \sqrt[3]{C} = \sqrt[3]{125e^{j(75^\circ + 1 \cdot 360^\circ)/3}} = 5e^{j(435^\circ)/3} = 5e^{j(145^\circ)}$$

oraz

$$3. \text{ pierwiastek } \rightarrow \sqrt[3]{C} = \sqrt[3]{125e^{j(75^\circ + 2 \cdot 360^\circ)/3}} = 5e^{j(795^\circ)/3} = 5e^{j(265^\circ)}$$

A.3.8. Logarytmy naturalne liczby zespolonej

Wyznaczenie logarytmu naturalnego liczby zespolonej $C = Me^{j\phi}$ jest proste, jeśli używa się postaci wykładniczej, gdyż wówczas

$$\ln C = \ln(Me^{j\phi}) = \ln M + \ln(e^{j\phi}) = \ln M + j\phi \quad (\text{A.28})$$

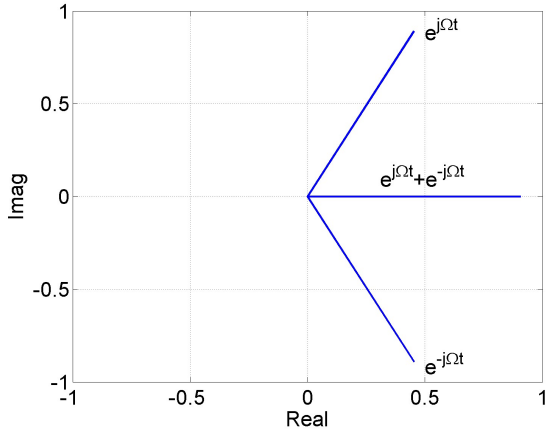


Fig. 1.3 Continuous-time complex exponential signal (1.4) on complex plane.

Euler's relations are observed in Fig. 1.3

$$x(t) = e^{j\Omega_0 t} = \cos(\Omega_0 t) + j \sin(\Omega_0 t), \quad (1.8)$$

and

$$e^{j\Omega_0 t} + e^{-j\Omega_0 t} = 2 \cos(\Omega_0 t), \quad e^{j\Omega_0 t} - e^{-j\Omega_0 t} = j 2 \sin(\Omega_0 t). \quad (1.9)$$

1.1.3 Sinusoidal signal

Sinusoidal signal is often defined with cosine function ('sinusoidal' refers to the shape of the function)

$$x(t) = A \cos(\Omega_0 t + \varphi) = A \cos(2\pi F_0 t + \varphi), \quad (1.10)$$

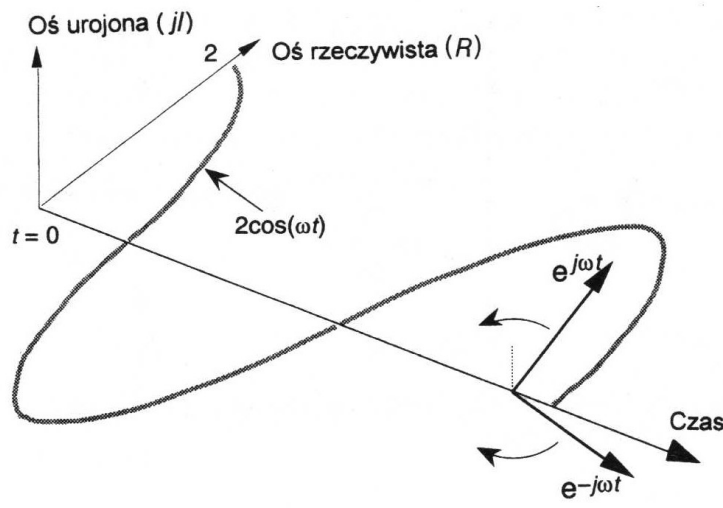
where t is time in seconds, Ω_0 is angular frequency in radians per second, F_0 is frequency in Hertz, φ is phase in radians, and $A > 0$ is amplitude in the units of measured physical quantity, e.g. volts.

Sinusoidal signal (1.10) is periodic with the period $T_0 = 2\pi/\Omega_0$.

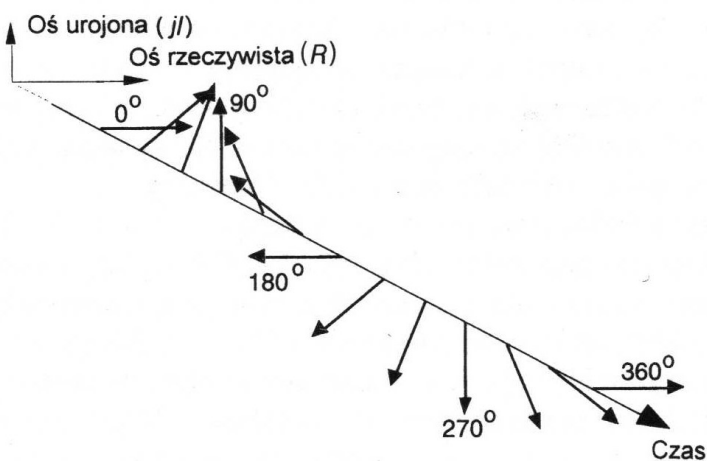
By using Euler's relation (1.9) sinusoidal signal may be expressed as a sum of complex exponentials

$$A \cos(\Omega_0 t + \varphi) = \frac{A}{2} e^{j\varphi} e^{j\Omega_0 t} + \frac{A}{2} e^{-j\varphi} e^{-j\Omega_0 t}.$$

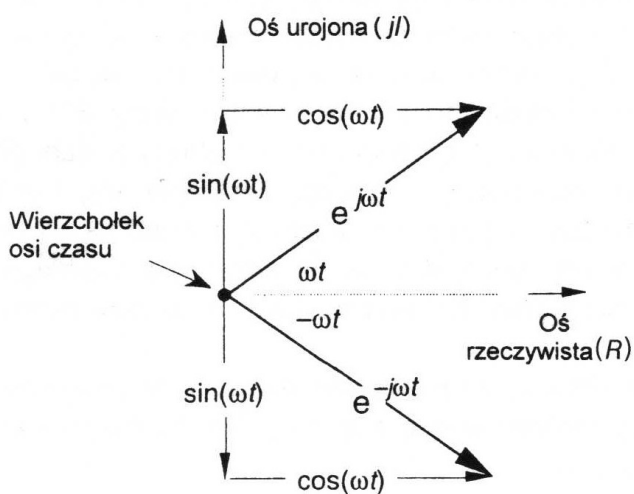
(1.11)



Rys. C.3. **K**
Przebieg cosinusoidalny
reprezentowany przez
dwa obracające się
wskaziki zespolone

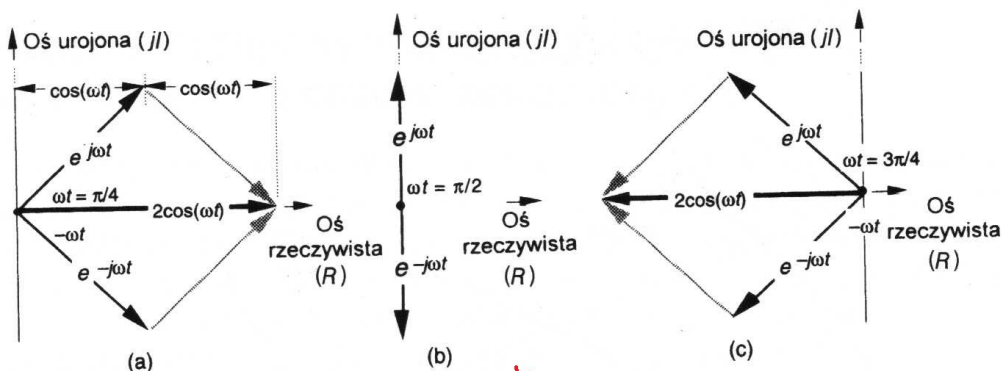


Rys. C.4.
Obrót wskaziku $e^{j\omega t}$ wokół
osi czasu



Rys. C.5.
Zespolone wskaziki
reprezentujące przebieg
cosinusoidalny na płaszczyźnie
zespolonej

Dodatni kąt ωt jest (arbitrarynie) zdefiniowany jako kąt mierzony w kierunku przeciwnym do ruchu wskazówek zegara pomiędzy osią rzeczywistą a wskazikiem. Gdy czas t rośnie, kąt ωt rośnie i wskazik $e^{j\omega t}$ obraca się w kierunku przeciwnym



Rys. C.6. Zespolone wskazy reprezentujące przebieg cosinusoidalny: (a) jeśli $\omega t = \pi/4$, (b) jeśli $\omega t = \pi/2$, (c) jeśli $\omega t = 3\pi/4$

do ruchu wskazówek zegara. Wskaz $e^{-j\omega t}$ obraca się zgodnie z kierunkiem wskazówek zegara z taką samą częstotliwością kątową, co wskaz $e^{j\omega t}$, to jest, jeśli ωt wynosi zero radianów, obydwa wskazy znajdują się na godzinie 3:00 wzdłuż osi rzeczywistej. W miarę upływu czasu, kiedy wskaz $e^{j\omega t}$ jest na godzinie dwunastej, wskaz $e^{-j\omega t}$ znajduje się na godzinie szóstej. Kontynuując obracanie się, wskazy te mijają się znów dokładnie na godzinie dziewiątej.

Spójrzmy dalej i zobaczymy, że suma wskazów $e^{j\omega t}$ i $e^{-j\omega t}$ reprezentuje rzeczywisty przebieg cosinusoidalny. Na rysunku C.6(a) kąt wskazu wynosi $\omega t = \pi/4$ (45 stopni). Pogrubiona strzałka, reprezentująca rzeczywisty przebieg cosinusoidalny $2\cos(\omega t)$ stanowi sumę wskazów $e^{j\omega t}$ i $e^{-j\omega t}$. Zauważmy, że koniec strzałki przebiegu cosinusoidalnego jest skierowany wzdłuż osi rzeczywistej. W chwilę później, kiedy wartość $\omega t = \pi/2$ radianów, wskaz $e^{j\omega t}$ obrócił się przeciwnie do ruchu wskazówek zegara, wskaz $e^{-j\omega t}$ obrócił się zgodnie z ruchem wskazówek zegara, koniec zaś strzałki przebiegu $2\cos(\omega t)$ przesunął się w lewo i znalazł się dokładnie w punkcie zerowym osi rzeczywistej, jak pokazano na rys. C.6(b). Wiemy, że jest to poprawne, ponieważ $2\cos(\pi/2) = 0$. Gdy czas płynie dalej i wartość $\omega t = 3\pi/4$ radiana, to dla tej chwili wskazy $e^{j\omega t}$ i $e^{-j\omega t}$ i ich wynikowy wskaz $2\cos(\omega t)$, który jest rzeczywisty i ujemny, zostały pokazane na rys. C.6(c). Gdy wskazy zespolone kontynuują obracanie się, koniec wskazu $2\cos(\omega t)$ ślizga się jedynie tam i z powrotem, pozostając wciąż na osi rzeczywistej. Na rysunku C.3 usiłowano to zilustrować przez pokazanie przebiegu $2\cos(\omega t)$, zawsze leżącego w płaszczyźnie osi rzeczywistej w naszej prezentacji trójwymiarowej.

Biorąc pod uwagę te wskazy, jest teraz jasne, dlaczego przebieg cosinusoidalny może być przyrównywany do sumy dwóch zespolonych wskazów poprzez zależność

$$\cos(\omega t) = \frac{e^{j\omega t} + e^{-j\omega t}}{2} \quad (\text{C.3})$$

będącą połową sumy równań (C.1) i (C.2). (W przykładzie na rys. C.3 użyto przebiegu cosinusoidalnego o amplitudzie równej 2 jedynie po to, aby uniknąć nieporządku na rys. C.3 do C.6 w mianowniku, równym 2 dla każdego z członów

1.1.4 Damped sinusoidal signal

By substituting the constant amplitude A in (1.10) by exponential signal (1.3) we obtain damped sinusoid

$$x(t) = Ce^{at} \cos(\Omega_0 t + \varphi), \quad a < 0, \quad (1.12)$$

which describes for example the response of RLC circuits or damped oscillatory mechanical system. Exponential signal in (1.12) is the envelope of sinusoidal signal.

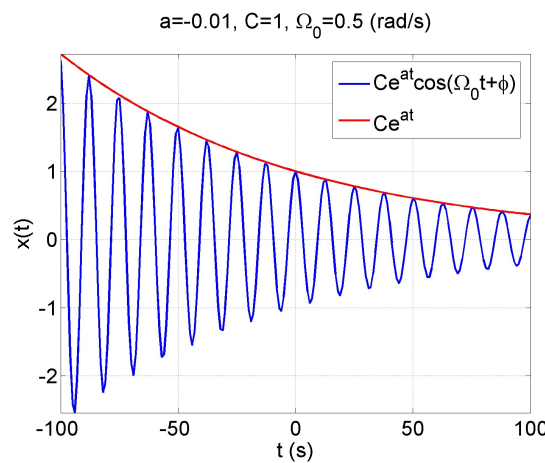


Fig. 1.4 Damped sinusoid (1.12).

1.1.5 Delta function

The delta function (unit impulse function, Dirac function) is usually defined by one of the three ways

I. By the equation

$$\int_{-\infty}^{\infty} \delta(t) dt = 1, \quad \delta(t) = 0 \quad \text{for } t \neq 0 \quad (1.13)$$

II. As a limit

$$\delta(t) = \lim_{n \rightarrow \infty} f_n(t) \quad (1.14)$$

of a sequence of functions satisfying $\int_{-\infty}^{\infty} f_n(t) dt = 1, \quad \lim_{n \rightarrow \infty} f_n(t) = 0 \quad \text{for } t \neq 0$

III. By the property

$$\int_{-\infty}^{\infty} \delta(t) f(t) dt = f(0) \quad (1.15)$$

where $f(t)$ is an arbitrary function, continuous at the origin.

Definitions (1.13-1.15) are informal but illustrate the concept of the delta function. Formal treatment of delta function is based on distribution theory.

A distribution, or generalized function, (or functional) $g(t)$ is a process of assigning to an arbitrary function $\varphi(t)$ of a given Class C a number $N_g[\varphi(t)]$. This number could be the value of $\varphi(t)$ or its derivatives for some $t=t_0$, the area under $\varphi(t)$ in some interval, or any other quantity depending on $\varphi(t)$ [Pap62].

In distribution theory generalized derivatives of discontinuous functions exist. The concept of generalized limit guarantees the convergence of certain limits that ordinary do not exist.

The definition (1.15) states that the delta function may select the value of the function (i.e. may sample the function) at the origin. This may also be done for arbitrary value t_0

$$\int_{-\infty}^{\infty} \delta(t - t_0) f(t) dt = f(t_0) \quad (1.16a)$$

or [Oppen83]

$$\delta(t - t_0) f(t) = \delta(t - t_0) f(t_0). \quad (1.16b)$$

1.2 Continuous-time systems

A *system* is any process that results in the transformation of signals. Thus, a system has an input signal, denoted by $x(t)$, and an output signal, denoted by $y(t)$, which are related by the system transformation (denoted by the arrow).

$$x(t) \rightarrow y(t). \quad (1.17)$$

A system is *casual* if the output at any time depends only on values of the input at the present time and in the past. In practice noncasual signal processing may also be applied for the signals that have already been recorded.

A system is *stable* if for the bounded input the output is also bounded.

A system is *time-invariant* if a time shift in the input signal causes the same time shift in the output signal, i.e. if $y(t)$ is an output for $x(t)$, than the output for $x(t-t_0)$ is $y(t-t_0)$.

A system is *linear* if it fulfils additivity property

$$x_1(t) + x_2(t) \rightarrow y_1(t) + y_2(t). \quad (1.18)$$

and scaling (homogeneity) property

$$ax(t) \rightarrow ay(t). \quad (1.19)$$

Both properties (1.18), (1.19) can be combined into a single superposition rule

$$ax_1(t) + bx_2(t) \rightarrow ay_1(t) + by_2(t), \quad (1.20)$$

where a, b are arbitrary constants. Equation (1.20) states that the output for the weighted sum of inputs equals the sum of weighted responses for each of input signal.

1.2.1 LTI systems

By applying (1.16a) for all values of variable t the function $x(t)$ is represented as a 'sum' (integral) of shifted by τ , and weighted by $x(\tau)$, delta functions

$$x(t) = \int_{-\infty}^{\infty} x(\tau) \delta(t - \tau) d\tau . \quad (1.21)$$

Consider a Linear Time Invariant (LTI) system with an arbitrary input $x(t)$ in the form (1.21)

$$x(t) = \int_{-\infty}^{\infty} x(\tau) \delta(t - \tau) d\tau \rightarrow y(t) . \quad (1.22)$$

By the linearity of the system the output is the superposition of the responses for each shifted delta function $h_\tau(t)$

$$y(t) = \int_{-\infty}^{\infty} x(\tau) h_\tau(t) d\tau , \quad (1.23)$$

where $\delta(t-\tau) \rightarrow h_\tau(t)$. For time invariant systems $h_\tau(t)=h_0(t-\tau)$. $h_0(t)$ is *unit impulse response* of LTI system and is denoted by $h(t)$. The response of LTI system for arbitrary input $x(t)$ is given by *convolution integral*

$$y(t) = \int_{-\infty}^{\infty} x(\tau) h(t - \tau) d\tau = x(t) * h(t) .$$

(1.24)

Continuous-time convolution satisfies:

I. Commutativity

$$x(t) * h(t) = h(t) * x(t) . \quad (1.25)$$

II. Associativity (cascade connection)

$$x(t) * [h_1(t) * h_2(t)] = [x(t) * h_1(t)] * h_2(t) . \quad (1.26)$$

III. Distributivity (parallel connection)

$$x(t) * [h_1(t) + h_2(t)] = [x(t) * h_1(t)] + [x(t) * h_2(t)] . \quad (1.27)$$

The system is stable if the impulse response is absolutely integrable

$$\int_{-\infty}^{\infty} |h(\tau)| d\tau < \infty . \quad (1.28)$$

To evaluate integral (1.24) for specific value of t we first obtain the signal $h(t-\tau)$ (regarded as a function of τ with fixed t) from $h(\tau)$ by a reflection about the origin plus a shift to the right by t if $t > 0$. We next multiply together signals $x(t)$ and $h(t-\tau)$ and $y(t)$ is obtained by integrating the resulting product from $\tau=-\infty$ to $\tau=+\infty$. Computation of (1.24) is illustrated in Fig. 1.5 for signals $x(t)=\begin{cases} 0.5, & |t|<1 \\ 0, & |t|>1 \end{cases}$ and $h(t)=\begin{cases} t+1, & |t|<1 \\ 0, & |t|>1 \end{cases}$. It is observed from (1.24) that in this example nonzero $y(t)$ is only possible for $|t|<2$, otherwise $x(\tau)$, or $h(t-\tau)$ equals zero. The

$$\text{convolution integral is } y(t)=\begin{cases} \frac{1}{4}(t+2)^2, & -2 < t < 0 \\ 1-\frac{1}{4}t^2, & 0 < t < 2 \\ 0, & |t| > 2 \end{cases}.$$

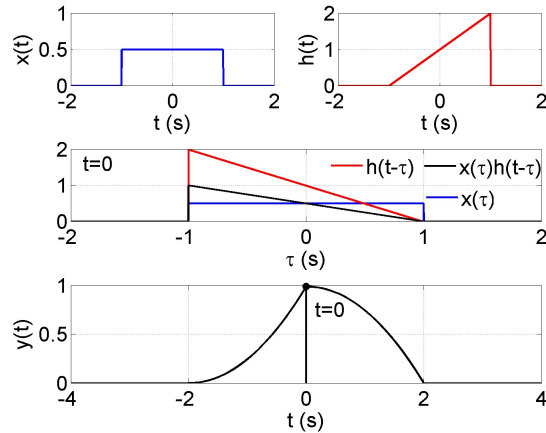


Fig. 1.5 Illustration of convolution integral $y(t)=\int_{-\infty}^{\infty} x(\tau)h(t-\tau)d\tau$ (1.24) computation.

$$y(t)=\begin{cases} \frac{1}{2}\int_{-1}^{t+1}(t-\tau+1)d\tau, & -2 < t < 0 \\ \frac{1}{2}\int_{t-1}^1(t-\tau+1)d\tau, & 0 < t < 2 \\ 0, & |t| > 2 \end{cases}, \quad y(t)=\begin{cases} \frac{1}{2}[t\tau-\frac{1}{2}\tau^2+\tau]_{-1}^{t+1}, & -2 < t < 0 \\ \frac{1}{2}[t\tau-\frac{1}{2}\tau^2+\tau]_{t-1}^1, & 0 < t < 2 \\ 0, & |t| > 2 \end{cases}$$

$$y(t)=\begin{cases} \frac{1}{2}[t(t+1)-\frac{1}{2}(t+1)^2+t+1]-\frac{1}{2}[-t-\frac{1}{2}-1]=\frac{1}{2}\left(\frac{1}{2}t^2+2t+2\right)=\frac{1}{4}(t+2)^2, & -2 < t < 0 \\ \frac{1}{2}[t-\frac{1}{2}+1]-\frac{1}{2}[t(t-1)-\frac{1}{2}(t-1)^2+t-1]=\frac{1}{2}\left(-\frac{1}{2}t^2+2\right)=1-\frac{1}{4}t^2, & 0 < t < 2 \\ 0, & |t| > 2 \end{cases}$$

digression convolution splines see

M. Unser, "Splines: A perfect fit for signal and image processing," IEEE Signal Processing Mag., vol. 16, no. 6, pp. 22–38, 1999.

Polynomial (convolution) splines of order P are defined as

$$\beta(t)^P = \underbrace{\beta(t)^0 * \beta(t)^0 * \dots * \beta(t)^0}_{(P+1) \text{ times}}, \quad \beta^0(t) = \begin{cases} 1, & |t| < 1 \\ 0, & |t| > 1 \end{cases}. \quad (1.29)$$

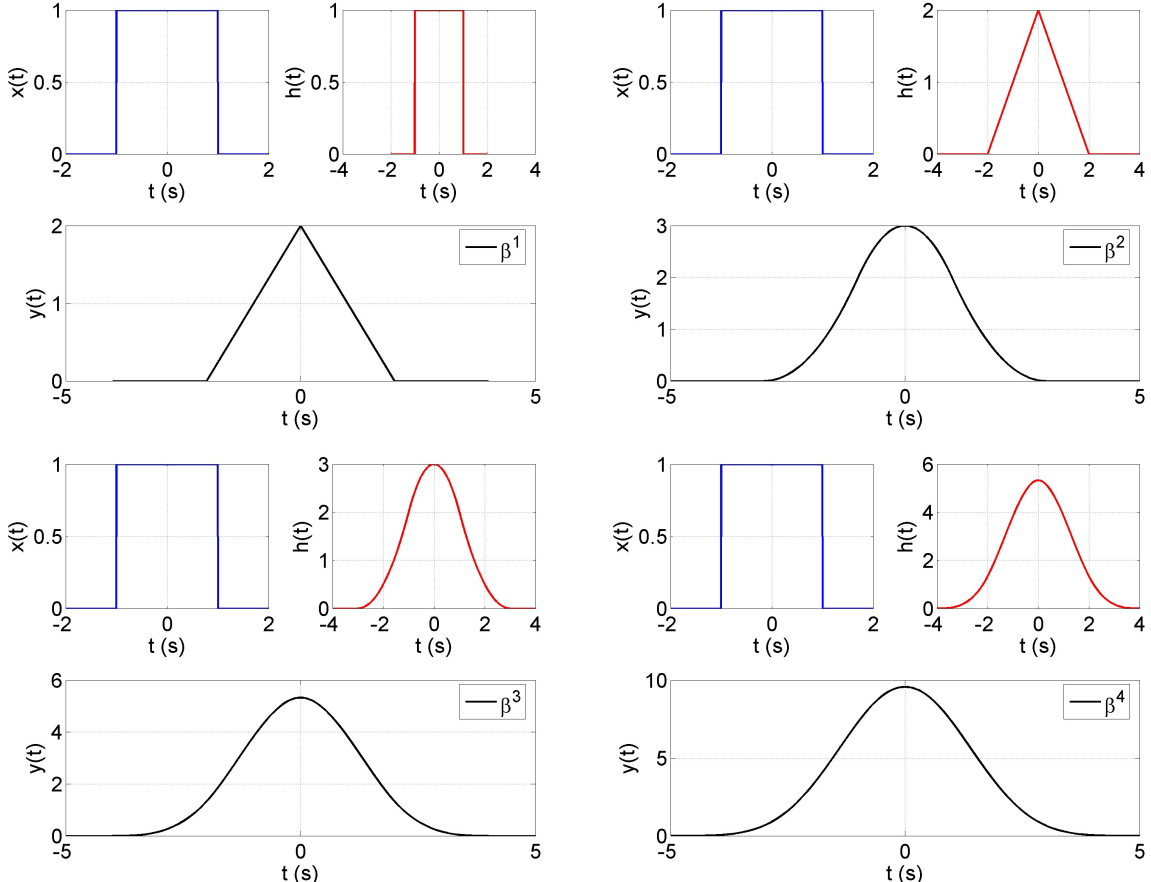


Fig. 1.6 Illustration of Polynomial (convolution) splines (1.29) computation.

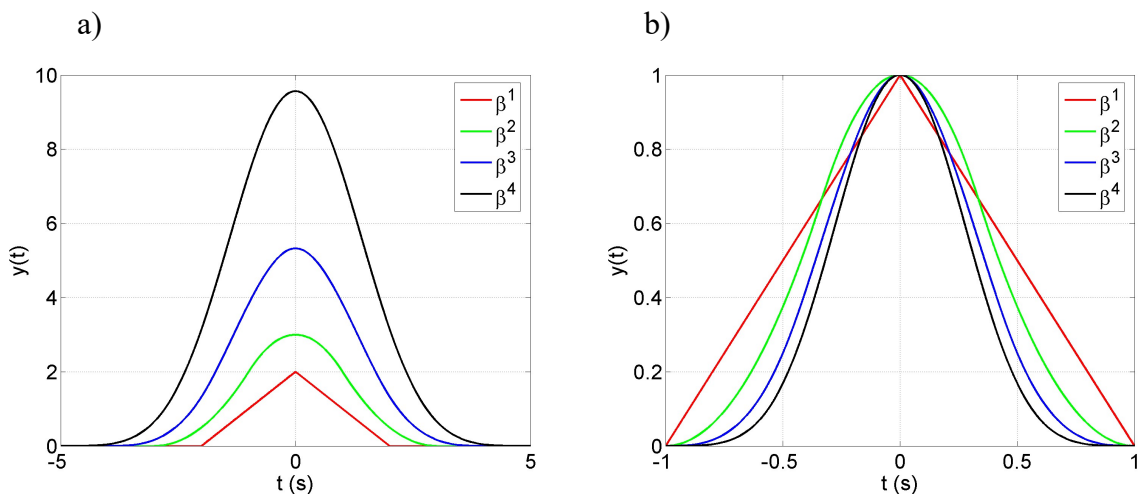


Fig. 1.7 Polynomial (convolution) splines: a) as computed from definition (1.29), b) rescaled to the time interval from -1 s to 1 s and the range of values from 0 to 1.

digression fractional splines

1.2.2 Frequency response of LTI systems

Let us consider an LTI system with impulse response $h(t)$. For an input signal being complex exponential signal $x(t) = e^{j\Omega_0 t}$ (1.4) the output is given by convolution integral (1.24)

$$y(t) = \int_{-\infty}^{\infty} h(\tau)x(t-\tau)d\tau = \int_{-\infty}^{\infty} h(\tau)e^{j\Omega_0(t-\tau)}d\tau = e^{j\Omega_0 t} \int_{-\infty}^{\infty} h(\tau)e^{-j\Omega_0 \tau}d\tau = H(\Omega_0)e^{j\Omega_0 t} \quad (1.30)$$

Thus the response to $x(t) = e^{j\Omega_0 t}$ is $y(t) = H(\Omega_0)e^{j\Omega_0 t}$ where in general

$$H(\Omega) = \int_{-\infty}^{\infty} h(\tau)e^{-j\Omega\tau}d\tau. \quad (1.31)$$

The complex valued function $H(\Omega)$ is a *frequency response* of LTI system; $|H(\Omega)|$ is a *magnitude response*, and angle $\{H(\Omega)\}$ is a *phase response*.

The importance of complex exponentials in the study of LTI systems stems from the fact that the response of an LTI system to a complex exponential input is the same complex exponential with only a change in complex amplitude, i.e. a change in amplitude and phase.

A signal for which the system output is just a constant times the input is referred to as an *eigenfunction*, and the amplitude factor is referred to as the *eigenvalue*.

Complex exponential $e^{j\Omega_0 t}$ is an eigenfunction of an LTI system. The $H(\Omega)$ (1.31) for a specified value of Ω_0 is the eigenvalue associated with the eigenfunction $e^{j\Omega_0 t}$.

1.2.3 Linear Constant-Coefficient Differential Equation

A general N th-order linear constant coefficient differential equation is given by

$$\sum_{k=0}^N a_k \frac{d^k y(t)}{dt^k} = \sum_{k=0}^M b_k \frac{d^k x(t)}{dt^k}. \quad (1.32)$$

The order refers to the highest derivative of the output $y(t)$. The solution $y(t)$ consists of two parts, a *particular* solution, satisfying (1.32), and a *homogeneous* solution, satisfying

$$\sum_{k=0}^N a_k \frac{d^k y(t)}{dt^k} = 0. \quad (1.33)$$

The differential equation (1.32) does not completely specify the output in terms of the input. In the general case we need a set of *auxiliary conditions* corresponding to the values of $y(t)$, $\frac{dy(t)}{dt}, \dots, \frac{d^{N-1}y(t)}{dt^{N-1}}$ at some point in time.

The system specified by (1.32) and auxiliary conditions is *linear* only if all of this auxiliary conditions are zero. Otherwise, the system is *incrementally linear* with the response due to auxiliary conditions alone added to the response due the input assuming zero auxiliary conditions.

For the system to be *linear* and *casual*, we must assume *initial rest*. That is, if $x(t)=0$ for $t \leq t_0$, we assume $y(t)=0$ for $t \leq t_0$, and therefore the response for $t > t_0$ can be calculated from (1.32) with the initial conditions $y(t_0) = \frac{dy(t_0)}{dt} = \dots = \frac{d^{N-1}y(t_0)}{dt^{N-1}} = 0$. In this case the system is linear time-invariant (LTI).

1.3 Fourier analysis



Jean Baptiste Joseph Fourier

Born	21 March 1768 Auxerre, Burgundy, Kingdom of France (now in Yonne, France)	Residence	France
Died	16 May 1830 (aged 62) Paris, Kingdom of France	Nationality	French
		Fields	Mathematician, physicist, and historian
		Institutions	École Normale École Polytechnique
		Alma mater	École Normale
		Doctoral advisor	Joseph Lagrange
		Doctoral students	Gustav Dirichlet Giovanni Plana Claude-Louis Navier
		Known for	Fourier series Fourier transform Fourier's law of conduction



THÉORIE
 ANALYTIQUE
DE LA CHALEUR,
 PAR M. FOURIER.



A PARIS,
 CHEZ FIRMIN DIDOT, PÈRE ET FILS,
 LIBRAIRES POUR LES MATHÉMATIQUES, L'ARCHITECTURE HYDRAULIQUE
 ET LA MARINE, RUE JACOB, N° 24.
 1822.
 262.

Digitized by Google

THE
 ANALYTICAL THEORY OF HEAT

BY
 Jean Baptiste JOSEPH FOURIER.



TRANSLATED, WITH NOTES,

BY
 ALEXANDER FREEMAN, M.A.,
 FELLOW OF ST JOHN'S COLLEGE, CAMBRIDGE.

EDITED FOR THE SYNDICS OF THE UNIVERSITY PRESS.

Cambridge:
 AT THE UNIVERSITY PRESS.
 LONDON: CAMBRIDGE WAREHOUSE, 17, PATERNOSTER ROW.
 CAMBRIDGE: DEIGHTON, BELL, AND CO.
 LEIPZIG: F. A. BROCKHAUS.
 1878
 [All Rights reserved.]

Digitized by Google

Analytical theory of heat p. 13

231—233. Any function whatever, $F(x)$, may be developed in the form

$$F(x) = A + \begin{cases} a_1 \cos x + a_2 \cos 2x + a_3 \cos 3x + \&c., \\ b_1 \sin x + b_2 \sin 2x + b_3 \sin 3x + \&c. \end{cases}$$

Each of the coefficients is a definite integral. We have in general

$$2\pi A = \int_{-\pi}^{+\pi} dx F(x), \quad \pi a_i = \int_{-\pi}^{+\pi} dx F(x) \cos ix,$$

and $\pi b_i = \int_{-\pi}^{+\pi} dx F(x) \sin ix.$

We thus form the general theorem, which is one of the chief elements of our analysis:

$$2\pi F(x) = \sum_{i=-\infty}^{+\infty} \left(\cos ix \int_{-\pi}^{+\pi} da F(a) \cos ia + \sin ix \int_{-\pi}^{+\pi} da F(a) \sin ia \right),$$

or $2\pi F(x) = \sum_{i=-\infty}^{+\infty} \int_{-\pi}^{+\pi} da F(a) \cos (ix - ia).$ 199

1.3.1 The Fourier Series

The representation of **periodic signal**, with period Ω_0 , as a linear combination of harmonically related complex exponentials of the form

$$x(t) = \sum_{k=-\infty}^{+\infty} a_k e^{jk\Omega_0 t} \quad (1.34)$$

where $a_k = A_k e^{j\varphi_k}$ is referred to as the *Fourier series* representation.

For real value periodic signal $x(t)$ it goes from Euler's relation (1.11) that $a_k = a_{-k}^*$ and (1.34) may be rewritten as

$$\begin{aligned} x(t) &= \sum_{k=-\infty}^{+\infty} a_k e^{jk\Omega_0 t} = a_0 + \sum_{k=1}^{+\infty} (A_k e^{j\varphi_k} e^{jk\Omega_0 t} + A_k e^{-j\varphi_k} e^{-jk\Omega_0 t}) = \\ &= a_0 + 2 \sum_{k=1}^{+\infty} A_k \cos(k\Omega_0 t + \varphi_k) \end{aligned} \quad (1.35)$$

The coefficients a_k of the *Fourier series* representation (1.34) are found by multiplying both sides of (1.34) by $e^{-jn\Omega_0 t}$

$$x(t)e^{-jn\Omega_0 t} = \sum_{k=-\infty}^{+\infty} a_k e^{jk\Omega_0 t} e^{-jn\Omega_0 t}. \quad (1.36)$$

Integrating both sides over one fundamental period from 0 to $T_0=2\pi/\Omega_0$, we have

$$\int_0^{T_0} x(t)e^{-jn\Omega_0 t} dt = \int_0^{T_0} \sum_{k=-\infty}^{+\infty} a_k e^{jk\Omega_0 t} e^{-jn\Omega_0 t} dt. \quad (1.37)$$

After changing the order of integration and summation, we obtain

$$\int_0^{T_0} x(t)e^{-jn\Omega_0 t} dt = \sum_{k=-\infty}^{+\infty} a_k \int_0^{T_0} e^{j(k-n)\Omega_0 t} dt. \quad (1.38)$$

The integral on the right side is

$$\int_0^{T_0} e^{j(k-n)\Omega_0 t} dt = \int_0^{T_0} \cos((k-n)\Omega_0 t) dt + j \int_0^{T_0} \sin((k-n)\Omega_0 t) dt. \quad (1.39)$$

For $k \neq n$ $\cos((k-n)\Omega_0 t)$ and $\sin((k-n)\Omega_0 t)$ are periodic sinusoids with fundamental period $T_0/|k-n|$. Therefore in (1.39) we are integrating over interval T_0 that is an integer number of periods of these signals. For $k \neq n$ both integrals in the right side of (1.39) are zero.

For $k=n$, $\cos((k-n)\Omega_0 t)$ equals 1, and thus the integral equals T_0 . In summary

$$\int_0^{T_0} e^{j(k-n)\Omega_0 t} dt = \begin{cases} T_0, & k = n \\ 0, & k \neq n \end{cases}, \quad (1.40)$$

and (1.38) reduces to $T_0 a_n$. Therefore

$$a_n = \frac{1}{T_0} \int_0^{T_0} x(t) e^{-jn\Omega_0 t} dt. \quad (1.41)$$

The integration in (1.41) may be done over any interval of length T_0 which is denoted by \int_{T_0} .

To summarize, if $x(t)$ has a Fourier series representation, then

$$x(t) = \sum_{k=-\infty}^{+\infty} a_k e^{jk\Omega_0 t}$$

$$a_k = \frac{1}{T_0} \int_{T_0} x(t) e^{-jk\Omega_0 t} dt$$

(1.42)

Upper equation (1.42) is referred to as the *synthesis equation*, and lower as the *analysis equation*.

The coefficients a_k are called the *Fourier series coefficients* or the *spectral coefficients* of $x(t)$.

The coefficient a_0 is the constant component of $x(t)$, or *dc* component, and is given by (1.42) with $k=0$

$$a_0 = \frac{1}{T_0} \int_{T_0} x(t) dt, \quad (1.43)$$

which is the average value of $x(t)$ over one period.

Example 1.1

Consider sinusoidal signal

$$x(t) = \sin(\Omega_0 t) = \frac{1}{2j} e^{j\Omega_0 t} - \frac{1}{2j} e^{-j\Omega_0 t}. \quad (1.44)$$

It is seen by comparing (1.42) and (1.44) that the only two nonzero Fourier coefficients are $a_1 = \frac{1}{2j}$, and $a_{-1} = -\frac{1}{2j}$.

Example 1.2

Consider periodic square wave depicted in Fig. 1.8 and defined over one period as

$$x(t) = \begin{cases} 1, & |t| < T_1 \\ 0, & T_1 < |t| < \frac{T_0}{2} \end{cases}. \quad (1.45)$$

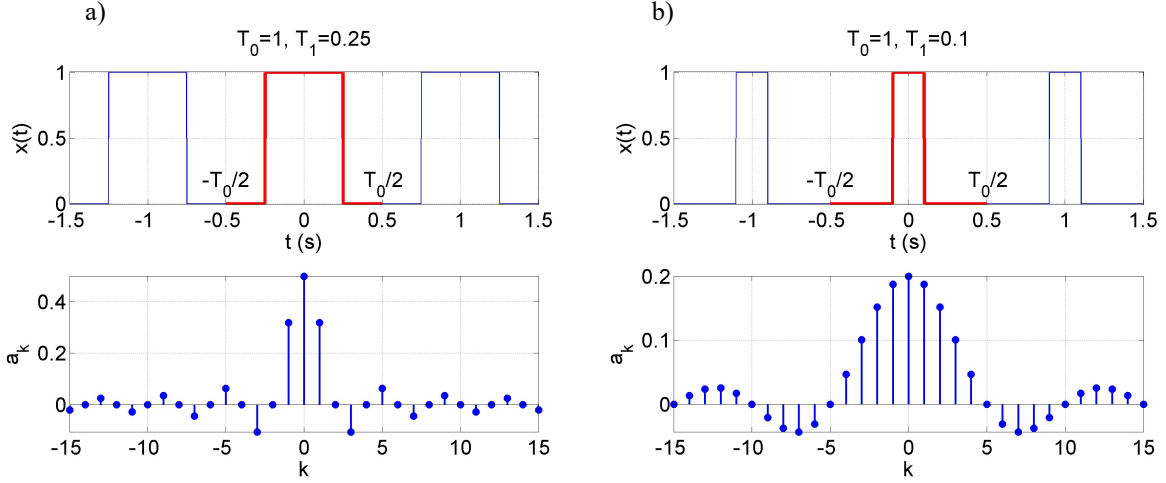


Fig. 1.8 Periodic square wave (1.45) and Fourier series coefficients from a_{-15} to a_{15} for:
a) $T_0=1$, $T_1=0.25$ (symmetric square wave), and b) $T_0=1$, $T_1=0.1$.

This signal is periodic with fundamental period T_0 (s) and fundamental frequency $\Omega_0=2\pi/T_0$ (rad/s). We will use (1.42) over interval $-(T_0/2) \leq t < T_0/2$.

For $k=0$ we get

$$a_o = \frac{1}{T_0} \int_{-T_1}^{T_1} dt = \frac{2T_1}{T_0}. \quad (1.46)$$

For $k \neq 0$ we get ($\Omega_0 T_0 = 2\pi$)

$$a_k = \frac{1}{T_0} \int_{-T_1}^{T_1} e^{-jk\Omega_0 t} dt = -\frac{1}{jk\Omega_0 T_0} e^{-jk\Omega_0 t} \Big|_{-T_1}^{T_1} = \frac{2}{2k\pi} \left(\frac{e^{jk\Omega_0 T_1} - e^{-jk\Omega_0 T_1}}{2j} \right) = \frac{\sin(k\Omega_0 T_1)}{k\pi} \quad (1.47)$$

For $T_0=4T_1$ we have $\Omega_0 T_0=\pi/2$ and $x(t)$ (1.45) is a symmetric square wave (Fig. 1.8a). From (1.46) and (1.47) follows

$$\begin{aligned} a_o &= \frac{1}{2} \\ a_k &= \frac{\sin(k\pi/2)}{k\pi}, \quad k \neq 0 \end{aligned} \quad (1.48)$$

In (1.48) $a_k=0$ for k even.

$$\begin{aligned} a_1 &= a_{-1} = \frac{1}{\pi} \\ a_3 &= a_{-3} = -\frac{1}{3\pi} \\ &\vdots \end{aligned} \quad (1.49)$$

Fourier series coefficients from a_{-15} to a_{15} for $T_0=1$, $T_1=0.25$ and $T_0=1$, $T_1=0.1$ are shown in Fig. 1.8. In this particular example, the Fourier coefficients are real, but in general

the Fourier coefficients are complex and consequently two graphs corresponding to real and imaginary parts or magnitude and phase of each coefficient are required.

In Fig. 1.8 horizontal axis could be scaled in frequency in Hertz ...- $3F_0$, - $2F_0$, - F_0 , 0, F_0 , $2F_0$, $3F_0$, ... instead on index k .

The range of Fourier series coefficients in this example is from $a_{-\infty}$ to a_{∞} .

By considering only a finite number of the Fourier series coefficients the signal $x(t)$ is approximated by $x_N(t)$

$$x_N(t) = \sum_{k=-N}^N a_k e^{jk\Omega_0 t}. \quad (1.50)$$

Approximation error is

$$e_N(t) = x(t) - x_N(t) = x(t) - \sum_{k=-N}^N a_k e^{jk\Omega_0 t}. \quad (1.51)$$

The quantitative measure of the size of the approximation error could be the total squared-error magnitude over one period (i.e. the energy in the approximation error over one period¹)

$$E_N = \int_{T_0} |e_N(t)|^2 dt = \int_{T_0} e_N(t) e_N^*(t) dt. \quad (1.52)$$

Optimal coefficients a_k in the sense of E_N (1.52) can be found by computing partial derivatives of (1.52) and equating them to zero. The coefficients a_k that minimize the energy in the error (1.52) are the Fourier series coefficients given by (1.42), thus If $x(t)$ has a Fourier series representation, the best approximation using only a finite number of harmonically related complex exponentials is obtained by truncating the Fourier series to the desired number of terms. The limit of E_N as $N \rightarrow \infty$ is zero.

Any periodic square-integrable over a period signal $x(t)$

$$\int_{T_0} |x(t)|^2 dt < \infty. \quad (1.53)$$

is *representable* through the Fourier series.

Fourier series is *equal* to $x(t)$ except at isolated values of t for which $x(t)$ is discontinuous (at these values of t the infinite Fourier series converges to the 'average' value of the discontinuity) if $x(t)$ satisfies the Dirichlet conditions.

¹ In general, for any signal $z(t)$ the quantity $E = \int_a^b |z(t)|^2 dt$ is referred to as the *energy* in $z(t)$ over the time interval $a \leq t \leq b$.

Dirichlet conditions:

Condition 1. Over any period $x(t)$ must be absolutely integrable

$$\int_{T_0} |x(t)| dt < \infty. \quad (1.54)$$

Condition 2. In any finite interval of time, $x(t)$ is of bounded variation, that is, there are no more than a finite number of maxima and minima during any single period of the signal.

Condition 3. In any finite interval of time there are only a finite number of discontinuities. Furthermore, each of these discontinuities must be finite.

Periodic signals violating Dirichlet conditions are:

- 1) Condition 1: $x(t) = \frac{1}{t}$, $0 < t \leq 1$ ([Fig.1.9 top](#)),
- 2) Condition 2: $x(t) = \sin\left(\frac{2\pi}{t}\right)$, $0 < t \leq 1$ ([Fig.1.9 middle](#)),
- 3) Condition 3: The signal composed of an infinite number of sections each of which is half the height and half the width of the previous section ([Fig.1.9 bottom](#)).

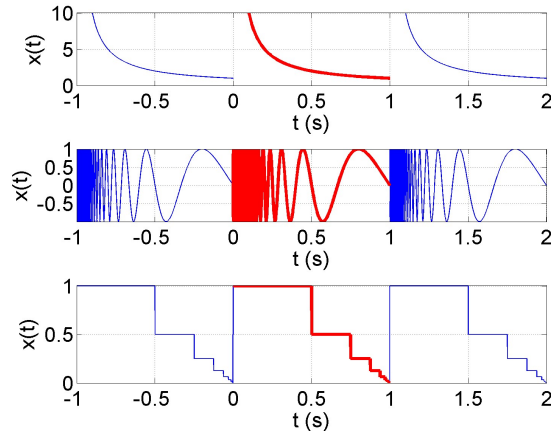


Fig. 1.9 Periodic signals that violate Dirichlet conditions.

The convergence of the Fourier representation of a square wave for the finite number of the Fourier series coefficients ([1.50](#)) is depicted in [Fig. 1.10](#). The maximum overshoot in the points of discontinuity is 9% of the height of the discontinuity no matter how large N becomes. This behavior is known as the *Gibbs phenomenon*.

[Fig.1.11](#) depicts the energy E_N in the approximation error over one period ([1.52](#)) for symmetric square wave in dependence of the finite number of the Fourier series coefficients N ([1.49](#)).

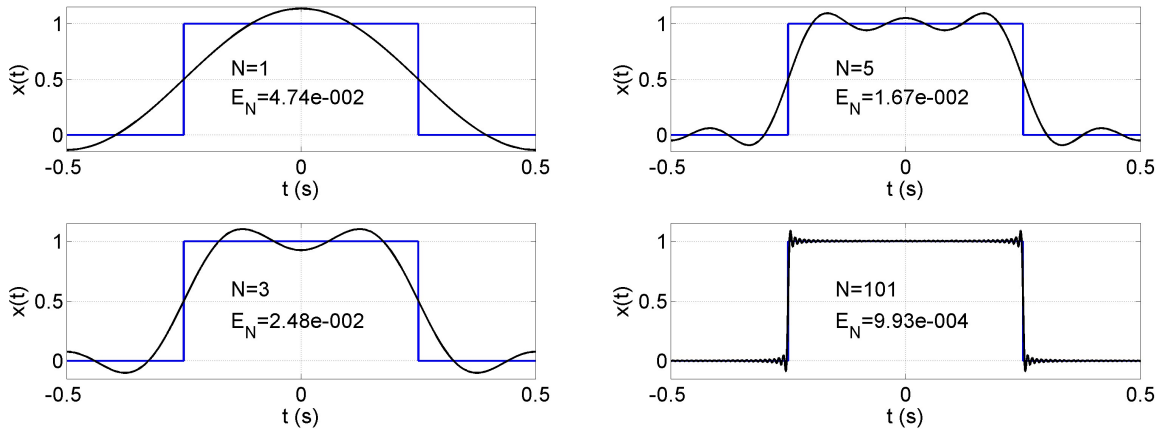


Fig. 1.10 Convergence of the Fourier representation of a square wave for the finite number of the Fourier series coefficients $a_{-N} \dots a_N$ (1.50)
 E_N is the energy in the approximation error over one period (1.52).

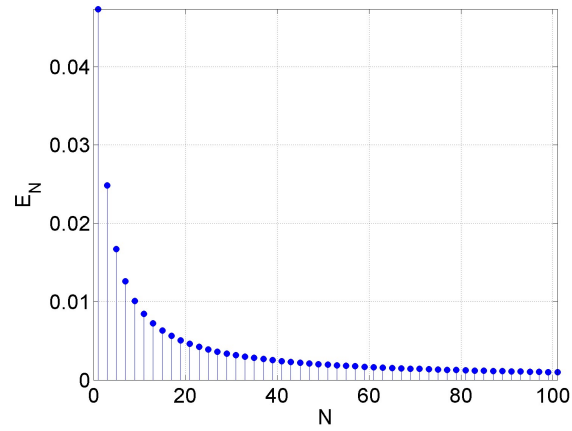


Fig. 1.11 The energy E_N in the approximation error over one period (1.52) for symmetric square wave in dependence of the finite number of the Fourier series coefficients $a_{-N} \dots a_N$ (1.50).

1.3.2 The Fourier Integral

An *aperiodic* signal can be thought of as the limit of a periodic signal as the period becomes arbitrary large.

As an example consider periodic square wave (1.45) for which the Fourier series coefficients are (1.46), (1.47)

$$a_k = \frac{2 \sin(k\Omega_0 T_1)}{k\Omega_0 T_0}. \quad (1.55)$$

Let us rewrite (1.55)

$$T_0 a_k = \frac{2 \sin(k\Omega_0 T_1)}{k\Omega_0} = \frac{2 \sin(\Omega T_1)}{\Omega} \Big|_{\Omega=k\Omega_0}. \quad (1.56)$$

Thus, with Ω thought of as a continuous variable, the function $\frac{2 \sin(\Omega T_1)}{\Omega}$ represents the envelope of $T_0 a_k$ and these coefficients are simply equally spaced samples of this envelope. Fig. 1.12 depicts the Fourier series coefficients $T_0 a_k$ and their envelope for the periodic square wave for fixed value of T_1 and several increasing values of T_0 . The set of Fourier series coefficients approaches the envelope function as $T_0 \rightarrow \infty$.

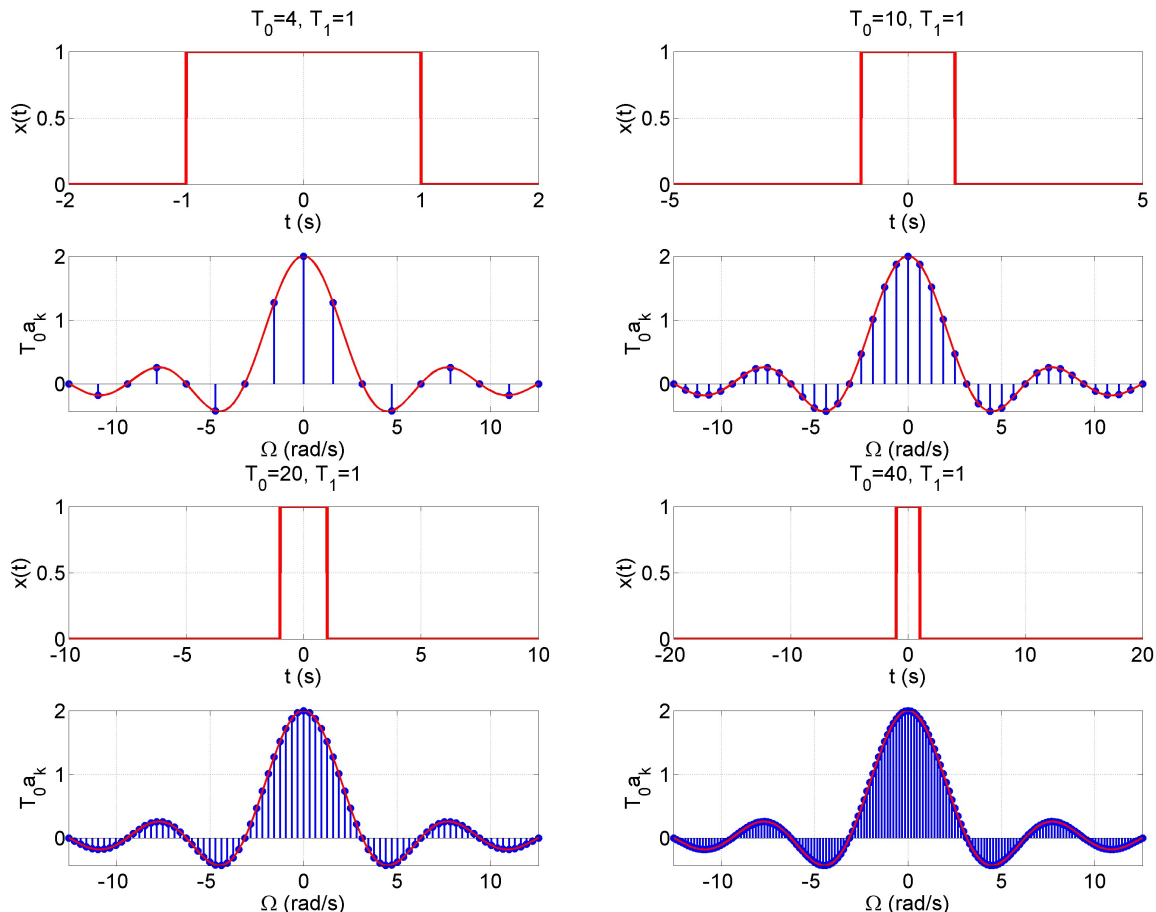


Fig. 1.12 Periodic square wave and its Fourier coefficients $T_0 a_k$ and their envelope (1.56).

Consider a general aperiodic signal $x(t)$ that is of finite duration. That is for some value T_1 , $x(t)=0$ if $|t|>T_1$. From this aperiodic signal we can construct periodic signal $\tilde{x}(t)$ for which $x(t)$ is one period. As we chose the period T_0 to be larger, $\tilde{x}(t)$ is identical to $x(t)$ over longer interval, and as $T_0\rightarrow\infty$, $\tilde{x}(t)$ is equal to $x(t)$ for any finite value of t .

The Fourier series representation (1.42) of $\tilde{x}(t)$ is

$$\begin{aligned}\tilde{x}(t) &= \sum_{k=-\infty}^{+\infty} a_k e^{jk\Omega_0 t} \\ a_k &= \frac{1}{T_0} \int_{-T_0/2}^{T_0/2} \tilde{x}(t) e^{-jk\Omega_0 t} dt\end{aligned}\quad (1.57)$$

Since $\tilde{x}(t)=x(t)$ for $|t|<T_0/2$ and since $x(t)=0$ outside this interval, (1.57) can be rewritten as

$$a_k = \frac{1}{T_0} \int_{-T_0/2}^{T_0/2} x(t) e^{-jk\Omega_0 t} dt = \frac{1}{T_0} \int_{-\infty}^{+\infty} x(t) e^{-jk\Omega_0 t} dt \quad (1.58)$$

By defining the envelope $X(\Omega)$ of $T_0 a_k$ as

$$X(\Omega) = \int_{-\infty}^{+\infty} x(t) e^{-j\Omega t} dt \quad (1.59)$$

the coefficients a_k can be expressed as

$$a_k = \frac{1}{T_0} X(k\Omega_0). \quad (1.60)$$

Combining (1.57) and (1.60) $\tilde{x}(t)$ can be expressed in terms of $X(\Omega)$ as

$$\tilde{x}(t) = \sum_{k=-\infty}^{+\infty} \frac{1}{T_0} X(k\Omega_0) e^{jk\Omega_0 t}, \quad (1.61)$$

or equivalently, since $2\pi/T_0=\Omega_0$

$$\tilde{x}(t) = \frac{1}{2\pi} \sum_{k=-\infty}^{+\infty} X(k\Omega_0) e^{jk\Omega_0 t} \Omega_0 \quad (1.62)$$

As $T_0\rightarrow\infty$ $\tilde{x}(t)$ approaches $x(t)$, and consequently (1.62) becomes representation of $x(t)$. Furthermore, $\Omega_0\rightarrow 0$ as $T_0\rightarrow\infty$, and the right side of (1.62) passes to an integral (for fixed t each term of the summation in (1.62) is the area of a rectangle of height $X(k\Omega_0) e^{jk\Omega_0 t}$ and width Ω_0 ; as $\Omega_0\rightarrow 0$, this by definition converges to the integral of $X(\Omega) e^{j\Omega t}$). Therefore, using the fact that $\tilde{x}(t)\rightarrow x(t)$ as $T_0\rightarrow\infty$ equations (1.62) and (1.59) become

$$\begin{aligned}x(t) &= \frac{1}{2\pi} \int_{-\infty}^{+\infty} X(\Omega) e^{j\Omega t} d\Omega \\ X(\Omega) &= \int_{-\infty}^{+\infty} x(t) e^{-j\Omega t} dt\end{aligned}$$

(1.63)

Equations (1.63) are referred to as the *Fourier transform pair* with the function $X(\Omega)$ referred to as the *Fourier transform* or the *Fourier integral* of $x(t)$ and the upper equation (1.63) as the *inverse Fourier Transform*.

Absolutely integrable signals that are continuous or have several discontinuities have Fourier Transforms.

Inverse Fourier transform is *equal* to $x(t)$ except at isolated values of t for which $x(t)$ is discontinuous (at these values of t it is equal to the average value of the discontinuity) if $x(t)$ satisfies the Dirichlet conditions.

Example 1.3

The spectrum of the delta function $\delta(t)$ is

$$X(\Omega) = \int_{-\infty}^{+\infty} \delta(t) e^{-j\Omega t} dt = 1 \quad (1.64)$$

That is, the unit impulse has a Fourier transform representation consisting of equal contributions of sinusoidal signals with all frequencies.

Example 1.4

Rectangular pulse signal

$$x(t) = \begin{cases} 1, & |t| < T_1 \\ 0, & |t| > T_1 \end{cases} \quad (1.65)$$

has a Fourier transform

$$X(\Omega) = \int_{-T_1}^{T_1} e^{-j\Omega t} dt = 2 \frac{\sin(\Omega T_1)}{\Omega}, \quad \Omega \neq 0, \quad (1.66)$$

and for $\Omega=0$ we have $X(0) = \int_{-T_1}^{T_1} dt = 2T_1$.

Example 1.5

Consider a signal $x(t)$ with the Fourier transform $X(\Omega)$ which is a single impulse of area 2π at $\Omega=\Omega_0$

$$X(\Omega) = 2\pi\delta(\Omega - \Omega_0). \quad (1.67)$$

From the inverse Fourier transform (1.63) it goes that $x(t)$ is a complex exponential signal

$$x(t) = \frac{1}{2\pi} \int_{-\infty}^{+\infty} 2\pi\delta(\Omega - \Omega_0) e^{j\Omega t} d\Omega = e^{j\Omega_0 t}. \quad (1.68)$$

The signal $x(t)$ with the Fourier transform $X(\Omega)=2\pi\delta(\Omega)$ is the constant signal $x(t)=1$.

The signal $x(t)$ with the Fourier transform

$$X(\Omega) = \pi\delta(\Omega - \Omega_0) + \pi\delta(\Omega + \Omega_0). \quad (1.69)$$

is cosine signal

$$x(t) = \frac{1}{2} e^{j\Omega_0 t} + \frac{1}{2} e^{-j\Omega_0 t} = \cos(\Omega_0 t). \quad (1.70)$$

Example 1.6

Consider exponential signal (1.3) that is non zero for $t > 0$

$$x(t) = \begin{cases} e^{-at}, & t > 0 \\ 0, & t < 0 \end{cases}. \quad (1.71)$$

For $a > 0$ from (1.63) we get

$$\begin{aligned} X(\Omega) &= \int_0^{+\infty} e^{-at} e^{-j\Omega t} dt = \int_0^{+\infty} e^{-(a+j\Omega)t} dt = \frac{1}{-(a+j\Omega)} e^{-(a+j\Omega)t} \Big|_0^{+\infty} = \\ &= \frac{1}{a+j\Omega}, \quad a > 0 \end{aligned} \quad (1.72)$$

This particular Fourier transform has both real and imaginary parts, to plot it as a function of Ω , $X(\Omega)$ is expressed in terms of its magnitude and phase, see Fig. 1.13

$$|X(\Omega)| = \frac{1}{\sqrt{a^2 + \Omega^2}}, \quad \angle X(\Omega) = -\tan^{-1}\left(\frac{\Omega}{a}\right) \quad (1.73)$$

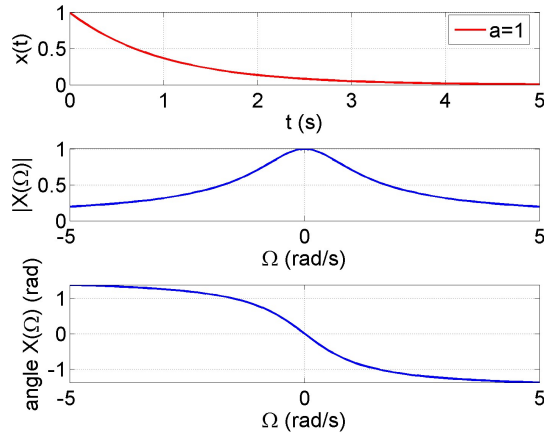


Fig. 1.13 Exponential signal (1.71) and its Fourier transform (1.72): magnitude response and phase response.

Table1.1 Some Properties of the Fourier Transform

Property	Aperiodic signal $x(t), y(t)$	Fourier transform $X(\Omega), Y(\Omega)$
<i>Linearity</i>	$ax(t)+by(t)$	$aX(\Omega)+bY(\Omega)$ (1.74)
<i>Duality (Fig. 1.14)</i>	If $f(u) = \int_{-\infty}^{+\infty} g(v)e^{-juv} dv$ then $g(t) \xrightarrow{FT} f(\Omega)$ and $f(t) \xrightarrow{FT} 2\pi g(-\Omega)$	
<i>The convolution property</i>	$x(t)*y(t)$	$X(\Omega)Y(\Omega)$ (1.75)
<i>The modulation property</i>	$x(t)y(t)$	$\frac{1}{2\pi} X(\Omega) * Y(\Omega)$ (1.76)
<i>Time shifting</i>	$x(t-t_0)$	$e^{-j\Omega t_0} X(\Omega)$ (1.77)
<i>Frequency shifting</i>	$e^{j\Omega_0 t} x(t)$	$X(\Omega - \Omega_0)$ (1.78)
<i>Time and frequency scaling</i>	$x(at)$	$\frac{1}{ a } X\left(\frac{\Omega}{a}\right)$ (1.79)
<i>Differentiation and Integration</i>	$\frac{d}{dt} x(t)$	$j\Omega X(\Omega)$ (1.80)
	$\int_{-\infty}^{\tau} x(t) dt$	$\frac{1}{j\Omega} X(\Omega) + \pi X(0)\delta(\Omega)$ (1.81)
	$tx(t)$	$j \frac{d}{d\Omega} X(\Omega)$ (1.82)
<i>Perseval's relation for aperiodic signals</i>		$\int_{-\infty}^{\infty} x(t) ^2 dt = \frac{1}{2\pi} \int_{-\infty}^{\infty} X(\Omega) ^2 d\Omega$ (1.83)

Duality

Fourier transform pair equations (1.63) $x(t) = \frac{1}{2\pi} \int_{-\infty}^{+\infty} X(\Omega) e^{j\Omega t} d\Omega$, $X(\Omega) = \int_{-\infty}^{+\infty} x(t) e^{-j\Omega t} dt$ are quite similar.

Compare rectangular pulse (1.65) and the Fourier transform of this signal (1.66)

$$x_1(t) = \begin{cases} 1, & |t| < T_1 \\ 0, & |t| > T_1 \end{cases} \xleftrightarrow{FT} X_1(\Omega) = 2 \frac{\sin(\Omega T_1)}{\Omega} \quad (1.84)$$

with the time signal $x(t)$ that has rectangular pulse Fourier transform

$$x_2(t) = \frac{\sin(Wt)}{\pi t} \xleftrightarrow{FT} X_2(\Omega) = \begin{cases} 1, & |\Omega| < W \\ 0, & |\Omega| > W \end{cases}. \quad (1.85)$$

Both signals and their Fourier transforms (1.84) and (1.85) are depicted in Fig. 1.14a.

Compare the delta function and its spectrum (1.64)

$$x_1(t) = \delta(t) \xleftrightarrow{FT} X_1(\Omega) = 1 \quad (1.86)$$

with the constant signal and its spectrum

$$x_2(t) = 1 \xleftrightarrow{FT} X_2(\Omega) = 2\pi\delta(\Omega). \quad (1.87)$$

Both signals and their Fourier transforms (1.86) and (1.87) are depicted in Fig. 1.14b.

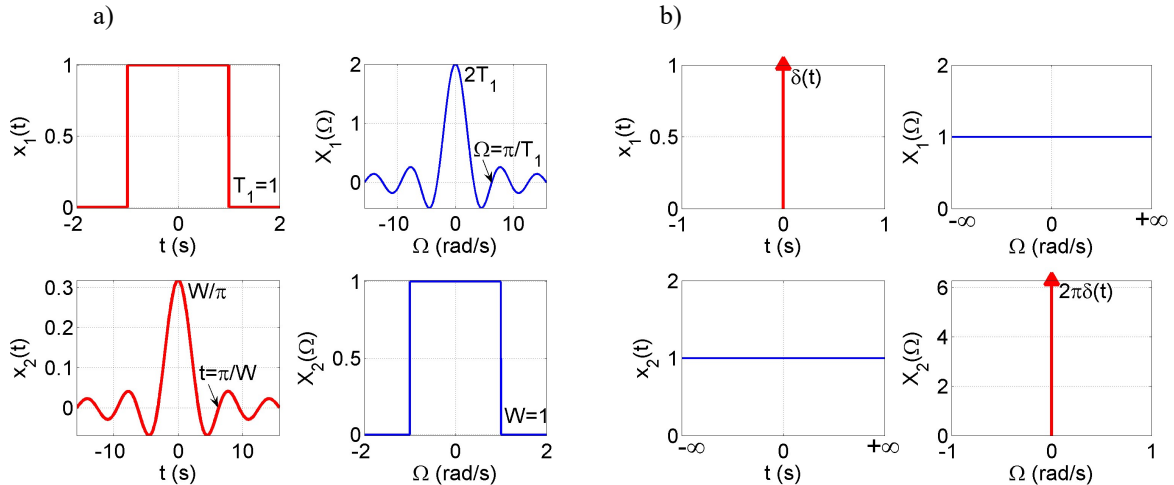


Fig. 1.14 Illustration of the Fourier transform duality property.

- a) Comparison of (1.84) and (1.85),
- b) Comparison of (1.86) and (1.87).

The convolution property

Let us compute the Fourier transform of the signal $y(t)$ which is the result of convolution integral

$$y(t) = x(t) * h(t) = \int_{-\infty}^{\infty} x(\tau)h(t-\tau)d\tau. \quad (1.88)$$

From the definition (1.63) we get

$$Y(\Omega) = \int_{-\infty}^{+\infty} \int_{-\infty}^{\infty} x(\tau)h(t-\tau)d\tau e^{-j\Omega t} dt. \quad (1.89)$$

Interchanging the order of integration and noting that $x(\tau)$ does not depend on t we have

$$Y(\Omega) = \int_{-\infty}^{+\infty} x(\tau) \left(\int_{-\infty}^{\infty} h(t-\tau) e^{-j\Omega t} dt \right) d\tau. \quad (1.90)$$

By the shifting property (1.77) the bracketed term is $e^{-j\Omega\tau} H(\Omega)$, and (1.90) becomes

$$Y(\Omega) = \int_{-\infty}^{+\infty} x(\tau) e^{-j\Omega\tau} H(\Omega) d\tau = H(\Omega) \int_{-\infty}^{+\infty} x(\tau) e^{-j\Omega\tau} d\tau = H(\Omega) X(\Omega). \quad (1.91)$$

[Oppen83, p.225]

TABLE 4.3 BASIC FOURIER TRANSFORM PAIRS

Signal	Fourier transform	Fourier series coefficients (if periodic)
$\sum_{k=-\infty}^{+\infty} a_k e^{jk\omega_0 t}$	$2\pi \sum_{k=-\infty}^{+\infty} a_k \delta(\omega - k\omega_0)$	a_k
$e^{j\omega_0 t}$	$2\pi \delta(\omega - \omega_0)$	$a_1 = 1$ $a_k = 0, \text{ otherwise}$
$\cos \omega_0 t$	$\pi[\delta(\omega - \omega_0) + \delta(\omega + \omega_0)]$	$a_1 = a_{-1} = \frac{1}{2}$ $a_k = 0, \text{ otherwise}$
$\sin \omega_0 t$	$\frac{\pi}{j} [\delta(\omega - \omega_0) - \delta(\omega + \omega_0)]$	$a_1 = -a_{-1} = \frac{1}{2j}$ $a_k = 0, \text{ otherwise}$
$x(t) = 1$	$2\pi \delta(\omega)$	$a_0 = 1, \quad a_k = 0, k \neq 0$ (has this Fourier series representation for any choice of $T_0 > 0$)
Periodic square wave $x(t) = \begin{cases} 1, & t < T_1 \\ 0, & T_1 < t \leq \frac{T_0}{2} \end{cases}$ and $x(t + T_0) = x(t)$	$\sum_{k=-\infty}^{+\infty} \frac{2 \sin k\omega_0 T_1}{k} \delta(\omega - k\omega_0)$	$\frac{\omega_0 T_1}{\pi} \operatorname{sinc}\left(\frac{k\omega_0 T_1}{\pi}\right) = \frac{\sin k\omega_0 T_1}{k\pi}$
$\sum_{n=-\infty}^{+\infty} \delta(t - nT)$	$\frac{2\pi}{T} \sum_{k=-\infty}^{+\infty} \delta\left(\omega - \frac{2\pi k}{T}\right)$	$a_k = \frac{1}{T} \text{ for all } k$
$x(t) = \begin{cases} 1, & t < T_1 \\ 0, & t > T_1 \end{cases}$	$2T_1 \operatorname{sinc}\left(\frac{\omega T_1}{\pi}\right) = \frac{2 \sin \omega T_1}{\omega}$	—
$\frac{W}{\pi} \operatorname{sinc}\left(\frac{Wt}{\pi}\right) = \frac{\sin Wt}{\pi t}$	$X(\omega) = \begin{cases} 1, & \omega < W \\ 0, & \omega > W \end{cases}$	—
$\delta(t)$	1	—
$u(t)$	$\frac{1}{j\omega} + \pi\delta(\omega)$	—
$\delta(t - t_0)$	$e^{-j\omega t_0}$	—
$e^{-at} u(t), \Re[e[a] > 0]$	$\frac{1}{a + j\omega}$	—
$t e^{-at} u(t), \Re[e[a] > 0]$	$\frac{1}{(a + j\omega)^2}$	—
$\frac{t^{n-1}}{(n-1)!} e^{-at} u(t), \Re[e[a] > 0]$	$\frac{1}{(a + j\omega)^n}$	—

Digression fractional splines

Polynomial (convolution) splines of order P are defined as

$$\beta(t)^P = \underbrace{\beta(t)^0 * \beta(t)^0 * \dots * \beta(t)^0}_{(P+1) \text{ times}}, \quad \beta^0(t) = \begin{cases} 1, & |t| < 1 \\ 0, & |t| > 1 \end{cases}. \quad (1.92)$$

Definition (1.92) may also be expressed as the inverse Fourier transform of the spectrum of $\beta^0(t)$ that equals $B^0(\Omega) = \frac{2\sin(\Omega)}{\Omega}$ raised to the power P

$$\beta(t)^P = \text{IFT}\{\text{FT}\{\beta^0(t)\}^{P+1}\} = \text{IFT}\left\{\left(\frac{2\sin(\Omega)}{\Omega}\right)^{P+1}\right\}. \quad (1.93)$$

Comparing definitions (1.92) and (1.93) it is seen that in the latter case fractional values of P are possible. For fractional P fractional splines are obtained.

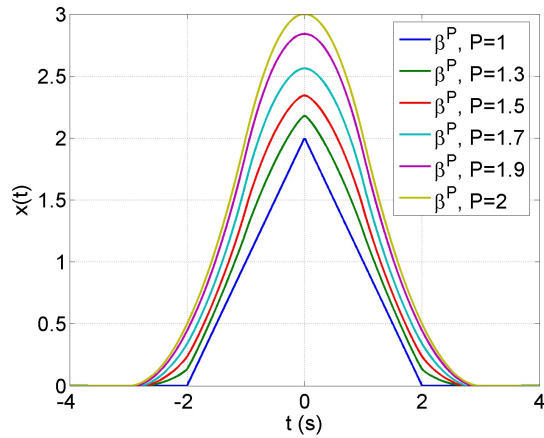


Fig. 1.15 Polynomial (convolution) splines for fractional values of P computed from (1.93) by the inverse Fourier transform (1.63).

1.4 Continuous-time filters

1.4.1 The Laplace transform

The unilateral Laplace transform $X(s)$ of a signal $x(t)$, $t > 0$ is defined as

$$X(s) = \int_0^\infty x(t)e^{-st} dt, \quad s = \sigma + j\Omega, \quad (1.94)$$

where σ and Ω are real. By substitution

$$s = j\Omega \quad (1.95)$$

into the Laplace transform definition (1.94) we obtain the Fourier transform definition (1.63) $X(\Omega) = \int_{-\infty}^{+\infty} x(t)e^{-j\Omega t} dt$, i.e. the Laplace transform computed on the *imaginary axis* is the Fourier transform.

Let us consider continuous-time LTI system described by linear constant coefficient differential equation (1.32). As an example, but without the lost of generality, let it be the 2nd order equation

$$a_2 \frac{d^2 y(t)}{dt^2} + a_1 \frac{dy(t)}{dt} + a_0 y(t) = b_1 \frac{dx(t)}{dt} + b_0 x(t). \quad (1.96)$$

By simplifying notation we have

$$a_2 y''(t) + a_1 y'(t) + a_0 y(t) = b_1 x'(t) + b_0 x(t). \quad (1.97)$$

Computing Laplace transform (1.94) of both sides of (1.97) we get

$$\int_0^\infty [a_2 y''(t) + a_1 y'(t) + a_0 y(t)] e^{-st} dt = \int_0^\infty [b_1 x'(t) + b_0 x(t)] e^{-st} dt, \quad (1.98)$$

By using linearity property and differentiation property

$$\int_0^\infty f'(t) e^{-st} dt = s \int_0^\infty f(t) e^{-st} dt - f(0+) = sF(s) - f(0+), \quad (1.99)$$

we get the following algebraic equation

$$a_2 s^2 Y(s) + a_1 s Y(s) + a_0 Y(s) = b_1 s X(s) + b_0 X(s). \quad (1.100)$$

Rearranging (1.100) we get the Laplace transmittance $H(s)$ of continuous-time LTI system described by linear constant coefficient differential equation (1.96):

$$H(s) = \frac{Y(s)}{X(s)} = \frac{b_1 s + b_0}{a_2 s^2 + a_1 s + a_0} = k \frac{s - z}{(s - p_1)(s - p_2)}. \quad (1.101)$$

The transmittance $H(s)$ is expressed as a ratio of two polynomials $Y(s)$ and $X(s)$. Zeros of $Y(s)$ are *zeros of transmittance $H(s)$* and zeros of $X(s)$ are *poles of transmittance $H(s)$* . If the polynomials coefficients b_n and a_n in (1.101) are required to be real, then zeros z and poles p , if complex must occur in complex conjugate pairs.

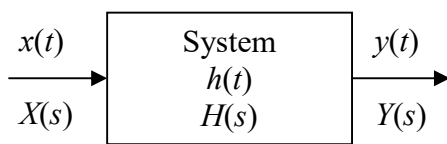


Fig. 1.16 Continuous-time LTI system.

Example 1.7

Consider following transmittance $H(s)$

$$H(s) = \frac{Y(s)}{X(s)} = \frac{s-1}{s^2 + 2s + 2} = \frac{s-1}{(s+1-j)(s+1+j)}. \quad (1.102)$$

Transmittance (1.102) has a single zero $z_1=1$, and one complex conjugate pole $p_{1,2}=-1\pm j$ depicted in Fig. 1.17a.

Frequency response is computed by substitution $s=j\Omega$. Magnitude characteristic is

$$|H(s = j\Omega)| = \frac{|j\Omega - 1|}{|(j\Omega)^2 + j2\Omega + 2|} = \frac{|j\Omega - 1|}{|j\Omega + 1 - j||j\Omega + 1 + j|} \quad (1.103)$$

From (1.103) amplitude gain for every frequency Ω may be computed. For example, the gain of constant component (*dc gain*) is

$$|H(\Omega = 0)| = \frac{|j0 - 1|}{|-0^2 + j2 \cdot 0 + 2|} = \frac{1}{2}. \quad (1.104)$$

Amplitude characteristic in the range from $\Omega=-5$ (rad/s) to $\Omega=5$ (rad/s) is depicted in Fig. 1.17. In general the range of frequencies is $-\infty < \Omega < +\infty$.

Imaginary axis is the frequency axis in the complex s -plane.

Zeros of transmittance $H(s)$ cause local minima in the magnitude response (i.e. attenuation of signals with those frequencies).

Poles of transmittance $H(s)$ cause local maxima in the magnitude response (i.e. amplification of signal with those frequencies).

The influence of zeros and poles on frequency response depends on their distance from imaginary axis, and increases as they get closer to the imaginary axis.

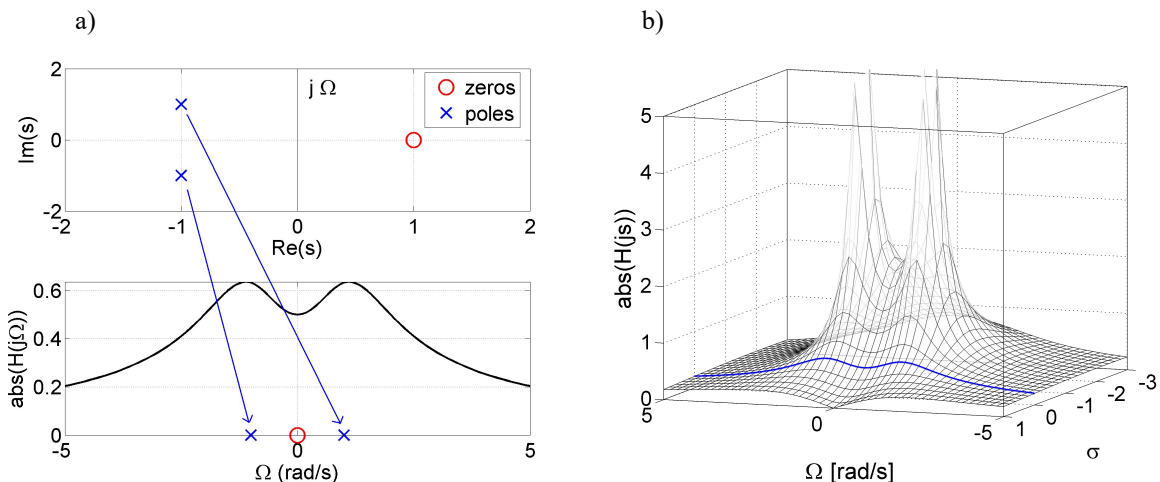


Fig.1.17 a) Zeros and poles of $H(s)$ (1.102) in the complex s -plain, and magnitude characteristic of $H(s)$.
b) magnitude characteristic of $H(s)$ (1.102) for some range of σ (1.94).

Example 1.8

Consider the following transmittance $H(s)$

$$H(s) = \frac{(s + a + jb)(s + a - jb)}{(s + c + jb)(s + c - jb)}, \quad (1.105)$$

where a , b , and c are real parameters. For stable filter $c > 0$. The filter with transmittance (1.105) has strong attenuation in narrow frequency band. It is called *notch filter*. Fig. 1.18 shows exemplary zero-pole plot, magnitude response, and impulse response of transmittance (1.105). Maximum attenuation is in frequency $\Omega = b$ rad/s.

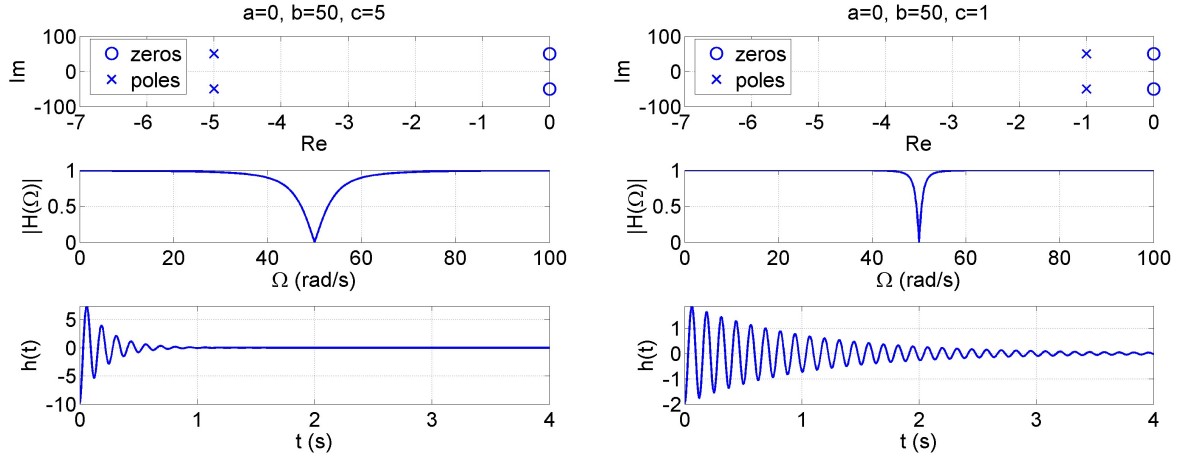


Fig. 1.18 Zero-pole plot, magnitude response and impulse response of exemplary notch filter with the transmittance $H(s)$ (1.105).

The localization of poles of transmittance $H(s)$ determines the stability of the system. Continuous-time system is stable if all poles of its transmittance $H(s)$ are placed in the left half plane of the complex s -plane, i.e. all poles have negative real part. Only then the impulse response of the system vanishes to zero.

If the poles are placed on the complex axis, then the impulse response oscillates infinitely.

If the poles are placed in the right half of the complex s -plane, i.e. the real part is positive then the impulse response grows infinitely.

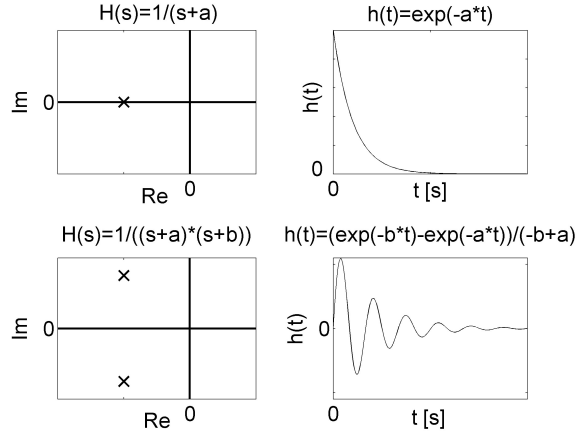


Fig.1.19 The placement of $H(s)$ transmittance poles of **stable** systems and their impulse responses.

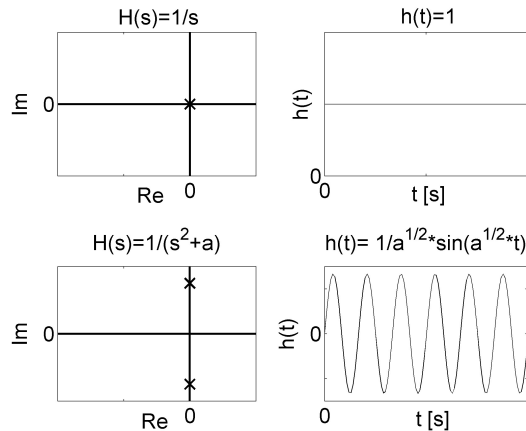


Fig.1.20 The placement of $H(s)$ transmittance poles of **conditionally stable** systems and their impulse responses.

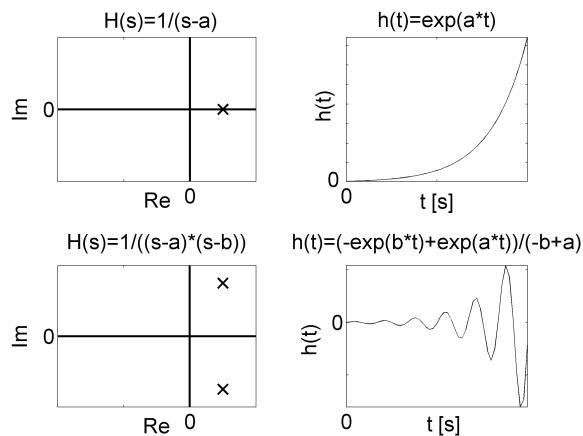


Fig.1.21 The placement of $H(s)$ transmittance poles of **unstable** systems and their impulse responses.

Matlab

```
[b,a] = zp2tf(z,p,k) Convert zero-pole-gain filter parameters to transfer function form
[z,p,k] = tf2zp(b,a) Convert transfer function filter parameters to zero-pole-gain form
[h,w] = freqs(b,a,f) Frequency response of analog filters
impulse(sys) Impulse response of LTI models
printsys(NUM,DEN,'s') Print system in pretty format
laplace Laplace transform (Symbolic Math Toolbox)
ilaplace Inverse Laplace transform (Symbolic Math Toolbox)
```

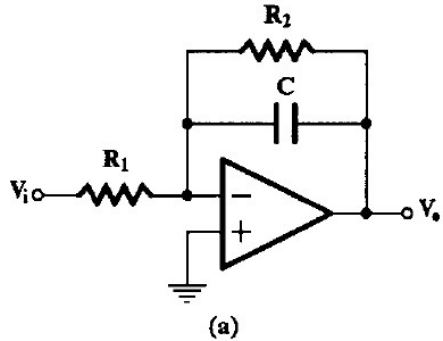
[Oppen83, p.604]

TABLE 9.2 LAPLACE TRANSFORMS OF ELEMENTARY FUNCTIONS

Transform pair	Signal	Transform	ROC
1	$\delta(t)$	1	All s
2	$u(t)$	$\frac{1}{s}$	$\Re\{s\} > 0$
3	$-u(-t)$	$\frac{1}{s}$	$\Re\{s\} < 0$
4	$\frac{t^{n-1}}{(n-1)!} u(t)$	$\frac{1}{s^n}$	$\Re\{s\} > 0$
5	$-\frac{t^{n-1}}{(n-1)!} u(-t)$	$\frac{1}{s^n}$	$\Re\{s\} < 0$
6	$e^{-\alpha t} u(t)$	$\frac{1}{s + \alpha}$	$\Re\{s\} > -\alpha$
7	$-e^{-\alpha t} u(-t)$	$\frac{1}{s + \alpha}$	$\Re\{s\} < -\alpha$
8	$\frac{t^{n-1}}{(n-1)!} e^{-\alpha t} u(t)$	$\frac{1}{(s + \alpha)^n}$	$\Re\{s\} > -\alpha$
9	$-\frac{t^{n-1}}{(n-1)!} e^{-\alpha t} u(-t)$	$\frac{1}{(s + \alpha)^n}$	$\Re\{s\} < -\alpha$
10	$\delta(t - T)$	e^{-sT}	All s
11	$[\cos \omega_0 t] u(t)$	$\frac{s}{s^2 + \omega_0^2}$	$\Re\{s\} > 0$
12	$[\sin \omega_0 t] u(t)$	$\frac{\omega_0}{s^2 + \omega_0^2}$	$\Re\{s\} > 0$
13	$[e^{-\alpha t} \cos \omega_0 t] u(t)$	$\frac{s + \alpha}{(s + \alpha)^2 + \omega_0^2}$	$\Re\{s\} > -\alpha$
14	$[e^{-\alpha t} \sin \omega_0 t] u(t)$	$\frac{\omega_0}{(s + \alpha)^2 + \omega_0^2}$	$\Re\{s\} > -\alpha$

[Deli99]

$$H(s) \equiv \frac{V_o}{V_i} = -\frac{1/CR_1}{s + 1/CR_2}$$



$$H(s) \equiv \frac{V_o}{V_i} = \frac{K/CR}{s + 1/CR} \quad K = 1 + \frac{R_2}{R_1}$$

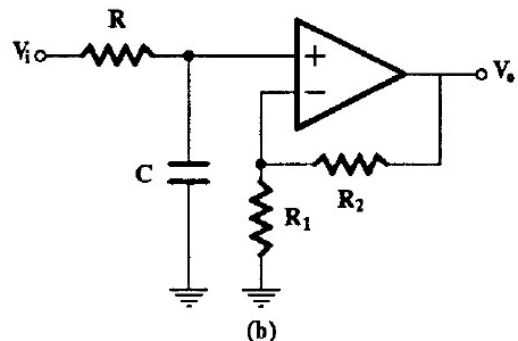


FIGURE 4.1

(a) A first-order lowpass circuit and (b) an alternative circuit.

$$H(s) = \frac{V_o}{V_i} = \frac{G/(C_1 C_2 R_1 R_2)}{s^2 + \left(\frac{1}{R_1 C_1} + \frac{1}{R_2 C_1} + \frac{1-G}{R_2 C_2} \right)s + \frac{1}{R_1 R_2 C_1 C_2}}$$

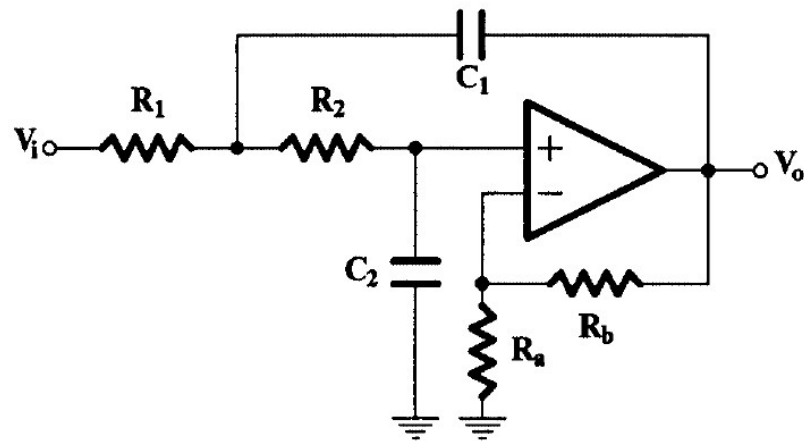


FIGURE 4.8

The Sallen-Key second-order lowpass circuit.

7.7 Classical Filter Design

Classical filter design means analog filter design. Why are we devoting a section in a book on DSP to analog filter design? There are two reasons. First, filtering is one of the few select subjects in analog signal processing about which every DSP expert should know something. Not only are there always analog antialiasing filters and reconstruction filters, but it is often worthwhile to perform other filtering in the analog domain. Good digital filters are notoriously computationally intensive, and in high-bandwidth systems there may be no alternative to performing at least some of the filtering using analog components. Second, the discipline of analog filter design was already well-developed when the more complex field of digital filter design was first developing. It strongly influenced much of the terminology and algorithms, although its stranglehold was eventually broken.

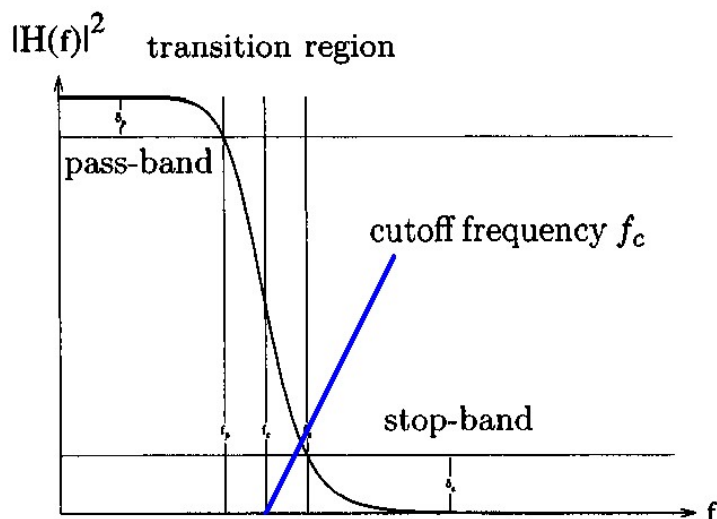


Figure 7.11: Desired frequency response of the analog low-pass filter to be designed. The pass-band is from $f = 0$ to the pass-band edge f_p , the transition region from f_p to f_s , and the stop-band from the top-band edge f_s to infinity. The frequency response is halfway between that of the pass-band and that of the stop-band at the cutoff frequency f_c . The maximal ripple in the pass-band is δ_p , and in the stop-band δ_s .

We will first focus on the simplest case, that of an analog low-pass filter. Our ideal will be the ideal low-pass filter, but that being unobtainable we strive toward its best approximation. The most important specification is the cutoff frequency f_c , below which we wish the signal to be passed, above which we wish the signal to be blocked. The pass-band and stop-band are separated by a transition region where we do not place stringent requirements on the frequency response. The end of the pass-band is called f_p and the beginning

of the stop-band f_s . Other specifications for a practical implementation are the transition width $\Delta = f_s - f_p$, the maximal deviation from unity gain in the pass-band δ_p , and the maximal amplitude in the stop-band δ_s . In a typical analog filter design problem f_c (or f_p or f_s) and the maximal allowed values for Δ , δ_p , and δ_s are given. Figure 7.11 depicts the ideal and approximate analog low-pass filters with these parameters.

Designing an analog filter essentially amounts to specifying the function $H(f)$ whose square is depicted in the figure. From the figure and our previous analysis we see that

$$\begin{aligned} |H(0)|^2 &= 1 \\ |H(f)|^2 &\approx 1 \quad \text{for } f < f_c \\ |H(f)|^2 &\approx 0 \quad \text{for } f > f_c \\ |H(f)|^2 &\rightarrow 0 \quad \text{for } f \rightarrow \infty \end{aligned}$$

are the requirements for an analog low-pass filter. The first functional forms that come to mind are based on arctangents and hyperbolic tangents, but these are natural when the constraints are at plus and minus infinity, rather than zero and infinity. Classical filter design relies on the form

$$|H(f)|^2 = \frac{1}{1 + p(f)} \quad (7.28)$$

where $p(f)$ is a polynomial that must obey

$$\begin{aligned} p(0) &= 0 \\ p(f) &\xrightarrow{f \rightarrow \infty} \infty \end{aligned}$$

and be well behaved. The classical design problem is therefore reduced to the finding of this polynomial.

In Figure 7.11 the deviation of the amplitude response from the ideal response is due entirely to its smoothly decreasing from unity at $f = 0$ in order to approach zero at high frequencies. One polynomial that obeys the constraints and has no extraneous extrema is the simple quadratic

$$p(f) = \left(\frac{f}{f_c}\right)^2$$

which when substituted back into equation (7.28) gives the ‘slowest’ filter depicted in Figure 7.12. The other filters there are derived from

$$p(f) = \left(\frac{f}{f_c}\right)^{2N}$$

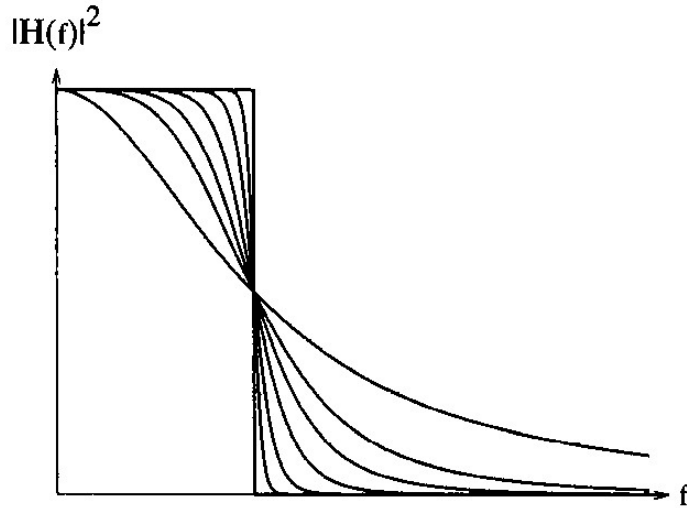


Figure 7.12: Frequency response of analog Butterworth low-pass filters. From bottom to top at low frequencies we have order $N = 1, 2, 3, 5, 10, 25, \infty$.

and are called the Butterworth low-pass filters of order n . It is obvious from the figure that the higher n is the narrower the transition.

Butterworth filters have advantages and disadvantages. The attenuation monotonically increases from DC to infinite frequency; in fact the first $2N - 1$ derivatives of $|H(f)|^2$ are identically zero at these two points, a property known as ‘maximal flatness’. An analog Butterworth filter has only poles and is straightforward to design. However, returning to the design specifications, for the transition region Δ to be small enough the order N usually has to be quite high; and there is no way of independently specifying the rest of the parameters.

In order to obtain faster rolloff in the filter skirt we have to give something up, and that something is the monotonicity of $|H(f)|^2$. A Butterworth filter ‘wastes’ a lot of effort in being maximally flat, effort that could be put to good use in reducing the size of the transition region. A filter that is allowed to oscillate up and down a little in either the pass-band, the stop-band or both can have appreciably smaller Δ . Of course we want the deviation from our specification to be minimal in some sense. We could require a minimal squared error between the specification and the implemented filter

$$\epsilon^2 = \int |H_{spec}(\omega) - H_{impl}(\omega)|^2 d\omega$$

but this would still allow large deviation from specification at some frequencies, at the expense of overexactness at others. It makes more sense to require *minimax error*, i.e., to require that the maximal deviation from specification

$$\max_{\omega} |H_{spec}(\omega) - H_{impl}(\omega)|$$

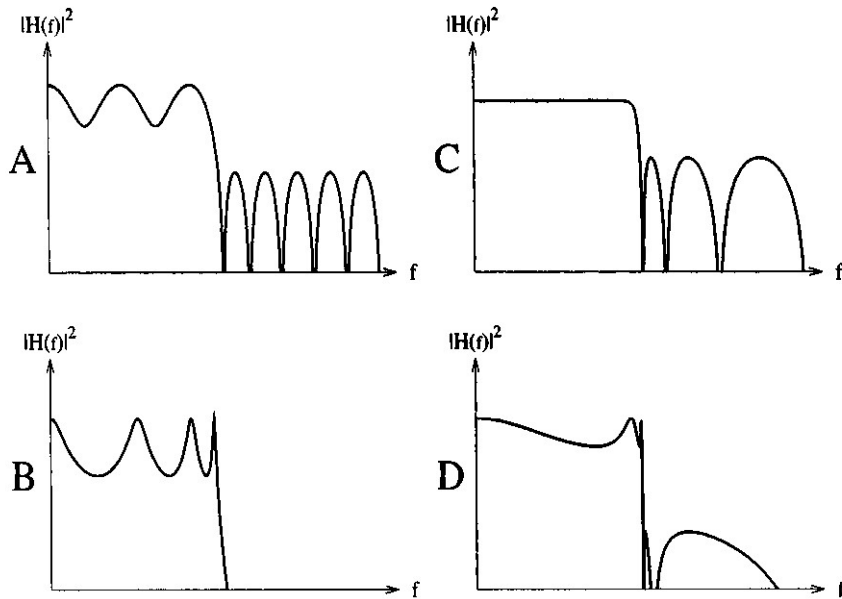


Figure 7.13: Frequency response of low-pass equiripple designs. In (A) we see an FIR filter designed using the Remez algorithm for comparison purposes. In (B) we see the IIR Chebyshev design, in (C) the inverse Chebyshev and in (D) the elliptical design.

be minimal. Achieving true minimax approximation is notoriously difficult in general, but approximation using Chebyshev polynomials (see Appendix A.10) is almost the same and straightforward to realize. This approximation naturally leads to equiripple behavior, where the error oscillates around the desired level with equal error amplitude, as shown in Figure 7.13.

The Chebyshev (also known as Chebyshev I) filter is equiripple in the pass-band, but maximally flat in the stop-band. It corresponds to choosing the polynomial

$$p(f) = \delta^2 T_N^2 \left(\frac{f}{f_p} \right)$$

and like the Butterworth approximation, the analog Chebyshev filter is all-pole. The inverse Chebyshev (or Chebyshev II) filter is equiripple in the stop-band but maximally flat in the pass-band. Its polynomial is

$$p(f) = \delta^2 \frac{T_N^2 \left(\frac{f_s}{f_p} \right)}{T_N^2 \left(\frac{f_s}{f} \right)}$$

The Chebyshev filter minimax approximates the desired response in the pass-band but not in the stop-band, while the inverse Chebyshev does just

the opposite. For both types of Chebyshev filters the parameter δ sets the ripple in the equiripple band. For the inverse Chebyshev, where the equiripple property holds in the stop-band, the attenuation is determined by the ripple; lower ripple means higher stop-band rejection.

Finally, the *elliptical* filter is equiripple in both pass-band and stop-band, and so approximates the desired response in the minimax sense for all frequencies. Its ‘polynomial’ is not a polynomial at all, but rather a rational function $U_N(\frac{f}{f_p})$. These functions are defined using the elliptical functions (see Appendices A.8 and A.10). Taking the idea from equation (A.59), we define the function

$$U_{r;k,q}(u) \equiv \operatorname{sn}_k(r \operatorname{sn}_q^{-1}(u)) \quad (7.29)$$

and when r and the complete elliptical integrals K_k and K_q obey certain relations that we will not go into here, this function becomes a rational function.

$$U_N(u) = a^2 \begin{cases} \frac{(u_1^2 - u^2)(u_3^2 - u^2) \cdots (u_{2N-1}^2 - u^2)}{(1 - u_1^2 u^2)(1 - u_3^2 u^2) \cdots (1 - u_{2N-1}^2 u^2)} & N \text{ even} \\ \frac{u(u_2^2 - u^2)(u_4^2 - u^2) \cdots (u_{2N}^2 - u^2)}{(1 - u_2^2 u^2)(1 - u_4^2 u^2) \cdots (1 - u_{2N}^2 u^2)} & N \text{ odd} \end{cases} \quad (7.30)$$

This rational function has several related interesting characteristics. For $u < 1$ the function lies between -1 and $+1$. Next,

$$U_N\left(\frac{1}{u}\right) = \frac{1}{U_N(u)}$$

and its zeros and poles are reciprocals of each other. Choosing all the N zeros in the range $0 < \zeta < 1$ forces all N poles to fall in the range $1 < \pi < \infty$. Although the zeros and poles are not equally spaced, the behavior of

$$|H(f)|^2 = \frac{1}{1 + U_N(\frac{f}{f_p})}$$

is equiripple in both the pass-band and the stop-band.

It is useful to compare the four types of analog filter—Butterworth, Chebyshev, inverse Chebyshev, and elliptical. A very strong statement can be made (but will not be proven here) regarding the elliptical filter; given any three of the four parameters of interest (pass-band ripple, stop-band ripple, transition width, and filter order) the elliptical filter minimizes the remaining parameter. In particular, for given order N and ripple tolerances the elliptical filter can provide the steepest pass-band to stop-band transition. The Butterworth filter is the weakest in this regard, and the two Chebyshev

types are intermediate. The Butterworth filter, however, is the best approximation to the Taylor expansion of the ideal response at both DC and infinite frequency. The Chebyshev design minimizes the maximum pass-band ripple, while the inverse Chebyshev maximizes the minimum stop-band rejection.

The design criteria as we stated them do not address the issue of phase response, and none of these filters is linear-phase. The elliptical has the worst phase response, oscillating wildly in the pass-band and transition region (phase response in the stop-band is usually unimportant). The Butterworth is the smoothest in this regard, followed by the Chebyshev and inverse Chebyshev.

Although this entire section focused on analog low-pass filter, the principles are more general. All analog filters with a single pass-band and/or stop-band can be derived from the low-pass designs discussed above. For example, we can convert analog low-pass filter designs into high-pass filters by the simple transformation $f \rightarrow \frac{1}{f}$. Digital filters are a somewhat more complex issue, to be discussed in the next section. For now it is sufficient to say that IIR filters are often derived from analog Butterworth, Chebyshev, inverse Chebyshev, or elliptical designs. The reasoning is not that such designs are optimal; rather that the theory of the present section predicated DSP and early practitioners preferred to exploit well-developed theory whenever possible.

EXERCISES

- 7.7.1 Show that a Butterworth filter of order N is maximally flat.
- 7.7.2 All Butterworth filters have their half gain (3 dB down) point at f_c . Higher order N makes the filter gain decrease faster, and the speed of decrease is called the ‘*rolloff*’. Show that for high frequencies the rolloff of the Butterworth filter is 6 dB per octave (i.e., the gain decreases 6 dB for every doubling in frequency) or 20 dB per decade. How should N be set to meet a specification involving a pass-band end frequency f_p , a stop-band start frequency f_s , and a maximum error tolerance δ ?
- 7.7.3 Show that the $2N$ poles of $|H(f)|^2$ for the analog Butterworth filter all lie on a circle of radius f_c in the s -plane, are equally spaced, and are symmetric with respect to the imaginary axis. Show that the poles of the Chebyshev I filter lie on an ellipse in the s -plane.
- 7.7.4 The HPNA 1.0 specification calls for a pulse consisting of 4 cycles of a 7.5 MHz square wave filtered by a five-pole Butterworth filter that extends from 5.5 MHz to 9.5 MHz. Plot this pulse in the time domain.

1.4.2 Butterworth filter

Notation $H(j\Omega)$

Magnitude characteristic of Butterworth filter is maximally flat in the passband. The magnitude-squared function of a continuous-time lowpass Butterworth filter is defined as

$$|H(j\Omega)|^2 = \frac{1}{1 + (j\Omega / j\Omega_c)^{2N}}, \quad (1.106)$$

where Ω is variable, and Ω_c is a constant value. By putting $s=j\Omega$ into (1.106) we get

$$|H(s)|^2 = H(s)H(-s) = \frac{1}{1 + (s / j\Omega_c)^{2N}}. \quad (1.107)$$

The poles s_k of transmittance (1.107) fulfill

$$1 + (s / j\Omega_c)^{2N} = 0. \quad (1.108)$$

From (1.108) the poles are

$$s_k = j^{2N}\sqrt{-1}\Omega_c = \Omega_c e^{j\frac{\pi(2k+N+1)}{2N}}, \quad k = 0, 1, \dots, 2N-1, \quad (1.109)$$

(the complex number $C = Me^{j\varphi} = Me^{j(\varphi+k2\pi)}$ has n different roots of degree n $\sqrt[n]{C} = \sqrt[n]{M} e^{j(\varphi+k2\pi)/n}$, $k = 0, 1, \dots, n-1$).

Equation (1.109) defines the poles of the product $H(s)H(-s)$. From those $2N$ poles we only select N poles of $H(s)$, that is the N poles from the left half complex s -plane, i.e. with the negative real part.

Fig. 1.22 shows magnitude characteristics of Butterworth filter for different orders N . For Ω_c the filter gain is

$$|H(j\Omega_c)| = \sqrt{\frac{1}{1 + (j\Omega_c / j\Omega_c)^{2N}}} = \frac{1}{\sqrt{2}}, \quad (1.110)$$

which in decibels equals $|H(j\Omega_c)| = 20\log_{10}(1/\sqrt{2}) = -3$ dB, thus Ω_c is called 3dB frequency. If the 3dB frequency is 1 rad/s then the filter is called analog lowpass filter prototype (in Matlab it can be designed by the function `buttap`).

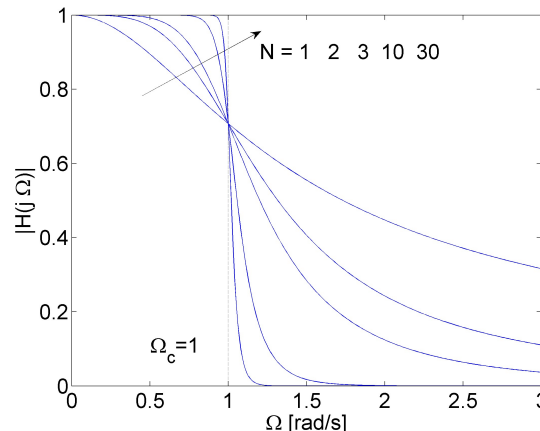


Fig. 1.22 Magnitude characteristics of Butterworth filter for different orders N .

[Fig.1.23](#) shows the poles of analog Butterworth filters for orders $N=2$, $N=3$, and $N=4$. In each case $2N$ poles are computed from (1.109) but only the poles with negative real part (distinguished in Fig. 1.23 in blue) are selected for the filter transmittance $H(s)$. The poles and transmittances depicted in Fig.1.23 are as follows

1. $s_{1,2} = -0.7071 \pm j0.7071$, $H(s) = \frac{1}{(s + 0.7071 + j0.7071)(s + 0.7071 - j0.7071)}$, $H(s) = \frac{1}{s^2 + 1.4142s + 1}$
2. $s_{1,3} = -0.5 \pm j0.866$, $s_2 = -1$, $H(s) = \frac{1}{s^3 + 2s^2 + 2s + 1}$
3. $s_{1,4} = -0.7654 \pm j1.8478$, $s_{2,3} = -1.8478 \pm j0.7654$, $w = \Omega_c^N = 2^4 = 16$
 $H(s) = \frac{16}{s^4 + 5.2263s^3 + 13.6569s^2 + 20.905s + 16}$

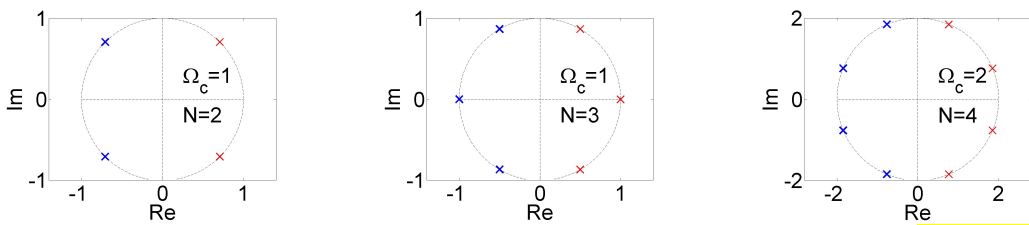


Fig.1.23 Poles of transmittance $H(s)$ of analog Butterworth filter of order 2, 3, and 4. **The cake.**

For the case when $\Omega_c \neq 1$ the transmittance $H(s)$ must be multiplied by the gain $w = \Omega_c^N$.

Example 1.8

Design analog lowpass Butterworth filter, i.e. specify the order N of the filter and 3 dB frequency Ω_c , and write the transmittance $H(s)$ of this filter, with magnitude response fulfilling the requirements

- the passband edge frequency $\Omega_{pass} = 50$ rad/s,
- the stopband edge frequency $\Omega_{stop} = 150$ rad/s,
- maximum passband attenuation $r_p = 1$ dB,
- minimum stopband attenuation $r_s = 30$ dB.

From (1.106) we have

$$\begin{cases} 20\log_{10}\left(\frac{1}{\sqrt{1+(\Omega_{pass}/\Omega_c)^{2N}}}\right) = -r_p [dB] \\ 20\log_{10}\left(\frac{1}{\sqrt{1+(\Omega_{stop}/\Omega_c)^{2N}}}\right) = -r_s [dB] \end{cases} \quad (1.111)$$

After some manipulations

$$\begin{cases} 20\log_{10}\left(\frac{1}{1+(\Omega_{pass}/\Omega_c)^{2N}}\right)^{-1/2} = -r_p, \\ 20\log_{10}\left(\frac{1}{1+(\Omega_{stop}/\Omega_c)^{2N}}\right)^{-1/2} = -r_s \end{cases} \quad (1.112)$$

$$\begin{cases} \log_{10}\left(\frac{1}{1+(\Omega_{pass}/\Omega_c)^{2N}}\right) = r_p/10, \\ \log_{10}\left(\frac{1}{1+(\Omega_{stop}/\Omega_c)^{2N}}\right) = r_s/10 \end{cases} \quad (1.113)$$

$$\begin{cases} (\Omega_{pass}/\Omega_c)^{2N} = 10^{r_p/10} - 1, \\ (\Omega_{stop}/\Omega_c)^{2N} = 10^{r_s/10} - 1 \end{cases} \quad (1.114)$$

$$\log_{10}\left(\frac{\Omega_{pass}}{\Omega_{stop}}\right)^{2N} = \log_{10}\left(\frac{10^{r_p/10} - 1}{10^{r_s/10} - 1}\right) \quad (1.115)$$

the filter order is:

$$N = \frac{1}{2} \log_{10}\left(\frac{10^{r_p/10} - 1}{10^{r_s/10} - 1}\right) / \log_{10}\left(\frac{\Omega_{pass}}{\Omega_{stop}}\right) = \frac{1}{2} \log_{10}\left(\frac{10^{1/10} - 1}{10^{30/10} - 1}\right) / \log_{10}\left(\frac{50}{150}\right) = 3.758 \quad (1.116)$$

The filter order is rounded up to the nearest integer, i.e. $N=4$.

Ω_c is evaluated from (1.114) for the passband edge frequency

$$\log_{10}(\Omega_{pass}/\Omega_c) = \frac{1}{2N} \log_{10}(10^{r_p/10} - 1), \quad (1.117)$$

$$\log_{10}(\Omega_{pass}/\Omega_c) = \log_{10}(10^{r_p/10} - 1)^{\frac{1}{2N}}, \quad (1.118)$$

$$\Omega_{pass}/\Omega_c = (10^{r_p/10} - 1)^{\frac{1}{2N}}, \quad (1.119)$$

$$\Omega_c = \frac{\Omega_{pass}}{(10^{r_p/10} - 1)^{\frac{1}{2N}}} = \frac{50}{(10^{1/10} - 1)^{\frac{1}{2^4}}} = 59.2, \quad (1.120a)$$

or for the stopband edge frequency

$$\Omega_c = \frac{\Omega_{stop}}{(10^{r_s/10} - 1)^{\frac{1}{2N}}} = \frac{150}{(10^{1/30} - 1)^{\frac{1}{2^4}}} = 63.26. \quad (1.120b)$$

The transmittance of the filter for $\Omega_c=59.02$ (1.120a) is

$$H(s) = \frac{12282667.0523}{s^4 + 154.6976s^3 + 11965.67s^2 + 542162.9667s + 12282667.0523}$$

$$= \frac{\Omega_c^N}{s^4 + 154.6976s^3 + 11965.67s^2 + 542162.9667s + \Omega_c^N}$$

Fig. 1.24 depicts magnitude characteristic and the requirements for designed analog lowpass Butterworth filter, and the zeros of this filter. It is seen that for Ω_c computed by (1.120a) attenuation requirement in passband is fulfilled exactly and in the stopband in excess, whereas for Ω_c computed by (1.120b) the situation is reversed.

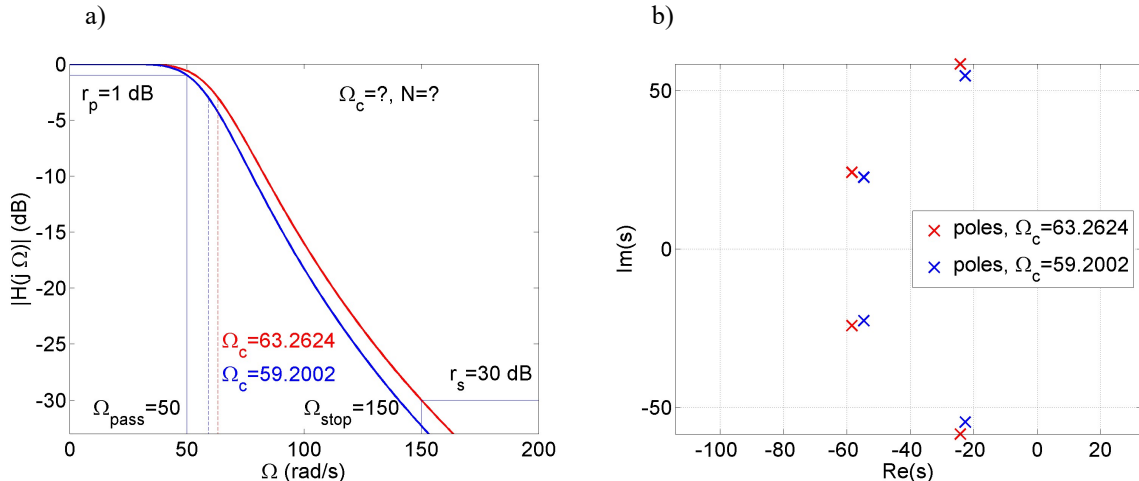


Fig. 1.24 a) Magnitude characteristic and requirements for designed analog lowpass Butterworth filter,
b) The poles of designed lowpass Butterworth filter.

1.4.3 Chebyshev type I and type II filters

The magnitude-squared function of a continuous-time lowpass Chebyshev type I filter is defined as

$$|H(j\Omega)|^2 = \frac{1}{1 + \varepsilon_p^2 V_N^2(\Omega/\Omega_c)}, \quad (1.121)$$

where ε_p is a parameter controlling the amplitude of ripples in the passband, and

$$V_N(x) = \begin{cases} \cos(N \arccos(x)), & |x| \leq 1 \\ \cosh(N \text{arccosh}(x)), & |x| > 1 \end{cases} \quad (1.122)$$

is the Chebyshev polynomial of order N .

[Spe68 p. 157-158]

30

CHEBYSHEV POLYNOMIALS

CHEBYSHEV'S DIFFERENTIAL EQUATION

30.1

$$(1-x^2)y'' - xy' + n^2y = 0 \quad n = 0, 1, 2, \dots$$

CHEBYSHEV POLYNOMIALS OF THE FIRST KIND

Solutions of 30.1 are given by

$$\text{30.2} \quad T_n(x) = \cos(n \cos^{-1} x) = x^n - \binom{n}{2} x^{n-2}(1-x^2) + \binom{n}{4} x^{n-4}(1-x^2)^2 - \dots$$

SPECIAL CHEBYSHEV POLYNOMIALS OF THE FIRST KIND

$$\text{30.3} \quad T_0(x) = 1$$

$$\text{30.7} \quad T_4(x) = 8x^4 - 8x^2 + 1$$

$$\text{30.4} \quad T_1(x) = x$$

$$\text{30.8} \quad T_5(x) = 16x^5 - 20x^3 + 5x$$

$$\text{30.5} \quad T_2(x) = 2x^2 - 1$$

$$\text{30.9} \quad T_6(x) = 32x^6 - 48x^4 + 18x^2 - 1$$

$$\text{30.6} \quad T_3(x) = 4x^3 - 3x$$

$$\text{30.10} \quad T_7(x) = 64x^7 - 112x^5 + 56x^3 - 7x$$

GENERATING FUNCTION FOR $T_n(x)$

30.11

$$\frac{1-tx}{1-2tx+t^2} = \sum_{n=0}^{\infty} T_n(x) t^n$$

SPECIAL VALUES

$$\text{30.12} \quad T_n(-x) = (-1)^n T_n(x)$$

$$\text{30.14} \quad T_n(-1) = (-1)^n$$

$$\text{30.16} \quad T_{2n+1}(0) = 0$$

$$\text{30.13} \quad T_n(1) = 1$$

$$\text{30.15} \quad T_{2n}(0) = (-1)^n$$

RECURRENCE FORMULA FOR $T_n(x)$

$$30.17 \quad T_{n+1}(x) - 2x T_n(x) + T_{n-1}(x) = 0$$

ORTHOGONALITY

$$30.18 \quad \int_{-1}^1 \frac{T_m(x) T_n(x)}{\sqrt{1-x^2}} dx = 0 \quad m \neq n$$

$$30.19 \quad \int_{-1}^1 \frac{\{T_n(x)\}^2}{\sqrt{1-x^2}} dx = \begin{cases} \pi & \text{if } n = 0 \\ \pi/2 & \text{if } n = 1, 2, \dots \end{cases}$$

ORTHOGONAL SERIES

$$30.20 \quad f(x) = \frac{1}{2} A_0 T_0(x) + A_1 T_1(x) + A_2 T_2(x) + \dots$$

where

$$30.21 \quad A_k = \frac{2}{\pi} \int_{-1}^1 \frac{f(x) T_k(x)}{\sqrt{1-x^2}} dx$$

CHEBYSHEV POLYNOMIALS OF THE SECOND KIND

$$\begin{aligned} 30.22 \quad U_n(x) &= \frac{\sin \{(n+1) \cos^{-1} x\}}{\sin (\cos^{-1} x)} \\ &= \binom{n+1}{1} x^n - \binom{n+1}{3} x^{n-2} (1-x^2) + \binom{n+1}{5} x^{n-4} (1-x^2)^2 - \dots \end{aligned}$$

SPECIAL CHEBYSHEV POLYNOMIALS OF THE SECOND KIND

$$30.23 \quad U_0(x) = 1$$

$$30.27 \quad U_4(x) = 16x^4 - 12x^2 + 1$$

$$30.24 \quad U_1(x) = 2x$$

$$30.28 \quad U_5(x) = 32x^5 - 32x^3 + 6x$$

$$30.25 \quad U_2(x) = 4x^2 - 1$$

$$30.29 \quad U_6(x) = 64x^6 - 80x^4 + 24x^2 - 1$$

$$30.26 \quad U_3(x) = 8x^3 - 4x$$

$$30.30 \quad U_7(x) = 128x^7 - 192x^5 + 80x^3 - 8x$$

GENERATING FUNCTION FOR $U_n(x)$

$$30.31 \quad \frac{1}{1-2tx+t^2} = \sum_{n=0}^{\infty} U_n(x) t^n$$

Magnitude characteristic of Chebyshev type I filter is equiripple in the passband and monotonic in the stopband, as shown in Fig. 1.25.

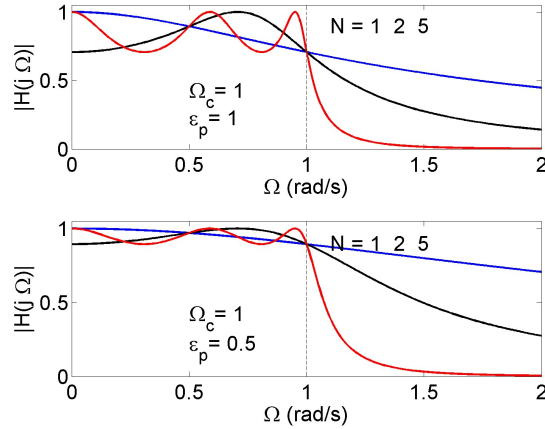


Fig.1.25 Magnitude characteristic of Chebyshev type I filter.

The poles of analog lowpass Chebyshev type I filter are placed on ellipse in the s -plane. The length of the semi-minor axis is $a\Omega_c$ and the length of semi-major axis is $b\Omega_c$ where

$$a = \frac{1}{2}(\alpha^{1/N} - \alpha^{-1/N}), \quad \alpha = \varepsilon_p^{-1} + \sqrt{1 + \varepsilon_p^{-2}}, \quad b = \frac{1}{2}(\alpha^{1/N} + \alpha^{-1/N}). \quad (1.123)$$

The poles of analog lowpass Chebyshev type I filter may be obtained from the poles of lowpass Butterworth filter. First, the poles of Butterworth filter are placed on the circle with the radius equal to semi-major axis $b\Omega_c$ and next the poles are moved to the right on ellipse as shown in Fig. 1.26.

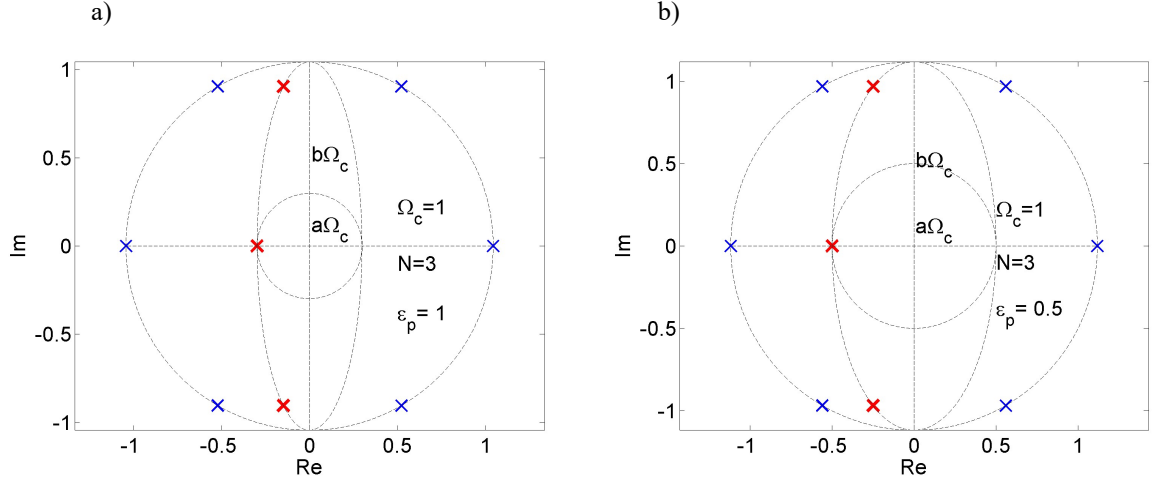


Fig. 1.26 The poles of Chebyshev type I filter (red) obtained from the poles of Butterworth filter (blue):
a) $\varepsilon_p = 1$, $s_{1,2} = -0.1490 \pm j0.9037$, $s_3 = -0.2980$,
b) $\varepsilon_p = 0.5$, $s_{1,2} = -0.2500 \pm j0.9682$, $s_3 = -0.5$.

The magnitude-squared function of a continuous-time lowpass Chebyshev type II filter is defined as

$$|H(j\Omega)|^2 = \frac{1}{1 + \frac{1}{\varepsilon_s^2 V_N^2(\Omega_c/\Omega)}} , \quad \Omega \neq 0, \quad (1.124)$$

where ε_s is a parameter controlling the amplitude of ripples in the stopband. Magnitude characteristic of Chebyshev type II filter is monotonic in the passband and equiripple in the stopband, as shown in Fig. 1.27.

The poles of lowpass Chebyshev type II filter can be found from the poles of Chebyshev type I filter from the equation

$$s_k^{II} = \frac{\Omega_c^2}{s_k^I}, \quad (1.125)$$

and the zeros are placed on imaginary axis in points $V_N(\Omega_c/\Omega) = 0$.

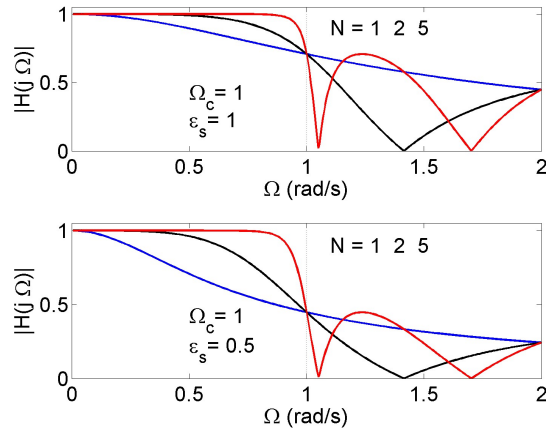


Fig. 1.27 Magnitude characteristics of Chebyshev type II.

Fig. 1.28a depicts magnitude characteristics of Chebyshev type I filter and Chebyshev type II filter that was obtained from Chebyshev type I filter, and Fig. 1.28b shows zero-pole plots for those two filters.

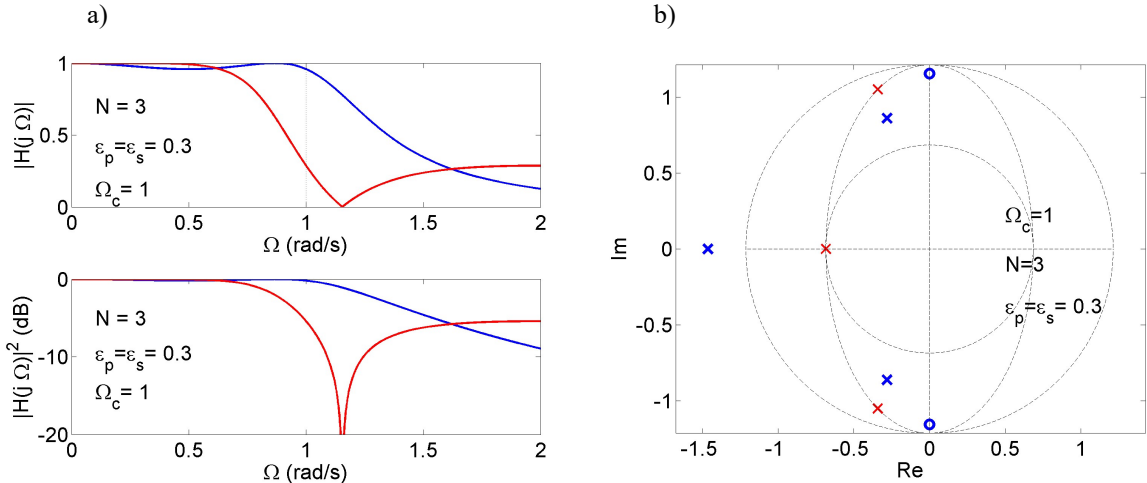


Fig.1.28 a) Magnitude characteristics of Chebyshev type I filter and Chebyshev type II filter that was obtained from Chebyshev type I filter.

b) Zero-pole plots for those two filters; for the Chebyshev type II filter the poles are $s_{1,2}=-0.2808 \pm 0.8615$, $s_3=-1.4617$ and the zeros are $z_{1,2}=\pm j1.1547$.

1.4.4 Elliptic filter

The magnitude-squared function of a continuous-time lowpass elliptic filter is defined with the Jacobian elliptic function. Magnitude characteristic of elliptic filter is equiripple in the passband and in the stopband. Elliptic filter has four parameters: filter order N , passband edge frequency Ω_c , amplitude of ripples in the passband ε_p , and amplitude of ripples in the stopband ε_s .

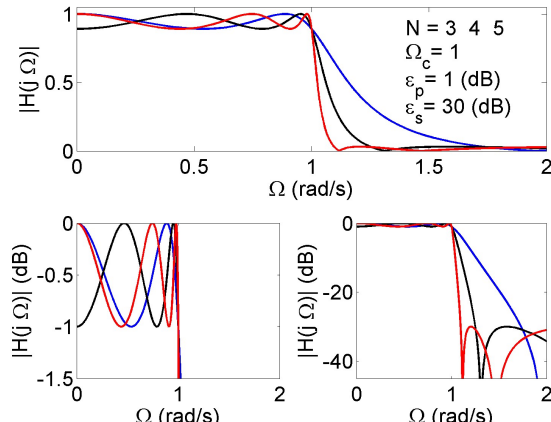


Fig.1.29 Magnitude characteristics of elliptic filter.

see [Britt93 p.93-107] for elliptic filter design

1.4.5 Bessel filter

Bessel filters are designed to have maximally flat group-delay characteristics, thus preserving the wave shape of filtered signals in the passband. As a consequence, there is no ringing in the impulse and step responses.

see [Britt93 p.109-116] for Bessel filter design

1.4.6 Comparison of analog filters

Tab. 1.2 and Figs. 1.30-1.33 compare the properties of continuous-time filters. All filters were designed for the same requirements. It is seen in Fig. 1.30 that for Bessel filter designing requirements are not fulfilled in the stopband.

Group delay shown in Fig. 1.32b is defined as

$$\text{Group delay}(\Omega) = -\frac{d}{d\Omega} \text{angle}(H(j\Omega)) \text{ (s).} \quad (1.126)$$

Table 1.2 Comparison of continuous-time filters properties.

Filter	Number of Parameters	Passband	Stopband	Zeros for LP	Selectivity	Phase in passband	Impulse response
Butterworth	2 N, Ω_c	Monotonic	Monotonic	no	Low	Slightly Nonlinear	Long with ringing
Chebyshev type I	3 $N, \Omega_c, \varepsilon_p$ (passband)	Equiripple	Monotonic	no	Medium	Slightly Nonlinear	Longest with ringing
Chebyshev type II	3 $N, \Omega_c, \varepsilon_s$ (stopband)	Monotonic	Equiripple	yes	Medium	Medium Nonlinear	Long with ringing
Elliptic	4 $N, \Omega_c, \varepsilon_p$ (passband) ε_s (stopband)	Equiripple	Equiripple	yes	Highest	Highly nonlinear	Longest with ringing
Bessel	2 N, Ω_c	Monotonic	Monotonic	no	Lowest	Almost linear	Shortest no ringing

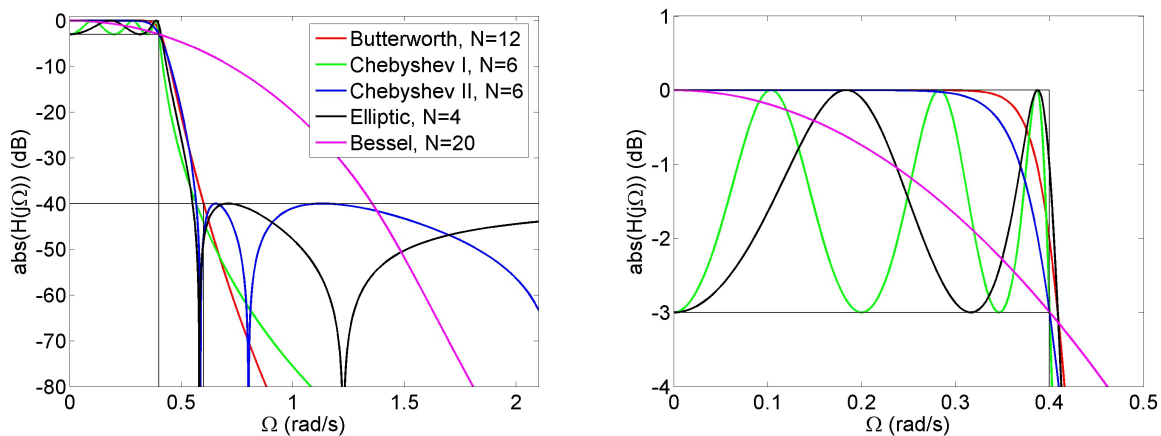


Fig. 1.30 Magnitude responses: $\Omega_{pass}=0.4$ rad/s, $\Omega_{stop}=0.6$ rad/s, $r_p=3$ dB, $r_s=40$ dB.

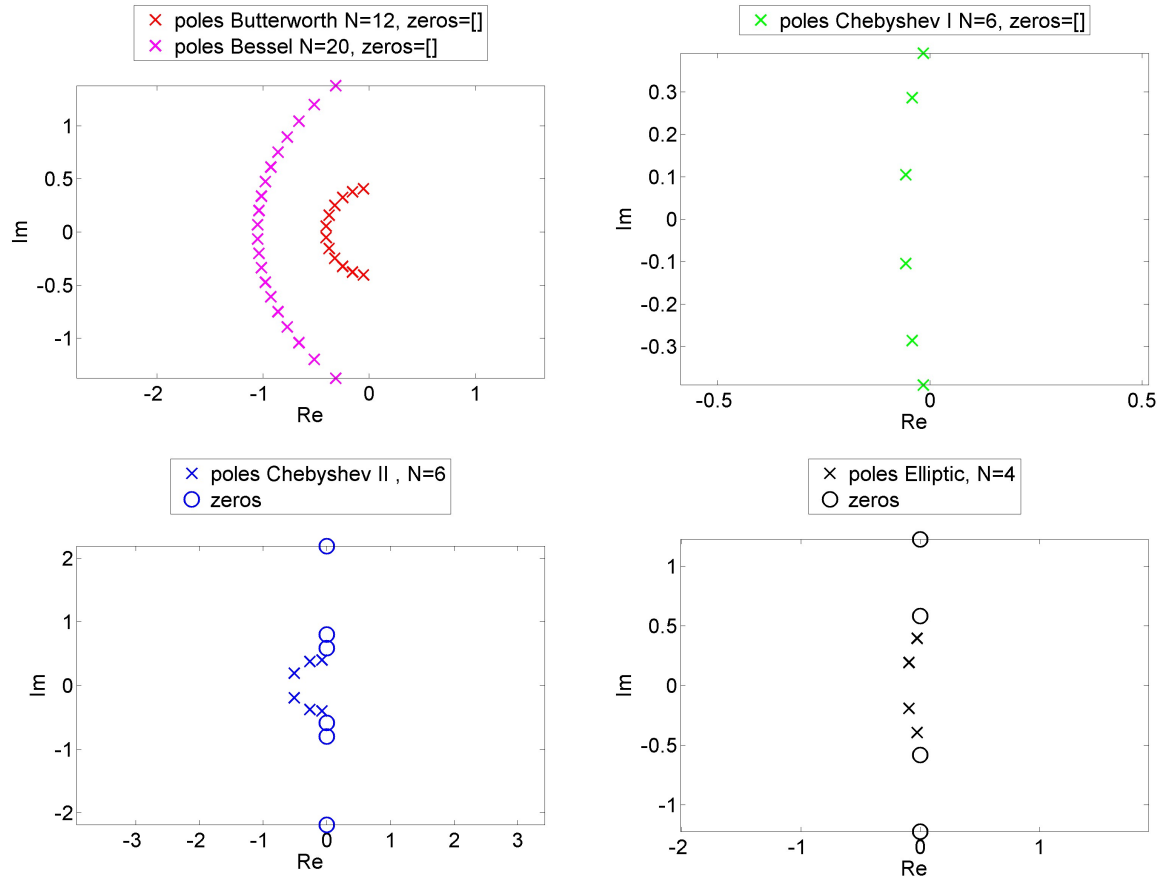


Fig.1.31 Zero-pole plots.

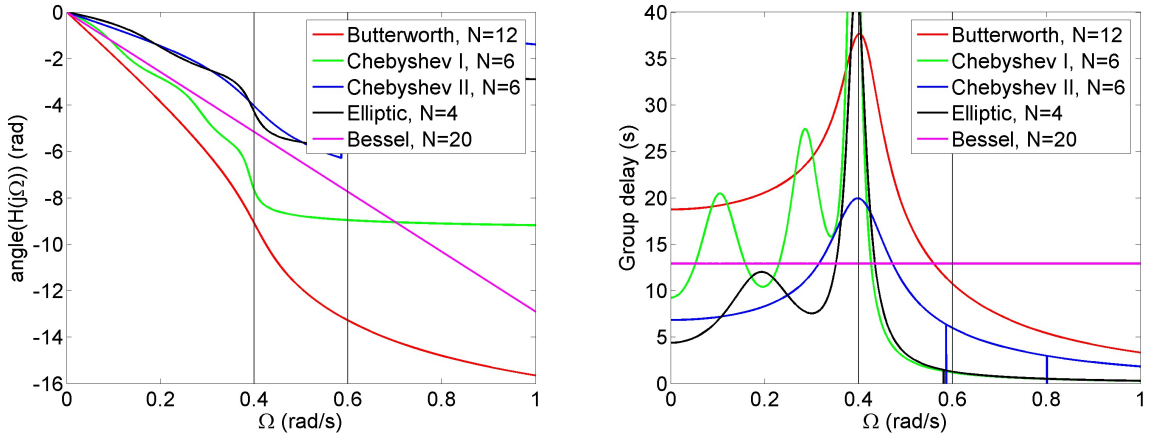


Fig.1.32 a) Phase responses, and b) Group delay.

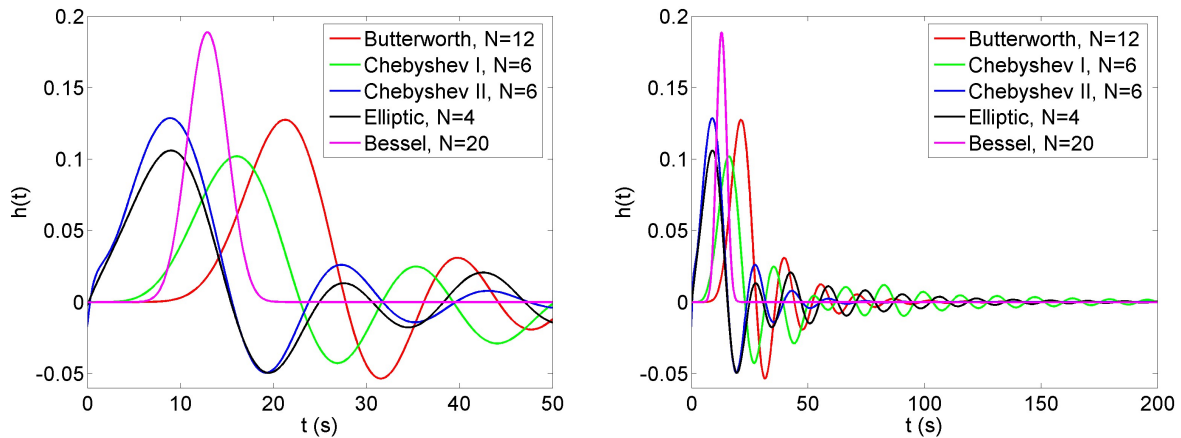


Fig.1.33 Impulse responses.

1.4.7 Frequency transformation: LP, HP, BP, BS filters

LP, HP, BP, BS filters are obtained from analog lowpass filter prototypes with a cutoff angular frequency of 1 rad/s by frequency transformations.

[Ziel05]

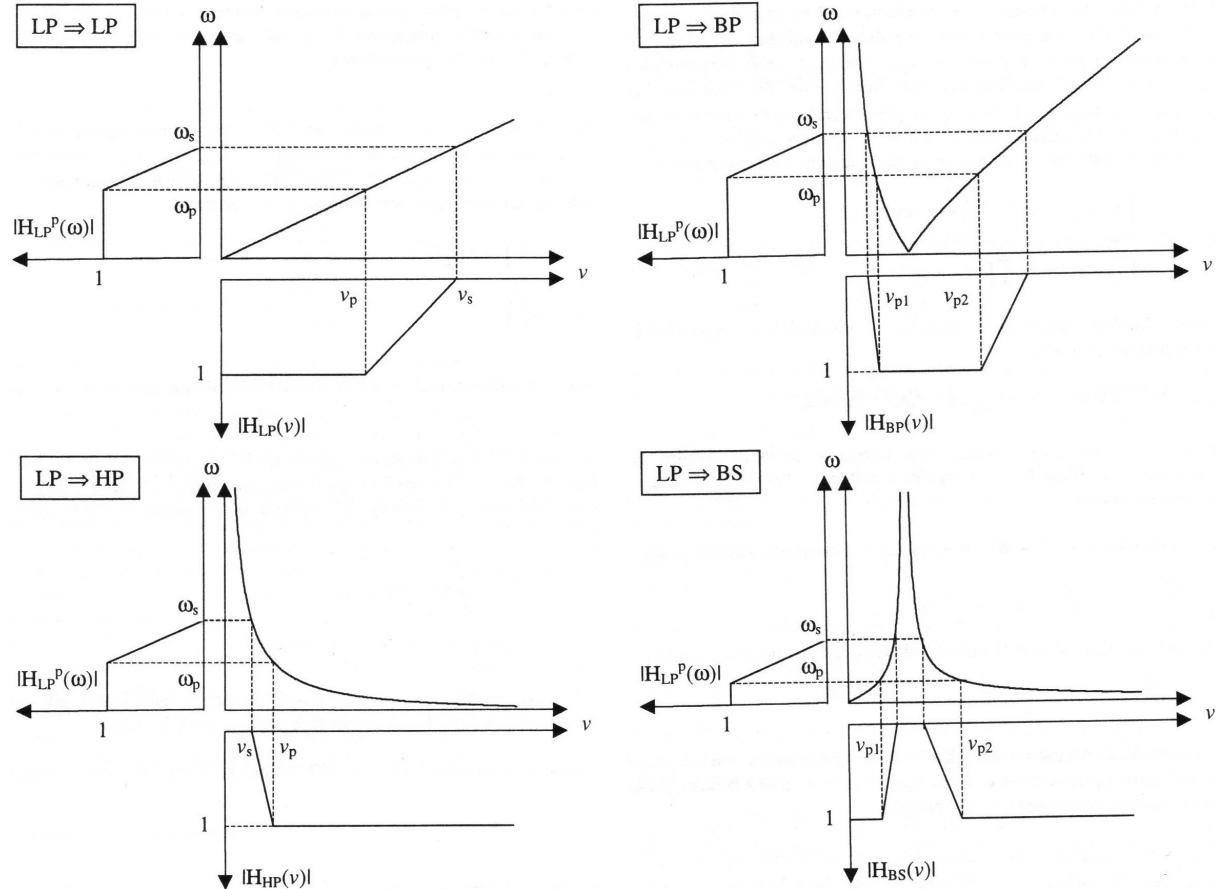


Table 1.3 Frequency transformations of analog prototype.

Filter	Transformation
LP (<i>lowpass</i>) with cutoff frequency ω_0 Matlab 1p2lp	$s' = s / \omega_0$ (1.127)
HP (<i>highpass</i>) with cutoff frequency ω_0 Matlab 1p2hp	$s' = \omega_0 / s$ (1.128)
BP (<i>bandpass</i>) from ω_1 to ω_2 Matlab 1p2bp	$s' = \frac{\omega_0}{\Delta\omega} \frac{(s/\omega_0)^2 + 1}{s/\omega_0}$ (1.129)
BS (<i>bandstop</i>) from ω_1 to ω_2 Matlab 1p2bs	$s' = \frac{\Delta\omega}{\omega_0} \frac{s/\omega_0}{(s/\omega_0)^2 + 1}$ (1.130)
where the bandwidth $\Delta\omega = \omega_2 - \omega_1$, and the middle frequency $\omega_0 = \sqrt{\omega_1\omega_2}$	

Table 1.4 Example of frequency transformation of analog Butterworth prototype filter $H(s) = \frac{1}{s^2 + \sqrt{2}s + 1}$

Filter	Transmittance	Remarks
LP	$H(s/\omega_0) = \frac{1}{(s/\omega_0)^2 + \sqrt{2}(s/\omega_0) + 1} = \frac{\omega_0^2}{s^2 + \omega_0\sqrt{2}s + \omega_0^2}$	Order 2 no zeros
HP	$H(\omega_0/s) = \frac{s^2}{s^2 + \omega_0\sqrt{2}s + \omega_0^2}$	Order 2 2 zeros
BP	$H\left(\frac{\omega_0}{\Delta\omega} \frac{(s/\omega_0)^2 + 1}{s/\omega_0}\right) = \frac{\Delta\omega^2 s^2}{s^4 + \sqrt{2}\Delta\omega s^3 + (2\omega_0^2 + \Delta\omega^2)s^2 + \sqrt{2}\Delta\omega\omega_0^2 s + \omega_0^4}$	Order 4 2 zeros
BS	$H\left(\frac{\Delta\omega}{\omega_0} \frac{s/\omega_0}{(s/\omega_0)^2 + 1}\right) = \frac{(s^2 + \omega_0^2)^2}{s^4 + \sqrt{2}\Delta\omega s^3 + (2\omega_0^2 + \Delta\omega^2)s^2 + \sqrt{2}\Delta\omega\omega_0^2 s + \omega_0^4}$	Order 4 2 zeros

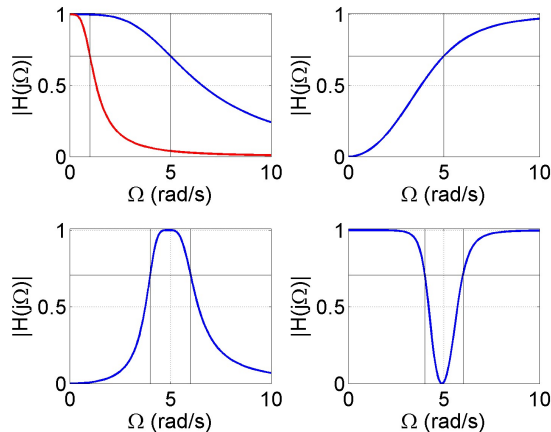


Fig.1.34 Magnitude characteristics of LP $\Omega_0=5$ rad/s, HP $\Omega_0=5$ rad/s, BP $\Omega_1=4$ rad/s, $\Omega_2=6$ rad/s, and BS $\Omega_1=4$ rad/s, $\Omega_2=6$ rad/s filters obtained from analog LP $\Omega_0=1$ rad/s prototype.

Frequency transformation of arbitrary transmittance $H(s)$ can be implemented by representing this transmittance $H(s)$ as a product of the two basic transmittances $H(s) = A/(s - B)$ and $H(s) = (s - A)/(s - B)$ and then transforming each of the basic transmittance with the use of mathematical equations.

2. Digital signal processing

2.1 Discrete-time signals and systems

Discrete-time signals are sequences (possible of infinite length) of samples. Discrete-time signals are obtained by sampling of continuous-time signals or as a result of counting events e.g. sunspot numbers, weekly Dow Jones stock market index, population indexes, etc.

Notation $x[n]$ (2.1) stands for all values of the sequence

$$x = \{x[n]\}, \quad n = \dots, -1, 0, 1, \dots, \quad x = \{\dots, x[-1], x[0], x[1], \dots\} = x[n]. \quad (2.1)$$

If $x[n]$ is obtained by uniform sampling, then

$$x[n] = x(nT), \quad \frac{1}{T} = F_s, \quad (2.2)$$

where F_s is the *sampling frequency* in Hertz, and T is the *sampling period* in seconds.

In practice discrete-time signals are processed by computers and the finite length of the signal must be assumed

$$x = \{x[n]\}, \quad n = 0, 1, \dots, N-1, \quad x = \{x[0], x[1], \dots, x[N-1]\} = x[n], \quad (2.3)$$

where N is the number o samples (values). Signal (2.3) is a *vector*, thus digital signal processing is processing of vectors and matrices.

Matlab digression on generating signals

%Continuous-time signal	%Discrete-time signal
%Parameters	%Parameters
Tmax	Fs
dt	N
%Computations	%Computations
t=0:dt:Tmax	t=(0:N-1)/Fs
N = length(t)	%fixed number of samples
	Tmax = max(t)

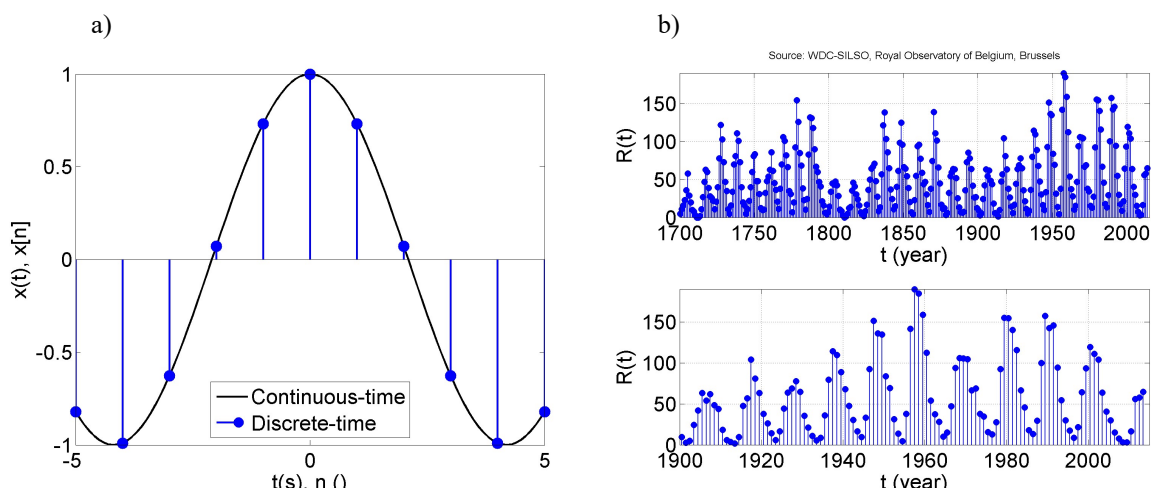


Fig.2.1 Discrete-time signals: a) sampling of continuous-time signal, b) sunspot numbers.

2.1.1 Exponential signal

Discrete-time exponential signal is defined as

$$x[n] = A\alpha^n = Ae^{\beta n}, \quad -\infty < n < \infty, \quad A, \alpha \in R, \quad (2.4)$$

where A and $\alpha = e^\beta$ are real and n is integer. If $|\alpha| > 1$ (i.e. $\beta > 0$) the signal grows exponentially with n , while if $|\alpha| < 1$ (i.e. $\beta < 0$) the signal decays exponentially. If α is positive, all the values of $A\alpha^n$ are of the same sign, but if α is negative, then the sign of $x[n]$ (2.4) alternates.

Table 2.1 Continuous-time and discrete time exponential signal.

$x(t) = Ce^{at}$	(1.3)	$x[n] = A\alpha^n = Ae^{\beta n}$	(2.4)
------------------	-------	-----------------------------------	-------

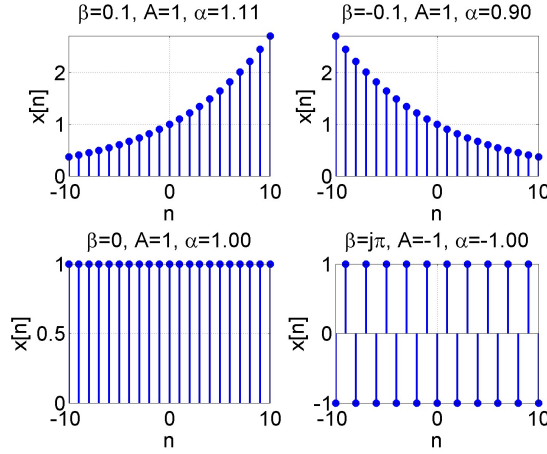


Fig. 2.2 Discrete-time exponential signals (2.1).

In case of oscillation $\beta = j\pi$.

2.1.2 Complex exponential signal

Discrete-time complex exponential signal is defined as

$$x[n] = e^{j\omega_0 n}, \quad -\infty < n < \infty, \quad (2.5)$$

where ω_0 is the frequency (angular frequency, pulsation) in radians.

Complex exponential signals with frequencies ω_0 and $(\omega_0 + 2\pi)$ are indistinguishable

$$x[n] = Ae^{j(\omega_0 + 2\pi)n} = Ae^{j\omega_0 n}e^{j2\pi n} = Ae^{j\omega_0 n}. \quad (2.6)$$

Discrete-time signal is periodic if

$$x[n] = x[n + N]. \quad (2.7)$$

Complex exponential signal is periodic only if $e^{j\omega_0(n+N)} = e^{j\omega_0 n}$, that is for $\omega_0 N = 2\pi m$, for some integer m .

Table 2.2 Continuous-time and discrete time complex exponential signal.

$x(t) = e^{j\Omega_0 t}$ (1.4)	$x[n] = e^{j\omega_0 n}$ (2.5)
Ω_0 - frequency in radians per second	ω_0 - frequency in radians.
Distinct signals for distinct values of Ω_0	Identical signals for exponentials at frequencies separated by 2π rad
Periodic for every Ω_0	Periodic, with period N , only if $\omega_0 = \frac{2\pi}{N}m$ for some integers $N > 0$ and m .
The number of oscillations increases with Ω_0 to infinity.	The number of oscillations changes periodically with ω_0 . For ω_0 increasing from $\omega_0=0$ to $\omega_0=\pi$ the number of oscillations increases, and for ω_0 increasing from $\omega_0=\pi$ to $\omega_0=2\pi$ the number of oscillations decreases.

2.1.3 Sinusoidal signal

Discrete-time sinusoidal signal is defined as

$$x[n] = A \cos(\omega_0 n + \phi), \quad -\infty < n < \infty, \quad (2.8)$$

where ω_0 is the frequency (angular frequency, pulsation) in radians, ϕ is the phase in radians, and $A > 0$ is the amplitude in the units of measured quantity (e.g. in volts).

Sinusoidal signal (2.8) is only periodic for $\omega_0 = \frac{2\pi}{N}m$, for some integer m .

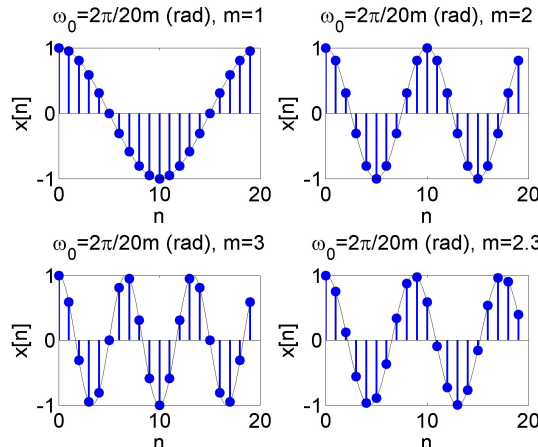


Fig. 2.3 Periodicity of discrete-time sinusoidal signal (2.8); fundamental periods N_p are:

$$\text{for } m=1, \omega_0=(2\pi/20)\cdot 1, \quad N_p=20$$

$$\text{for } m=2, \omega_0=(2\pi/20)\cdot 2=2\pi/10, \quad N_p=10$$

$$\text{for } m=3, \omega_0=(2\pi/20)\cdot 3, \quad N_p=20$$

$$\text{for } m=3, \omega_0=(2\pi/20)\cdot 2.3, \quad \text{aperiodic}$$

Sinusoidal signals with frequencies ω_0 and $\omega_0+2\pi$ are indistinguishable because $A \cos(\omega_0 n + 2\pi n + \phi) = A \cos(\omega_0 n + \phi)$

For discrete-time sinusoidal signal the number of oscillations increases as ω_0 increases from $\omega_0=0$ to $\omega_0=\pi$ rad, and the number of oscillations decreases when ω_0 increases from $\omega_0=\pi$ rad to $\omega_0=2\pi$ rad as shown in Fig.2.4.

From Fig.2.4. it is seen that the range of frequencies for discrete-time sinusoidal signal is $\langle 0, \pi \rangle$ rad.

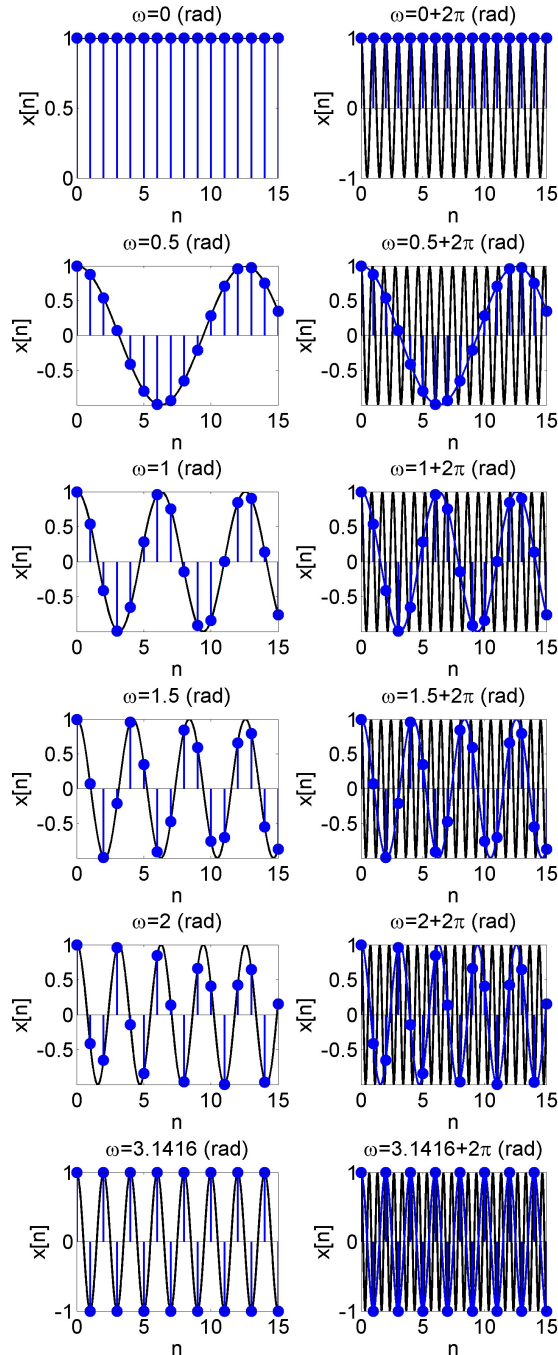


Fig. 2.4 Oscillations of continuous-time and discrete-time sinusoidal signals.

If discrete-time sinusoidal signal is obtained from sampling of continuous-time sinusoidal signal, i.e. $x[n] = x(nT)$, $\frac{1}{T} = F_s$, then the frequency of this signal may be expressed in Hertz with the use of sampling frequency F_s

$$x[n] = x(nT) = A \cos(\Omega_0 nT + \phi) = A \cos(2\pi \frac{F_0}{F_s} n + \phi), \quad (2.9)$$

where F_0 is the frequency in Hertz. By comparing (2.8) and (2.9) it goes that

$$\omega_0 = 2\pi \frac{F_0}{F_s}. \quad (2.10)$$

As observed in Fig. 2.4 the maximum value of ω_0 is π rad, thus from (2.10) we get the condition

$$F_s > 2F_0, \quad (2.11)$$

i.e. the sampling frequency must be two times higher than the frequency of the sinusoidal signal.

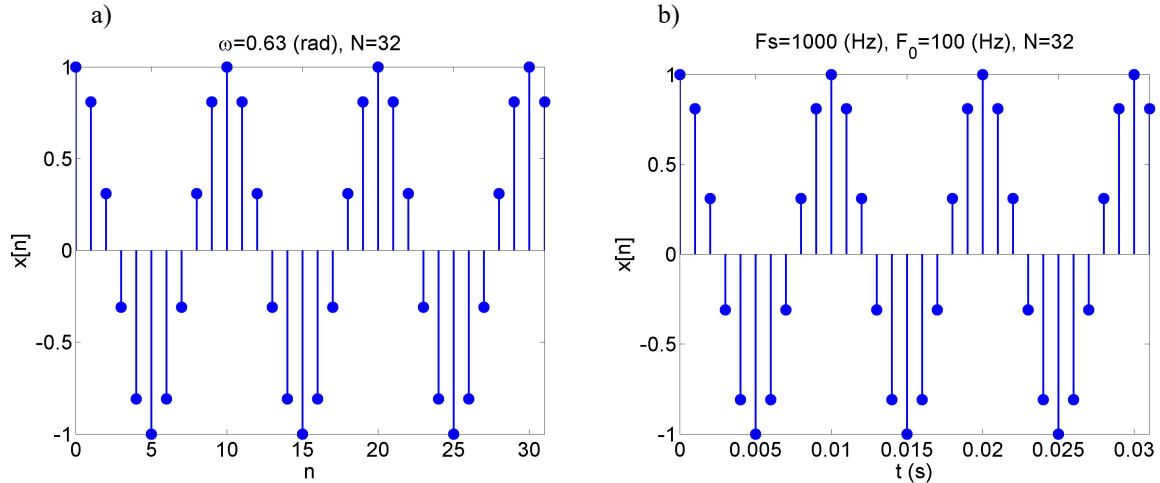


Fig. 2.5 Discrete-time sinusoidal signal: a) frequency ω_0 in radians (2.8), b) frequency F_0 in Hertz (2.9). The values of samples are identical in both cases.

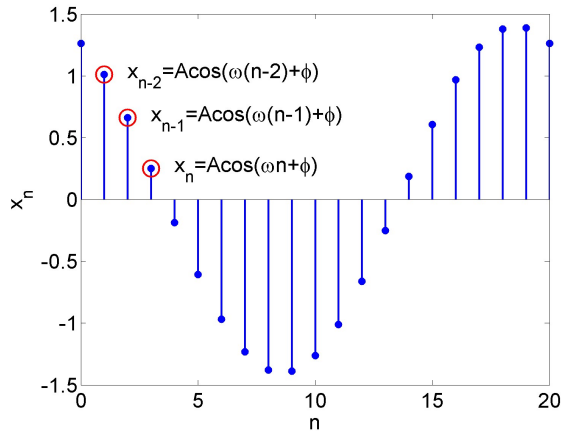


Fig. 2.6 Arbitrary three successive samples for deriving sinusoid difference equation (2.14).

Discrete-time sinusoidal signal fulfills second order difference equation. Let us write arbitrary three successive samples $x[n-2], x[n-1], x[n]$ defined by (2.8)

$$\begin{aligned} x[n-2] &= A \cos(\omega_0(n-2) + \phi) \\ x[n-1] &= A \cos(\omega_0(n-1) + \phi), \\ x[n] &= A \cos(\omega_0 n + \phi) \end{aligned} \quad (2.12)$$

Multiplying both sides of $x[n-1] = A \cos(\omega_0(n-1) + \phi)$ by $2 \cos(\omega_0)$ we get

$$\begin{aligned} 2 \cos(\omega_0) x[n-1] &= 2 A \cos(\omega_0 n + \phi - \omega_0) \cos(\omega_0) = \\ &= A \cos(\omega_0 n + \phi - 2\omega_0) + A \cos(\omega_0 n + \phi) =, \\ &= x[n-2] + x[n] \end{aligned} \quad (2.13)$$

and finally

$$x[n] = 2 \cos(\omega_0) x[n-1] - x[n-2]. \quad (2.14)$$

2.1.4 Damped sinusoidal signal

Discrete-time damped sinusoidal signal is defined as

$$x[n] = A \cos(\omega_0 n + \phi) e^{-dn}, \quad -\infty < n < \infty, \quad (2.15)$$

where ω_0 is the frequency (angular frequency, pulsation) in radians, d is the damping factor, ϕ is the phase in radians, and $A > 0$ is the amplitude in the units of measured quantity.

Discrete-time damped sinusoidal signal fulfills second order difference equation. Let us write arbitrary three successive samples $x[n-2], x[n-1], x[n]$ defined by (2.15)

$$\begin{aligned} x[n-2] &= A \cos(\omega_0(n-2) + \phi) e^{-d(n-2)} \\ x[n-1] &= A \cos(\omega_0(n-1) + \phi) e^{-d(n-1)}, \\ x[n] &= A \cos(\omega_0 n + \phi) e^{-dn} \end{aligned} \quad (2.16)$$

Multiplying both sides of $x[n-1] = A \cos(\omega_0(n-1) + \phi) e^{-d(n-1)}$ by $2 \cos(\omega_0) e^{-d}$ we get

$$\begin{aligned} 2 \cos(\omega_0) e^{-d} x[n-1] &= 2 A \cos(\omega_0(n-1) + \phi) \cos(\omega_0) e^{-d(n-1)} e^{-d} = \\ &= A \cos(\omega_0 n + \phi - 2\omega_0) e^{-dn} + A \cos(\omega_0 n + \phi) e^{-dn} =, \\ &= x[n-2] e^{-2d} + x[n] \end{aligned} \quad (2.17)$$

and finally

$$x[n] = 2 \cos(\omega_0) e^{-d} x[n-1] - e^{-2d} x[n-2]. \quad (2.18)$$

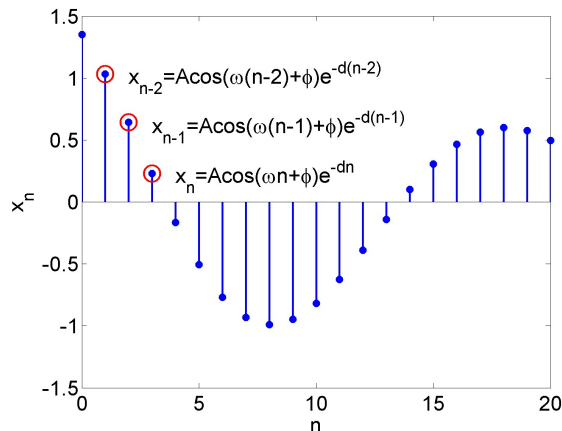


Fig. 2.7 Arbitrary three successive samples for deriving damped sinusoid difference equation (2.18).

2.1.5 Unite impulse

Unite impulse (also called unit sample, and Kronecker delta) is defined as

$$\delta[n] = \begin{cases} 1, & n = 0, \\ 0, & n \neq 0. \end{cases} \quad (2.19)$$

The fragment of unit impulse for $-5 \leq n \leq 5$ is shown in Fig. 2.8.

The sum of all elements of unite impulse equals 1

$$\sum_{k=-\infty}^{k=\infty} \delta[k] = 1. \quad (2.20)$$

Unite impulse may sample the value of discrete-time signal in arbitrary index n_0

$$x[n]\delta[n - n_0] = x[n_0]\delta[n - n_0]. \quad (2.21)$$

Arbitrary discrete-time signal $x[n]$ may be represented as a sum of scaled (by the values of $x[n]$), and shifted unite impulses

$$x[n] = \sum_{k=-\infty}^{\infty} x[k]\delta[n - k]. \quad (2.22)$$

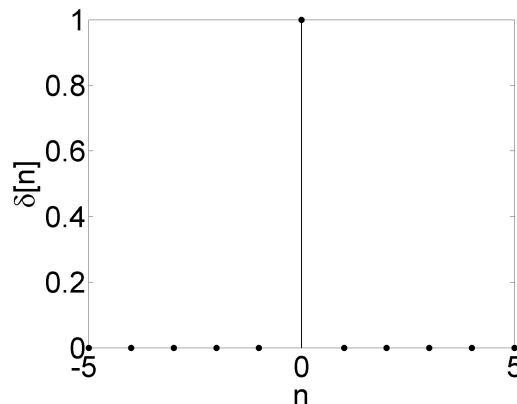


Fig.2.8 The Fragment of unite impulse for $-5 \leq n \leq 5$.

Table 2.3 Dirac function and Kronecker delta.

Continuous-time	Discrete-time
$\int_{-\infty}^{\infty} \delta(t)dt = 1, \quad \delta(t) = 0 \quad \text{for } t \neq 0 \quad (1.13)$	$\delta[n] = \begin{cases} 1, & n = 0, \\ 0, & n \neq 0. \end{cases} \quad (2.19)$
$\delta(t - t_0)f(t) = \delta(t - t_0)f(t_0) \quad (1.16b)$	$x[n]\delta[n - n_0] = x[n_0]\delta[n - n_0] \quad (2.21)$
$x(t) = \int_{-\infty}^{\infty} x(\tau)\delta(t - \tau)d\tau \quad (1.21)$	$x[n] = \sum_{k=-\infty}^{\infty} x[k]\delta[n - k] \quad (2.22)$
Not realizable.	Easy to obtain and manipulate.

2.2 Discrete-time systems

A *system* is any process that results in the transformation of signals. A discrete-time system has an input signal, denoted by $x[n]$, and an output signal, denoted by $y[n]$, which are related by the system transformation (similarly as (1.17) for continuous-time systems)

$$x[n] \rightarrow y[n]. \quad (2.23)$$

The transformation of the input signal $x[n]$ made by the system may also be denoted as

$$y[n] = T\{x[n]\}. \quad (2.24)$$

Example 2.1

The *delay system* is defined by the equation

$$y[n] = x[n - n_d], \quad -\infty < n < \infty, \quad n_d = \text{const}, \quad (2.25)$$

where n_d is a fixed positive integer called the delay of the system.

Example 2.2

The *moving-average system* is defined as

$$\begin{aligned} y[n] &= \frac{1}{M_1 + M_2 + 1} \sum_{k=-M_1}^{M_2} x[n - k] = \\ &= \frac{1}{M_1 + M_2 + 1} (x[n + M_1] + x[n + M_1 - 1] + \dots + x[n] + x[n - 1] + \dots + x[n - M_2]) \end{aligned} . \quad (2.26)$$

The system computes n th output sample as the average of $(M_1 + M_2 + 1)$ samples of the input signal $x[n]$ around the n th sample. Exemplary computations of (2.26) for $M_1 = M_2 = 1$ are illustrated in Fig. 2.9.

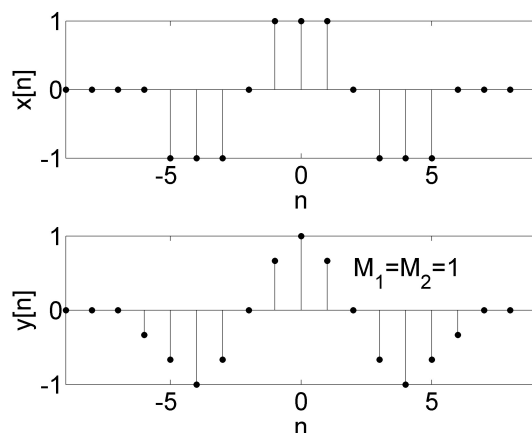


Fig.2.9 Exemplary moving-average system (2.26) input output relation for $M_1 = M_2 = 1$.

2.2.1 LTI systems

The definitions of *stability*, *causality*, *time-invariance*, and *linearity* are the same as in the case of continuous-time systems (see section 1.2).

For the causal system the output $y[n]$ for the fixed index n_0 depends only on the current and previous input samples, that is $x[n \leq n_0]$. Casual system is *nonanticipative*. The *backward difference* $y[n] = x[n] - x[n-1]$ is causal system, and the *forward difference* $y[n] = x[n+1] - x[n]$ is not causal system. Moving average (2.26) is not causal system.

The system is time-invariant (shift-invariant) if the shift in the input signal makes the same shift in the output signal, that is

$$\text{If } y[n] = T\{x[n]\} \text{ then } y[n-n_0] = T\{x[n-n_0]\}. \quad (2.27)$$

The system is linear if it is *additive*

$$T\{x_1[n] + x_2[n]\} = T\{x_1[n]\} + T\{x_2[n]\} \quad (2.28)$$

and *homogeneous (scalable)*

$$T\{ax[n]\} = aT\{x[n]\} \quad (2.29)$$

Additivity and homogeneity may be expressed in a single *principle of superposition*

$$T\{ax_1[n] + bx_2[n]\} = aT\{x_1[n]\} + bT\{x_2[n]\}. \quad (2.30)$$

A system is *stable* if and only if every bounded input sequence produces a bounded output sequence. The input $x[n]$ is bounded if there exists a fixed positive finite value B_x such that $|x[n]| \leq B_x < \infty, \forall n$.

Let us consider the output $y[n]$ of the LTI system for the input signal $x[n]$ represented as a shifted sum of scaled unite impulses (2.22)

$$y[n] = T\left\{\sum_{k=-\infty}^{\infty} x[k]\delta[n-k]\right\}. \quad (2.31)$$

In (2.31) the values of $x[k]$ are scaling coefficients of unite impulses. From the superposition property (2.30) we get

$$y[n] = \sum_{k=-\infty}^{\infty} x[k]T\{\delta[n-k]\} = \sum_{k=-\infty}^{\infty} x[k]h_k[n], \quad (2.32)$$

where $h_k[n] = T\{\delta[n-k]\}$ is the response of the system to shifted unite impulses $\delta[n-k]$. From the time-invariance property we have

$$\text{If } h[n] = T\{\delta[n]\} \text{ then } h[n-k] = T\{\delta[n-k]\}, \quad (2.33)$$

and (2.32) may be rewritten as

$$y[n] = \sum_{k=-\infty}^{\infty} x[k]h[n-k] = x[n] * h[n]. \quad (2.34)$$

Equation (2.34) is a *convolution sum*. LTI system is completely characterized by its impulse response $h[n]$.

Example 2.3

Convolution sum (2.34) is computed as follows:

- a) for the fixed n sum over k ,
- b) increase n , and go to a).

$$h[n] = [\dots, 0, h[1], h[2], h[3], 0, \dots] = [\dots, 0, 1, 3, 5, 0, \dots], \quad x[n] = [\dots, 0, x[1], x[2], x[3], 0, \dots] = [\dots, 0, 2, 4, 6, 0, \dots]$$

$$y[n] = \sum_{k=-\infty}^{\infty} x[k]h[n-k]$$

$$y[1] = \sum_{k=-\infty}^{\infty} x[k]h[1-k] = \dots, 0 + x[1]h[0] + x[2]h[-1] + x[3]h[-2] + 0, \dots = \dots, 0 + 2 \cdot 0 + 4 \cdot 0 + 6 \cdot 0 + 0, \dots = 0$$

$$y[2] = \sum_{k=-\infty}^{\infty} x[k]h[2-k] = \dots, 0 + x[1]h[1] + x[2]h[0] + x[3]h[-1] + 0, \dots = \dots, 0 + 2 \cdot 1 + 4 \cdot 0 + 6 \cdot 0 + 0, \dots = 2$$

$$y[3] = \sum_{k=-\infty}^{\infty} x[k]h[3-k] = \dots, 0 + x[1]h[2] + x[2]h[1] + x[3]h[0] + 0, \dots = \dots, 0 + 2 \cdot 3 + 4 \cdot 1 + 6 \cdot 0 + 0, \dots = 10$$

$$y[4] = \sum_{k=-\infty}^{\infty} x[k]h[4-k] = \dots, 0 + x[1]h[3] + x[2]h[2] + x[3]h[1] + 0, \dots = \dots, 0 + 2 \cdot 5 + 4 \cdot 3 + 6 \cdot 1 + 0, \dots = 28$$

$$y[5] = \sum_{k=-\infty}^{\infty} x[k]h[5-k] = \dots, 0 + x[1]h[4] + x[2]h[3] + x[3]h[2] + 0, \dots = \dots, 0 + 2 \cdot 0 + 4 \cdot 5 + 6 \cdot 3 + 0, \dots = 38$$

$$y[6] = \sum_{k=-\infty}^{\infty} x[k]h[6-k] = \dots, 0 + x[1]h[5] + x[2]h[4] + x[3]h[3] + 0, \dots = \dots, 0 + 2 \cdot 0 + 4 \cdot 0 + 6 \cdot 5 + 0, \dots = 30$$

$$y[n] = x[n] * h[n] = [\dots, 0, 2, 10, 28, 38, 30, 0, \dots]$$

$$\begin{array}{r} h[-n] = [\dots, 0, 5, 3, \boxed{1}, 0, \dots] \\ x[n] = [\dots, 0, \boxed{2}, 4, 6, 0, \dots] \\ \hline y[1] = 1 \cdot 2 = 2 \end{array}$$

$$\begin{array}{r} h[-n] = [\dots, 0, 5, 3, \boxed{1}, 0, \dots] \\ x[n] = [\dots, 0, \boxed{2}, 4, 6, 0, \dots] \\ \hline y[2] = 3 \cdot 2 + 1 \cdot 4 = 10 \end{array}$$

$$\begin{array}{r} h[-n] = [\dots, 0, \boxed{5}, 3, \boxed{1}, 0, \dots] \\ x[n] = [\dots, 0, \boxed{2}, 4, 6, 0, \dots] \\ \hline y[3] = 5 \cdot 2 + 3 \cdot 4 + 1 \cdot 6 = 28 \end{array}$$

$$\begin{array}{r} h[-n] = [\dots, 0, \boxed{5}, 3, \boxed{1}, 0, \dots], \\ x[n] = [\dots, 0, \boxed{2}, 4, 6, 0, \dots] \\ \hline y[4] = 5 \cdot 4 + 3 \cdot 6 = 38 \end{array}$$

$$\begin{array}{r} h[-n] = [\dots, 0, \boxed{5}, 3, \boxed{1}, 0, \dots], \\ x[n] = [\dots, 0, \boxed{2}, 4, 6, 0, \dots] \\ \hline y[5] = 5 \cdot 6 = 30 \end{array}$$

Fig.2.10 Computing convolution sum.

One of the signals is time reversed, next signals are shifted along each other, multiplied, and summed.

It is observed in the [Example 2.3](#) that the number of nonzero samples N_y in output signal $y[n]$ equals to the sum of number of nonzero samples N_x in signal $x[n]$, and N_h in $h[n]$ minus 1, that is

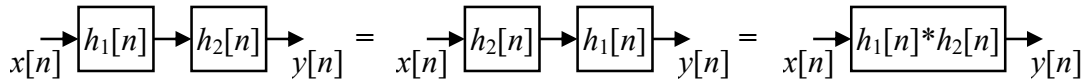
$$N_y = N_x + N_h - 1, \quad (2.35)$$

Convolution sum [\(2.34\)](#) may be interpreted as a polynomial multiplication. In the [Example 2.3](#) if the vectors $x[n]=[2, 4, 6]$ and $h[n]=[1, 3, 5]$ represent polynomials coefficients with decreasing power of variable, then the convolution sum $y[n]=x[n]*h[n]=[2, 10, 28, 38, 30]$ represents coefficients of the product polynomial, i.e. if $y_x(x)=2x^2+4x+6$ and $y_h(x)=x^2+3x+5$ then $y_y(x)=y_x(x)y_h(x)=2x^4+10x^3+28x^2+38x+30$.

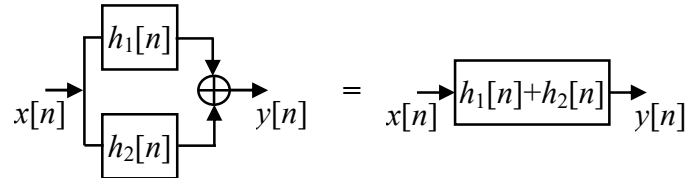
Discrete-time LTI systems have the following properties (the same as continuous-time LTI systems [\(1.25\)-\(1.27\)](#)):

1. Commutativity: $x[n]*h[n] = h[n]*x[n]$ (2.36)

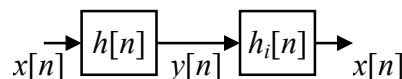
2. Associativity (cascade connection) $x[n]*(h_1[n]*h_2[n]) = (x[n]*h_1[n])*h_2[n]$ (2.37)



3. Distributivity (parallel connection) $x[n]*(h_1[n]+h_2[n]) = x[n]*h_1[n] + x[n]*h_2[n]$ (2.38)



4. Inverse system $h_i[n]$ (if exists) $h[n]*h_i[n] = \delta[n]$ (2.39)



Similarly as for continuous-time systems, let us now consider discrete-time LTI system with an impulse response $h[n]$ for an input signal being complex exponential signal $x[n] = e^{j\omega_0 n}$ (2.5). The output of this system is given by convolution sum (2.34)

$$y[n] = \sum_{k=-\infty}^{\infty} h[k] e^{j\omega_0(n-k)} = e^{j\omega_0 n} \left(\sum_{k=-\infty}^{\infty} h[k] e^{-j\omega_0 k} \right) = e^{j\omega_0 n} H(e^{j\omega_0}). \quad (2.40)$$

It is seen from (2.40) that the output of LTI system to the complex sinusoidal input signal is the complex sinusoidal signal with the same frequency multiplied by a complex number $H(e^{j\omega_0})$, i.e. the amplitude and phase of the complex sinusoidal output signal may be changed (but not frequency). The complex valued function $H(e^{j\omega})$ is the *frequency response* of an LTI system, and it may be represented as

$$H(e^{j\omega}) = \operatorname{Re}\{H(e^{j\omega})\} + j \operatorname{Im}\{H(e^{j\omega})\} = |H(e^{j\omega})| e^{j \arg\{|H(e^{j\omega})|\}}, \quad (2.41)$$

where $|H(e^{j\omega})|$ is a frequency-magnitude, or simple magnitude response, and $\arg\{|H(e^{j\omega})|\}$ is frequency-phase, or simply phase response.

Frequency response of discrete-time LTI system is periodic with the period 2π rad

$$H(e^{j(\omega+2\pi)}) = \sum_{k=-\infty}^{\infty} h[k] e^{-j(\omega+2\pi)k} = \sum_{k=-\infty}^{\infty} h[k] e^{-j\omega k} e^{-j2\pi k} = H(e^{j\omega}), \quad (2.42)$$

thus it is enough to compute $|H(e^{j\omega})|$ over one period.

2.2.2 Linear Constant-Coefficient Difference Equation

LTI system is fully described by impulse response $h[n]$. The output $y[n]$ of LTI system is the convolution sum (2.34) of the input $x[n]$ and the impulse response $h[n]$. In practice discrete-time systems have a structure presented in Fig. 2.11, where $b[n]$ and $a[n]$ are vectors of length $M+1$ and $N+1$, respectively.

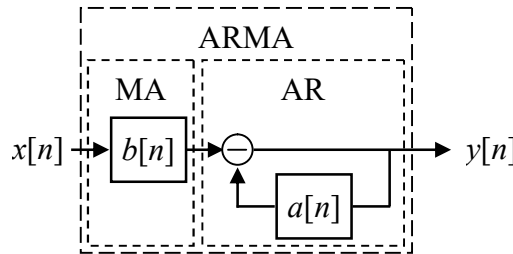


Fig.2.11 The structure of discrete-time systems.

MA	Moving Average FIR system
AR	Autoregressive IIR system
ARMA	Autoregressive Moving Average IIR system

For the system shown in Fig. 2.11 the input $x[n]$ and the output $y[n]$ satisfy N th-order linear constant coefficients difference equation

$$\boxed{\sum_{k=0}^N a[k]y[n-k] = \sum_{m=0}^M b[m]x[n-m].} \quad (2.43)$$

Difference equation (2.43) is a counterpart of differential equation (1.32) for continuous-time systems. By excluding $y[n]a[0]$ from the left sum in (2.43) we get the relation for the current output sample

$$y[n] = \sum_{m=0}^M \frac{b[m]}{a[0]} x[n-m] - \sum_{k=1}^N \frac{a[k]}{a[0]} y[n-k] \quad (2.44)$$

that depends on the current and the previous inputs $x[n]$, $x[n-1], \dots, x[n-M]$, and previous outputs $y[n-1], \dots, y[n-N]$.

The discrete-time system described by (2.43) is LTI system and causal system, if it is initially at rest, i.e. if $x[n]=0$ then $y[n]=0$ for $n < n_0$.

The vector $a[n]$ in (2.43) and Fig.2.11 represents *negative feedback* in the system. As the current output depends on previous outputs the impulse response may be of infinite length; thus the system is called *Infinite Impulse Response* (IIR).

Without negative feedback (2.43) reduces to convolution sum $y[n] = \sum_{k=-\infty}^{\infty} x[k]h[n-k] = x[n]*h[n]$ (2.34), then the impulse response is finite and equals $b[n]$, and the system is called *Finite Impulse Response* (FIR).

2.3 Fourier analysis

2.3.1 The Discrete Time Fourier Transform

The Inverse Discrete Time Fourier Transform (synthesis) is defined as

$$x[n] = \frac{1}{2\pi} \int_{-\pi}^{\pi} X(e^{j\omega}) e^{j\omega n} d\omega. \quad (2.45)$$

The Discrete Time Fourier Transform (analysis) is defined as

$$X(e^{j\omega}) = \sum_{n=-\infty}^{\infty} x[n] e^{-j\omega n}. \quad (2.46)$$

To show that (2.45) and (2.46) are the pair of inverse transforms let us put $X(e^{j\omega})$ into (2.45)

$$x[n] = \frac{1}{2\pi} \int_{-\pi}^{\pi} \left(\sum_{m=-\infty}^{\infty} x[m] e^{-j\omega m} \right) e^{j\omega n} d\omega = \sum_{m=-\infty}^{\infty} x[m] \left(\frac{1}{2\pi} \int_{-\pi}^{\pi} e^{j\omega(n-m)} d\omega \right). \quad (2.47)$$

Basis functions $e^{j\omega n}$ are orthogonal and the integral in the bracket equals

$$\frac{1}{2\pi} \int_{-\pi}^{\pi} e^{j\omega(n-m)} d\omega = \frac{\sin(\pi(n-m))}{\pi(n-m)} = \begin{cases} 1, & m=n \\ 0, & m \neq n \end{cases} = \delta[n-m], \quad (2.48)$$

finally we get

$$x[n] = \sum_{m=-\infty}^{\infty} x[m] \delta[n-m] = x[n]. \quad (2.49)$$

Synthesis equation (2.45) represents a discrete-time signal $x[n]$ as a weighted sum (integral) of complex exponentials. The complex weights $X(e^{j\omega})$ are called *the spectrum of the signal* $x[n]$. Frequency ω in radians is continuous variable, thus the spectrum $X(e^{j\omega})$ of discrete-time signal is continuous. The spectrum $X(e^{j\omega})$ is periodic with the period 2π rad. The complex spectrum $X(e^{j\omega})$ is often represented by magnitude $|X(e^{j\omega})|$ and phase $\arg\{X(e^{j\omega})\}$ characteristics

$$X(e^{j\omega}) = \operatorname{Re}\{X(e^{j\omega})\} + j \operatorname{Im}\{X(e^{j\omega})\} = |X(e^{j\omega})| e^{j \arg\{X(e^{j\omega})\}}. \quad (2.50)$$

Phase characteristic $\arg\{X(e^{j\omega})\}$ is not unique because $\arg\{\exp(j\varphi)\} = \arg\{\exp(j(\varphi \pm 2\pi))\}$.

By comparing (2.40) with (2.46) it is seen that the frequency response $H(e^{j\omega})$ of LTI system is the Fourier transform of its impulse response $h[n]$

$$H(e^{j\omega}) = \sum_{n=-\infty}^{\infty} h[n] e^{-j\omega n}. \quad (2.51)$$

The Fourier transform exists for all signals for which infinite sum in (2.46) is convergent. A sufficient condition for convergence is *absolute summability* of $x[n]$

$$|X(e^{j\omega})| = \left| \sum_{n=-\infty}^{\infty} x[n] e^{-j\omega n} \right| \leq \sum_{n=-\infty}^{\infty} |x[n]| \|e^{-j\omega n}\| \leq \sum_{n=-\infty}^{\infty} |x[n]| < \infty. \quad (2.52)$$

Since a stable sequence is, by definition, absolutely summable, all stable sequences have Fourier transforms; also any stable system has a finite and continuous frequency response.

Some signals are not absolutely summable but are square summable, i.e.

$$\lim_{M \rightarrow \infty} \int_{-\pi}^{\pi} |X(e^{j\omega}) - X_M(e^{j\omega})|^2 d\omega = 0, \quad (2.53)$$

where $X(e^{j\omega})$ is an ideal frequency characteristic, e.g. rectangular pulse, and $X_M(e^{j\omega}) = \sum_{n=-M}^M x[n] e^{-j\omega n}$ is its approximation (see for example the case of ideal lowpass filter explained in chapter 2.4.3). Convergence in the mean-square sense (2.53) means that as $M \rightarrow \infty$ the aptitude of oscillations of $X(e^{j\omega}) - X_M(e^{j\omega})$ may remain the same (Gibbs phenomenon), but the energy of those oscillations decay to zero.

Example 2.4

Infinite length constant sequence $x[n]=1$, $-\infty < n < \infty$ is neither absolutely summable nor square summable. Fourier transform of infinite length constant sequence is the periodic impulse train

$$X(e^{j\omega}) = \sum_{r=-\infty}^{\infty} 2\pi\delta(\omega + 2\pi r). \quad (2.54)$$

It is straightforward to verify that by putting (2.54) into definition (2.45) we get the desired result

$$x[n] = \frac{1}{2\pi} \int_{-\pi}^{\pi} \sum_{r=-\infty}^{\infty} 2\pi\delta(\omega + 2\pi r) e^{j\omega n} d\omega = 1. \quad (2.55)$$

To compute the Fourier transform of a finite length constant signal $x_M[n]=1$, $-M \leq n \leq M$ we use the DTFT definition (2.46)

$$X_M(e^{j\omega}) = \sum_{n=-M}^M e^{-j\omega n}. \quad (2.56)$$

and observe that (2.56) is a sum of terms in geometric (power) series that for the first N terms

equals $\sum_{n=0}^{N-1} a^n = \begin{cases} N, & a=0 \\ \frac{1-a^N}{1-a}, & a \neq 0 \end{cases}$. To apply this closed form formula we rewrite (2.56)

$$X_M(e^{j\omega}) = \sum_{n=-M}^M e^{-j\omega n} = \sum_{n=0}^{2M} e^{-j\omega(n-M)} = e^{j\omega M} \sum_{n=0}^{2M} e^{-j\omega n} = e^{j\omega M} \frac{1 - e^{-j\omega(2M+1)}}{1 - e^{-j\omega}} = \frac{e^{j\omega(2M+1)/2} - e^{-j\omega(2M+1)/2}}{e^{j\omega/2} - e^{-j\omega/2}} = \frac{\sin(\omega(2M+1)/2)}{\sin(\omega/2)}, \omega \neq 0, \quad (2.57)$$

and for $\omega=0$ $X_M(e^{j\omega})=2M+1$.

Jawna postać szeregu geometrycznego

W literaturze cyfrowego przetwarzania sygnałów często napotykamy takie wyrażenia dla szeregu geometrycznego jak

$$\sum_{n=p}^{N-1} r^n = \frac{r^p - r^N}{1-r} \quad (\text{B.1})$$

$$\sum_{n=0}^{N-1} e^{-j2\pi nm/N} = \frac{1 - e^{-j2\pi m}}{1 - e^{-j2\pi nm/N}} \quad (\text{B.2})$$

Niestety, wielu autorów czyni takie stwierdzenie, jak „i wiemy, że”, a następnie obdarza równaniami (B.1) lub (B.2) nic nie podejrzewającego Czytelnika, od którego oczekuje się, że przyjmie te wyrażenia na wiarę. Możemy się zastanawiać, w jaki sposób można otrzymać równania (B.1) lub (B.2). Aby odpowiedzieć na to pytanie, rozważmy wyrażenie ogólne dla szeregu geometrycznego, takiego jak

$$S = \sum_{n=p}^{N-1} ar^n = ar^p + ar^{p+1} + ar^{p+2} + \dots + ar^{N-1} \quad (\text{B.3})$$

gdzie N , N i p są liczbami całkowitymi, a i r są zaś dowolnymi stałymi. Przemnożenie równania (B.3) przez r daje

$$Sr = \sum_{n=p}^{N-1} ar^{n+1} = ar^{p+1} + ar^{p+2} + \dots + ar^{N-1} + ar^N \quad (\text{B.4})$$

Odjęcie równania (B.4) od równania (B.3) daje wyrażenie

$$S - Sr = S(1 - r) = ar^p - ar^N$$

lub

$$S = a \cdot \frac{r^p - r^N}{1 - r} \quad (\text{B.5})$$

I oto mamy to, co chcieliśmy osiągnąć. *Jawna postać* tego szeregu, to

Jawna postać ogólnego szeregu geometrycznego:

$$\sum_{n=p}^{N-1} ar^n = a \cdot \frac{r^p - r^N}{1 - r} \quad (\text{B.6})$$

(Przez jawną postać mamy na myśli rozważenie szeregu nieskończonego i przetworzenie go w prostszą postać matematyczną bez sumowania.) Jeśli $a = 1$, to równanie (B.6) staje się równaniem (B.1). Możemy szybko sprawdzić równanie (B.6) na przykładzie. Przyjmując, przykładowo, $N = 5$, $p = 0$, $a = 2$ i $r = 3$ możemy utworzyć następującą listę:

n	$ar^n = 2 \cdot 3^n$
0	$2 \cdot 3^0 = 2$
1	$2 \cdot 3^1 = 6$
2	$2 \cdot 3^2 = 18$
3	$2 \cdot 3^3 = 54$
4	$2 \cdot 3^4 = 162$
Sumą tej kolumny jest	
	$\sum_{n=0}^4 2 \cdot 3^n = 242$

Wstawiając wartości N , p , a i r z naszego przykładu do równania (B.6), otrzymujemy wartość

$$\sum_{n=p}^{N-1} ar^n = a \cdot \frac{r^p - r^N}{1 - r} = 2 \cdot \frac{3^0 - 3^5}{1 - 3} = 2 \cdot \frac{1 - 243}{-2} = 242 \quad (\text{B.7})$$

która jest równa sumie w prawej kolumnie listy.

W końcu, wyrażenia we wcześniejszym równaniu (B.2) odpowiadają przyjęciu $p = 0$, $a = 1$ i $r = e^{-j2\pi m/N}$ w równaniu (B.6)¹⁾. Zatem wstawienie tych członów z równania (B.2) do równania (B.6) daje nam

$$\sum_{n=0}^{N-1} e^{-j2\pi nm/N} = 1 \cdot \frac{e^{-j2\pi m0/N} - e^{-j2\pi mN/N}}{1 - e^{-j2\pi m/N}} = \frac{1 - e^{-j2\pi m}}{1 - e^{-j2\pi m/N}} \quad (\text{B.8})$$

potwierdzając prawdziwość równania (B.2).

¹⁾ Na podstawie tożsamości $a^{xy} = (a^x)^y$, możemy powiedzieć, że $e^{-j2\pi nm/N} = (e^{-j2\pi m/N})^n$, zatem $r = e^{-j2\pi m/N}$.

Exemplary magnitude plots of (2.57) are shown in Fig. 2.12 for two constant discrete-time signals with length 7 ($M=3$), and 31 ($M=15$) samples. In the spectra so called *mainlobes* and *side-lobes* are observed. Mainlobes occur in the frequencies $k2\pi$ rad, $k=\dots,-1,0,1,\dots$. The height of the mainlobes equals the sum of all samples in $x[n]$, which in general is always the case for $\omega_0=0+k2\pi$ rad. The width of the mainlobes decreases as the length of the sequence increases. Maximum amplitude of side-lobes does not depend on the length of the sequence. The spectrum is periodic with the period 2π rad.

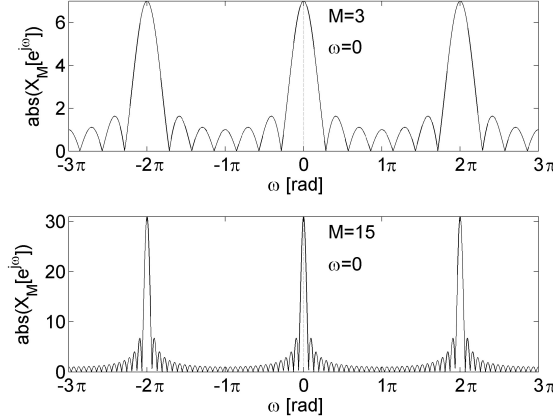


Fig.2.12 Fourier transforms of finite length constant signal $x_M[n]=1$, $-M \leq n \leq M$.

Example 2.5

Let us consider a sequence $x[n]$ with the following Fourier transform

$$X(e^{j\omega}) = \sum_{r=-\infty}^{\infty} 2\pi\delta(\omega - \omega_0 + 2\pi r). \quad (2.58)$$

Using the inverse Fourier transform we find out that $x[n]$ is a infinite length complex exponential

$$x[n] = \frac{1}{2\pi} \int_{-\pi}^{\pi} X(e^{j\omega}) e^{j\omega n} d\omega = \frac{1}{2\pi} \int_{-\pi}^{\pi} 2\pi\delta(\omega - \omega_0) e^{j\omega n} d\omega = e^{j\omega_0 n}, \quad -\infty < n < \infty, \quad (2.59)$$

For $\omega_0=0$ (2.59) simplifies to infinite length constant sequence.

Fourier transform of finite length exponential signal $x_M[n]=e^{j\omega_0 n}$, $-M \leq n \leq M$ is computed similarly as (2.57)

$$X_M(e^{j\omega}) = \sum_{n=-M}^M e^{j\omega_0 n} e^{-j\omega n} = \sum_{n=-M}^M e^{-j(\omega-\omega_0)n} = \frac{\sin((\omega-\omega_0)(2M+1)/2)}{\sin((\omega-\omega_0)/2)}, \quad \omega \neq \omega_0, \quad (2.60)$$

and for $\omega=\omega_0$ $X_M(e^{j\omega})=2M+1$. Exemplary magnitude plots of (2.60) are depicted in Fig.2.13. Comparing to Fig.2.12 mainlobes in Fig.2.13 are placed in frequencies $\omega_0=1+k2\pi$ rad.

The Fourier transform of finite length sinusoidal signal $x_M[n] = \cos(\omega_0 n) = \frac{1}{2}e^{j\omega_0 n} + \frac{1}{2}e^{-j\omega_0 n}$, $-M \leq n \leq M$ is

$$X_M(e^{j\omega}) = \begin{cases} \frac{1}{2} \frac{\sin((\omega - \omega_0)(2M+1)/2)}{\sin((\omega - \omega_0)/2)} + \frac{1}{2} \frac{\sin((\omega + \omega_0)(2M+1)/2)}{\sin((\omega + \omega_0)/2)}, & \omega \neq \omega_0, \omega \neq -\omega_0 \\ \frac{2M+1}{2} + \frac{1}{2} \frac{\sin((\omega_0(2M+1))}{\sin(\omega_0)}, & \text{otherwise} \end{cases}. \quad (2.61)$$

Exemplary magnitude plots of (2.61) are depicted in Fig.2.14. Comparing to Fig.2.13 there are two mainlobes in one period in Fig.2.14 placed in frequencies $\omega_0 = \pm 1 + k2\pi$ rad. The spectrum of complex signal is *one-sided*, and the spectrum of real signal is *two-sided*. The height of the mainlobe in case of real value sinusoid is two times lower than in the case of complex exponential.

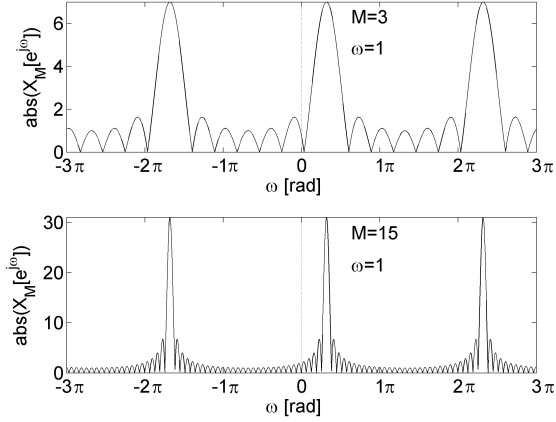


Fig.2.13 Fourier transforms of finite length complex exponential signal $x_M[n] = e^{j\omega_0 n}$, $-M \leq n \leq M$.

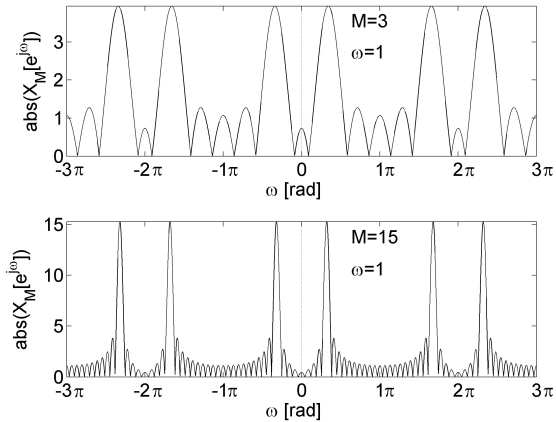


Fig.2.14 Fourier transforms of finite length sinusoidal signal $x_M[n] = \cos(\omega_0 n)$, $-M \leq n \leq M$.

Table 2.4 Fourier transform pairs.

$$x[n] = \quad X(e^{j\omega}) =$$

$$\delta[n] \quad 1 \quad (2.62)$$

$$\delta[n - n_0] \quad e^{-j\omega n_0} \quad (2.63)$$

$$1, \quad (-\infty < n < \infty) \quad \sum_{k=-\infty}^{\infty} 2\pi\delta(\omega + 2\pi k) \quad (2.64)$$

$$\boxed{\frac{\sin(\omega_c n)}{\pi n}} \quad \boxed{\begin{cases} 1, & |\omega| < \omega_c \\ 0, & \omega_c < |\omega| \leq \pi \end{cases}} \quad (2.65)$$

$$\boxed{\begin{cases} 1, & 0 \leq n \leq N \\ 0, & \text{otherwise} \end{cases}} \quad \boxed{\frac{\sin(\omega \cdot (N+1)/2)}{\sin(\omega/2)} e^{-j\omega N/2}} \quad (2.66)$$

$$e^{j\omega_0 n} \quad \sum_{k=-\infty}^{\omega} 2\pi\delta(\omega - \omega_0 + 2\pi k) \quad (2.67)$$

$$\boxed{\cos(\omega_0 n + \phi)} \quad \boxed{\sum_{k=-\infty}^{\infty} [\pi e^{j\phi} \delta(\omega - \omega_0 + 2\pi k) + \pi e^{-j\phi} \delta(\omega + \omega_0 + 2\pi k)]} \quad (2.68)$$

$$a^n u[n], \quad |a| < 1 \quad \frac{1}{1 - ae^{-j\omega}} \quad (2.69)$$

$$u[n] \quad \frac{1}{1 - e^{-j\omega}} + \sum_{k=-\infty}^{\infty} \pi\delta(\omega + 2\pi k) \quad (2.70)$$

The Fourier transform of unite impulse is constant (2.62), thus the spectrum of the unite impulse contains sinusoids with all frequencies. For LTI systems frequency response $H(e^{j\omega})$ is the Fourier transform of impulse response $h[n]$.

(2.65) is an impulse response of lowpass filter and its frequency response, and (2.66) is rectangular window and its frequency response.

Table 2.5 Fourier transform symmetries.

Complex signal

$$x^*[n] \quad X^*(e^{-j\omega}) \quad (2.71)$$

$$x^*[-n] \quad X^*(e^{j\omega}) \quad (2.72)$$

$$\operatorname{Re}\{x[n]\} \quad X_e(e^{-j\omega}) \quad (2.73)$$

$$j \operatorname{Im}\{x[n]\} \quad X_o(e^{-j\omega}) \quad (2.74)$$

$$x_e[n] \quad X_R(e^{j\omega}) = \operatorname{Re}\{X(e^{j\omega})\} \quad (2.75)$$

$$x_o[n] \quad jX_I(e^{j\omega}) = j \operatorname{Im}\{X(e^{j\omega})\} \quad (2.76)$$

Real signal

$$X(e^{j\omega}) = X^*(e^{-j\omega}), \text{ FT is conjugate symmetric} \quad (2.77)$$

$$X_R(e^{j\omega}) = X_R(e^{-j\omega}), \text{ real part is even} \quad (2.78)$$

$$X_I(e^{j\omega}) = -X_I(e^{-j\omega}), \text{ imaginary part is odd} \quad (2.79)$$

$$|X(e^{j\omega})| = |X(e^{-j\omega})|, \text{ magnitude is even} \quad (2.80)$$

$$\arg\{X(e^{j\omega})\} = -\arg\{X(e^{-j\omega})\}, \text{ phase is odd} \quad (2.81)$$

Fourier transform symmetries are illustrated in Fig.2.15 for real signal $x[n]=1$, $n=0,1,2,\dots,6$.

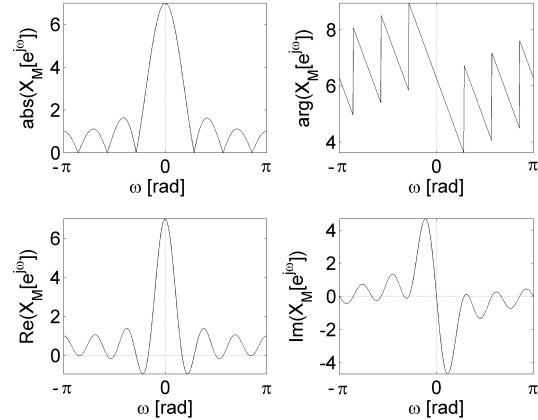


Fig. 2.15 Fourier transform symmetries for real signal $x[n]=1$, $n=0,1,2,\dots,6$.

Table 2.6 Fourier transform theorems.

sequence	Fourier transform	
$ax[n] + by[n]$	$aX(e^{j\omega}) + bY(e^{j\omega})$, linearity	(2.82)
$x[n - n_d]$	$e^{-j\omega n_d} X(e^{j\omega})$, time shifting	(2.83)
$e^{j\omega_0 n} x[n]$	$X(e^{j(\omega-\omega_0)})$, frequency shifting	(2.84)
$x[-n]$	$X(e^{-j\omega})$ $X^*(e^{j\omega})$ if $x[n]$ real	, time reversal (2.85)
$nx[n]$	$j \frac{dX(e^{j\omega})}{d\omega}$, differentiation in frequency	(2.86)
$x[n] * y[n]$	$X(e^{j\omega})Y(e^{j\omega})$, the convolution theorem	(2.87)
$x[n] \cdot y[n]$	$\frac{1}{2\pi} \int_{-\pi}^{\pi} X(e^{j\Theta})Y(e^{j(\omega-\Theta)}) d\Theta$, the modulation or windowing theorem	(2.88)

Fourier transform preserves the energy

$$\sum_{n=-\infty}^{\infty} |x[n]|^2 = \frac{1}{2\pi} \int_{-\pi}^{\pi} |X(e^{j\omega})|^2 d\omega, \quad (2.89)$$

where $|X(e^{j\omega})|^2$ is called the energy density spectrum.

Example 2.6

To prove the convolution theorem (2.87) we compute from the definition (2.46) the Fourier transform of convolution sum (2.34)

$$\sum_{n=-\infty}^{\infty} \left(\sum_{k=-\infty}^{\infty} x[k]h[n-k] \right) e^{-j\omega n} = \sum_{k=-\infty}^{\infty} x[k] \sum_{n=-\infty}^{\infty} h[n-k] e^{-j\omega n}. \quad (2.90)$$

The change of summation order in (2.90) is easy to observe when we write down a few terms

$$\begin{aligned} & \vdots \\ & \dots x[k_{-1}]h[n_{-1}+1]e^{j\omega n_{-1}} + x[k_0]h[n_{-1}+0]e^{j\omega n_{-1}} + x[k_1]h[n_{-1}-1]e^{j\omega n_{-1}} \dots \\ & \dots x[k_{-1}]h[n_0+1]e^{j\omega n_0} + x[k_0]h[n_0+0]e^{j\omega n_0} + x[k_1]h[n_0-1]e^{j\omega n_0} \dots \\ & \dots x[k_{-1}]h[n_1+1]e^{j\omega n_1} + x[k_0]h[n_1+0]e^{j\omega n_1} + x[k_1]h[n_1-1]e^{j\omega n_1} \dots \\ & \vdots \end{aligned} \quad (2.91)$$

The left hand part of (2.90) is summation of (2.91) along rows (constant n) whereas the right hand side of (2.90) is summation of (2.91) along columns. By changing the index to $m=n-k$ we have the final result

$$\sum_{k=-\infty}^{\infty} x[k] \sum_{m=-\infty}^{\infty} h[m] e^{-j\omega(k+m)} = \sum_{k=-\infty}^{\infty} x[k] e^{-j\omega k} \sum_{m=-\infty}^{\infty} h[m] e^{-j\omega m} = X(e^{j\omega})H(e^{j\omega}), \quad (2.92)$$

i.e. the spectrum of the convolution sum $x[n]*h[n]$ is the product of spectra $X(e^{j\omega})H(e^{j\omega})$.

2.3.2 The Discrete Fourier Transform

Let us consider infinite length, periodic with period N , discrete-time signal $\tilde{x}[n] = \tilde{x}[n+rN]$ for any integer n, r . Fundamental frequency of $\tilde{x}[n]$ is $\omega=2\pi/N$ rad. Fourier series representation (1.42) of $\tilde{x}[n]$ is

$$\tilde{x}[n] = \frac{1}{N} \sum_{k=-\infty}^{+\infty} \tilde{X}[k] e^{j \frac{2\pi}{N} kn}. \quad (2.93)$$

In (2.93) $\tilde{X}[k]$ are the *discrete Fourier series coefficients*. The multiplicative constant $1/N$ will be explained later, see (2.98).

The Fourier series representation of continuous-time signal generally requires infinitely many harmonically related complex exponentials, whereas the discrete Fourier series for any discrete-time signal with period N requires only N harmonically related complex exponentials, because discrete-time exponentials in (2.93) are periodic in k with period N

$$e^{j(2\pi/N)(k+lN)n} = e^{j(2\pi/N)kn} e^{j2\pi ln} = e^{j(2\pi/N)kn}, l - \text{integer}. \quad (2.94)$$

Considering (2.94) it is sufficient to sum in (2.93) for N successive values of k , e.g. for $k=0, 1, \dots, N-1$

$$\tilde{x}[n] = \frac{1}{N} \sum_{k=0}^{N-1} \tilde{X}[k] e^{j \frac{2\pi}{N} kn}. \quad (2.95)$$

To find discrete Fourier series coefficients $\tilde{X}[k]$ let us multiply both sides of (2.95) by $e^{-j \frac{2\pi}{N} rn}$ and sum from $n=0$ do $n=N-1$

$$\sum_{n=0}^{N-1} \tilde{x}[n] e^{-j \frac{2\pi}{N} rn} = \sum_{n=0}^{N-1} \frac{1}{N} \sum_{k=0}^{N-1} \tilde{X}[k] e^{j \frac{2\pi}{N} (k-r)n}. \quad (2.96)$$

After changing the order of summation we get

$$\sum_{n=0}^{N-1} \tilde{x}[n] e^{-j \frac{2\pi}{N} rn} = \sum_{k=0}^{N-1} \tilde{X}[k] \left(\frac{1}{N} \sum_{n=0}^{N-1} e^{j \frac{2\pi}{N} (k-r)n} \right). \quad (2.97)$$

The sum in the right side bracket is

$$\frac{1}{N} \sum_{n=0}^{N-1} e^{j \frac{2\pi}{N} (k-r)n} = \begin{cases} 1, & k-r = mN, \quad m - \text{an integer} \\ 0, & \text{otherwise} \end{cases}. \quad (2.98)$$

Equation (2.98) is illustrated in Fig. 2.16.

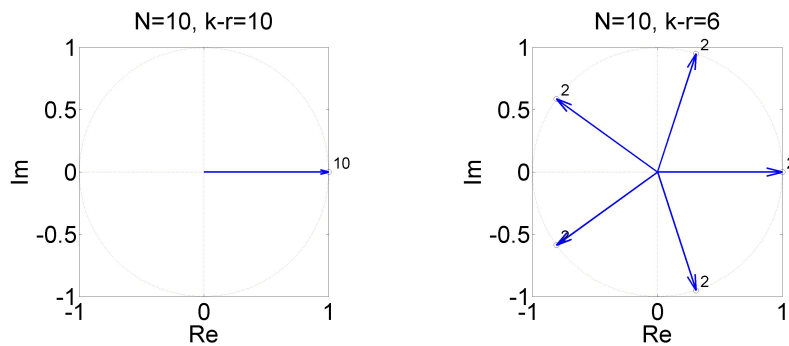


Fig. 2.16 Illustration of (2.98).

Equation (2.97) may be rewritten as

$$\sum_{n=0}^{N-1} \tilde{x}[n] e^{-j \frac{2\pi}{N} rn} = \tilde{X}[r]. \quad (2.99)$$

Finally, discrete Fourier series coefficients are given by

$$\tilde{X}[k] = \sum_{n=0}^{N-1} \tilde{x}[n] e^{-j \frac{2\pi}{N} kn}. \quad (2.100)$$

The sequence $\tilde{X}[k]$ is periodic with period N

$$\tilde{X}[k+N] = \sum_{n=0}^{N-1} \tilde{x}[n] e^{-j \frac{2\pi}{N} (k+N)n} = \sum_{n=0}^{N-1} \tilde{x}[n] e^{-j \frac{2\pi}{N} kn} e^{-j 2\pi n} = \tilde{X}[k]. \quad (2.101)$$

Let us consider finite-duration sequence $x[n]$ of length N samples such that $x[n]=0$ outside the range $0 \leq n \leq N-1$. We may always define periodic sequence $\tilde{x}[n]$ in a way that $x[n]$ is one period of $\tilde{x}[n]$

$$\tilde{x}[n] = \sum_{r=-\infty}^{\infty} x[n-rN], \quad x[n] = \begin{cases} \tilde{x}[n], & 0 \leq n \leq N-1, \\ 0, & \text{otherwise} \end{cases}. \quad (2.102)$$

By computing discrete Fourier series $\tilde{X}[k]$ (2.100) of (2.102) and considering one period of $\tilde{X}[k]$ we get the *Discrete Fourier Transform* (DFT) analysis equation

$$X[k] = \sum_{n=0}^{N-1} x[n] e^{-j \frac{2\pi}{N} kn}, \quad k = 0, 1, \dots, N-1$$

(2.103)

The Inverse *Discrete Fourier Transform* (IDFT) synthesis equation is defined as

$$x[n] = \frac{1}{N} \sum_{k=0}^{N-1} X[k] e^{j \frac{2\pi}{N} kn}, \quad n = 0, 1, \dots, N-1.$$

(2.104)

DFT (2.103) is periodic with period N and the sequence $x[n]$ (2.104) is also assumed to be periodic with period N , therefore DFT and IDFT may be defined for arbitrary range of N successive indexes k and n , e.g.

$$X[k] = \sum_{n=-M}^{M-1} x[n] e^{-j \frac{2\pi}{N} kn}, \quad x[n] = \frac{1}{N} \sum_{k=-M}^{M-1} X[k] e^{j \frac{2\pi}{N} kn}, \quad N=2M \quad (2.105a)$$

$$X[k] = \sum_{n=-M}^M x[n] e^{-j \frac{2\pi}{N} kn}, \quad x[n] = \frac{1}{N} \sum_{k=-M}^M X[k] e^{j \frac{2\pi}{N} kn}, \quad N=2M+1 \quad (2.105b)$$

[Lyons04 p26]

Figure 3-12. Spectral replication when the DFT input is 3.4 cycles per sample interval.

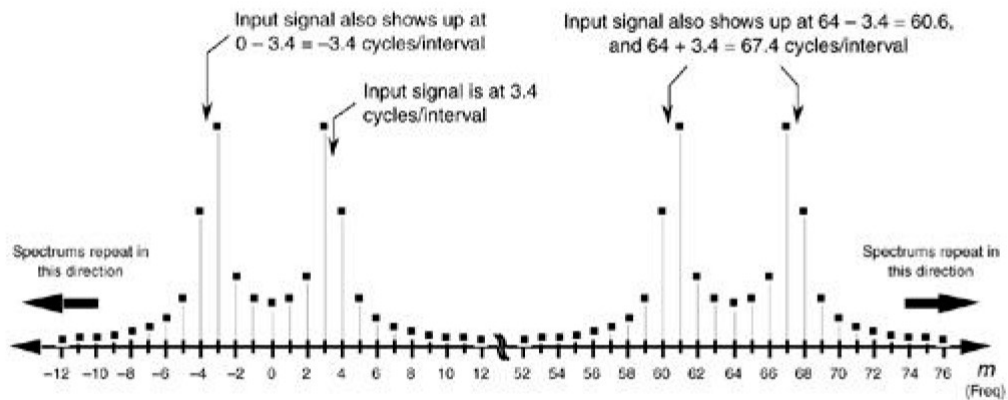
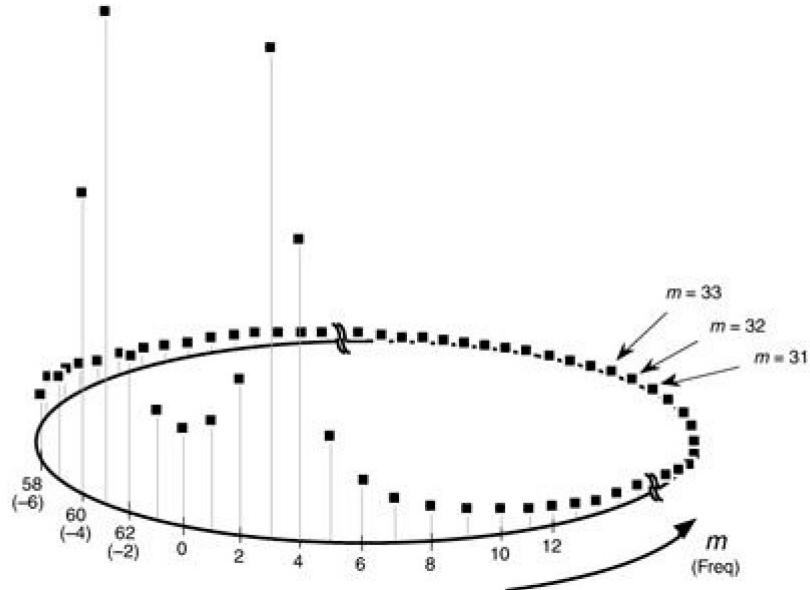


Figure 3-11. Cyclic representation of the DFT's spectral replication when the DFT input is 3.4 cycles per sample interval.



Example 2.7

The DFT (2.103) of $x[n]=[1,2,3,4]$ is $X[k]=[10, -2+j2, -2, -2-j2]$

$$X[0] = \sum_{n=0}^{4-1} x[n]e^{-j(2\pi/4)0n} = x[0] + x[1] + x[2] + x[3] = 10, \text{ for } k=0 \text{ we sum all samples in the sequence } x[n]$$

$$X[1] = \sum_{n=0}^3 x[n]e^{-j(2\pi/4)1n} = x[0]e^0 + x[1]e^{-j(2\pi/4)} + x[2]e^{-j(2\pi/4)2} + x[3]e^{-j(2\pi/4)3} = 1 - j2 - 3 + j4 = -2 + j2,$$

$$X[2] = \sum_{n=0}^3 x[n]e^{-j(2\pi/4)2n} = x[0]e^0 + x[1]e^{-j(2\pi/4)2} + x[2]e^{-j(2\pi/4)2\cdot2} + x[3]e^{-j(2\pi/4)2\cdot3} = 1 - 2 + 3 - 4 = -2,$$

$$X[3] = \sum_{n=0}^3 x[n]e^{-j(2\pi/4)3n} = x[0]e^0 + x[1]e^{-j(2\pi/4)3} + x[2]e^{-j(2\pi/4)3\cdot2} + x[3]e^{-j(2\pi/4)3\cdot3} = 1 + j2 - 3 - j4 = -2 - j2.$$

The DFT (2.103) in matrix form is

$$\begin{bmatrix} X[0] \\ X[1] \\ X[2] \\ X[3] \end{bmatrix} = \begin{bmatrix} 1 & 1 & 1 & 1 \\ 1 & -j & -1 & j \\ 1 & -1 & 1 & -1 \\ 1 & j & -1 & -j \end{bmatrix} \begin{bmatrix} x[0] \\ x[1] \\ x[2] \\ x[3] \end{bmatrix} = \begin{bmatrix} 10 \\ -2 + j2 \\ -2 \\ -2 - j2 \end{bmatrix}.$$

Computing DFT from definition (2.103) requires N^2 complex multiplications and $N(N-1)$ complex additions.

By comparing DTFT (2.46) $X(e^{j\omega}) = \sum_{n=-\infty}^{\infty} x[n]e^{-j\omega n}$ and DFT (2.103) $X[k] = \sum_{n=0}^{N-1} x[n]e^{-j\frac{2\pi}{N}kn}$

we see that DFT computes DTFT for frequencies $\omega_k = \frac{2\pi}{N}k$ rad, thus DFT samples continuous-frequency spectrum $X(e^{j\omega})$ of discrete-time signal $x[n]$ in frequencies ω_k , i.e. the frequency of DFT bin with index k is $\frac{2\pi}{N}k$ rad.

Fig. 2.17a depicts sequence $x[n]=\{1, 2, 3, 4\}$ and its DTFT and DFT. Basis functions of DTFT and DFT are shown in Fig. 2.17b. DFT bins are inner products of the sequence $x[n]$ and complex exponential basis functions.

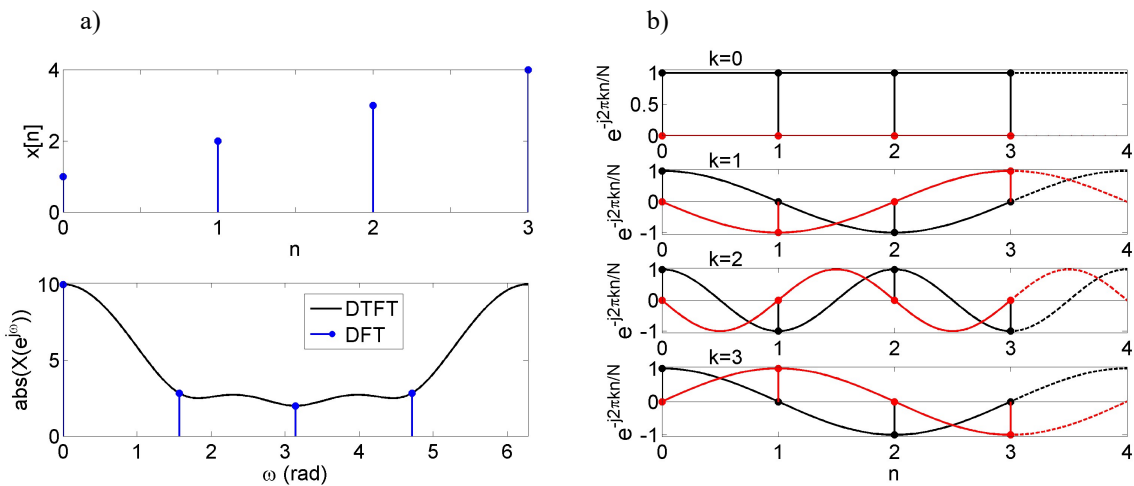


Fig. 2.17 a) Exemplary sequence $x[n]$ and DTFT and DFT of this sequence,
b) Complex exponential basis functions for $N=4$.

DFT has the property of *periodic convolution*. For finite-length sequences $x_1[n]$ and $x_2[n]$, both of length N , with DFTs $X_1[k]$ and $X_2[k]$, the sequence $x_3[n]$ with the DFT being a product $X_3[k]=X_1[k]X_2[k]$ is *circular convolution*

$$x_3[n] = \sum_{m=0}^{N-1} x_1[m]x_2[(n-m)_N], \quad n = 0, 1, \dots, N-1, \quad (2.106)$$

where $x_2[(n-m)_N]$ stands for circular shift explained in Fig. 2.18; or the DFT of circular convolution is the product of DFTs.

Table 2.7 Convolution property of DTFT and DFT.

DTFT - linear convolution	DFT - circular convolution
$y[n] = \sum_{k=-\infty}^{\infty} x[k]h[n-k], \quad Y(e^{j\omega}) = X(e^{j\omega})H(e^{j\omega})$	$x_3[n] = \sum_{m=0}^{N-1} x_1[m]x_2[(n-m)_N], \quad X_3[k] = X_1[k]X_2[k]$

Fig. 2.18 depicts circular shift of finite-length sequence $x[n]$ of length N . It is assumed that $x[n]$ is a one period of infinite periodic sequence $\tilde{x}[n]$. By shifting $\tilde{x}[n]$ to the right the samples at the end of period are removed, but at the same time at the beginning of the period the samples from the end of left neighboring period are placed.

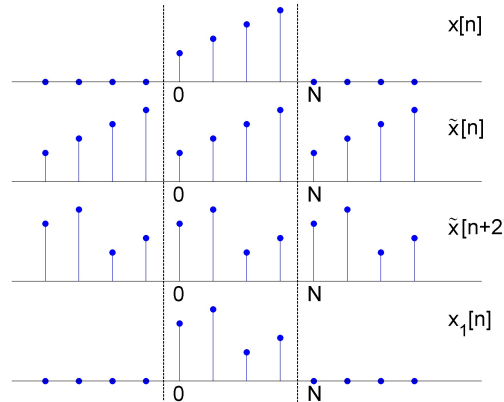


Fig. 2.18 Circular shift of finite-length sequence.

Circular convolution of two constant sequences is also constant sequence, see Fig. 2.19a, however if before computing circular convolution both sequences are extended by appending zeros, then the result of circular convolution may be equivalent to linear convolution as in Fig. 2.19a. One period of circular convolution is equivalent to linear convolution if finite-length sequences $x_1[n]$ and $x_2[n]$ with lengths N_1 and N_2 are extended by appending zeros to the length N_1+N_2-1 . As to sum up linear convolution may be computed by DFT in following steps:

1. Determine the lengths N_1 and N_2 of sequences $x_1[n]$ and $x_2[n]$,
2. Append zeros at the end of $x_1[n]$ and $x_2[n]$ to the length N_1+N_2-1 ,
3. Compute DFTs $X_1[k]$ and $X_2[k]$,
4. Compute inverse DFT of the product $X_1[k]X_2[k]$.

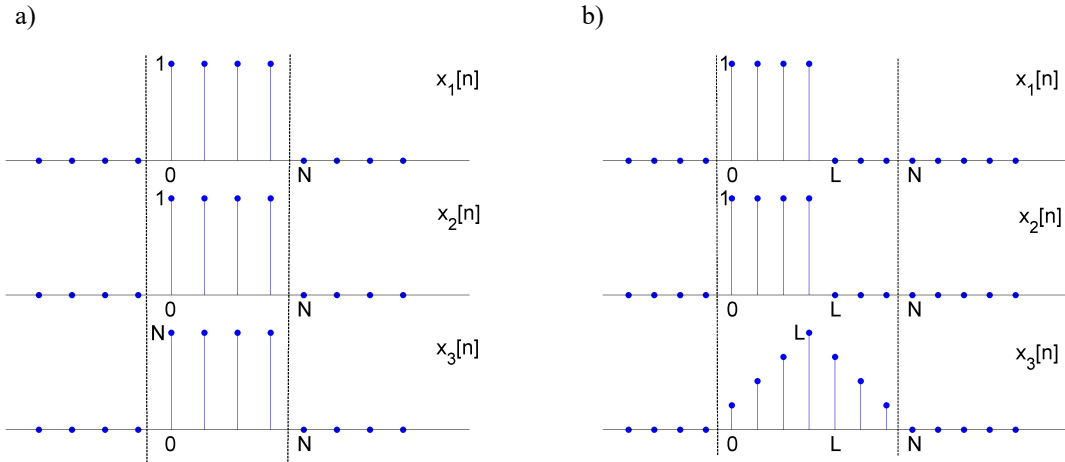


Fig. 2.19 a) Circular convolution,
b) Circular convolution equivalent to linear convolution.

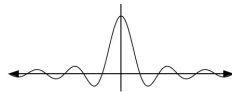
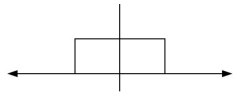
TABLE 8.2

Finite-Length Sequence (Length N)	N -point DFT (Length N)
1. $x[n]$	$X[k]$
2. $x_1[n], x_2[n]$	$X_1[k], X_2[k]$
3. $ax_1[n] + bx_2[n]$	$aX_1[k] + bX_2[k]$
4. $X[n]$	$Nx[((-k))_N]$
5. $x[((n - m))_N]$	$W_N^{km} X[k]$
6. $W_N^{-tn} x[n]$	$X[((k - \ell))_N]$
7. $\sum_{m=0}^{N-1} x_1(m)x_2[((n - m))_N]$	$X_1[k]X_2[k]$
8. $x_1[n]x_2[n]$	$\frac{1}{N} \sum_{\ell=0}^{N-1} X_1(\ell)X_2[((k - \ell))_N]$
9. $x^*[n]$	$X^*((-k))_N$
10. $x^*[((-n))_N]$	$X^*[k]$
11. $\mathcal{R}e\{x[n]\}$	$X_{ep}[k] = \frac{1}{2}\{X[((k))_N] + X^*((-k))_N\}$
12. $j\mathcal{J}m\{x[n]\}$	$X_{op}[k] = \frac{1}{2}\{X[((k))_N] - X^*((-k))_N\}$
13. $x_{ep}[n] = \frac{1}{2}\{x[n] + x^*[((-n))_N]\}$	$\mathcal{R}e\{X[k]\}$
14. $x_{op}[n] = \frac{1}{2}\{x[n] - x^*[((-n))_N]\}$	$j\mathcal{J}m\{X[k]\}$
Properties 15–17 apply only when $x[n]$ is real.	
15. Symmetry properties	$\begin{cases} X[k] = X^*((-k))_N \\ \mathcal{R}e\{X[k]\} = \mathcal{R}e\{X[((-k))_N]\} \\ \mathcal{J}m\{X[k]\} = -\mathcal{J}m\{X[((-k))_N]\} \\ X[k] = X[((-k))_N] \\ \angle\{X[k]\} = -\angle\{X[((-k))_N]\} \end{cases}$
16. $x_{ep}[n] = \frac{1}{2}\{x[n] + x[((-n))_N]\}$	$\mathcal{R}e\{X[k]\}$
17. $x_{op}[n] = \frac{1}{2}\{x[n] - x[((-n))_N]\}$	$j\mathcal{J}m\{X[k]\}$

[Poll99 p417]

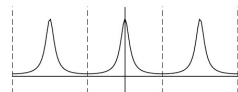
The Fourier integral: Ref. (13.78), (13.79)

$$x(t) = \frac{1}{2\pi} \int_{-\infty}^{\infty} \xi(\omega) e^{i\omega t} d\omega \quad \longleftrightarrow \quad \xi(\omega) = \int_{-\infty}^{\infty} x(t) e^{-i\omega t} dt$$



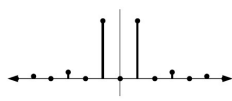
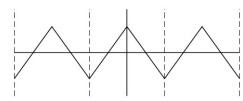
The discrete-time Fourier transform: Ref. (13.52), (13.53)

$$x_t = \frac{1}{2\pi} \int_{-\pi}^{\pi} \xi(\omega) e^{i\omega t} d\omega \quad \longleftrightarrow \quad \xi(\omega) = \sum_{t=-\infty}^{\infty} x_t e^{-i\omega t}$$



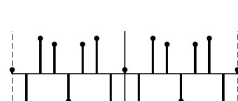
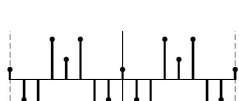
The classical Fourier series: Ref. (13.14), (13.15)

$$x(t) = \sum_{j=-\infty}^{\infty} \xi_j e^{i\omega_j t} \quad \longleftrightarrow \quad \xi_j = \frac{1}{T} \int_0^T x(t) e^{-i\omega_j t} dt$$



The discrete Fourier transform: Ref. (14.46), (14.51)

$$x_t = \sum_{j=0}^{T-1} \xi_j e^{i\omega_j t} \quad \longleftrightarrow \quad \xi_j = \frac{1}{T} \sum_{t=0}^{T-1} x_t e^{-i\omega_j t}$$



D.S.G. POLLICK: TIME-SERIES ANALYSIS

Table 14.1. The classes of Fourier transformations*

	Aperiodic in frequency Continuous in time	Periodic in frequency Discrete in time
Aperiodic in time Continuous in frequency	<i>Fourier integral</i>	<i>Discrete-time FT</i>
Periodic in time Discrete in frequency	<i>Fourier series</i>	<i>Discrete FT</i>

* Each cell of the table contains the name of a transform which is the product of a Fourier transformation mapping from the time domain to the frequency domain. The nature of the transform is determined by the nature of the signal (i.e., the time-domain function)—which is continuous or discrete, and periodic or aperiodic.

	Continuous time	Discrete time
Discrete in frequency	Periodic in time, aperiodic in frequency FS (Fourier Series) $x(t) = \sum_{k=-\infty}^{+\infty} a_k e^{jk\Omega_0 t}$ $a_k = \frac{1}{T_0} \int_{T_0} x(t) e^{-jk\Omega_0 t} dt$	Periodic in time, periodic in frequency DFT (Discrete Fourier Transform) $x[n] = \frac{1}{N} \sum_{k=0}^{N-1} X[k] e^{j\frac{2\pi}{N} kn}$ $X[k] = \sum_{n=0}^{N-1} x[n] e^{-j\frac{2\pi}{N} kn}$
Continuous in frequency	Aperiodic in time, aperiodic in frequency FT (Fourier Transform) $x(t) = \frac{1}{2\pi} \int_{-\infty}^{+\infty} X(\Omega) e^{j\Omega t} d\Omega$ $X(\Omega) = \int_{-\infty}^{+\infty} x(t) e^{-j\Omega t} dt$	Aperiodic in time, periodic in frequency DTFT (Discrete Time Fourier Transform) $x[n] = \frac{1}{2\pi} \int_{-\pi}^{\pi} X(e^{j\omega}) e^{j\omega n} d\omega$ $X(e^{j\omega}) = \sum_{n=-\infty}^{\infty} x[n] e^{-j\omega n}$

2.4 Discrete-time filters

2.4.1 The z-Transform

The z-Transform is used for analysis of discrete-time systems and signals similarly as Laplace transform is used for analysis of continuous-time systems and signals.

The z-Transform of discrete-time signal $x[n]$ is defined as

$$Z\{x[n]\} = X(z) = \sum_{n=-\infty}^{\infty} x[n]z^{-n}, \quad z = re^{j\omega}, \quad (2.107)$$

where r and ω are real. By substitution

$$z = e^{j\omega} \quad (2.108)$$

into the z-Transform definition (2.107) we obtain the Discrete Time Fourier Transform definition (2.46) $X(e^{j\omega}) = \sum_{n=-\infty}^{\infty} x[n]e^{-j\omega n}$, i.e. the z-Transform computed on the *unit circle* is DTFT.

Fig. 2.20 shows frequency interpretation of the Laplace transform and the z-Transform. In case of the Laplace transform the Fourier transform is obtained on the imaginary axis and the range of frequencies is infinite. In case of the z-Transform the DTFT is obtained on the unit circle and the range of frequencies is from $\omega=0$ to $\omega=2\pi$ rad. The DTFT is periodic with the period 2π rad.

If the discrete-time signal was obtained by sampling then $\omega=\pi$ rad corresponds to $F_s/2$ Hz, where F_s is the sampling frequency.

In Matlab convention frequency $\omega=\pi$ rad corresponds to normalized frequency 1 without a unit.

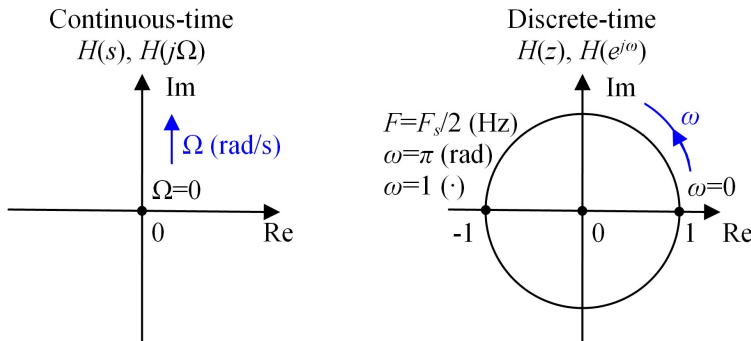


Fig. 2.20 Frequency interpretation of the Laplace transform and z-Transform.

In general case z-Transform may be interpreted as the DTFT of the product of $x[n]$ and r^{-n}

$$X(z) = X(re^{j\omega}) = \sum_{n=-\infty}^{\infty} x[n](re^{j\omega})^{-n} = \sum_{n=-\infty}^{\infty} (x[n]r^{-n})e^{-j\omega n}. \quad (2.109)$$

The z-transform is convergent if the sequence $x[n]r^{-n}$ is absolutely summable, i.e.

$$\sum_{n=-\infty}^{\infty} |x[n]r^{-n}| < \infty. \quad (2.110)$$

By computing z-Transform of difference equation $\sum_{k=0}^N a[k]y[n-k] = \sum_{m=0}^M b[m]x[n-m]$

(2.43) and by using the time-shifting property

$$x[n-n_0] \xrightarrow{Z} z^{-n_0} X(z) \quad (2.111)$$

we get

$$\sum_{k=0}^N a[k]z^{-k} Y(z) = \sum_{m=0}^M b[m]z^{-m} X(z). \quad (2.112)$$

The transmittance is

$$H(z) = \frac{Y(z)}{X(z)} = \frac{\sum_{m=0}^M b_m z^{-m}}{\sum_{k=0}^N a_k z^{-k}} = \frac{b_0 + b_1 z^{-1} + \dots + b_M z^{-M}}{a_0 + a_1 z^{-1} + \dots + a_N z^{-N}}, \quad (2.113)$$

where, for convenience, $a[k]=a_k$, $b[m]=b_m$. The transmittance (2.113) is the ratio of polynomials in z^{-1} . The denominator of (2.113) represents system negative feedback.

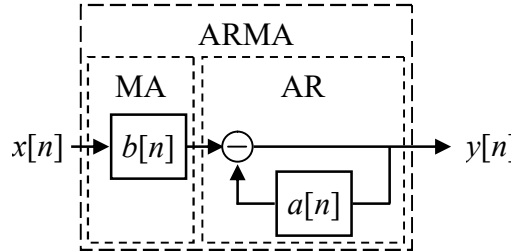


Fig.2.11 The structure of discrete-time systems. (repeated figure)

MA	Moving Average FIR system
AR	Autoregressive IIR system
ARMA	Autoregressive Moving Average IIR system

If $M=0$ and $N>0$ then $H(z)$ is a transmittance of IIR (*Infinite Impulse Response*) recursive system.

If $M>0$ and $N=0$ then $H(z)$ is a transmittance of FIR (*Finite Impulse Response*) non-recursive system.

If $M>0$ and $N>0$ then $H(z)$ is a transmittance of IIR system.

The transmittance (2.113) may be written in factored form as

$$H(z) = w \frac{\prod_{m=1}^M (1-c_m z^{-1})}{\prod_{k=1}^N (1-d_k z^{-1})} = w \frac{(1-c_1 z^{-1}) \dots (1-c_M z^{-1})}{(1-d_1 z^{-1}) \dots (1-d_N z^{-1})}, \quad (2.114)$$

where w is the gain, and each of the factors $(1-c_m z^{-1})$ in the numerator contributes a transmittance zero at $z=c_m$ and pole at $z=0$, and each of the factors $(1-d_k z^{-1})$ in the denominator contributes a transmittance zero at $z=0$ and pole at $z=d_k$.

The transmittance (2.113) may be written as a ratio of polynomials of z rather than z^{-1}

$$H(z) = \frac{Y(z)}{X(z)} = \frac{b_0 + b_1 z^{-1} + \dots + b_M z^{-M}}{a_0 + a_1 z^{-1} + \dots + a_N z^{-N}} = \frac{z^N (b_0 z^M + b_1 z^{M-1} + \dots + b_M)}{z^M (a_0 z^N + a_1 z^{N-1} + \dots + a_N)} = w \frac{z^N (z - c_1) \dots (z - c_M)}{z^M (z - d_1) \dots (z - d_N)}. \quad (2.115)$$

Zeros of transmittance $H(z)$ cause local minima in magnitude response and poles of transmittance $H(z)$ cause local maxima in magnitude response of the system. The strength of impact of zeros and poles increases as they get closer to the unit circle.

Example 2.8

Consider discrete-time system defined by zeros $c = [1.1e^{j\pi/2} \quad 1.1e^{-j\pi/2}]$, poles $d = [0.7e^{j\pi/8} \quad 0.7e^{-j\pi/8}]$, and gain $w=1$. The transmittance of this system is

$$H(z) = \frac{(1-1.1e^{j\pi/2}z^{-1})(1-1.1e^{-j\pi/2}z^{-1})}{(1-0.7e^{j\pi/8}z^{-1})(1-0.7e^{-j\pi/8}z^{-1})} = \frac{1+1.21z^{-2}}{1-1.2934z^{-1}+0.49z^{-2}}, \quad (2.116a)$$

or

$$H(z) = \frac{(z-1.1e^{j\pi/2})(z-1.1e^{-j\pi/2})}{(z-0.7e^{j\pi/8})(z-0.7e^{-j\pi/8})} = \frac{z^2+1.21}{z^2-1.2934z+0.49}. \quad (2.116b)$$

Magnitude response is computed by substitution $z = e^{j\omega}$ (2.108)

$$|H(e^{j\omega})| = \frac{|(e^{j\omega}-c)| \cdot |(e^{j\omega}-c^*)|}{|(e^{j\omega}-d)| \cdot |(e^{j\omega}-d^*)|}. \quad (2.117)$$

In (2.117) each absolute value is the distance of the zero or pole from the point on unite circle, what is graphically shown in Fig. 2.12.

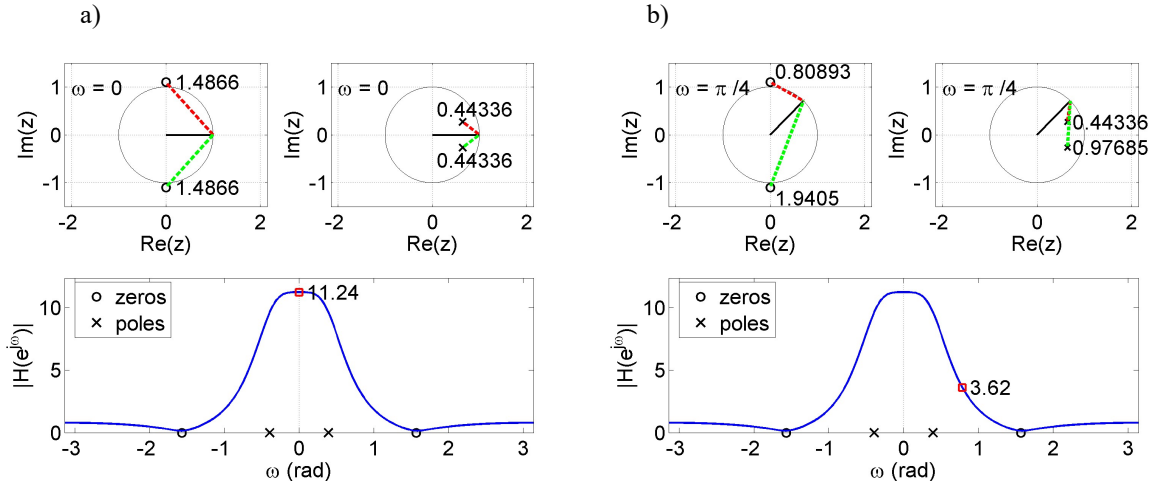


Fig. 2.21 Influence of zeros and poles of $H(z)$ (2.116a) on magnitude response: a) $\omega=0$, b) $\omega=\pi/4$ rad.

DC gain of (2.116a) is

$$|H(e^{j0})| = \left| \frac{1+1.21}{1-1.2934+0.49} \right| = 11.24, \quad (2.118a)$$

or from (2.117)

$$|H(e^{j0})| = \frac{1.4866 \cdot 1.4866}{0.44336 \cdot 0.44336} = 11.24. \quad (2.118a)$$

If we chose the gain of the system $w=1/11.24$ then DC gain will be 1, and the shape of magnitude response remain the same.

In order to use the discrete-time system with the transmittance $H(z)$ we must obtain difference equation associated with this transmittance

$$H(z) = \frac{Y(z)}{X(z)} = \frac{1+1.21z^{-2}}{1-1.2934z^{-1}+0.49z^{-2}} \rightarrow Y(z) = X(z) + 1.21X(z)z^{-2} + 1.2934Y(z)z^{-1} - 0.49Y(z)z^{-2}. \quad (2.119)$$

By using the time-shifting property (2.111) we get

$$y[n] = x[n] + 1.21x[n-2] + 1.2934y[n-1] - 0.49y[n-2]. \quad (2.120)$$

For unite sample input signal $\delta[n]$ (2.19) the output is called impulse response and is shown in Fig.2.22 as computed from (2.120).

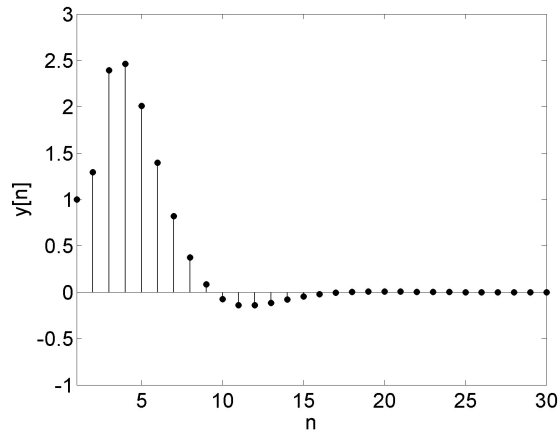


Fig.2.22 Impulse response of the discrete-time system (2.116a).

Figs.2.23-2.25 show zero-pole plots of continuous-time and discrete-time systems and their impulse responses. The plots for continuous-time systems are only shown for comparison.

Discrete-time system is stable only if the poles of $H(z)$ lay inside unit circle, i.e. $|p|<1$. If the poles lay on the unit circle the impulse response oscillates infinitely. If the poles lay outside unit circle the impulse response grows infinitely.

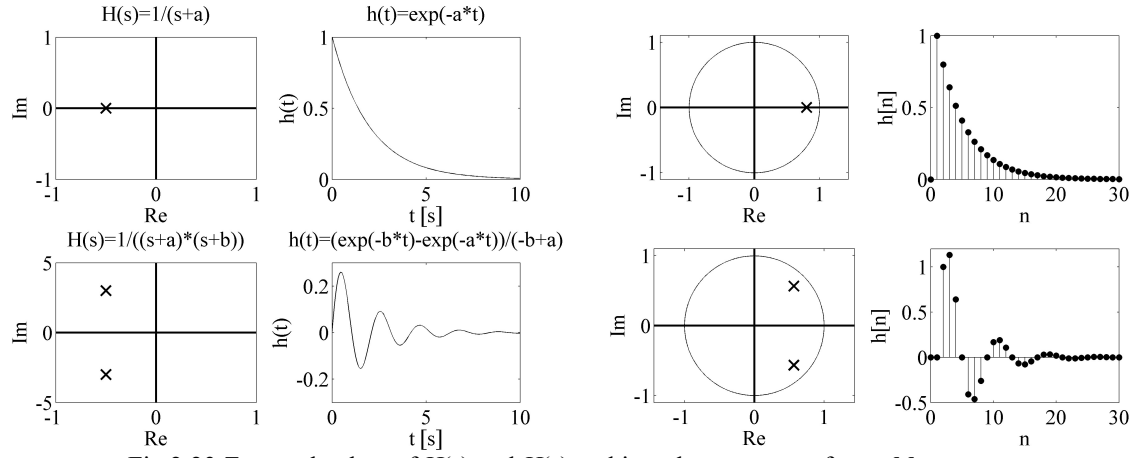


Fig.2.23 Zero-pole plots of $H(s)$ and $H(z)$ and impulse responses for **stable** systems.

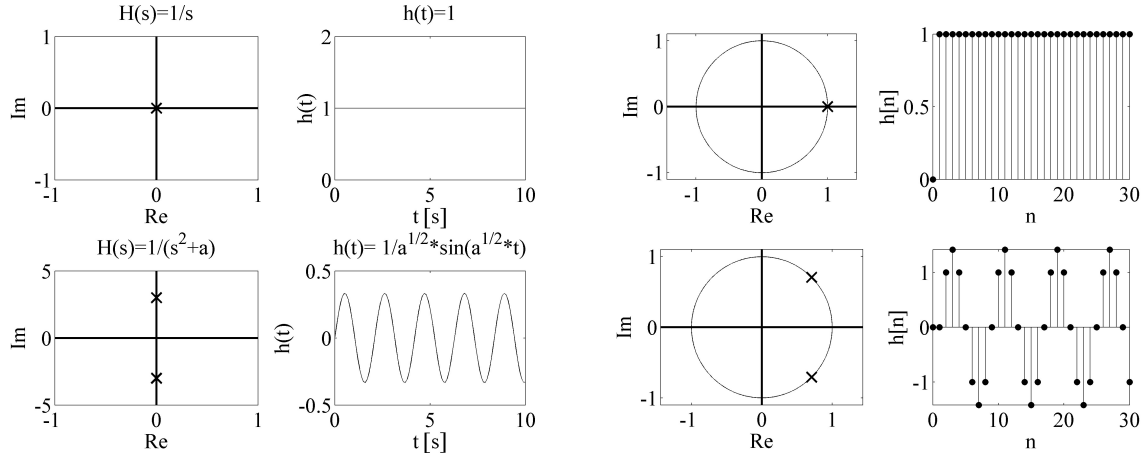


Fig.2.24 Zero-pole plots of $H(s)$ and $H(z)$ and impulse responses for **conditionally stable** systems.

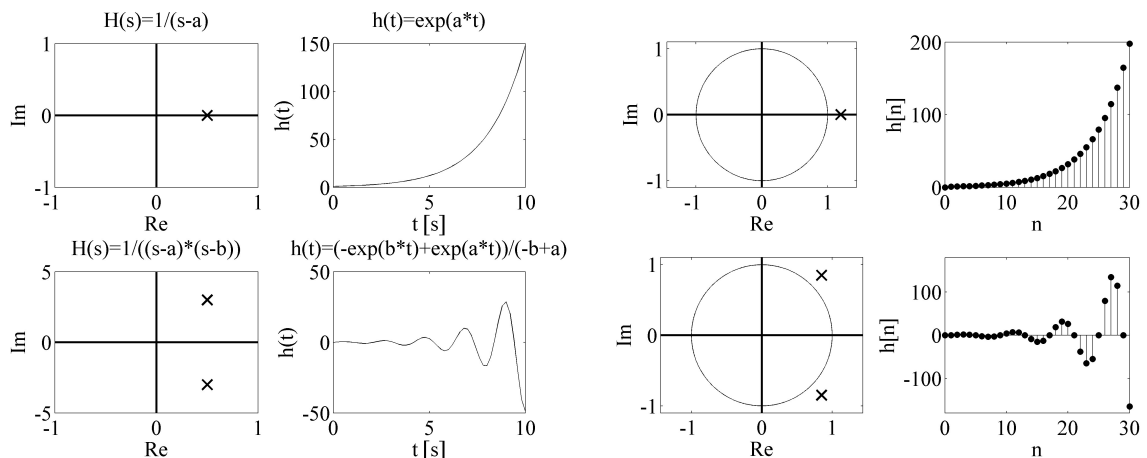


Fig.2.25 Zero-pole plots of $H(s)$ and $H(z)$ and impulse responses for **unstable** systems.

Example 2.9

Let us consider discrete-time system with a single pole equal a

$$H(z) = \frac{Y(z)}{X(z)} = \frac{1}{z-a}. \quad (2.121)$$

The difference equation is

$$y[n+1] = x[n] + ay[n]. \quad (2.122)$$

The impulse response is computed for $x[n]=\delta[n]$ (the system is initially at rest i.e. $y[n]=0, n \leq 0$)

$$\begin{aligned} n=0, \quad y[1] &= x[0] + ay[0] = 1, \\ n=1, \quad y[2] &= x[1] + ay[1] = a, \\ n=2, \quad y[3] &= x[2] + ay[2] = a^2, \\ n=3, \quad y[4] &= x[3] + ay[3] = a^3, \end{aligned} \quad (2.123)$$

generally

$$y[n] = a^n, \quad n \geq 0. \quad (2.124)$$

The system is stable if its impulse response is limited, i.e. $\sum_{n=-\infty}^{\infty} |y[n]| < \infty$. The sum of power series (2.124) is limited for $|a| < 1$

$$\sum_{n=0}^{\infty} |a|^n = \frac{1}{1-|a|} < \infty \quad \text{for } |a| < 1. \quad (2.125)$$

The system (2.121) is stable only if $|a| < 1$, that is only if the pole is inside the unit circle on the complex z -plane,

Example 2.10

Consider the following transmittance $H(z)$

$$H(z) = \frac{(z - r_1 e^{j\omega})(z - r_1 e^{-j\omega})}{(z - r_2 e^{j\omega})(z - r_2 e^{-j\omega})}, \quad (2.126)$$

where $0 \leq \omega \leq \pi$ rad, $0 < r_2 < 1$, and r_1 is real parameter. The filter with transmittance (2.126) has strong attenuation in narrow frequency band. It is called *notch filter*. Fig. 2.26 shows exemplary zero-pole plot, magnitude response, and impulse response of transmittance (2.126).

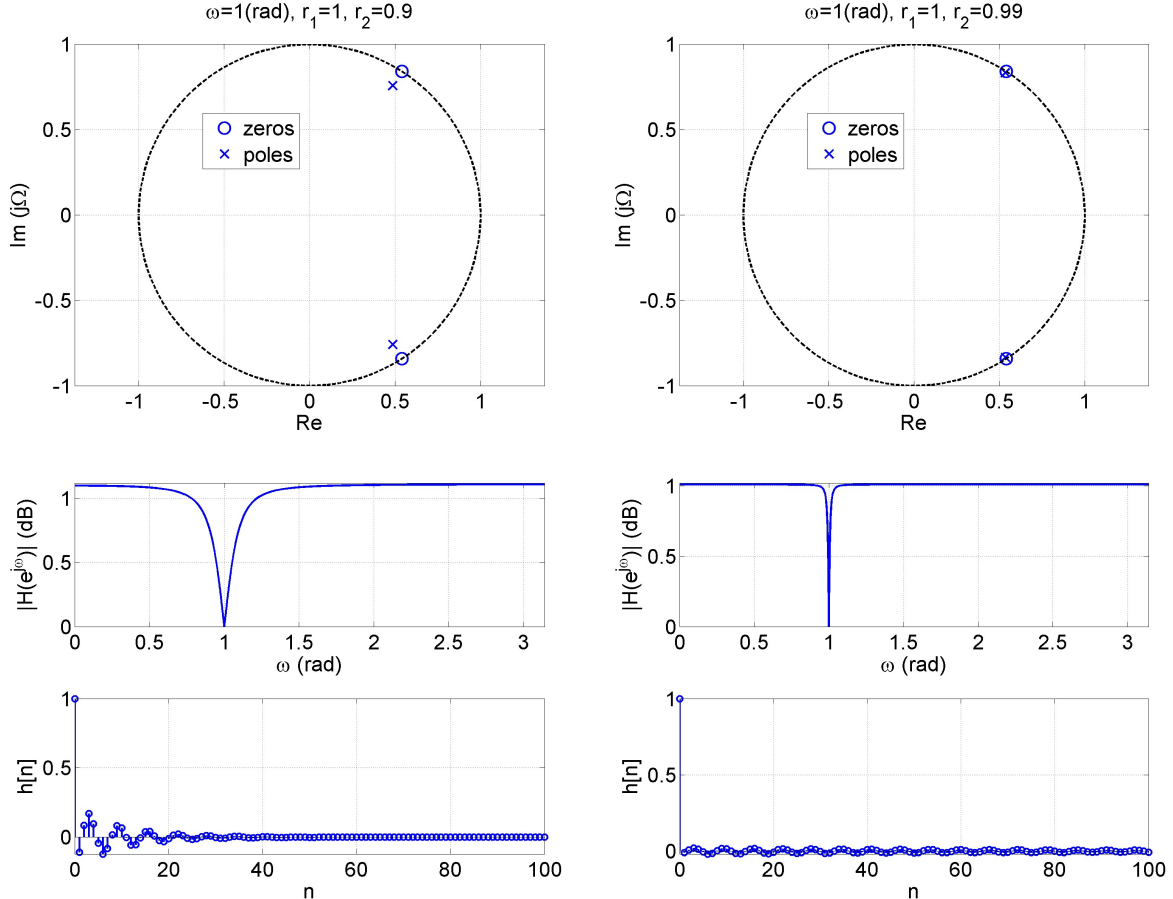


Fig.2.26 Zero-pole plot, magnitude response and impulse response of exemplary notch filter with the transmittance $H(z)$ (2.126).

Minimum-phase systems

Magnitude response does not define the transmittance $H(z)$ uniquely.

Discrete-time minimum-phase system has all its poles and zeros of transmittance $H(z)$ inside the unit circle.

Minimum-phase system has a stable *inverse system* with transmittance $1/H(z)$.

From all systems with the same magnitude response minimum-phase system has minimum group delay.

[Fig. 2.27](#) compares two discrete-time systems having the same magnitude responses. Both systems have the same poles $0.7e^{\pm j\pi/8}$. The zeros of non minimum-phase filter are $1.1e^{\pm j\pi/2}$, and the zeros of minimum-phase filter are the inverse, i.e. $1/1.1e^{\pm j\pi/2} \approx 0.909e^{\pm j\pi/2}$.

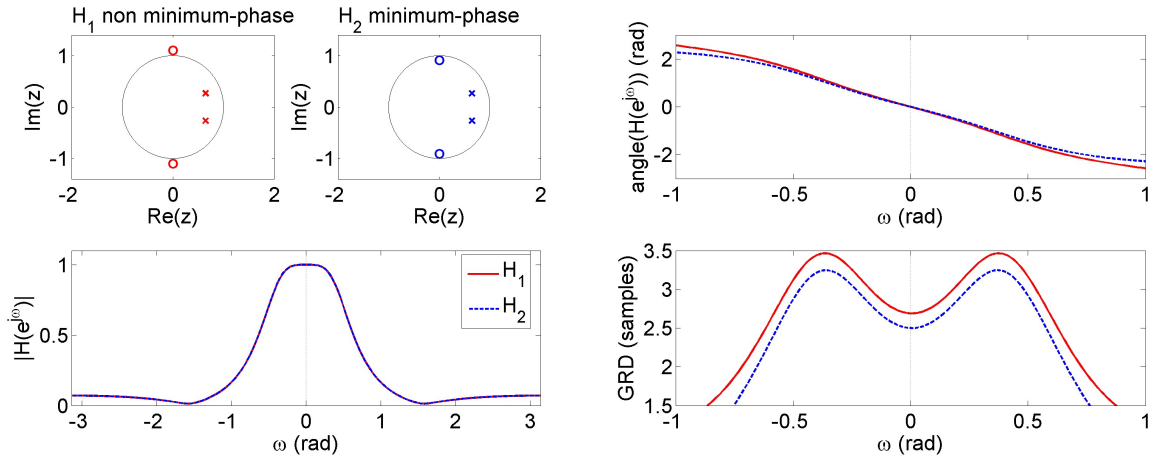


Fig.2.27 Zero-pole plots and frequency responses of discrete-time systems:

red - non minimum-phase system,
blue - minimum-phase system.

Group delay shown in [Fig. 2.27](#) is defined as

$$\text{GRD}(\omega) = -\frac{d}{d\omega} \text{angle}(H(e^{j\omega})) \text{ (sample)}. \quad (2.127)$$

All-pass systems

All-pass system has constant, i.e. independent of ω , magnitude response. Let us consider the system with transmittance

$$H_{ap}(z) = \frac{(z-c)(z-c^*)}{\left(z - \frac{1}{c^*}\right)\left(z - \frac{1}{c}\right)}, \quad c = Ce^{j\varphi}, \quad |c| > 1. \quad (2.128)$$

The Fourier transform of (2.128) is

$$\begin{aligned} H_{ap}(e^{j\omega}) &= \frac{(e^{j\omega}-c)(e^{j\omega}-c^*)}{\left(e^{j\omega} - \frac{1}{c^*}\right)\left(e^{j\omega} - \frac{1}{c}\right)} = \frac{(e^{j\omega}-c)(e^{j\omega}-c^*)}{\frac{1}{c^*}(e^{j\omega}c^*-1)\frac{1}{c}(e^{j\omega}c-1)} = cc^* \frac{(e^{j\omega}-c)(e^{j\omega}-c^*)}{(e^{j\omega}c^*-1)(e^{j\omega}c-1)} = \\ &= cc^* \frac{(e^{j\omega}-c)(e^{j\omega}-c^*)}{e^{j\omega}\left(c^* - \frac{1}{e^{j\omega}}\right)e^{j\omega}\left(c - \frac{1}{e^{j\omega}}\right)} = cc^* \frac{(e^{j\omega}-c)(e^{j\omega}-c^*)}{e^{j2\omega}(c^* - e^{-j\omega})(c - e^{-j\omega})} = \\ &= e^{-j2\omega}cc^* \frac{(e^{j\omega}-c)(e^{j\omega}-c^*)}{(e^{-j\omega}-c^*)(e^{-j\omega}-c)} \end{aligned} \quad , \quad (2.129)$$

and the magnitude response is

$$|H_{ap}(e^{j\omega})| = |cc^*| \frac{|e^{j\omega}-c| |e^{j\omega}-c^*|}{|e^{-j\omega}-c| |e^{-j\omega}-c^*|} = C^2. \quad (2.130)$$

Fig. 2.28 shows zero-pole plot and magnitude response of exemplary second order all-pass system. The gain of this system is $w=0.5$. It is shown that for $\omega=0$ and for $\omega=\pi/3$ rad magnitude response equals 1, i.e. $0.5 \cdot (0.63 \cdot 0.63) / (0.44 \cdot 0.44) = 1$ and $0.5 \cdot (0.88 \cdot 1.63) / (1.14 \cdot 0.62) = 1$.

All-pass filters are used for correction of phase responses.

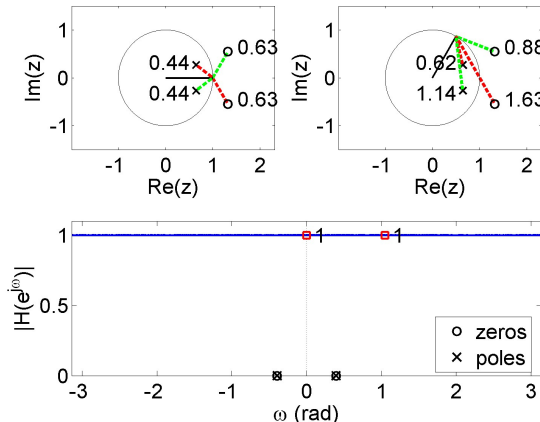


Fig.2.28 Zero-pole plots and magnitude response of all-pass discrete-time systems.

Inverse systems

Inverse system $H_i(z)$ is defined as

$$H(z)H_i(z)=1, \quad (2.131)$$

thus

$$H_i(z)=\frac{1}{H(z)}, \quad (2.132)$$

where $H(z)$ is minimum-phase system.

Impulse responses of $H(z)$ and $H_i(z)$ fulfill

$$h[n]*h_i[n]=\delta[n]. \quad (2.133)$$

[Fig. 2.29](#) shows zero-pole plots and magnitude responses of minimum-phase and inverse discrete-time systems.

Inverse systems are used for correction of magnitude responses.

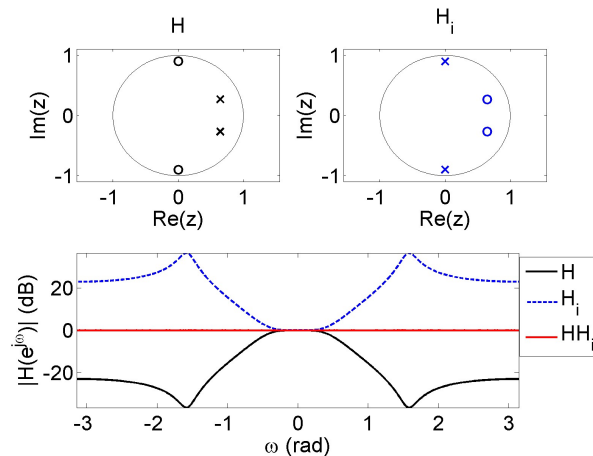


Fig.2.29 Zero-pole plots and magnitude response of minimum-phase and inverse discrete-time systems.

Minimum-phase and all-pass decomposition

Non minimum-phase system may be expressed as a cascade connection of minimum-phase system $H_{min}(z)$, and all-pass system $H_{ap}(z)$

$$H(z)=H_{min}(z)H_{ap}(z). \quad (2.134)$$

Let us consider following system

$$H(z)=\frac{(z-c)(z-c^*)}{(z-d)(z-d^*)}, \quad |c|>1. \quad (2.135)$$

We have

$$H(z)=\frac{(z-c)(z-c^*)}{(z-d)(z-d^*)}=\frac{(z-c)(z-c^*)}{(z-d)(z-d^*)}\frac{\left(z-\frac{1}{c^*}\right)\left(z-\frac{1}{c}\right)}{\left(z-\frac{1}{c^*}\right)\left(z-\frac{1}{c}\right)}=\frac{\left(z-\frac{1}{c^*}\right)\left(z-\frac{1}{c}\right)}{(z-d)(z-d^*)}\frac{(z-c)(z-c^*)}{\left(z-\frac{1}{c^*}\right)\left(z-\frac{1}{c}\right)}=H_{min}(z)H_{ap}(z), \quad (2.136)$$

and the magnitude response of $H_{min}(z)$ and $H(z)$ is the same, expect gain

$$\left|H(e^{j\omega})\right|=\left|H_{min}(e^{j\omega})\right|\left|H_{ap}(e^{j\omega})\right|=w\left|H_{min}(e^{j\omega})\right|. \quad (2.137)$$

[Oppen99 p282]

5.6.2 Frequency-Response Compensation

In many signal-processing contexts, a signal has been distorted by an LTI system with an undesirable frequency response. It may then be of interest to process the distorted signal with a compensating system, as indicated in Figure 5.25. This situation may arise, for example, in transmitting signals over a communication channel. If perfect compensation is achieved, then $s_c[n] = s[n]$, i.e., $H_c(z)$ is the inverse of $H_d(z)$. However, if we assume that the distorting system is stable and causal and require the compensating system to be stable and causal, then perfect compensation is possible only if $H_d(z)$ is a minimum-phase system, so that it has a stable, causal inverse.

Based on the previous discussions, assuming that $H_d(z)$ is known or approximated as a rational system function, we can form a minimum-phase system $H_{d\min}(z)$ by reflecting all the zeros of $H_d(z)$ that are outside the unit circle to their conjugate reciprocal locations inside the unit circle. $H_d(z)$ and $H_{d\min}(z)$ have the same frequency-response magnitude and are related through an all-pass system $H_{ap}(z)$, i.e.,

$$H_d(z) = H_{d\min}(z)H_{ap}(z). \quad (5.104)$$

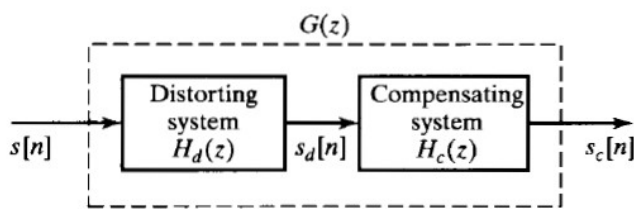


Figure 5.25 Illustration of distortion compensation by linear filtering.

Table 2.8 Continuous-time and discrete-time LTI systems.

Convolution integral $y(t) = \int_{-\infty}^{\infty} x(\tau)h(t-\tau)d\tau = x(t) * h(t)$ (1.24)	Convolution sum $y[n] = \sum_{k=-\infty}^{\infty} x[k]h[n-k] = x[n] * h[n]$ (2.34)
Response to single sinusoid $x(t) = e^{j\Omega_0 t}$ $y(t) = e^{j\Omega_0 t} \int_{-\infty}^{\infty} h(\tau)e^{-j\Omega_0 \tau} d\tau = e^{j\Omega_0 t} H(j\Omega_0)$ (1.31) $H(j\Omega) = \int_{-\infty}^{\infty} h(\tau)e^{-j\Omega\tau} d\tau, \quad -\infty < \Omega < +\infty$ Aperiodic spectrum	Response to single sinusoid $x[n] = e^{j\omega_0 n}$ $y[n] = e^{j\omega_0 n} \sum_{k=-\infty}^{\infty} h[k]e^{-j\omega_0 k} = e^{j\omega_0 n} H(e^{j\omega_0})$ (2.40) $H(e^{j\omega}) = \sum_{k=-\infty}^{\infty} h[k]e^{-j\omega k}$ Spectrum periodic with 2π rad
Linear constant coefficient differential equation $\sum_{k=0}^N a_k \frac{d^k y(t)}{dt^k} = \sum_{k=0}^M b_k \frac{d^k x(t)}{dt^k}$ (1.29)	Linear constant coefficients difference equation $\sum_{k=0}^N a[k]y[n-k] = \sum_{m=0}^M b[m]x[n-m]$ (2.43)
Laplace transform $H(s)$ $X(s) = \int_0^{\infty} x(t)e^{-st} dt, \quad s = \sigma + j\Omega$ (3.1) Frequency interpretation $s = j\Omega$ (3.2)	z-Transform $H(z)$ $Z\{x[n]\} = X(z) = \sum_{n=-\infty}^{\infty} x[n]z^{-n}, \quad z = re^{j\omega}$ (2.43) Frequency interpretation $z = e^{j\omega}$ (2.108)
Transmittance $H(s) = \frac{Y(s)}{X(s)} = \frac{\sum_{m=0}^M b_m s^m}{\sum_{k=0}^K a_k s^k} = W \frac{\prod_{m=1}^M (s - z_m)}{\prod_{k=1}^K (s - p_k)}$	Transmittance $H(z) = \frac{Y(z)}{X(z)} = \frac{\sum_{m=0}^M b_m z^{-m}}{\sum_{k=0}^K a_k z^{-k}} = W \frac{\prod_{m=1}^M (1 - z_m z^{-1})}{\prod_{k=1}^K (1 - p_k z^{-1})}$
Stable for poles in the left half of the complex plane, $\operatorname{Re}(p) < 0$	Stable for poles in the unit circle in the complex plane, $ p < 1$

2.4.2 IIR recursive filters

IIR filters have selective magnitude responses with low orders of transmittance $H(z)$. IIR filters may be designed from analog prototypes with *bilinear transformation*.

Bilinear transformation

Bilinear transformation is an algebraic transformation that maps complex s -plane into complex z -plane, as depicted in Fig. 2.30. The transmittance of discrete-time filter $H(z)$ is obtained from the transmittance of continuous-time filter $H_c(s)$ by substitution

$$s = \frac{2}{T} \left(\frac{1-z^{-1}}{1+z^{-1}} \right), \text{ i.e. } H(z) = H_c \left(\frac{2}{T} \left(\frac{1-z^{-1}}{1+z^{-1}} \right) \right), \quad (2.138)$$

where T is the sampling period in seconds. Solving (2.138) for z and putting $s=\sigma+j\Omega$ we get

$$z = \frac{1 + (T/2)s}{1 - (T/2)s} = \frac{1 + \sigma T/2 + j\Omega T/2}{1 - \sigma T/2 - j\Omega T/2}. \quad (2.139)$$

For $\sigma=0$ $|z| = \frac{|1 + j\Omega T/2|}{|1 - j\Omega T/2|} = 1$, thus entire $j\Omega$ -axis in the s -plane is mapped into the unit circle $e^{j\omega}$ in the z -plane. For $\sigma < 0$ we have $|z| < 1$, and for $\sigma > 0$ we have $|z| > 1$, thus the left half of s -plane is mapped inside the unit circle in the z -plane, and the right half of s -plane is mapped outside the unit circle in the z -plane.

By bilinear transformation stable continuous-time filters are mapped into stable discrete-time filters.

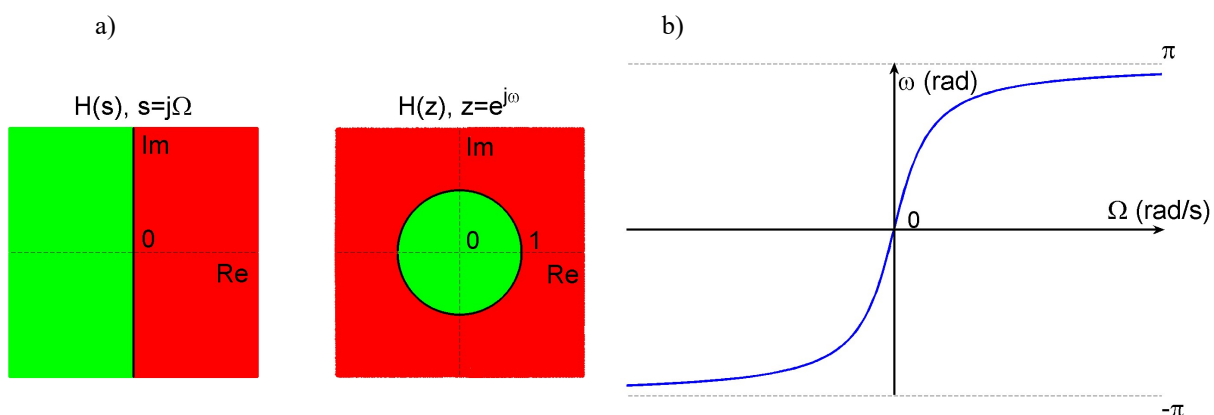


Fig.2.30 Bilinear transformation:
 a) mapping s -plane into z -plane,
 b) dependence between frequency Ω of continuous-time system and frequency ω of discrete-time system.

The dependence between frequency Ω of continuous-time system and frequency ω of discrete-time system shown in Fig. 2.30b is nonlinear. From definition (2.138) we have

$$\begin{aligned} j\Omega &= \frac{2}{T} \left(\frac{1 - e^{-j\omega}}{1 + e^{-j\omega}} \right) = \frac{2}{T} \left(\frac{1 - e^{-j\omega/2} e^{-j\omega/2}}{1 + e^{-j\omega/2} e^{-j\omega/2}} \right) = \frac{2}{T} \left(\frac{e^{-j\omega/2} (e^{j\omega/2} - e^{-j\omega/2})}{e^{-j\omega/2} (e^{j\omega/2} + e^{-j\omega/2})} \right) = \\ &= \frac{2}{T} \left(j \frac{\frac{e^{j\omega/2} - e^{-j\omega/2}}{2j}}{\frac{e^{j\omega/2} + e^{-j\omega/2}}{2}} \right) = \frac{j2}{T} \left(\frac{\sin(\omega/2)}{\cos(\omega/2)} \right) = j \frac{2}{T} \operatorname{tg}(\omega/2) \end{aligned} \quad (2.139)$$

and finally

$$\Omega = \frac{2}{T} \operatorname{tg}(\omega/2), \quad \omega = \operatorname{arctg}(\Omega T/2). \quad (2.140)$$

Analog prototype must be designed for cutoff frequency $\Omega = \frac{2}{T} \operatorname{tg}(\omega/2)$.

Example 2.11

Design discrete-time lowpass elliptic filter for sampling frequency $F_s=100$ Hz with magnitude response fulfilling the requirements:

- the passband edge frequency $f_{pass}=20$ Hz,
- the stopband edge frequency $f_{stop}=25$ Hz,
- maximum passband attenuation $r_p=3$ dB,
- minimum stopband attenuation $r_s=30$ dB.

Discrete-time filter design goes in following steps:

1. Compute discrete-time filter edge frequencies in radians

$$\omega_{pass} = 2\pi \frac{f_{pass}}{F_s} = 2\pi \frac{20}{100} = 1.26 \text{ rad}, \quad \omega_{stop} = 2\pi \frac{f_{stop}}{F_s} = 2\pi \frac{25}{100} = 1.57 \text{ rad}. \quad (2.141)$$

2. Compute continuous-time filter corrected edge frequencies in radians per second

$$\Omega_{pass} = \frac{2}{T} \tan(\omega_{pass}/2) = \frac{2}{1/100} \tan(1.26/2) = 145.31 \text{ rad/s}, \quad \Omega_{stop} = 200 \text{ rad/s}. \quad (2.142)$$

As shown in Fig. 2.31 continuous-time filter is designed for $F_{pass}=23.13$ Hz and $F_{stop}=31.83$ Hz.

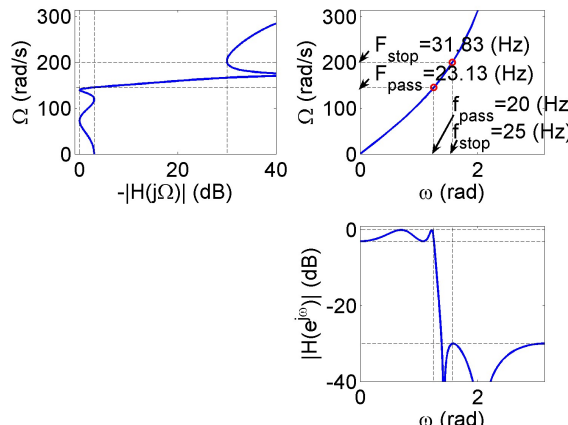


Fig.2.31 Correction of continuous-time filter edge frequencies before bilinear transformation.

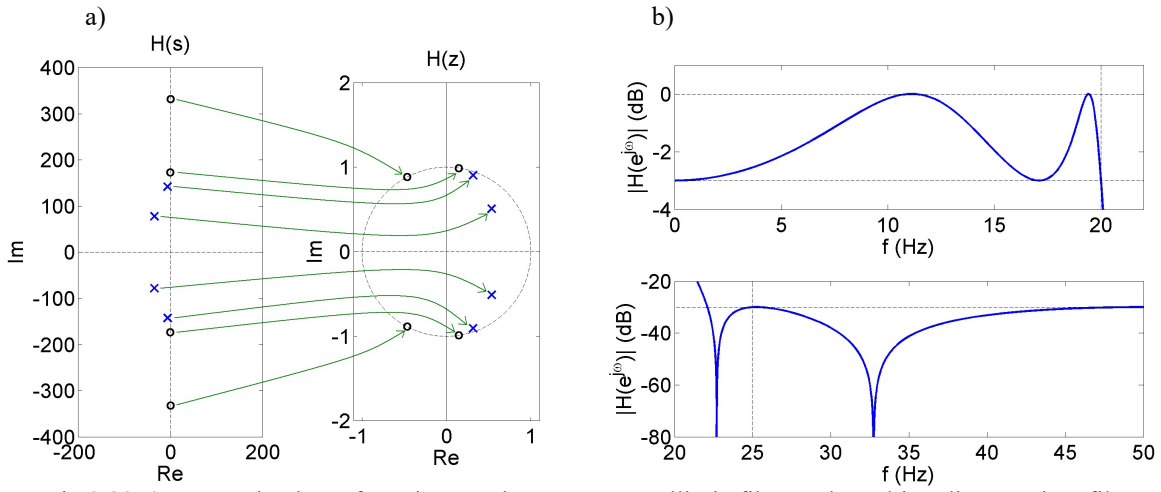


Fig.2.32 a) Zero-pole plots of continuous-time prototype elliptic filter and resulting discrete-time filter,
b) Verification of discrete-time filter magnitude response.

3. Compute the transmittance $H(s)$ of continuous-time filter. Zeros and poles of $H(s)$ are shown in Fig. 2.32a.
4. Map each zero and pole of $H(s)$ from s -plane to z -plane by bilinear transformation (2.138), as shown in Fig. 2.32a.
5. Verify if magnitude response of obtained transmittance $H(z)$ fulfill designing requirements. From Fig. 2.32b it is seen that passband and stopband attenuation is as required.

Bilinear transformation maps entire $j\Omega$ -axis in the s -plane into the unit circle $e^{j\omega}$ in the z -plane, thus zeros of $H(s)$ in $j\Omega=\pm\infty$ are mapped into zeros of $H(z)$ in $e^{\pm j\pi}=-1$. Multiple zeros of $H(s)$ in $j\Omega=\pm\infty$ occur if the degree of the polynomial in the nominator is lower than the degree of the polynomial in the denominator. The difference between degrees of those polynomials is the number of zeros of $H(s)$ in $j\Omega=\pm\infty$, and thus the number of zeros of $H(z)$ in -1 . E.g. the transmittance $H(s)=1/(s^2+1.41s+1)$ has a double zero in $j\Omega=\infty$ and by applying bilinear transformation the $H(z)$ has a double zero in -1 , and analog prototype Butterworth filter designed for requirements from Example 2.11, see Fig. 2.33, has zero degree polynomial in nominator and eleventh degree polynomial in denominator thus it has 11 zeros in $j\Omega=\pm\infty$, and discrete-time filter obtained by bilinear transformation has 11 zeros in -1 .

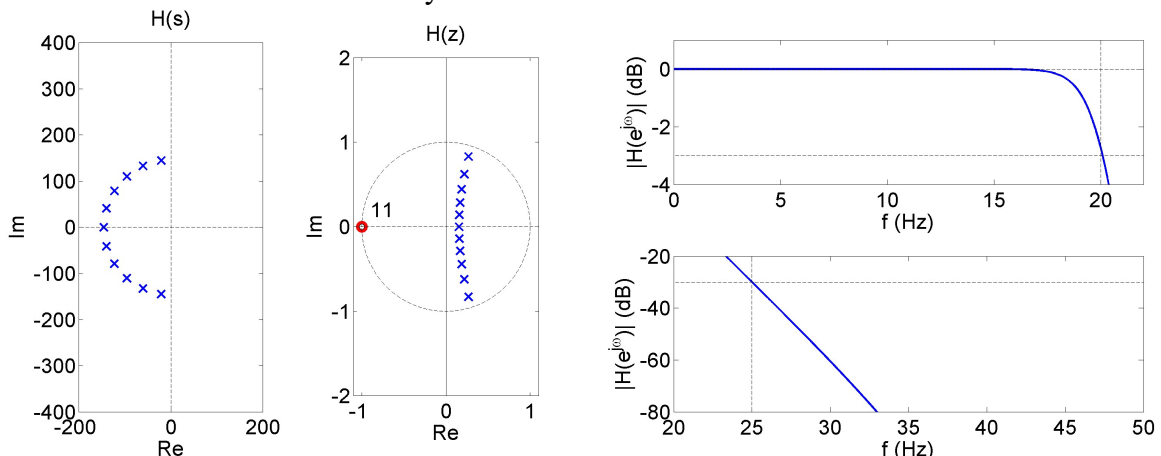


Fig.2.33 a) Zero-pole plots of continuous-time prototype Butterworth filter and resulting discrete-time filter,
b) Verification of discrete-time filter magnitude response.

Bilinear transformation may be implemented by representing transmittance $H(s)$ as a product of the two basic transmittances $H(s) = A/(s - B)$ and $H(s) = (s - A)/(s - B)$ and then transforming each of the basic transmittance with the use of mathematical equations.

$$H(s) = \frac{A}{s - B} \quad \Rightarrow \quad H(z) = \frac{-AT(z+1)}{z(BT-2)+BT+2} = \frac{-AT}{BT-2} \frac{z+1}{z+\frac{BT+2}{BT-2}}, \quad (2.143)$$

$$H(s) = \frac{s-A}{s-B} \quad \Rightarrow \quad H(z) = \frac{z(AT-2)+AT+2}{z(BT-2)+BT+2} = \frac{AT-2}{BT-2} \frac{z+\frac{AT+2}{AT-2}}{z+\frac{BT+2}{BT-2}}. \quad (2.144)$$

As seen in (2.143) $H(s)=0$ for $j\Omega=\infty$ is mapped in $H(z)=0$ in $e^{j\omega}=-1$.

2.4.3 FIR non recursive filters

Magnitude response of an ideal lowpass (LP) filter presented in Fig. 2.34a is defined as

$$H_{LP}(e^{j\omega}) = \begin{cases} 1, & |\omega| < \omega_c \\ 0, & \omega_c < |\omega| \leq \pi \end{cases}. \quad (2.145)$$

Impulse response of an ideal LP filter is computed by the inverse DTFT (2.45)

$$h_{LP}[n] = \frac{1}{2\pi} \int_{-\omega_c}^{\omega_c} e^{j\omega n} d\omega = \frac{1}{2\pi j n} [e^{j\omega n}]_{-\omega_c}^{\omega_c} = \frac{1}{2\pi j n} (e^{j\omega_c n} - e^{-j\omega_c n}) = \frac{\sin(\omega_c n)}{\pi n} = \begin{cases} \frac{\sin(\omega_c n)}{\pi n}, & n \neq 0 \\ \frac{\omega_c}{\pi}, & n = 0 \end{cases}. \quad (2.146)$$

Impulse response (2.146) is noncasual and the range of n is infinite $-\infty < n < \infty$.

Finite length causal filter, with length $N=2M+1$, is obtained from (2.146) by computing $h_{LP}[n]$ for $-M \leq n \leq M$ and shifting it by M indexes

$$h_{LP}^{2M+1}[n] = \frac{\sin(\omega_c(n-M))}{\pi(n-M)}, \quad n = 0, 1, 2, \dots, 2M, \quad (2.147)$$

where the upper subscript $2M+1$ in $h_{LP}^{2M+1}[n]$ denotes the length of impulse response and $h_{LP}^{2M+1}[M] = \omega_c / \pi$.

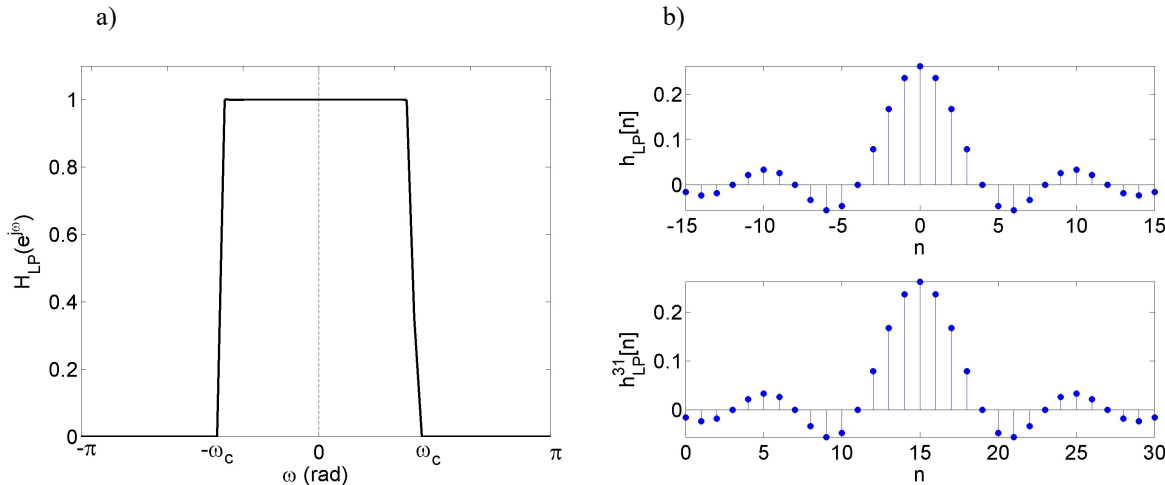


Fig.2.34 a) Magnitude response of ideal, noncasual lowpass filter,
b) Fragment of infinite impulse response of noncasual filter and finite impulse response of causal filter.

Increasing the length N of impulse response does not minimize the absolute error of magnitude response, i.e.

$$\lim_{N \rightarrow \infty} \max |H_{LP}^N(e^{j\omega}) - H_{LP}(e^{j\omega})| \neq 0, \quad (2.148)$$

but it does minimize the energy of the error of magnitude response

$$\lim_{N \rightarrow \infty} \int_{-\pi}^{\pi} |H_{LP}^N(e^{j\omega}) - H_{LP}(e^{j\omega})|^2 d\omega = 0. \quad (2.149)$$

Properties (2.148-2.149) are illustrated in Fig. 2.35.

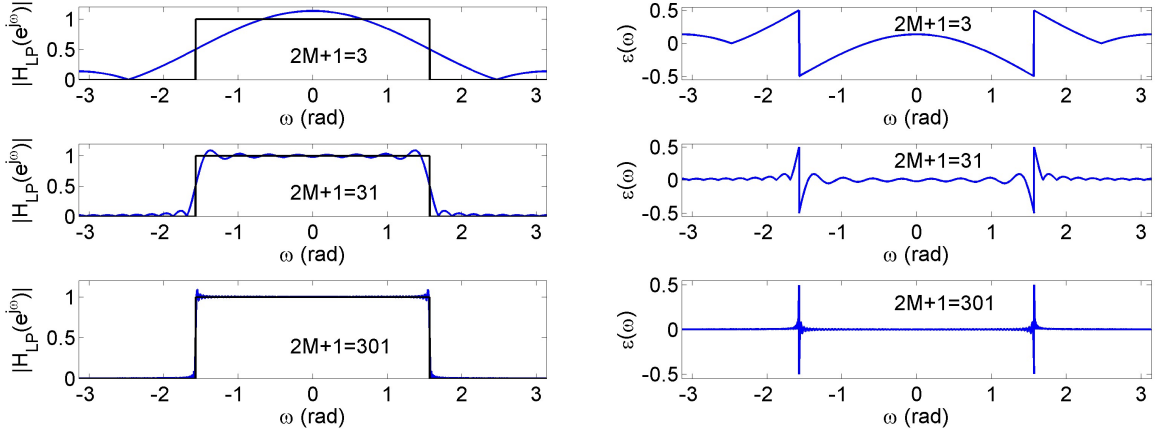


Fig.2.35 a) Magnitude response of LP filter for different length of impulse response $h_{LP}^{2M+1}[n]$,

$$\text{b) Error of magnitude response } \varepsilon(\omega) = |H_{LP}^N(e^{j\omega})| - H_{LP}(e^{j\omega}).$$

Impulse responses of HP, BP and BS filters may be derived by inverse DTFT similarly as (2.146). They may also be obtained by summing impulse responses of LP filter and all-pass filter as shown in Fig. 2.36, e.g. HP filter is obtained as

$$h_{HP}[n] = h_{ALL}[n] - h_{LP}[n] = \frac{\sin(\pi n)}{\pi n} - \frac{\sin(\omega_c n)}{\pi n} = \begin{cases} \frac{\sin(\pi n) - \sin(\omega_c n)}{\pi n}, & n \neq 0 \\ 1 - \frac{\omega_c}{\pi}, & n = 0 \end{cases}. \quad (2.150)$$

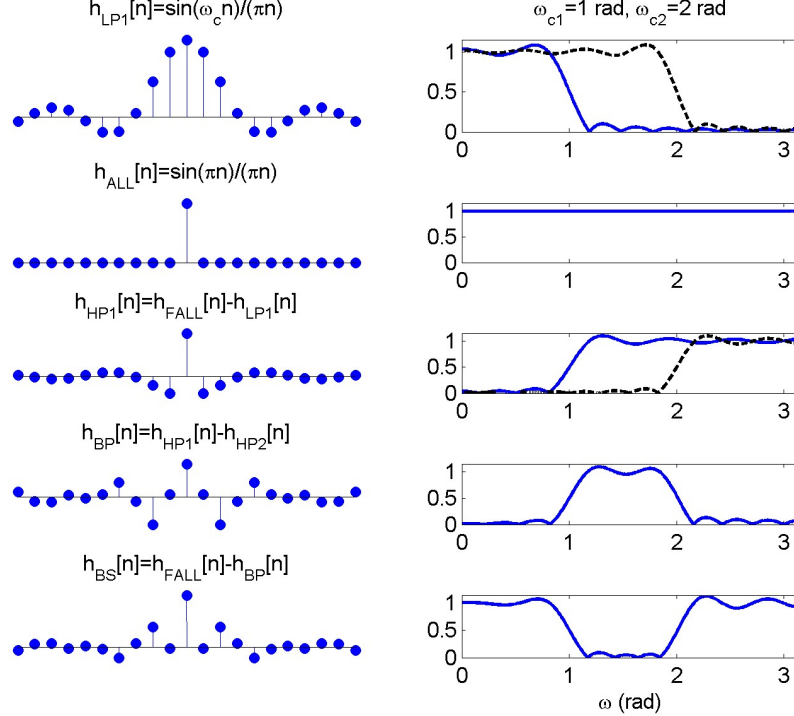


Fig.2.36 HP, BP, and BS filters obtained by summing impulse responses of LP filters and all-pass filter.

The magnitude response of LP filter may be easily shifted in frequency by π rad (i.e. the half of sampling frequency F_s) or by $\pi/2$ rad (i.e. $F_s/4$ Hz) by multiplying $h_{LP}[n]$ by $\cos(\pi n)=1,-1,1,-1,\dots$ or $\sin(\pi/2n)=0,1,0,-1,0,1,\dots$ as depicted in Fig. 2.37. This multiplication by -1, 0 or 1 is very efficient computationally because it is only the change of sign, replacing the sample with value zero, or leaving unchanged sample, and in fact no computations are required.

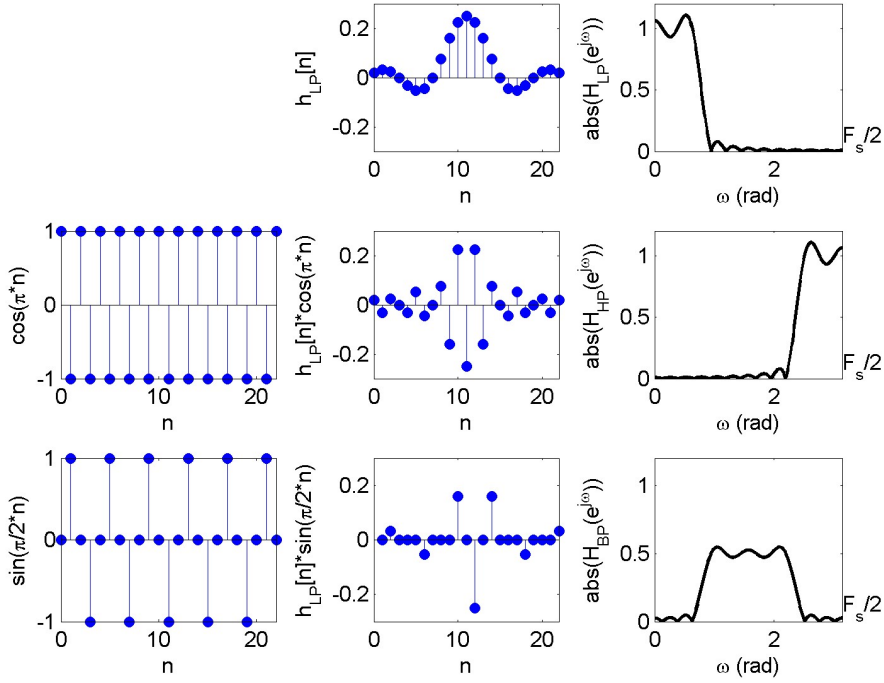


Fig.2.37 Shifting the magnitude response of LP filter by π rad ($F_s/2$) and by $\pi/2$ rad (i.e. $F_s/4$).

LTI systems with linear phase

LTI systems with linear phase response have constant group delay (2.127) that means all sinusoids in the passband are delayed by the same number of samples (time) and the system preserves the shape of the input signal.

For linear phase property impulse response of LTI system must be symmetric. The four cases of possible symmetries are depicted in Fig. 2.38a. Tab. 2.9 summaries main properties of linear phase LTI systems.

[Hay99p190]

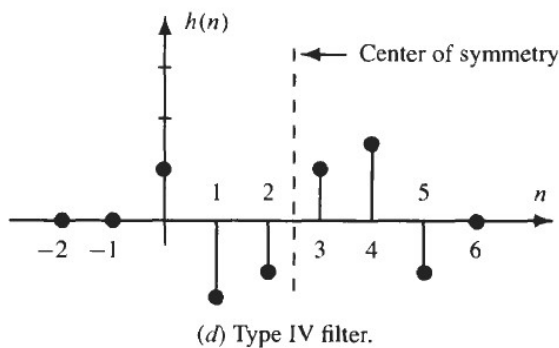
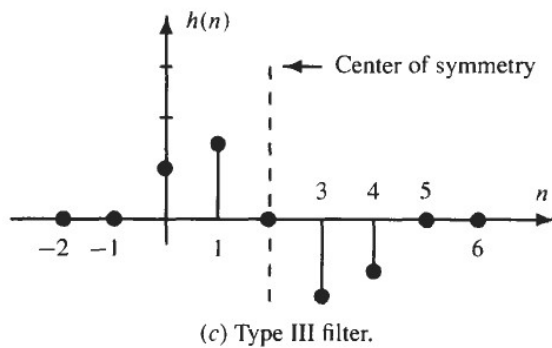
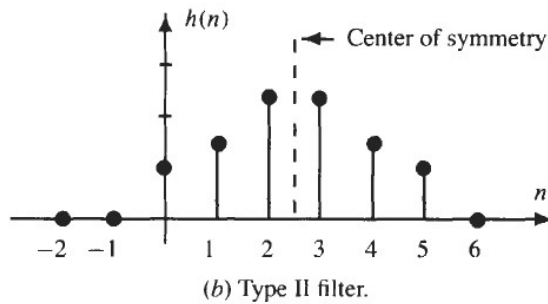
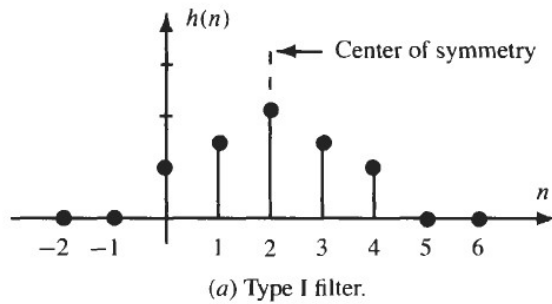


Fig. 5-3. Symmetries in the unit sample response for generalized linear phase systems.

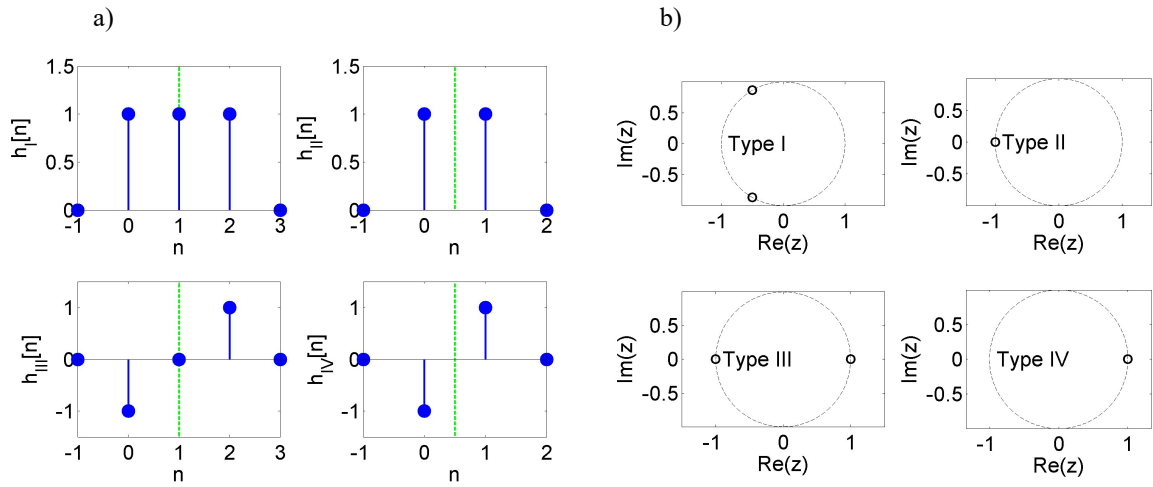


Fig.2.38 a) The symmetries of impulse responses for linear phase LTI system,
b) zero plots of $H(z)$ transmittances of linear phase LTI systems.

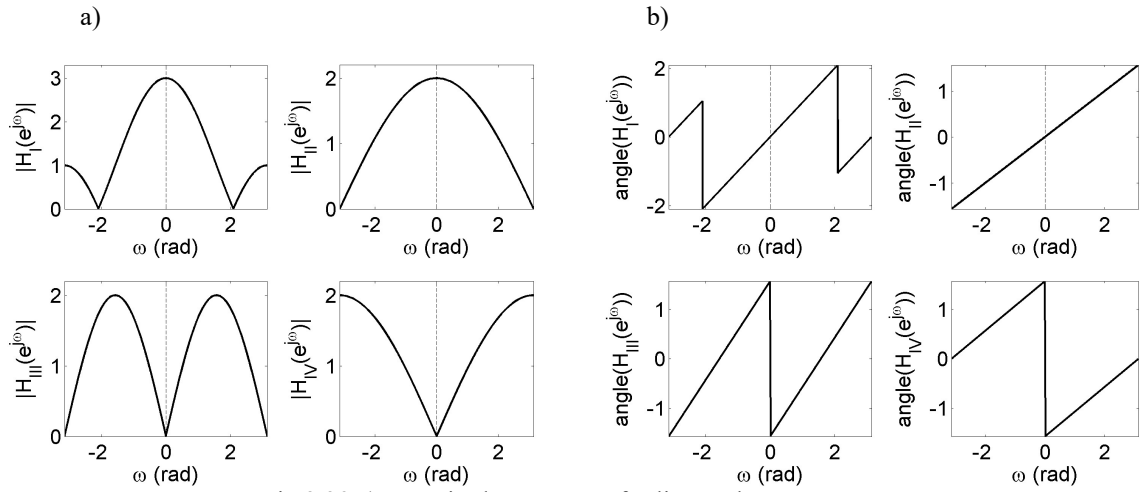


Fig.2.39 a) Magnitude responses for linear phase LTI system,
b) Phase responses of linear phase LTI systems.

Table 2.9 Linear phase LTI systems.

	Type I length $2M+1$	Type II length $2M$	Type III length $2M+1$	Type IV length $2M$
Noncasual	$h[n], -M \leq n \leq M$ $h[n]=h[-n]$ $H(e^{j\omega}) = h[0] + 2 \sum_{n=1}^M h[n] \cos(\omega n)$ $\text{angle}(H(e^{j\omega}))=0$ $\text{GRD}(\omega)=0$	$h[n], -M+1 \leq n \leq M$ $h[n]=h[-n+1]$ $H(e^{j\omega}) = 2e^{-j0.5\omega} \sum_{n=1}^M h[n] \cos(\omega(n-0.5))$ $\text{angle}(H(e^{j\omega}))=-0.5\omega \text{ rad}$ $\text{GRD}(\omega)=0.5 \text{ samples}$	$h[n], -M \leq n \leq M$ $h[n]=-h[-n], h[0]=0$ $H(e^{j\omega}) = -j2 \sum_{n=1}^M h[n] \sin(\omega n)$ $\text{angle}(H(e^{j\omega}))=-\pi/2 \text{ rad}$ $\text{GRD}(\omega)=0$	$h[n], -M+1 \leq n \leq M$ $h[n]=-h[-n+1]$ $H(e^{j\omega}) = 2e^{-j(0.5\omega+\pi/2)} \sum_{n=1}^M h[n] \sin(\omega(n-0.5))$ $\text{angle}(H(e^{j\omega}))=-0.5\omega+\pi/2 \text{ rad}$ $\text{GRD}(\omega)=0.5 \text{ samples}$
Casual	$h^{2M+1}[n]=h[n-M], 0 \leq n \leq 2M$ $h^{2M+1}[n]=h^{2M+1}[2M+1-n]$ $H^{2M+1}(e^{j\omega}) = e^{-j\omega M} \left(h[M] + 2 \sum_{n=1}^M h[n] \cos(\omega(M+n)) \right)$ $\text{angle}(H^{2M+1}(e^{j\omega}))=-\omega M \text{ rad}$ $\text{GRD}(\omega)=M \text{ samples}$	$h^{2M}[n]=h[n-M+1], 0 \leq n \leq 2M-1$ $h^{2M}[n]=h^{2M}[2M-1-n]$ $H^{2M}(e^{j\omega}) = 2e^{-j\omega(M-0.5)} \sum_{n=1}^M h[n] \cos(\omega(M+n-1.5))$ $\text{angle}(H^{2M}(e^{j\omega}))=-\omega(M-0.5) \text{ rad}$ $\text{GRD}(\omega)=M-0.5 \text{ samples}$	$h^{2M+1}[n]=h[n-M], h[0]=0, 0 \leq n \leq 2M$ $h^{2M+1}[n]=-h^{2M+1}[2M+1-n], h[M]=0$ $H^{2M+1}(e^{j\omega}) = 2e^{-j(\omega M+\pi/2)} \sum_{n=1}^M h[n] \sin(\omega(M+n))$ $\text{angle}(H^{2M+1}(e^{j\omega}))=-\omega M+\pi/2 \text{ rad}$ $\text{GRD}(\omega)=M \text{ samples}$	$h^{2M}[n]=-h[n-M+1], 0 \leq n \leq 2M-1$ $h^{2M}[n]=-h^{2M}[2M-1-n]$ $H^{2M}(e^{j\omega}) = 2e^{-j(\omega(M-0.5)+\pi/2)} \sum_{n=1}^M h[n] \sin(\omega(M+n-1.5))$ $\text{angle}(H^{2M}(e^{j\omega}))=-\omega(M-0.5)+\pi/2 \text{ rad}$ $\text{GRD}(\omega)=M-0.5 \text{ samples}$
Zeros of transmittance $H(z)$	none all bandpass filters possible	$z=-1$ only LP, BP filters	$z=\pm 1$ only BP filters	$z=1$ only HP, BP filters
Exemplary impulse response	$h_I[n]=[1 \ 1 \ 1]$	$h_{II}[n]=[1 \ 1]$	$h_{III}[n]=[-1 \ 0 \ 1]$	$h_{IV}[n]=[-1 \ 1]$

Type I linear phase LTI system

From DTFT definition (2.46) the frequency response of noncasual system $h[n]$, $-M \leq n \leq M$ is

$$H(e^{j\omega}) = \sum_{n=-M}^M h[n]e^{-j\omega n}. \quad (2.151)$$

Let us assume Type I impulse response symmetry $h[n]=h[-n]$, then frequency response simplifies to

$$\begin{aligned} H(e^{j\omega}) &= \sum_{n=-M}^M h[n]e^{-j\omega n} = \sum_{n=-M}^{-1} h[n]e^{-j\omega n} + h[0] + \sum_{n=1}^M h[n]e^{-j\omega n} = \\ &= h[0] + \sum_{n=1}^M h[n]e^{j\omega n} + \sum_{n=1}^M h[n]e^{-j\omega n} = \\ &= h[0] + 2 \sum_{n=1}^M h[n] \frac{e^{j\omega n} + e^{-j\omega n}}{2} = h[0] + 2 \sum_{n=1}^M h[n] \cos(\omega n) \end{aligned} \quad . \quad (2.152)$$

Frequency response (2.152) is real and thus phase response is zero, and group delay is also zero.

The frequency response of causal system $h^{2M+1}[n]=h[n-M]$, $0 \leq n \leq 2M$ is obtained from (2.152) by time shifting property (2.83) of DTFT

$$\begin{aligned} H^{2M+1}(e^{j\omega}) &= e^{-j\omega M} H(e^{j\omega}) = \\ &= e^{-j\omega M} \left(h[M] + 2 \sum_{n=1}^M h[n] \cos(\omega(M+n)) \right). \end{aligned} \quad (2.153)$$

The group delay (2.127) for causal system (2.153) is M samples (the length of the impulse response is $2M+1$).

Type II linear phase LTI system

For noncasual system $h[n]$, $-M+1 \leq n \leq M$ with impulse response symmetry $h[n]=h[-n+1]$ the frequency response is

$$\begin{aligned} H(e^{j\omega}) &= \sum_{n=-M+1}^M h[n]e^{-j\omega n} = \sum_{n=-M+1}^0 h[n]e^{-j\omega n} + \sum_{n=1}^M h[n]e^{-j\omega n} = \\ &= \sum_{n=1}^M h[n]e^{j\omega(n-1)} + \sum_{n=1}^M h[n]e^{-j\omega n} = \\ &= e^{-j0.5\omega} \sum_{n=1}^M h[n]e^{j\omega n} e^{-j0.5\omega} + e^{-j0.5\omega} \sum_{n=1}^M h[n]e^{-j\omega n} e^{j0.5\omega} = \\ &= 2e^{-j0.5\omega} \sum_{n=1}^M h[n] \frac{e^{j\omega(n-0.5)} + e^{-j\omega(n-0.5)}}{2} = 2e^{-j0.5\omega} \sum_{n=1}^M h[n] \cos(\omega(n-0.5)) \end{aligned} \quad . \quad (2.154)$$

Phase response of (2.154) is linear because $\text{angle}(H(e^{j\omega}))=-0.5\omega$, and group delay (2.127) is $\text{GRD}(\omega)=0.5$ samples.

The frequency response of causal system $h^{2M}[n]=h[n-M+1]$, $0 \leq n \leq 2M-1$ is obtained from (2.152) by time shifting property (2.83) of DTFT

$$\begin{aligned} H^{2M}(e^{j\omega}) &= e^{-j\omega(M-1)} H(e^{j\omega}) = \\ &= 2e^{-j\omega(M-0.5)} \sum_{n=1}^M h[n] \cos(\omega(M+n-1.5)). \end{aligned} \quad (2.155)$$

The group delay (2.127) for causal system (2.155) is $M-0.5$ samples (the length of the impulse response is $2M$).

Type III linear phase LTI system

For noncasual system $h[n]$, $-M \leq n \leq M$ having Type III impulse response symmetry $h[n] = -h[-n]$, $h[0] = 0$ frequency response is

$$\begin{aligned} H(e^{j\omega}) &= \sum_{n=-M}^M h[n]e^{-j\omega n} = \sum_{n=-M}^{-1} h[n]e^{-j\omega n} + h[0] + \sum_{n=1}^M h[n]e^{-j\omega n} = \\ &= -\sum_{n=1}^M h[n]e^{j\omega n} + \sum_{n=1}^M h[n]e^{-j\omega n} = \\ &= -j2 \sum_{n=1}^M h[n] \frac{e^{j\omega n} - e^{-j\omega n}}{2j} = 2e^{-j\pi/2} \sum_{n=1}^M h[n] \sin(\omega n) \end{aligned} . \quad (2.156)$$

Frequency response (2.156) is imaginary and phase response is constant angle($H(e^{j\omega})$) = $-\pi/2$, thus group delay is zero.

The frequency response of causal system $h^{2M+1}[n] = -h[n-M]$, $h[M] = 0$, $0 \leq n \leq 2M$ is obtained from (2.156) by time shifting property (2.83) of DTFT

$$\begin{aligned} H^{2M+1}(e^{j\omega}) &= e^{-j\omega M} H(e^{j\omega}) = \\ &= 2e^{-j(\omega M + \pi/2)} \sum_{n=1}^M h[n] \sin(\omega(M+n)) \end{aligned} . \quad (2.157)$$

The group delay (2.127) for causal system (2.157) is M samples (the length of the impulse response is $2M+1$).

Type IV linear phase LTI system

For noncasual system $h[n]$, $-M+1 \leq n \leq M$ with impulse response symmetry $h[n] = -h[-n+1]$ the frequency response is

$$\begin{aligned} H(e^{j\omega}) &= \sum_{n=-M+1}^M h[n]e^{-j\omega n} = \sum_{n=-M+1}^0 h[n]e^{-j\omega n} + \sum_{n=1}^M h[n]e^{-j\omega n} = \\ &= -\sum_{n=1}^M h[n]e^{j\omega(n-1)} + \sum_{n=1}^M h[n]e^{-j\omega n} = \\ &= -j2e^{-j0.5\omega} \sum_{n=1}^M h[n] \frac{e^{j\omega(n-0.5)} - e^{-j\omega(n-0.5)}}{2j} = 2e^{-j(0.5\omega + \pi/2)} \sum_{n=1}^M h[n] \sin(\omega(n-0.5)) \end{aligned} . \quad (2.158)$$

Phase response of (2.158) is linear angle($H(e^{j\omega})$) = $-0.5\omega + \pi/2$, and group delay (2.127) is $\text{GRD}(\omega) = 0.5$ samples.

The frequency response of causal system $h^{2M}[n] = h[n-M+1]$, $0 \leq n \leq 2M-1$ is obtained from (2.152) by time shifting property (2.83) of DTFT

$$\begin{aligned} H^{2M}(e^{j\omega}) &= e^{-j\omega(M-1)} H(e^{j\omega}) = \\ &= 2e^{-j(\omega(M-0.5) + \pi/2)} \sum_{n=1}^M h[n] \sin(\omega(M+n-1.5)) \end{aligned} . \quad (2.159)$$

The group delay (2.127) for causal system (2.159) is $M-0.5$ samples (the length of the impulse response is $2M$).

Designing of FIR filters by window method

In window method the infinite length impulse response $h_d[n]$ of the FIR filter with desired frequency response $H_d(e^{j\omega})$ is computed by inverse DTFT (2.45)

$$h_d[n] = \frac{1}{2\pi} \int_{-\pi}^{\pi} H_d(e^{j\omega}) e^{j\omega n} d\omega, \quad (2.160)$$

see (2.146) for LP filter example, and then it is multiplied by finite length time window

$$h[n] = h_d[n]w[n], \quad w[n] = \begin{cases} w[n], & n = 0, 1, 2, \dots, N \\ 0, & \text{otherwise.} \end{cases} \quad (2.161)$$

The DTFT of the product (2.161) is the convolution integral of DTFTs of the infinite length impulse response $h_d[n]$ and finite length time window $w[n]$

$$H(e^{j\omega}) = \frac{1}{2\pi} \int_{-\pi}^{\pi} H_d(e^{j\Theta})W(e^{j(\omega-\Theta)})d\Theta. \quad (2.162)$$

Fig. 2.40 illustrates (2.161) and (2.162) for rectangular window defined as $w[n]=1$, $n=0, 1, \dots, N-1$. Finite length impulse response $h[n]$ is the fragment selected by window $w[n]$ from the infinite length impulse response $h_d[n]$. The frequency response $H(e^{j\omega})$ of $h[n]$ is the convolution integral of $H_d(e^{j\omega})$ and $W(e^{j\omega})$. While computing this integral both spectra are shifted along each other, thus ripples in the passband and stopband in $H(e^{j\omega})$ have the same amplitude. For the filter designed with rectangular window ripples in the stopband are on the level -21 dB and this attenuation does not depend on the filter length, see Fig. 2.41. By increasing filter length the transition band becomes narrower, i.e. the magnitude response becomes sharper.

Filter designed with rectangular window has the narrowest transition band (advantage) and the lowest attenuation of sidelobes (disadvantage). Other time windows sacrifice the width of transition band for higher attenuation of sidelobes.

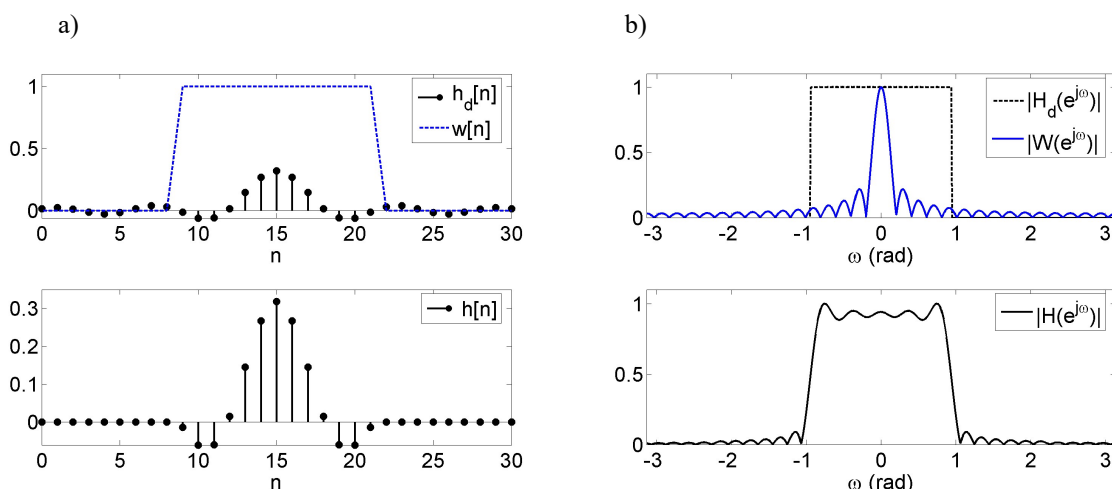


Fig. 2.40 a) Infinite length impulse response $h_d[n]$ of LP filter and finite length impulse response $h[n]$ obtained by multiplication with rectangular window,

b) Magnitude responses of infinite length LP filter and rectangular window, and magnitude response of finite length LP filter as a convolution of above two characteristics.

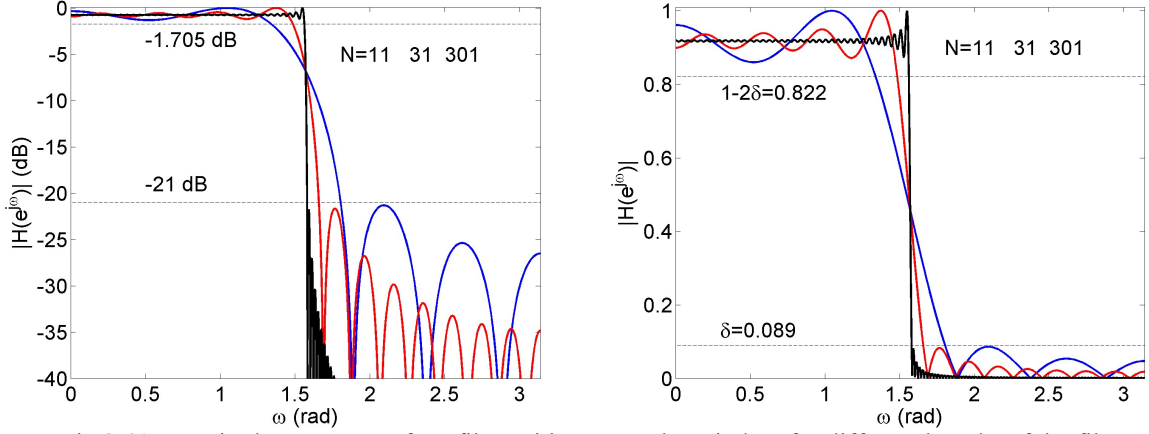


Fig.2.41 Magnitude responses of LP filter with rectangular window for different lengths of the filter.

Time windows

Rectangular window

Rectangular window is defined as

$$w_R[n] = \begin{cases} 1, & n = 0, 1, 2, \dots, N \\ 0, & \text{otherwise.} \end{cases} \quad (2.163)$$

Note that according the definition (2.163) the length of the window is $N+1$.

From DTFT definition (2.46), the frequency response of rectangular window (2.163) is for $\omega \neq 0$

$$\begin{aligned} W_R(e^{j\omega}) &= \sum_{n=0}^N e^{-j\omega n} = \frac{1 - e^{-j\omega(N+1)}}{1 - e^{-j\omega}} = \\ &= \frac{2je^{-j\omega(N+1)/2} \frac{e^{j\omega(N+1)/2} - e^{-j\omega(N+1)/2}}{2j}}{2je^{-j\omega/2} \frac{e^{j\omega/2} - e^{-j\omega/2}}{2j}} = . \end{aligned} \quad (2.164a)$$

$$= e^{-j\omega N/2} \frac{\sin(\omega(N+1)/2)}{\sin(\omega/2)}, \quad \omega \neq 0$$

and for $\omega=0$

$$W_R(e^{j\omega}) = \sum_{n=0}^N e^{-j\omega n} = \sum_{n=0}^N 1 = N+1, \quad \omega=0. \quad (2.164b)$$

TABLE I
WINDOWS AND FIGURES OF MERIT

WINDOW	HIGHEST SIDE- LOBE LEVEL (dB)	SIDE- LOBE FALL- OFF (dB/OCT)	COHERENT GAIN	EQUIV. NOISE BW (BINS)	3.0-dB BW (BINS)	SCALLOP LOSS (dB)	WORST CASE PROCESS LOSS (dB)	6.0-dB BW (BINS)	OVERLAP CORRELATION (PCNT)	
									75% OL	50% OL
RECTANGLE	-13	-6	1.00	1.00	0.89	3.92	3.92	1.21	75.0	50.0
TRIANGLE	-27	-12	0.50	1.33	1.28	1.82	3.07	1.78	71.9	25.0
COS ² (X)	a = 1.0	-23	-12	0.64	1.23	1.20	2.10	3.01	1.65	75.5
HANNING	a = 2.0	-32	-18	0.50	1.50	1.44	1.42	3.18	2.00	65.9
	a = 3.0	-39	-24	0.42	1.73	1.66	1.08	3.47	2.32	56.7
	a = 4.0	-47	-30	0.38	1.94	1.86	0.86	3.75	2.59	48.6
HAMMING		-43	-6	0.54	1.36	1.30	1.78	3.10	1.81	70.7
RIESZ		-21	-12	0.67	1.20	1.16	2.22	3.01	1.59	76.5
RIEMANN		-26	-12	0.59	1.30	1.26	1.89	3.03	1.74	73.4
DE LA VALLE-POUSSIN		-53	-24	0.38	1.92	1.82	0.90	3.72	2.55	49.3
TUKEY	a = 0.25	-14	-18	0.88	1.10	1.01	2.96	3.39	1.38	74.1
	a = 0.50	-15	-18	0.75	1.22	1.15	2.24	3.11	1.57	72.7
	a = 0.75	-19	-18	0.63	1.36	1.31	1.73	3.07	1.80	70.5
BOHMAN		-46	-24	0.41	1.79	1.71	1.02	3.54	2.38	54.5
POISSON	a = 2.0	-19	-6	0.44	1.30	1.21	2.09	3.23	1.69	69.9
	a = 3.0	-24	-6	0.32	1.65	1.45	1.46	3.64	2.08	54.8
	a = 4.0	-31	-6	0.25	2.08	1.75	1.03	4.21	2.58	40.4
HANNING-POISSON	a = 0.5	-35	-18	0.43	1.61	1.54	1.26	3.33	2.14	61.3
	a = 1.0	-39	-18	0.38	1.73	1.64	1.11	3.50	2.30	56.0
	a = 2.0	NONE	-18	0.29	2.02	1.87	0.87	3.94	2.65	44.6
CAUCHY	a = 3.0	-31	-6	0.42	1.48	1.34	1.71	3.40	1.90	61.6
	a = 4.0	-35	-6	0.33	1.76	1.50	1.36	3.83	2.20	48.8
	a = 5.0	-30	-6	0.28	2.06	1.68	1.13	4.28	2.53	38.3
GAUSSIAN	a = 2.5	-42	-6	0.51	1.39	1.33	1.69	3.14	1.86	67.7
	a = 3.0	-55	-6	0.43	1.64	1.55	1.26	3.40	2.18	57.5
	a = 3.5	-69	-6	0.37	1.90	1.79	0.94	3.73	2.52	47.2
DOLPH-CHEBYSHEV	a = 2.5	-50	0	0.53	1.39	1.33	1.70	3.12	1.85	69.6
	a = 3.0	-60	0	0.48	1.51	1.44	1.44	3.23	2.01	64.7
	a = 3.5	-70	0	0.45	1.62	1.55	1.25	3.35	2.17	60.2
	a = 4.0	-80	0	0.42	1.73	1.65	1.10	3.48	2.31	55.9
KAISER-BESSEL	a = 2.0	-46	-6	0.49	1.50	1.43	1.46	3.20	1.99	65.7
	a = 2.5	-57	-6	0.44	1.65	1.57	1.20	3.38	2.20	59.5
	a = 3.0	-69	-6	0.40	1.80	1.71	1.02	3.56	2.39	53.9
	a = 3.5	-82	-6	0.37	1.93	1.83	0.89	3.74	2.57	48.8
BARCILON-TEMES	a = 3.0	-53	-6	0.47	1.56	1.49	1.34	3.27	2.07	63.0
	a = 3.5	-58	-6	0.43	1.67	1.59	1.18	3.40	2.23	58.6
	a = 4.0	-68	-6	0.41	1.77	1.69	1.05	3.52	2.36	54.4
EXACT BLACKMAN		-51	-6	0.46	1.57	1.52	1.33	3.29	2.13	62.7
BLACKMAN		-58	-18	0.42	1.73	1.68	1.10	3.47	2.35	56.7
MINIMUM 3-SAMPLE BLACKMAN-HARRIS		-67	-6	0.42	1.71	1.66	1.13	3.45	1.81	57.2
* MINIMUM 4-SAMPLE BLACKMAN-HARRIS		-92	-6	0.36	2.00	1.90	0.83	3.85	2.72	46.0
* 61 dB 3-SAMPLE BLACKMAN-HARRIS		-61	-6	0.45	1.61	1.56	1.27	3.34	2.19	61.0
74 dB 4-SAMPLE BLACKMAN-HARRIS		-74	-6	0.40	1.79	1.74	1.03	3.56	2.44	53.9
4-SAMPLE KAISER-BESSEL	a = 3.0	-69	-6	0.40	1.80	1.74	1.02	3.56	2.44	53.9
	KAISER-BESSEL									7.4

*REFERENCE POINTS FOR DATA ON FIGURE 12 – NO FIGURES TO MATCH THESE WINDOWS.

Cosine windows

Cosine windows are defined as a weighted sum of harmonic cosine functions

$$w_{\cos}[n] = \begin{cases} \sum_{m=0}^M (-1)^m A[m] \cos\left(\frac{2\pi}{N} mn\right), & n = 0, 1, 2, \dots, N \\ 0, & \text{otherwise.} \end{cases} \quad (2.165)$$

Cosine window defined by (2.165) may be interpreted as a sum of modulated (i.e. frequency shifted) rectangular windows, thus the frequency response of cosine window may be expressed as the weighted sum of frequency shifted responses of rectangular window (2.164)

$$W_{\cos}(e^{j\omega}) = \sum_{m=0}^M (-1)^m \frac{A[m]}{2} W_R(e^{j(\omega - \omega_m)}) + (-1)^m \frac{A[m]}{2} W_R(e^{j(\omega + \omega_m)}), \quad (2.166)$$

where $\omega_m = \frac{2\pi}{N+1}m$.

The examples of cosine windows are:

- $\sin^\alpha(x)$ windows (including Hann window),
- Hamming window,
- Blackman window.

$\sin^\alpha(x)$ cosine windows

The $\sin^\alpha(x)$ windows are defined as

$$w_\alpha[n] = \sin^\alpha\left(\frac{\pi}{N}n\right), \quad n = 0, 1, 2, \dots, N, \quad (2.167)$$

with α normally being an integer.

For $\alpha=0$ we get rectangular window from (2.167).

For $\alpha=0, 2, 4, \dots$ $\sin^\alpha(x)$ windows are called Rife-Vincent class I windows.

For $\alpha=2$ we get Hann window also called (incorrectly) Hanning window

$$w_{\alpha=2}[n] = \sin^2\left(\frac{\pi}{N}n\right) = 0.5 - 0.5\cos\left(\frac{2\pi}{N}n\right), \quad n = 0, 1, 2, \dots, N. \quad (2.168)$$

Equation (2.168) defines *symmetric window* that preserves the symmetry of FIR impulse response, and thus linear phase property. In signal analysis *periodic windows* are used that preserve the periodicity (if exists) of the signal. The periodic window is also defined by equation (2.168) but the range of n goes from 0 to $N-1$, that is $n=0, 1, 2, \dots, N-1$. The symmetric and periodic Hann windows are shown in Fig. 2.42.

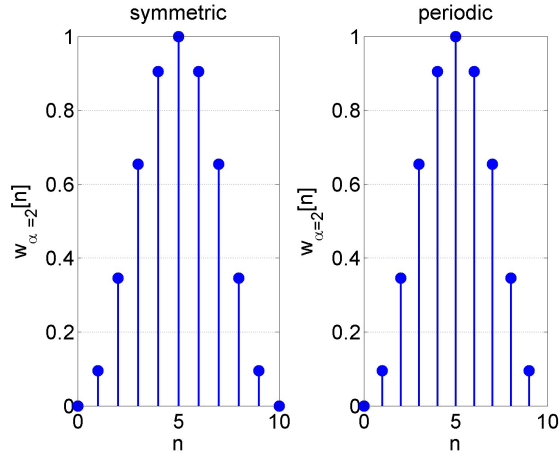


Fig.2.42 Symmetric and periodic Hann windows.

Hann window (2.168) is a sum of rectangular window and rectangular window multiplied by cosine function, i.e. shifted in frequency from $\omega=0$ to $\omega=\pm 2\pi/N$ rad

$$W_{\alpha=2}(e^{j\omega}) = -0.25W_R(e^{j(\omega-\omega_l)}) + 0.5W_R(e^{j\omega}) - 0.25W_R(e^{j(\omega+\omega_l)}), \quad \omega_l = \frac{2\pi}{N+1}. \quad (2.169)$$

Fig. 2.43a illustrates equation (2.169), it is seen that the mainlobe of Hann window is two times wider than the mainlobe of rectangular window, but side lobes for Hann window are smaller. Comparison of magnitude characteristics in dB for rectangular window and Hann window is shown in Fig. 2.43b. For rectangular window the first side lobe is on the level -13 dB, and for Hann window -31 dB.

Fig. 2.44 shows $\sin^\alpha(x)$ windows for $\alpha=0,1,2,\dots,6$, and their magnitude characteristics. $\sin^\alpha(x)$ windows have the fastest decaying sidelobes.

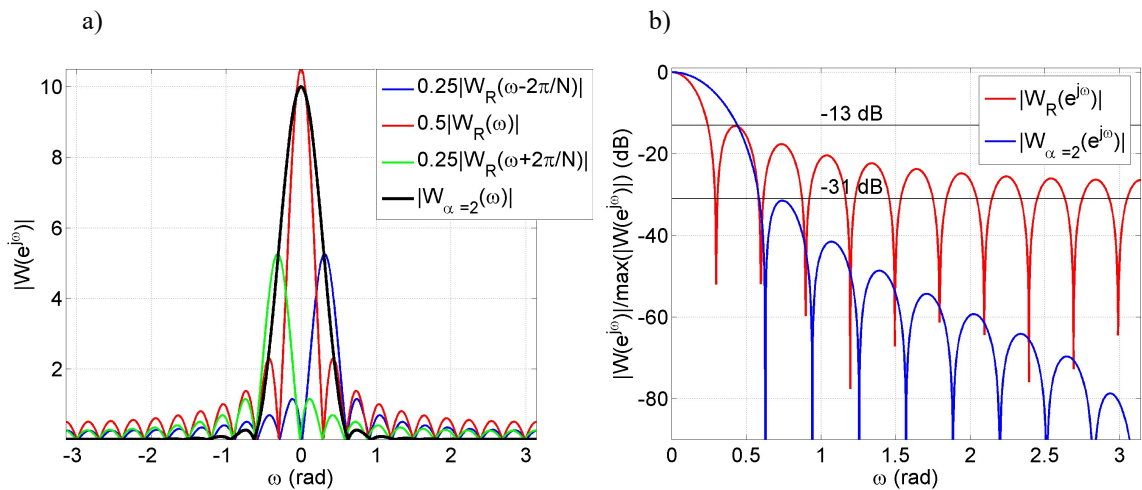


Fig.2.43 a)Magnitude response of symmetric Hann window as a sum of scaled and frequency shifted spectra of three rectangular windows, $N=20$.

b) Comparison of magnitude characteristics of rectangular window and Hann window, $N=20$.

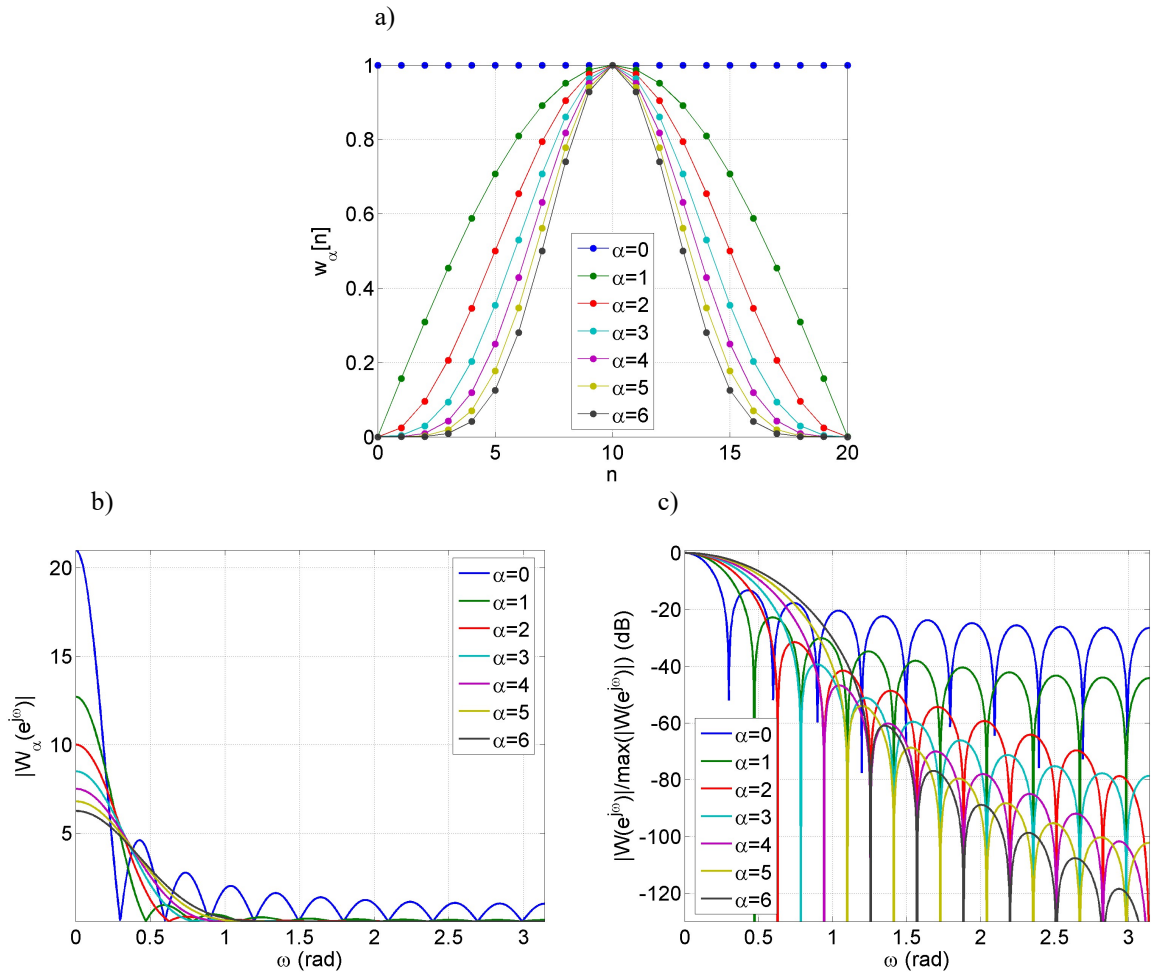


Fig.2.44 Symmetric $\sin^\alpha(x)$ windows and their magnitude characteristics.

Hamming cosine window

The Hamming window is defined as

$$w_H[n] = 0.54 - 0.46 \cos\left(\frac{2\pi}{N}n\right), \quad n = 0, 1, 2, \dots, N. \quad (2.170)$$

The first side lobe in the magnitude spectrum of Hamming window is on the level -41 dB, and the width of the mainlobe is similar to Hann window.

Blackman cosine window

The Blackman window is defined as

$$w_B[n] = 0.42 - 0.5 \cos\left(\frac{2\pi}{N}n\right) + 0.08 \cos\left(\frac{4\pi}{N}n\right), \quad n = 0, 1, 2, \dots, N. \quad (2.171)$$

The first side lobe in the magnitude spectrum of Blackman window is on the level -57 dB.

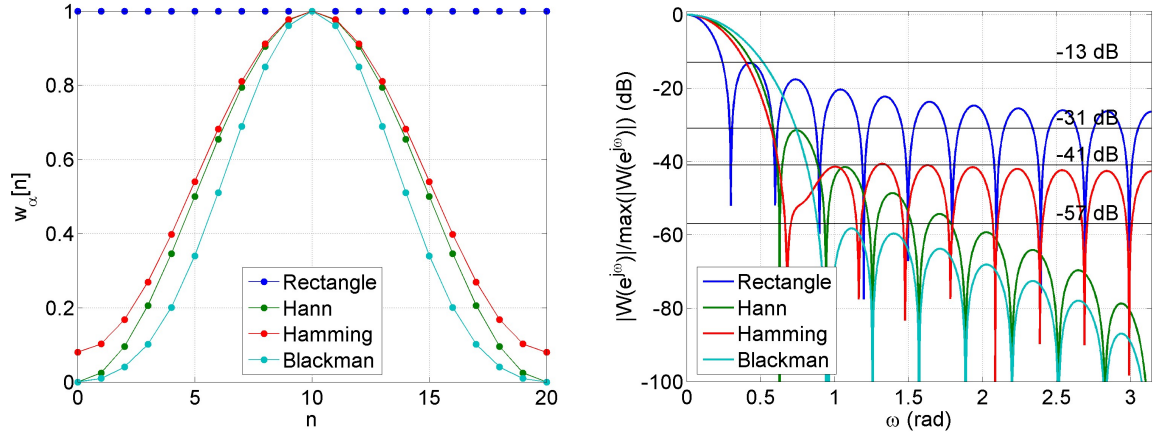


Fig.2.45 Symmetric cosine windows and their magnitude characteristics.

Self-convolution windows

Self-convolution window of order P is defined by $P+1$ convolutions of rectangular window

$$w_P[n] = \underbrace{w_0[n] * w_0[n] * \dots * w_0[n]}_{(P+1) \text{ times}}, \quad P = 0, 1, 2, \dots, \quad (2.172)$$

where $w_0[n] = w_R[n]$. The length of symmetric window $w_P[n]$ is $N_p + 1$, and

$$N_p = (P+1)N_0, \quad (2.173)$$

where $N_0 + 1$ is the length of $w_0[n]$. Note also that the maximum value of the convolution window defined by (2.172) increases rapidly with the order P . Convolution window is often normalized by mean value.

It goes from the DTFT convolution property (2.87) that the spectrum of self-convolution window (2.172) of order P and length $N_p + 1$ is given by the $P+1$ -th power of the spectrum of rectangular window with length $N_0 = \frac{N_p}{P+1} + 1$.

$$\begin{aligned} W_P(e^{j\omega}) &= [W_0(e^{j\omega})]^{P+1} = \left[e^{-j\omega N_0 / 2} \frac{\sin(\omega(N_0 + 1)/2)}{\sin(\omega/2)} \right]^{P+1} = \\ &= e^{-j\omega N_p / 2} \left[\frac{\sin\left(\omega\left(\frac{N_p + P + 1}{2(P+1)}\right)\right)}{\sin(\omega/2)} \right]^{P+1}, \quad \omega \neq 0. \end{aligned} \quad (2.174a)$$

$$W_P(e^{j\omega}) = (N_0 + 1)^{P+1}, \quad \omega = 0. \quad (2.174b)$$

Explicit equations for self-convolution windows (2.172) are splines, however the samples of $w_P[n]$ may easily be obtained by DFT, e.g.:

```
P = 1;
N0 = 12;
Np = (P+1)*N0
Wk = ( fft( ones(1,N0+1), Np+1 ) ).^(P+1);
wn = ifft(Wk);
wn = wn/(Wk(1)/(Np+1)); %normalization by mean value
```

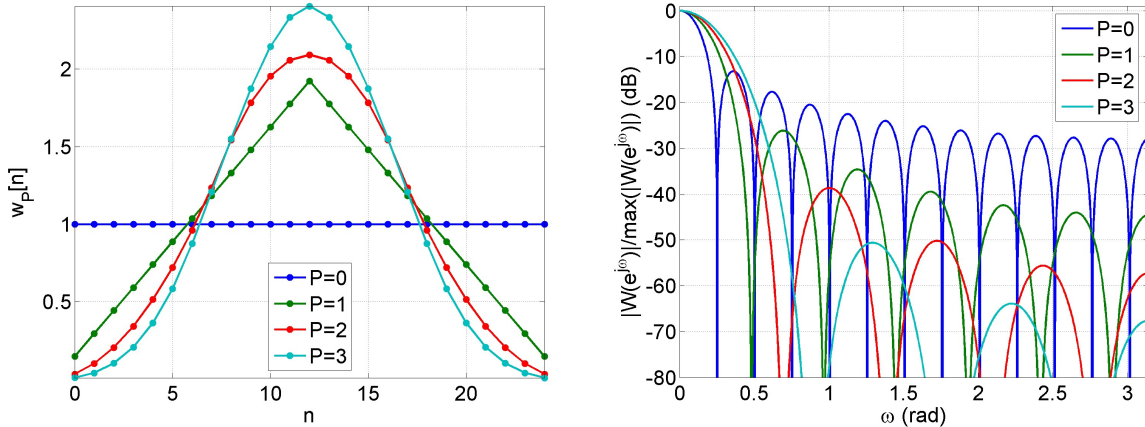


Fig.2.46 Symmetric self-convolution windows and their magnitude characteristics.

Kaiser-Bessel window

The trade-off between the mainlobe width and the side lobe area may be expressed as an optimality criterion, e.g. for a restricted energy, determine the function of restricted time duration which maximizes the energy in the band of frequencies. Above problem was solved by Slepian et. al. and involves prolate spheroidal wave functions that are difficult to manipulate. However Kaiser found that a near-optimal window could be formed using Bessel functions. The Kaiser-Bessel window is defined as

$$w[n] = \begin{cases} \frac{I_0[\beta(1 - [(n-\alpha)/\alpha]^2)^{1/2}]}{I_0(\beta)}, & n = 0, 1, 2, \dots, N, \\ 0, & \text{otherwise} \end{cases}, \quad (2.175)$$

where $\alpha=N/2$, and $I_0(\cdot)$ represents the zeroth-order modified Bessel functions of the first kind (in Matlab function **besseli**)

Kaiser-Bessel window has two parameters: 1) the length $N+1$, and 2) the shape parameter β . By increasing N the transition band is narrowed, and by increasing β the attenuation of the side lobes is increased. Fig. 2.47 shows exemplary Kaiser-Bessel windows for different β and their magnitude characteristics.

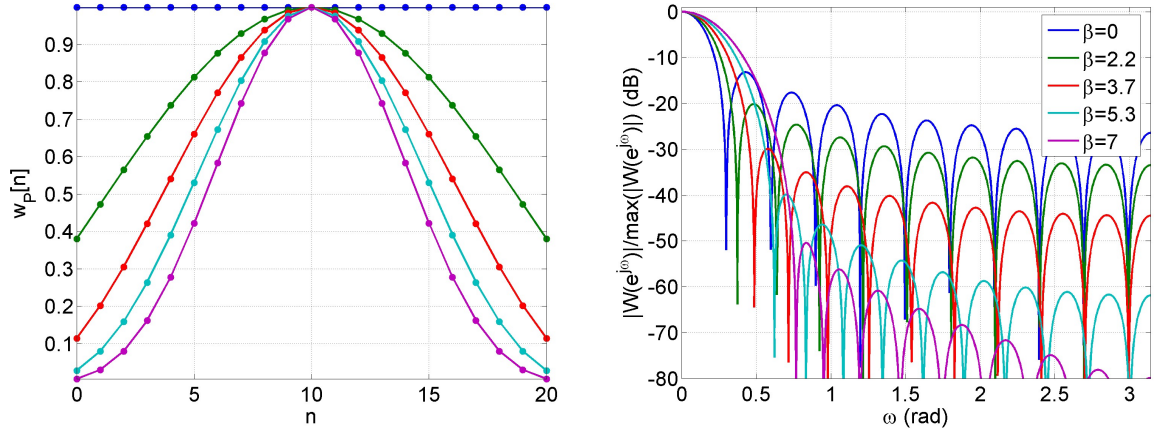


Fig.2.47 Symmetric Kaiser-Bessel windows and their magnitude characteristics.

Kaiser determined empirically the value of β and N for obtaining required attenuation of FIR filter

$$\beta = \begin{cases} 0.1102(A - 8.7), & A > 50 \\ 0.5842(A - 21)^{0.4} + 0.07886(A - 21), & 21 \leq A \leq 50 \\ 0, & A < 21 \end{cases}, \quad (2.176)$$

where $A = -20\log_{10}(\delta)$, $\Delta\omega = \omega_s - \omega_p$ and the meaning of passband and stopband attenuation δ and transition region width $\Delta\omega$ are explained in Fig. 2.48. Parameter N is predicted as

$$N = \frac{A - 8}{2.285\Delta\omega}. \quad (2.177)$$

Equation (2.177) is not strict and the final design may require the fine tuning of parameters N and β by the trial and error.

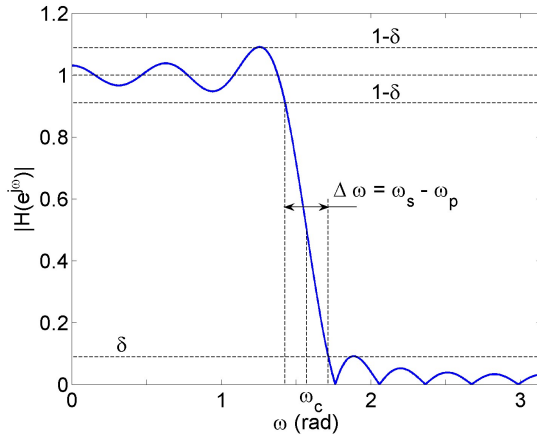


Fig.2.48 Magnitude response of the FIR filter designed by window method.

Example 2.12

Design discrete-time lowpass FIR filter with Kaiser-Bessel window with magnitude response fulfilling the requirements:

- the passband edge frequency $\omega_p=0.4\pi$ rad,
- the stopband edge frequency $\omega_s=0.6\pi$ rad,
- maximum passband attenuation $r_p=1$ dB,
- minimum stopband attenuation $r_s=60$ dB.

The FIR filter design goes in the following steps:

1. Compute δ in the passband and in the stopband:

$$\text{passband} \quad \delta_p = (1 - 10^{-r_p/20})/2 = 0.0544,$$

$$\text{stopband} \quad \delta_s = 10^{-r_s/20} = 0.001.$$

For FIR filter designed by window method $\delta_p=\delta_s$, and thus the lower δ is chosen $\delta = \min\{\delta_p, \delta_s\} = 0.001$.

2. Compute β and N using (2.176) and (2.177), and then the Kaiser-Bessel window (2.175). In the example $\beta=5.6533$ and $N=37$. Note that if Type I impulse response symmetry is required then the length of the filter impulse response must be odd.

3. Compute impulse response of FIR filter for the frequency $\omega_c=(\omega_s+\omega_p)/2$ (2.147), and multiply it by the window.

4. Check the magnitude response of the designed FIR filter.

Fig. 2.49a shows magnitude response of the designed FIR filter. It is seen that that requirements in stopband are not fulfilled. By the trial and error parameter N was changed from 37 to 39 and β from $\beta=5.6533$ to $\beta=5.7663$. Resulting magnitude response is presented in Fig. 2.49b.

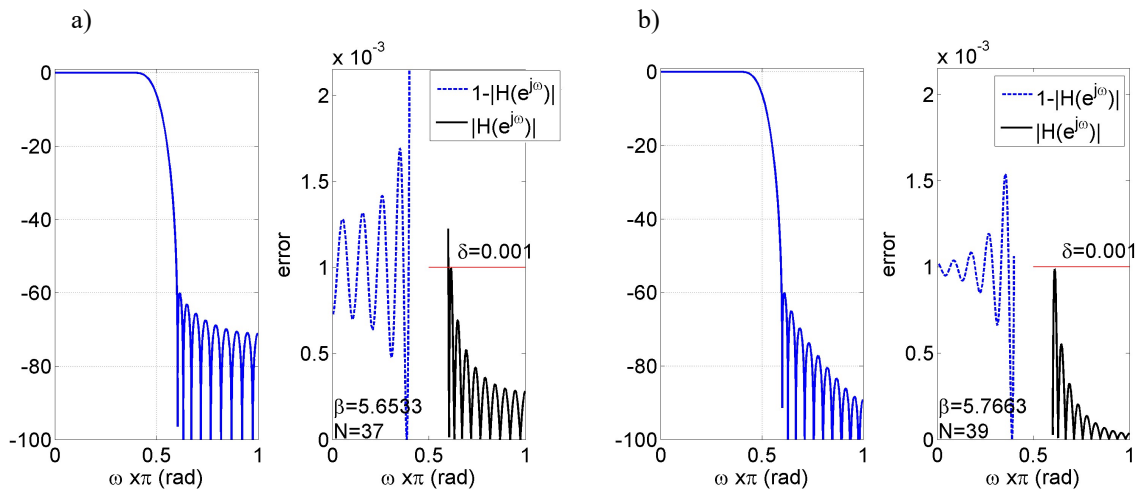


Fig.2.49 a) Magnitude response of designed FIR filter, and approximation error in respect to ideal lowpass filter.
b) Magnitude response after trial and error tuning of N and β , and approximation error.

Optimum approximations of FIR filters

The problem of optimum FIR filter design may be stated as follows. Find the impulse response $h[n]$ of FIR filter as to minimize the distance between the desired frequency response $D(e^{j\omega})$ and filter frequency response $H(e^{j\omega})$

$$E(e^{j\omega}) = D(e^{j\omega}) - H(e^{j\omega}) \quad (2.178)$$

in the sense of the chosen metric. In practice two metrics are used:

Mean Square distance denoted as L_2

$$E_2 = \left[\frac{1}{2\pi} \int_{-\pi}^{\pi} |E(e^{j\omega})|^2 d\omega \right]^{1/2}, \quad (2.179)$$

and *Chebyshev* distance denoted as L_∞

$$E_\infty = \max_{\omega} |E(e^{j\omega})|. \quad (2.180)$$

Additionally, the error (2.178) may be weighted by continuous function $W(e^{j\omega})$ having real, positive values

$$E_w(e^{j\omega}) = W(e^{j\omega})E(e^{j\omega}) = W(e^{j\omega})[D(e^{j\omega}) - H(e^{j\omega})] = D_w(e^{j\omega}) - H_w(e^{j\omega}). \quad (2.181)$$

By using weighting function $W(e^{j\omega})$ it is possible to obtain different attenuation in the passband and the stopband, which is not possible in the window method.

FIR filter designed by window method with rectangular window with constant weighting function $W(e^{j\omega})=1$ is optimal in *Mean Square* sense (2.179).

FIR filter optimal in minimum of maximal errors (2.180) has equiripple magnitude response in the passband and in the stopband.

Optimum Mean Square FIR filters

Let us consider FIR filter with Type I impulse response symmetry, see [Table 2.9](#). Frequency response of this filter is

$$H(e^{j\omega}) = h[0] + 2 \sum_{n=1}^M h[n] \cos(\omega n) = \sum_{n=0}^M a[n] \cos(\omega n), \quad (2.182)$$

where

$$h[n] = \begin{cases} a[n], & n = 0 \\ a[n]/2, & 1 \leq n \leq M \end{cases}. \quad (2.183)$$

The cost function is

$$\begin{aligned} E_2 &= \left[\frac{1}{2\pi} \int_{-\pi}^{\pi} |E(e^{j\omega})|^2 d\omega \right]^{1/2} = \\ &= \left[\frac{1}{2\pi} \int_{-\pi}^{\pi} D^2(e^{j\omega}) d\omega - \frac{1}{2\pi} \int_{-\pi}^{\pi} 2D(e^{j\omega})H(e^{j\omega}) d\omega + \frac{1}{2\pi} \int_{-\pi}^{\pi} H^2(e^{j\omega}) d\omega \right]^{1/2}. \end{aligned} \quad (2.184)$$

The objective is to find minimum of E_2 (2.184) in respect to filter coefficients $h[n]$, or equivalently $a[n]$.

Example 2.13

For $M=2$ we have the following derivatives of E_2 (2.185) in respect to filter coefficients $a[n]$ (the first integral does not depend on $a[n]$)

$$\begin{aligned}\frac{dE_2}{da[0]} &= -\frac{1}{\pi} \int_{-\pi}^{\pi} D(e^{j\omega}) \cos(0) d\omega + \frac{1}{\pi} \int_{-\pi}^{\pi} \cos(0)(a[0]\cos(0) + a[1]\cos(\omega) + a[2]\cos(2\omega)) d\omega \\ \frac{dE_2}{da[1]} &= -\frac{1}{\pi} \int_{-\pi}^{\pi} D(e^{j\omega}) \cos(\omega) d\omega + \frac{1}{\pi} \int_{-\pi}^{\pi} \cos(\omega)(a[0]\cos(0) + a[1]\cos(\omega) + a[2]\cos(2\omega)) d\omega \\ \frac{dE_2}{da[2]} &= -\frac{1}{\pi} \int_{-\pi}^{\pi} D(e^{j\omega}) \cos(2\omega) d\omega + \frac{1}{\pi} \int_{-\pi}^{\pi} \cos(2\omega)(a[0]\cos(0) + a[1]\cos(\omega) + a[2]\cos(2\omega)) d\omega\end{aligned}. \quad (2.185)$$

Optimum coefficients $a[n]$ are computed by equating derivatives (2.185) to zero

$$\begin{aligned}\int_{-\pi}^{\pi} a[0]\cos(0)\cos(0)d\omega + \int_{-\pi}^{\pi} a[1]\cos(0)\cos(\omega)d\omega + \int_{-\pi}^{\pi} a[2]\cos(0)\cos(2\omega)d\omega &= \int_{-\pi}^{\pi} D(e^{j\omega})\cos(0)d\omega \\ \int_{-\pi}^{\pi} a[0]\cos(\omega)\cos(0)d\omega + \int_{-\pi}^{\pi} a[1]\cos(\omega)\cos(\omega)d\omega + \int_{-\pi}^{\pi} a[2]\cos(\omega)\cos(2\omega)d\omega &= \int_{-\pi}^{\pi} D(e^{j\omega})\cos(\omega)d\omega \\ \int_{-\pi}^{\pi} a[0]\cos(2\omega)\cos(0)d\omega + \int_{-\pi}^{\pi} a[1]\cos(2\omega)\cos(\omega)d\omega + \int_{-\pi}^{\pi} a[2]\cos(2\omega)\cos(2\omega)d\omega &= \int_{-\pi}^{\pi} D(e^{j\omega})\cos(2\omega)d\omega\end{aligned}, \quad (2.186a)$$

or in matrix notation

$$\begin{bmatrix} \int_{-\pi}^{\pi} \cos(0)\cos(0)d\omega & \int_{-\pi}^{\pi} \cos(0)\cos(\omega)d\omega & \int_{-\pi}^{\pi} \cos(0)\cos(2\omega)d\omega \\ \int_{-\pi}^{\pi} \cos(\omega)\cos(0)d\omega & \int_{-\pi}^{\pi} \cos(\omega)\cos(\omega)d\omega & \int_{-\pi}^{\pi} \cos(\omega)\cos(2\omega)d\omega \\ \int_{-\pi}^{\pi} \cos(2\omega)\cos(0)d\omega & \int_{-\pi}^{\pi} \cos(2\omega)\cos(\omega)d\omega & \int_{-\pi}^{\pi} \cos(2\omega)\cos(2\omega)d\omega \end{bmatrix} \begin{bmatrix} a[0] \\ a[1] \\ a[2] \end{bmatrix} = \begin{bmatrix} \int_{-\pi}^{\pi} D(e^{j\omega})\cos(0)d\omega \\ \int_{-\pi}^{\pi} D(e^{j\omega})\cos(\omega)d\omega \\ \int_{-\pi}^{\pi} D(e^{j\omega})\cos(2\omega)d\omega \end{bmatrix}. \quad (2.186b)$$

The frequency response of the real value signal is symmetric, see Table 2.5, and integrals in (2.186) may be computed on the interval $0 \leq \omega \leq \pi$ rad. Integrals on the left hand side of equation (2.186) do not depend on desired frequency response of the filter, and for fixed length of the filter the left hand matrix is the same no matter if the filter is e.g. lowpass or highpass.

The integrals of (2.186) are

$$\begin{bmatrix} [\omega]_0^\pi & [\sin(\omega)]_0^\pi & [\sin(2\omega)/2]_0^\pi \\ [\sin(\omega)]_0^\pi & [\sin(\omega)\cos(\omega)/2 + \omega/2]_0^\pi & [\sin(\omega)/2 + \sin(3\omega)/6]_0^\pi \\ [\sin(2\omega)/2]_0^\pi & [\sin(\omega)/2 + \sin(3\omega)/6]_0^\pi & [\sin(2\omega)\cos(2\omega)/4 + \omega/2]_0^\pi \end{bmatrix} \begin{bmatrix} a[0] \\ a[1] \\ a[2] \end{bmatrix} = \begin{bmatrix} D(e^{j\omega})[\omega]_0^\pi \\ D(e^{j\omega})[\sin(\omega)]_0^\pi \\ D(e^{j\omega})[\sin(2\omega)/2]_0^\pi \end{bmatrix}. \quad (2.187)$$

Let us assume lowpass filter with desired frequency response defined as

$$D(e^{j\omega}) = \begin{cases} 1, & |\omega| < \omega_c \\ 0, & \omega_c < \omega \leq \pi \end{cases}, \quad (2.188)$$

where ω_c is cutoff frequency in radians. For $\omega_c = \pi/2$ rad from (2.187) we get

$$\begin{bmatrix} 1 & 0 & 0 \\ 0 & 1/2 & 0 \\ 0 & 0 & 1/2 \end{bmatrix} \begin{bmatrix} a[0] \\ a[1] \\ a[2] \end{bmatrix} = \begin{bmatrix} 1/2 \\ 1/\pi \\ 0 \end{bmatrix}, \quad (2.189)$$

and coefficients $a[n]$ are

$$\begin{bmatrix} a[0] \\ a[1] \\ a[2] \end{bmatrix} = \begin{bmatrix} 1 & 0 & 0 \\ 0 & 2 & 0 \\ 0 & 0 & 2 \end{bmatrix} \begin{bmatrix} 1/2 \\ 1/\pi \\ 0 \end{bmatrix}. \quad (2.190)$$

Impulse response of optimum filter is $h[n] = [a[2]/2, a[1]/2, a[0], a[1]/2, a[2]/2] = [0, 1/\pi, 1/2, 1/\pi, 0]$. Observe that the same impulse response could be obtained from (2.146).

In general case optimum coefficients $a[n]$ are given by

$$\mathbf{a} = \mathbf{R}^{-1}\mathbf{c}, \quad (2.191)$$

where

$$\mathbf{R}[n, m] = \int_{\omega} \cos(\omega n) \cos(\omega m) d\omega, \quad n, m = 0, 1, 2, \dots, M, \quad (2.192)$$

$$\mathbf{c}[n] = \int_{\omega} D(e^{j\omega}) \cos(\omega n) d\omega. \quad (2.193)$$

The filter designed by (2.191) is the same as the filter designed by window method with rectangular window, however by introducing weighting function $W(e^{j\omega})$ we can trade off ripples in the stopband for ripples in the passband, and vice versa, which is not possible in window method.

Let us assume following weighting function $W(e^{j\omega})$

$$W(e^{j\omega}) = \begin{cases} W_p, & |\Omega| < \Omega_c \\ W_s, & \Omega_c < |\Omega| \leq \pi \end{cases}, \quad (2.194)$$

where W_p is weighting coefficient in the passband and W_s in the stopband.

Weighted filter frequency response is

$$H_w(e^{j\omega}) = W(e^{j\omega}) \sum_{n=0}^M a[n] \cos(\omega n), \quad (2.195)$$

and weighted desired frequency response for LP filter is

$$D_w(e^{j\omega}) = \begin{cases} W_p, & |\omega| < \omega_c \\ 0, & \omega_c < |\omega| \leq \pi \end{cases}. \quad (2.196)$$

The weighted cost function is

$$E_2 = \left[\frac{1}{2\pi} \int_{\omega} D_w^2(e^{j\omega}) d\omega - \frac{1}{2\pi} \int_{\omega} 2D_w(e^{j\omega}) H_w(e^{j\omega}) d\omega + \frac{1}{2\pi} \int_{\omega} H_w^2(e^{j\omega}) d\omega \right]^{1/2}. \quad (2.197)$$

Optimum coefficients $a[n]$ are given by

$$\mathbf{a} = \mathbf{R}_w^{-1}\mathbf{c}_w, \quad (2.191)$$

where

$$\mathbf{R}_w[n, m] = \int_{\omega} W(e^{j\omega}) \cos(\omega n) \cos(\omega m) d\omega, \quad n, m = 0, 1, 2, \dots, M, \quad (2.192)$$

$$\mathbf{c}_w[n] = \int_{\omega} W(e^{j\omega}) D(e^{j\omega}) \cos(\omega n) d\omega. \quad (2.193)$$

[Fig. 2.50](#) shows exemplary magnitude responses of Mean Square optimal, weighted FIR filters. In summary:

- decreasing ripples in passband increases ripples in the stopband, and vice versa, thus it is only possible to change the ratio W_p/W_s and not W_p and W_s independently,
- for $W_p/W_s \neq 1$ frequency response is shifted along frequency axis thus we lose the control of the transition band (cutoff frequency),
- filter coefficients are given by explicit formula and are easy to compute.

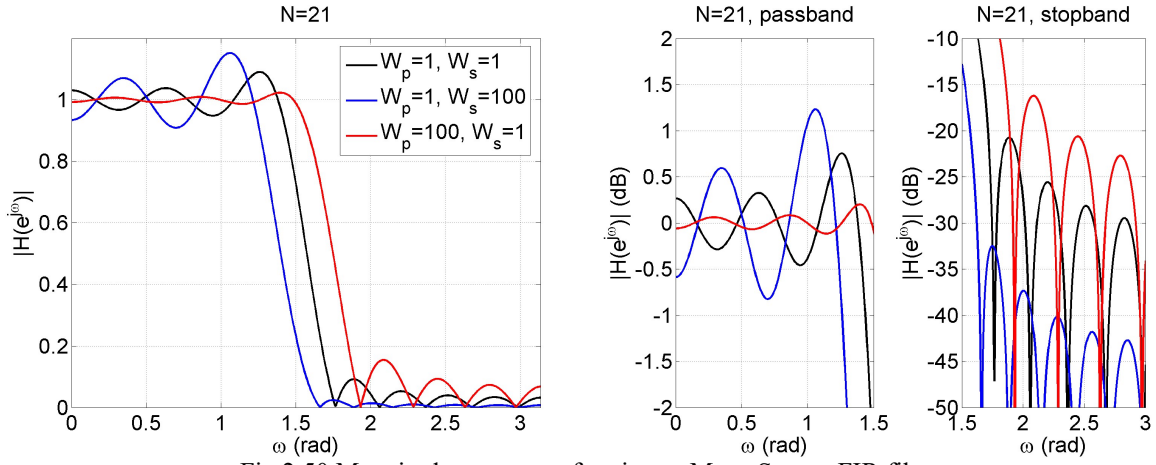


Fig.2.50 Magnitude response of optimum Mean Square FIR filters.

Optimum Min Max FIR filters

According to *alternation theorem* (tw. o przerzutach) approximation error $E(e^{j\omega}) = D(e^{j\omega}) - H(e^{j\omega})$ (2.178) for the length $N=2M+1$ FIR filter optimal in L_∞ sense (2.180) has at least $M+2$ local minima and maxima that occur alternatively in frequencies ω_k , $k=0,1,2,\dots,M+1$. Fig. 2.51a shows equiripple magnitude response of optimum in min max sense (i.e. minimum of maximal errors) (2.180) FIR filter.

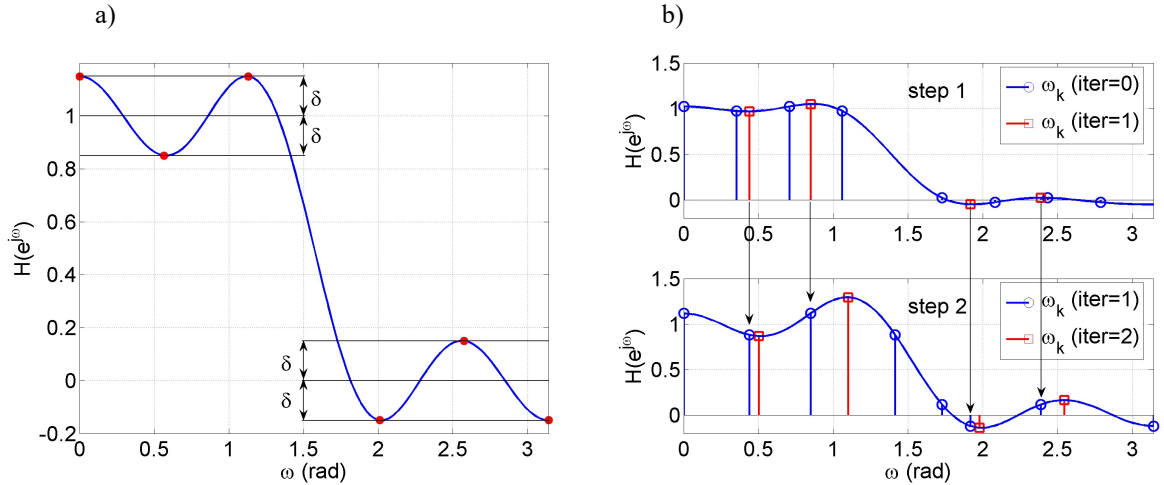


Fig.2.51 a) Equiripple magnitude response of optimum Min Max FIR filter,
b) Two successive steps of Remez algorithm, $\omega_k(\text{iter}=0)$ is initial set of frequencies.

Base on Fig. 2.51a we can write

$$W(e^{j\omega_k})[D(e^{j\omega_k}) - H(e^{j\omega_k})] = (-1)^k \delta, \quad k = 0, 1, 2, \dots, M+1, \quad (2.194)$$

where δ is an absolute maximum value of error function $E(e^{j\omega})$ (2.178). Filter coefficients $a[n]$ (2.183) along with ripples amplitude δ are computed form the set of equation (2.194)

$$D(e^{j\omega_k}) - \sum_{n=0}^M a[n] \cos(\omega_k n) = (-1)^k \delta / W(e^{j\omega_k}), \quad (2.195)$$

$$\sum_{n=0}^M a[n] \cos(\omega_k n) + (-1)^k \delta / W(e^{j\omega_k}) = D(e^{j\omega_k}), \quad (2.196)$$

$$\begin{bmatrix} 1 & \cos(\omega_0) & \cdots & \cos(\omega_0 M) & 1/W(e^{j\omega_0}) \\ 1 & \cos(\omega_1) & & \cos(\omega_1 M) & -1/W(e^{j\omega_1}) \\ 1 & \cos(\omega_2) & & \cos(\omega_2 M) & 1/W(e^{j\omega_2}) \\ \vdots & \vdots & \ddots & \vdots & \vdots \\ 1 & \cos(\omega_{M+1}) & & \cos(\omega_{M+1} M) & (-1)^k / W(e^{j\omega_{M+1}}) \end{bmatrix} \begin{bmatrix} a[0] \\ a[1] \\ \vdots \\ a[M] \\ \delta \end{bmatrix} = \begin{bmatrix} D(e^{j\omega_0}) \\ D(e^{j\omega_1}) \\ \vdots \\ D(e^{j\omega_2}) \\ \vdots \\ D(e^{j\omega_{M+1}}) \end{bmatrix}, \quad (2.197)$$

or

$$[\mathbf{R} \quad \mathbf{w}] \begin{bmatrix} \mathbf{a} \\ \delta \end{bmatrix} = \mathbf{c}, \quad (2.198)$$

where

$$\mathbf{R}[k, m] = \cos(\omega_k m), \quad k = 0, 1, 2, \dots, M+1, \quad m = 0, 1, 2, \dots, M, \quad (2.199)$$

$$\mathbf{w}[k] = (-1)^k / W(e^{j\omega_k}), \quad (2.200)$$

$$\mathbf{c}[k] = D(e^{j\omega_k}). \quad (2.201)$$

The solution is

$$\begin{bmatrix} \mathbf{a} \\ \delta \end{bmatrix} = [\mathbf{R} \quad \mathbf{w}]^{-1} \mathbf{c}. \quad (2.202)$$

Straightforward computation of (2.202) is not possible because the set of frequencies ω_k is unknown. For computing (2.202) Parks and McClellan proposed iterative Remez algorithm.

Algorithm 2.1 - Iterative computation of optimal FIR filter by Remez algorithm

I. Initialization

Assume a set of equidistant ω_k on the interval $\langle 0, \pi \rangle$ rad.

II. Computations

If the magnitude response is equiripple

end computations

else

compute the new set of ω_k as the set of frequencies of minima and maxima in the approximation error $E(e^{j\omega})$.

The first two steps of Algorithm 2.1 are depicted in Fig. 2.51b. In each iteration filter coefficients $a[n]$ and frequency response $H(e^{j\omega})$ are computed for actual set of ω_k frequencies.

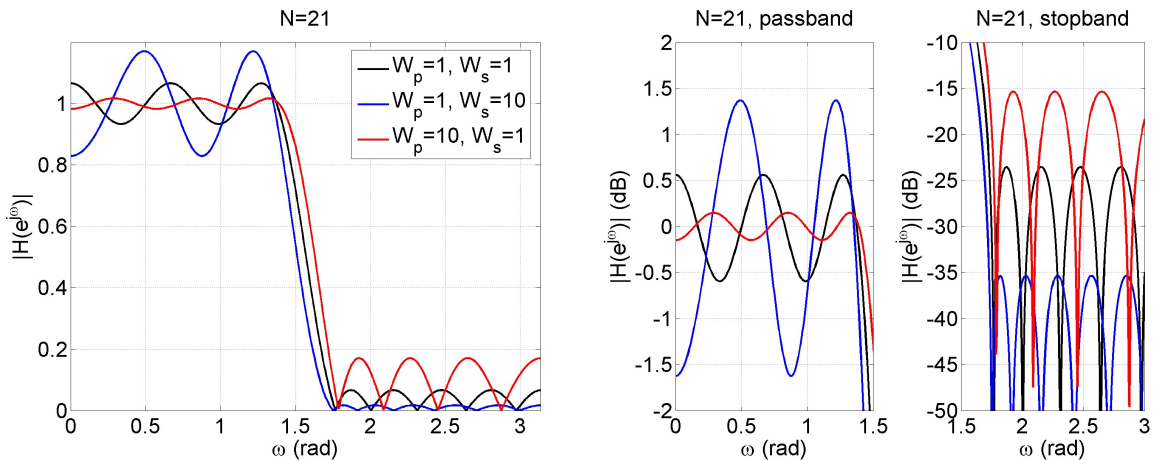


Fig.2.52 Magnitude response of optimum Min Max FIR filters.

Fig. 2.52 shows exemplary magnitude responses of Min Max optimal, weighted FIR filters. In summary:

- decreasing ripples in passband increases ripples in the stopband, and vice versa, thus it is only possible to change the ratio W_p/W_s and not W_p and W_s independently,
- filter coefficients are computed by iterative algorithm.

Table 2.10 Comparison of FIR designing methods.

	Ripples in the passband and stopband	Computation of the impulse response	Edge frequency
Window method	the same amplitude $\delta_p=\delta_s$ ripples higher near to the band edge	simple	fixed
Optimum Mean Square filters	adjustable ratio δ_p/δ_s ripples higher near to the band edge	simple	may shift
Optimum Min Max filters	adjustable ratio δ_p/δ_s equiripple	difficult (iterative)	fixed

2.4.4 Structures for discrete-time systems

344

Structures for Discrete-Time Systems Chap. 6

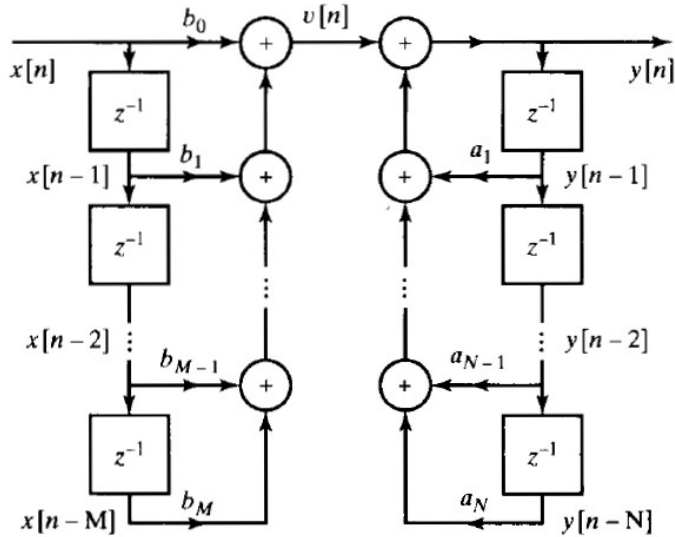


Figure 6.3 Block diagram representation for a general N th-order difference equation.

$$y[n] = \sum_{k=1}^N a_k y[n-k] + \sum_{k=0}^M b_k x[n-k]. \quad (6.9)$$

The block diagram of Figure 6.3 is an explicit pictorial representation of Eq. (6.9). More precisely, it represents the pair of difference equations

$$v[n] = \sum_{k=0}^M b_k x[n-k], \quad (6.10a)$$

$$y[n] = \sum_{k=1}^N a_k y[n-k] + v[n]. \quad (6.10b)$$

A block diagram can be rearranged or modified in a variety of ways without changing the overall system function. Each appropriate rearrangement represents a *different* computational algorithm for implementing the *same* system. For example, the block diagram of Figure 6.3 can be viewed as a cascade of two systems, the first representing the computation of $v[n]$ from $x[n]$ and the second representing the computation of $y[n]$ from $v[n]$. Since each of the two systems is a linear time-invariant system (assuming initial-rest conditions for the delay registers), the order in which the two systems are cascaded can be reversed, as shown in Figure 6.4, without affecting the overall system function. In Figure 6.4, for convenience, we have assumed that $M = N$. Clearly, there is no loss of generality, since if $M \neq N$, some of the coefficients a_k or b_k in the figure would be zero, and the diagram could be simplified accordingly.

In terms of the system function $H(z)$ in Eq. (6.8), Figure 6.3 can be viewed as an implementation of $H(z)$ through the decomposition

$$H(z) = H_2(z)H_1(z) = \left(\frac{1}{1 - \sum_{k=1}^N a_k z^{-k}} \right) \left(\sum_{k=0}^M b_k z^{-k} \right) \quad (6.11)$$

or, equivalently, through the pair of equations

$$V(z) = H_1(z)X(z) = \left(\sum_{k=0}^M b_k z^{-k} \right) X(z), \quad (6.12a)$$

$$Y(z) = H_2(z)V(z) = \left(\frac{1}{1 - \sum_{k=1}^N a_k z^{-k}} \right) V(z). \quad (6.12b)$$

Figure 6.4, on the other hand, represents $H(z)$ as

$$H(z) = H_1(z)H_2(z) = \left(\sum_{k=0}^M b_k z^{-k} \right) \left(\frac{1}{1 - \sum_{k=1}^N a_k z^{-k}} \right) \quad (6.13)$$

or, equivalently, through the equations

$$W(z) = H_2(z)X(z) = \left(\frac{1}{1 - \sum_{k=1}^N a_k z^{-k}} \right) X(z), \quad (6.14a)$$

$$Y(z) = H_1(z)W(z) = \left(\sum_{k=0}^M b_k z^{-k} \right) W(z). \quad (6.14b)$$

In the time domain, Figure 6.4 and, equivalently, Eqs. (6.14a) and (6.14b) can be represented by the pair of difference equations

$$w[n] = \sum_{k=1}^N a_k w[n-k] + x[n], \quad (6.15a)$$

$$y[n] = \sum_{k=0}^M b_k w[n-k]. \quad (6.15b)$$

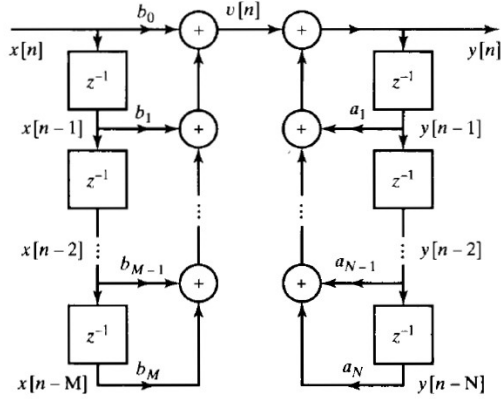


Figure 6.3 Block diagram representation for a general N th-order difference equation.

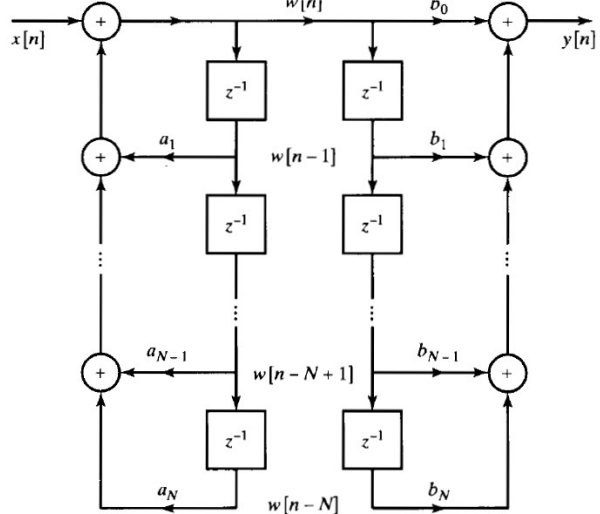


Figure 6.4 Rearrangement of block diagram of Figure 6.3. We assume for convenience that $N = M$. If $N \neq M$, some of the coefficients will be zero.

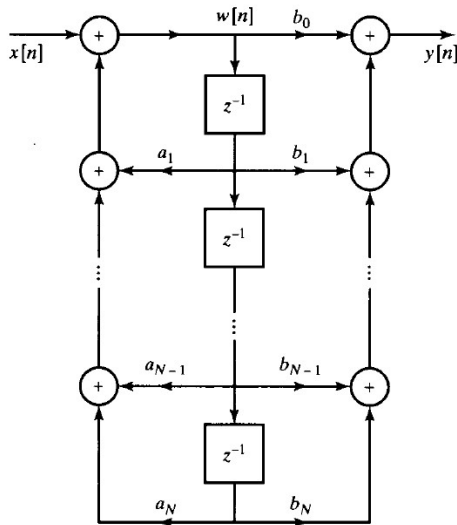


Figure 6.5 Combination of delays in Figure 6.4.

2.5 Sampling of signals

Discrete-time representation of continuous-time signal is typically obtained by periodic sampling

$$x[n] = x_c(nT), \quad -\infty < n < \infty, \quad (2.203)$$

where T is the *sampling period* in seconds, and its inverse is the sampling frequency in Hertz

$$F_s = \frac{1}{T} \text{ (Hz).} \quad (2.204a)$$

Sampling frequency may also be expressed in radians per second

$$\Omega_s = 2\pi F_s = \frac{2\pi}{T} \text{ (rad/s).} \quad (2.204b)$$

Equation (2.203) describes an ideal *continuous-to-discrete-time (C/D) converter*. In practice sampling is done with electronic circuits called *analog to digital converters (ADC)* that also quantize output samples.

The fundamental problem of sampling is: Is it possible to reconstruct continuous-time signal $x_c(t)$ from its samples $x[n]$, and if it is possible, then how to do it?

In general such reconstruction is not possible, however it is possible if we put some constraints (no very hard) on $x_c(t)$.

The operation of sampling may be expressed as multiplication of $x_c(t)$ with Dirac impulse train and then preserving only the values (samples) that occur in the sampling times, as depicted in Fig. 2.53.

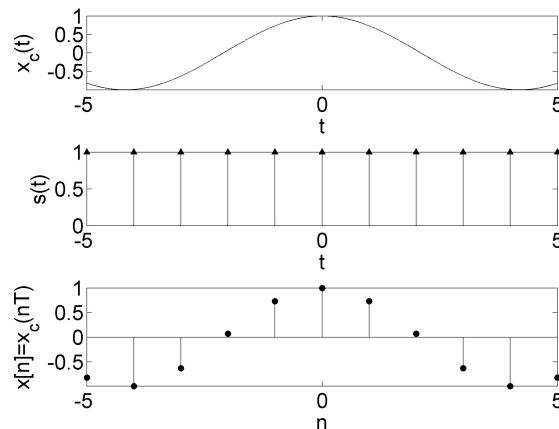


Fig.2.53 Sampling of continuous-time signal.

Dirac impulse train is defined as

$$s(t) = \sum_{n=-\infty}^{\infty} \delta(t-nT), \quad (2.205)$$

and its Fourier transform is also Dirac impulse train

$$S(j\Omega) = \frac{2\pi}{T} \sum_{k=-\infty}^{\infty} \delta(\Omega - k\Omega_s). \quad (2.206)$$

Continuous-time sampled signal is

$$x_s(t) = x_c(t)s(t) = x_c(t) \sum_{n=-\infty}^{\infty} \delta(t-nT) = \sum_{n=-\infty}^{\infty} x_c(nT)\delta(t-nT). \quad (2.207)$$

and its Fourier transform (from the modulation property $\frac{1}{2\pi} X(\Omega) * Y(\Omega)$ (1.76)) is

$$X_s(j\Omega) = \frac{1}{T} \sum_{k=-\infty}^{\infty} X_c(j(\Omega - \Omega_s k)), \quad (2.208)$$

where $X_c(j\Omega)$ is the Fourier transform of $x_c(t)$.

It is seen from (2.208) that the Fourier transform of continuous-time sampled signal $x_s(t)=x_c(t)s(t)$ consist of periodically repeated copies of the Fourier transform of continuous-time signal $x_c(t)$ shifted by integer multiples of sampling frequency. The spectrum of the discrete signal is periodic.

2.5.1 Sampling of lowpass signals

The spectrum of lowpass, continuous-time sampled signal $x_s(t)$ is shown in Fig. 2.54.

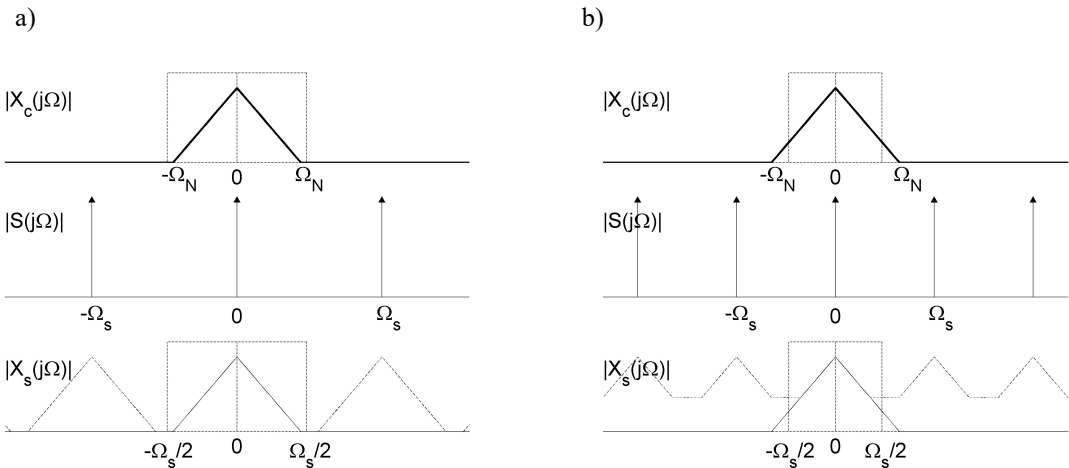


Fig. 2.54 The spectrum of continuous-time sampled signal $x_s(t)$

- a) $\Omega_s > 2\Omega_N$, correct sampling - possible reconstruction,
- b) $\Omega_s < 2\Omega_N$, incorrect sampling (aliasing distortion) - reconstruction not possible.

It is seen from Fig. 2.54, that one period of spectrum $X_s(j\Omega)$ is identical to the spectrum of low-pass signal $x_c(t)$ if

$$\Omega_s - \Omega_N > \Omega_N \text{ or } \Omega_s > 2\Omega_N, \quad (2.209)$$

where Ω_N is the highest frequency component in the spectrum $X_c(j\Omega)$; and only in this case continuous-time signal may be reconstructed from sampled signal. The sampling frequency must be two times higher than the highest frequency in the lowpass signal. If the condition (2.209) is not fulfilled then the copies of $X_s(j\Omega)$ overlap and add together, see Fig. 2.54b, which leads to distortion called *aliasing*.

Nyquist sampling Theorem [Oppen99, p. 146]

Let $x_c(t)$ be a **bandlimited** (lowpass) signal with

$$X_c(j\Omega) = 0, \quad |\Omega| > \Omega_N. \quad (2.210)$$

Then $x_c(t)$ is uniquely determined by its samples $x[n] = x_c(nT)$, $n = 0, \pm 1, \pm 2, \dots$ if

$$\Omega_s = \frac{2\pi}{T} > 2\Omega_N \text{ (rad/s)}, \quad (2.211a)$$

or

$$F_s > 2F_N \text{ (Hz)}. \quad (2.211b)$$

The frequency Ω_N (i.e. the half of sampling frequency) is called *Nyquist frequency*, and the frequency $2\Omega_N$ (i.e. the sampling frequency) is called the *Nyquist rate*.

In general continuous-time signals are not bandlimited, and the constrain (2.211) must be ensured by the use of lowpass continuous-time filters, so called **anti-aliasing filters**. For example, periodic square wave (1.45), Fig. 1.8 may not be uniquely represented by samples because its Fourier transform is not bandlimited.

Let us now express the DTFT of $x[n]$ in terms of FT of $X_s(j\Omega)$. From the definition of FT (1.63) the spectrum of $x_s(t)$ (2.207) is

$$X_s(\Omega) = \int_{-\infty}^{+\infty} x_s(t) e^{-j\Omega t} dt = \int_{-\infty}^{+\infty} \sum_{n=-\infty}^{\infty} x_c(nT) \delta(t - nT) e^{-j\Omega t} dt = \sum_{n=-\infty}^{\infty} x_c(nT) e^{-j\Omega T n}. \quad (2.212)$$

since $x[n] = x_c(nT)$ we have from DTFT definition (2.46)

$$X(e^{j\omega}) = \sum_{n=-\infty}^{\infty} x[n] e^{-j\omega n} = \sum_{n=-\infty}^{\infty} x_c(nT) e^{-j\omega n}, \quad (2.213)$$

thus

$$X_s(j\Omega) = X(e^{j\omega}) \Big|_{\omega=\Omega T} = X(e^{j\Omega T}). \quad (2.214)$$

DTFT of $x[n]$ is a frequency scaled, by $\omega = \Omega T$, version of $X_s(j\Omega)$. Inserting (2.208) into (2.214) we get

$$X(e^{j\Omega T}) = \frac{1}{T} \sum_{k=-\infty}^{\infty} X_c\left(j(\Omega - \Omega_s k)\right), \quad (2.215a)$$

or by using $\omega = \Omega T$, $\Omega_s = \frac{2\pi}{T}$

$$X(e^{j\omega}) = \frac{1}{T} \sum_{k=-\infty}^{\infty} X_c\left(j\left(\frac{\omega}{T} - \frac{2\pi}{T} k\right)\right). \quad (2.215b)$$

The normalization (scaling) of $X_s(j\Omega)$ is such that the sampling frequency $\Omega = \Omega_s$ rad/s is normalized to $\omega = 2\pi$ rad.

Example 2.13

The spectrum of sine signal $x_c = \cos(\Omega_0 t)$ consists from the sum of two Dirac functions $X_c(\Omega) = \pi\delta(\Omega - \Omega_0) + \pi\delta(\Omega + \Omega_0)$ (1.69-1.70). Fig. 2.55 shows the spectra of sampled sine signal for $\Omega_s > 2\Omega_0$ and $\Omega_s < 2\Omega_0$. For the case $\Omega_s > 2\Omega_0$ there is no aliasing, one period of $X_s(j\Omega)$ is the same as $X_c(j\Omega)$, and the signal may be reconstructed from its samples. For the case $\Omega_s < 2\Omega_0$ the spectrum $X_s(j\Omega)$ contains the signal $x_s = \cos((\Omega_s - \Omega_0)t)$, i.e. the higher frequency signal $\cos(\Omega_0 t)$ takes the identity (*alias*) of the lower frequency signal $\cos((\Omega_s - \Omega_0)t)$.

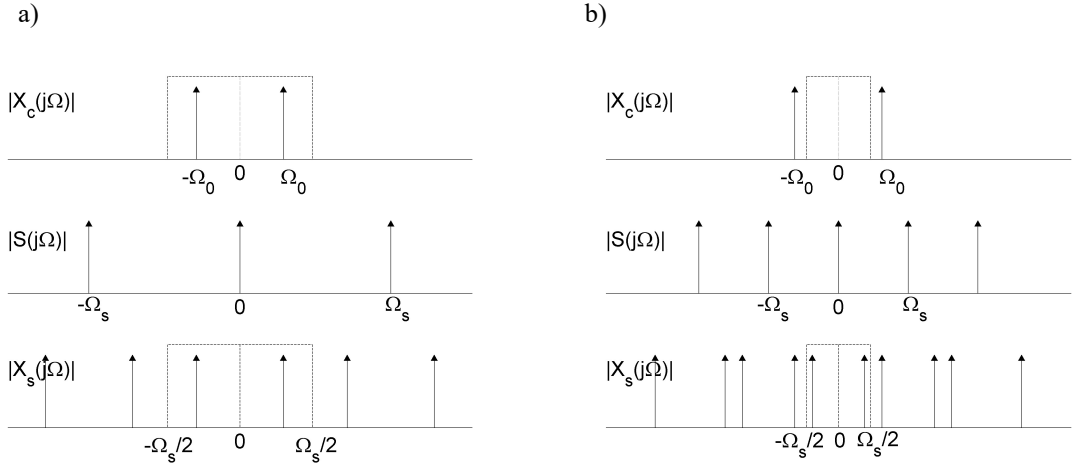


Fig. 2.55 The spectrum of sinusoidal signal $x_c = \cos(\Omega_0 t)$ sampled with frequency:

- a) $\Omega_s > 2\Omega_0$, no aliasing, correct frequency Ω_0 is observed in $X_s(j\Omega)$,
- b) $\Omega_s < 2\Omega_0$, aliasing, incorrect frequency $\Omega_s - \Omega_0$ is observed in $X_s(j\Omega)$.

Fig. 2.56 depicts finite-length, 10 Hz sinusoidal signal sampled with 1 Hz. As a result of aliasing we observe the sinusoidal signal with frequency 1 Hz (similar, so called stroboscopic, effect is observed in the movies when the wheels of a passing by car seem to spinning backwards in slow motion).

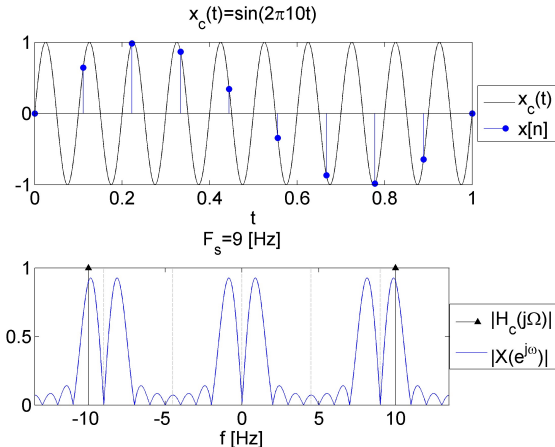


Fig. 2.56 Sampling of 10 Hz finite length sinusoidal signal with frequency 9 Hz.

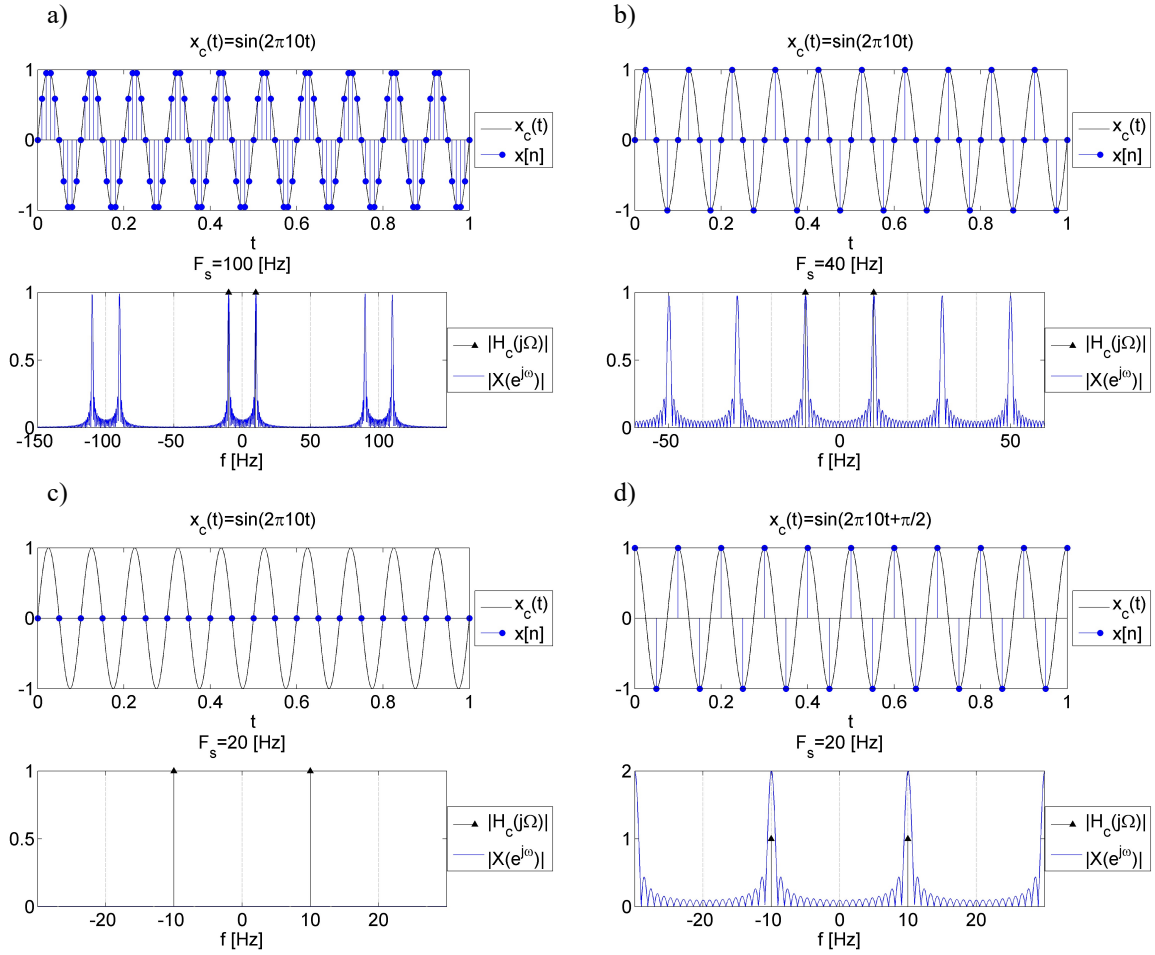


Fig.2.57 10 Hz finite length sinusoidal signal:

- sampled with frequency 100 Hz (i.e. 10 samples per period),
- sampled with frequency 40 Hz (i.e. 4 samples per period),
- sampled with frequency 20 Hz (i.e. 2 samples per period),
- sampled with frequency 20 Hz (i.e. 2 samples per period).

Fig. 2.57 shows four examples of sinusoidal signal sampling. Discrete-time sinusoidal signal $x[n]=\sin(\pi/2n)=...0,1,0,-1...$, Fig. 2.57b, is used as modulation sequence for shifting frequency response by $\pi/2$ rad (i.e. $F_s/4$ Hz), see Fig.2.37, and discrete-time sinusoidal signal $x[n]=\cos(\pi n)=...,1,-1,...$. Fig. 2.57d, is used as modulation sequence for shifting frequency response by π rad (i.e. $F_s/2$ Hz), see Fig.2.37.

It is seen from Fig. 2.57c that two samples per period are not sufficient to uniquely represent sinusoidal signal. The sinusoidal signal must be sampled faster than two samples per period.

Sinusoidal signal is a bandpass signal and we may take advantage of the aliasing and sample the bandpass signal with slow rate as explain next.

Communication in the Presence of Noise*

CLAUDE E. SHANNON†, MEMBER, IRE

II. THE SAMPLING THEOREM

Let us suppose that the channel has a certain bandwidth W in cps starting at zero frequency, and that we are allowed to use this channel for a certain period of time T . Without any further restrictions this would mean that we can use as signal functions any functions of time whose spectra lie entirely within the band W , and whose time functions lie within the interval T . Although it is not possible to fulfill both of these conditions exactly, it is possible to keep the spectrum within the band W , and to have the time function very small outside the interval T . Can we describe in a more useful way the functions which satisfy these conditions? One answer is the following:

THEOREM 1: *If a function $f(t)$ contains no frequencies higher than W cps, it is completely determined by giving its ordinates at a series of points spaced $1/2W$ seconds apart.*

This is a fact which is common knowledge in the communication art. The intuitive justification is that, if $f(t)$ contains no frequencies higher than W , it cannot change to a substantially new value in a time less than one-half cycle of the highest frequency, that is, $1/2W$. A mathematical proof showing that this is not only approximately, but exactly, true can be given as follows. Let $F(\omega)$ be the spectrum of $f(t)$. Then

$$f(t) = \frac{1}{2\pi} \int_{-\infty}^{\infty} F(\omega) e^{i\omega t} d\omega \quad (2)$$

$$= \frac{1}{2\pi} \int_{-2\pi W}^{+2\pi W} F(\omega) e^{i\omega t} d\omega, \quad (3)$$

since $F(\omega)$ is assumed zero outside the band W . If we let

$$t = \frac{n}{2W} \quad (4)$$

where n is any positive or negative integer, we obtain

$$f\left(\frac{n}{2W}\right) = \frac{1}{2\pi} \int_{-2\pi W}^{+2\pi W} F(\omega) e^{i\omega \frac{n}{2W}} d\omega. \quad (5)$$

On the left are the values of $f(t)$ at the sampling points. The integral on the right will be recognized as essentially the n th coefficient in a Fourier-series expansion of the function $F(\omega)$, taking the interval $-W$ to $+W$ as a fundamental period. This means that the values of the samples $f(n/2W)$ determine the Fourier coefficients in the series expansion of $F(\omega)$. Thus they determine $F(\omega)$, since $F(\omega)$ is zero for frequencies greater than W , and for lower frequencies $F(\omega)$ is determined if its Fourier coefficients are determined. But $F(\omega)$ determines the original function $f(t)$ completely, since a function is determined if its spectrum is known. Therefore the original samples determine the function $f(t)$ completely. There is one and only one function whose spectrum is limited to a band W , and which passes through given values at sampling points separated $1/2W$ seconds apart. The function can be simply reconstructed from the samples by using a pulse of the type

$$\frac{\sin 2\pi W t}{2\pi W t}. \quad (6)$$

This function is unity at $t=0$ and zero at $t=n/2W$, i.e., at all other sample points. Furthermore, its spectrum is constant in the band W and zero outside. At each sample point a pulse of this type is placed whose amplitude is adjusted to equal that of the sample. The sum of these pulses is the required function, since it satisfies the conditions on the spectrum and passes through the sampled values.

Mathematically, this process can be described as follows. Let x_n be the n th sample. Then the function $f(t)$ is represented by

$$f(t) = \sum_{n=-\infty}^{\infty} x_n \frac{\sin \pi(2Wt - n)}{\pi(2Wt - n)}. \quad (7)$$

A similar result is true if the band W does not start at zero frequency but at some higher value, and can be proved by a linear translation (corresponding physically to single-sideband modulation) of the zero-frequency case. In this case the elementary pulse is obtained from $\sin x/x$ by single-side-band modulation.

2.5.2 Sampling of bandpass signals

Let us consider continuous-time bandpass signal $x_c(t)$ with the Fourier transform $X_c(j\Omega)$ shown in Fig. 2.58. The bandwidth of this signal equals B , and the spectrum is concentrated at frequency Ω_c , i.e.

$$X_c(j\Omega) = 0, \quad |\Omega| < \Omega_c - B/2 \quad \text{or} \quad |\Omega| > \Omega_c + B/2. \quad (2.216)$$

The maximum frequency component in the $X_c(j\Omega)$ has frequency $\Omega_N = \Omega_c + B/2$. Fig. 2.58a shows the spectrum of sampled signal for $\Omega_s > 2\Omega_N$, that is for the case when the sampling condition for lowpass signal (2.211a) is fulfilled. Fig. 2.58b shows the spectrum of sampled signal for $\Omega_s = 1.95\Omega_N$, it is observed that aliasing distorts the spectrum. Figs. 2.58c,d,e show the spectrum of sampled signal for $\Omega_s = 1.1\Omega_N$, $\Omega_s = 0.7\Omega_N$ and $\Omega_s = 0.52\Omega_N$, however aliases do not disturb the spectrum, they have the same shape as $X_c(j\Omega)$, and may be used for reconstruction of $x_c(t)$. The last Fig. 2.58e again shows the spectrum distorted by aliasing, this time for $\Omega_s = 0.49\Omega_N$. From Fig. 2.58 we may observe the limits of sampling frequency for which aliases do not disturb the spectrum. From Fig. 2.58b it goes that

$$m\Omega_s < 2\Omega_c - B, \quad (2.217)$$

and from Fig. 2.58f

$$(m+1)\Omega_s > 2\Omega_c + B, \quad (2.218)$$

where m is the number of aliases in the range from $-\Omega_c + B/2$ to $\Omega_c - B/2$ as depicted in Fig. 2.58. In Figs. 2.58c,d,e conditions (2.217) and (2.218) are fulfilled, and aliases fit into the gaps in the spectrum of bandpass signal without disturbing this spectrum. If equality sign is used in (2.217) and (2.218) then neighboring aliases butt up against each.

By combining (2.217) and (2.218) we may formulate sampling conditions for bandpass signal.

Bandpass signal $x_c(t)$ with Fourier transform (2.216) is uniquely determined by its samples $x[n] = x_c(nT)$, $n = 0, \pm 1, \pm 2, \dots$ if

$$\Omega_s > 2B \quad \text{and} \quad \frac{2\Omega_c + B}{m+1} < \Omega_s < \frac{2\Omega_c - B}{m}, \quad (2.219)$$

where $\Omega_s = \frac{2\pi}{T}$, and m is the number of aliases in the range from $-\Omega_c + B/2$ to $\Omega_c - B/2$.

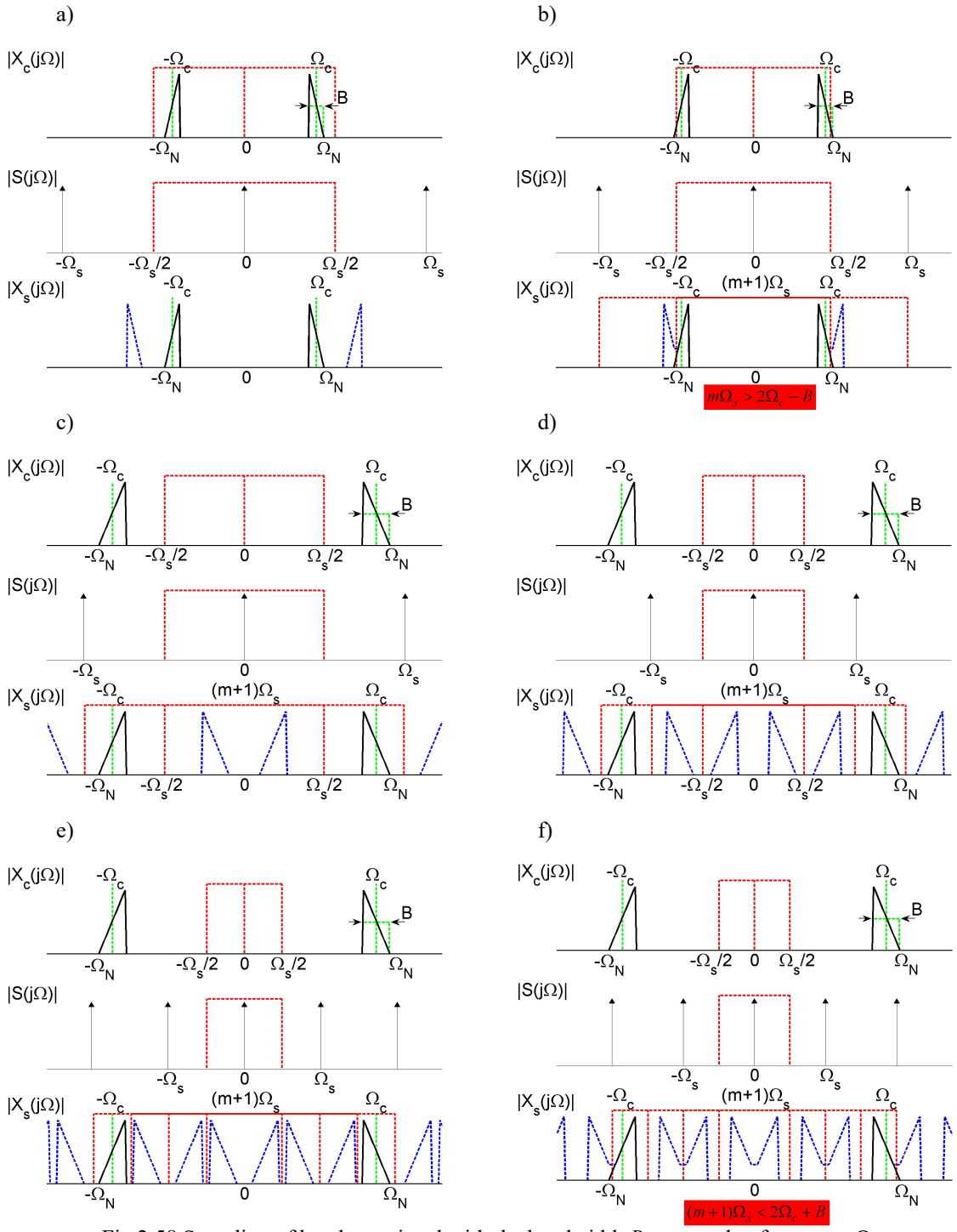


Fig.2.58 Sampling of bandpass signal with the bandwidth B , centered at frequency Ω_c with the highest frequency component Ω_N

- a) $\Omega_s > 2\Omega_N$, $\Omega_s = 2.30\Omega_N$, no aliasing, lowpass sampling
- b) $\Omega_s < 2\Omega_N$, $\Omega_s = 1.95\Omega_N$, aliasing, **distorted spectrum**
- c) $\Omega_s < 2\Omega_N$, $\Omega_s = 1.10\Omega_N$, aliasing, no distortion
- d) $\Omega_s < 2\Omega_N$, $\Omega_s = 0.70\Omega_N$, aliasing, no distortion
- e) $\Omega_s < 2\Omega_N$, $\Omega_s = 0.52\Omega_N$, aliasing, no distortion
- f) $\Omega_s < 2\Omega_N$, $\Omega_s = 0.49\Omega_N$, aliasing, **distorted spectrum**

2.5.3 Reconstruction of continuous-time signal from samples

Reconstruction of continuous-time signal from samples is done by applying lowpass continuous-time filter to the continuous-time signal defined by samples

$$x_s(t) = \sum_{n=-\infty}^{\infty} x[n] \delta(t - nT). \quad (2.220)$$

The output of the filter is

$$x_r(t) = \sum_{n=-\infty}^{\infty} x[n] h_r(t - nT), \quad (2.221)$$

where $x_r(t)$ is the reconstructed signal and $h_r(t)$ is the impulse response of reconstruction filter. Reconstruction filter selects one period of discrete-time signal spectrum that is identical to the spectrum of continuous-time signal. Cutoff frequency of reconstruction filter is the half of sampling frequency $\Omega_c = \Omega_s/2 = \pi/T$ rad/s. The filter has a gain T to compensate the factor $1/T$ in (2.215). The impulse response is (1.85)

$$h_r(t) = T \frac{\sin(\Omega_c t)}{\pi t} = T \frac{\sin\left(\frac{\pi}{T}t\right)}{\pi t}, \quad (2.222)$$

and $h_r(t=0)=1$. It is seen that $h_r(nT)=0$ for $n=\dots, -2, -1, 1, 2, \dots$ which means that reconstructed signal has the values of samples in sampling times.

Substituting (2.222) into (2.221) we get

$$x_r(t) = \sum_{n=-\infty}^{\infty} x[n] \frac{\sin\left(\frac{\pi}{T}(t - nT)\right)}{\frac{\pi}{T}(t - nT)}, \quad (2.223)$$

From (2.223) it is seen that between the samples signal is interpolated by the function $\sin(x)/x$.

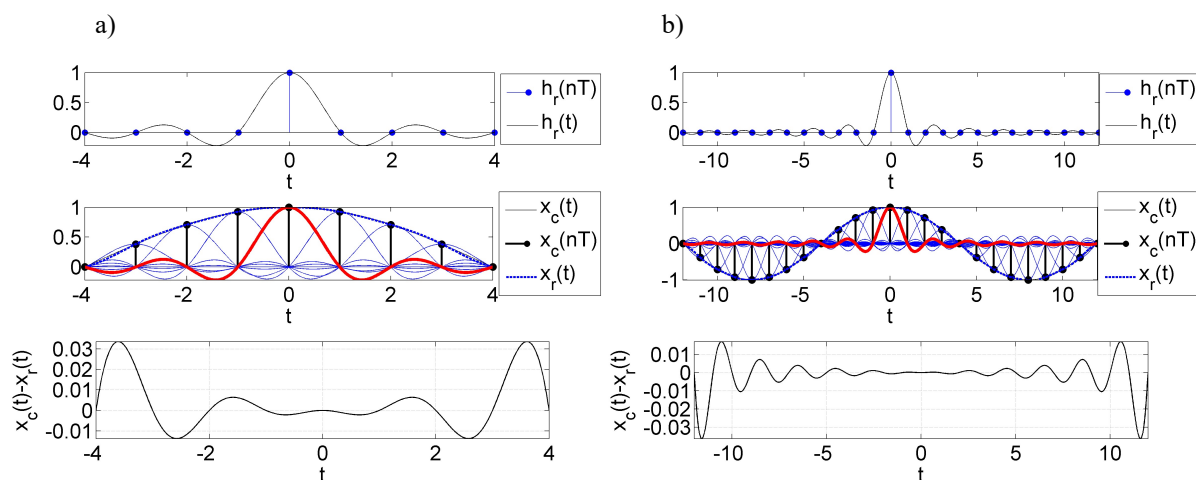


Fig.2.58 Reconstruction of continuous-time signal by lowpass filtering for two finite length signals.

2.5.4 Changing the sampling rate of discrete-time signals

The sampling rate of a sequence can be reduced by integer factor M by selecting from the sequence $x[n]$ every M th sample

$$x_d[n] = x[nM] = x_c(nMT). \quad (2.224)$$

The system defined by (2.224) is called *compressor* and is denoted in block diagrams by $\downarrow M$, see Fig.2.61. Sampling frequency of $x[n]$ is Ω_s rad/s and sampling frequency of downsampled signal $x_d[n]$ is Ω_s/M rad/s. To avoid aliasing the bandwidth of $x[n]$ must be limited by lowpass digital filter to $(\Omega_s/M)/2$ rad/s.

The spectra of $x[n]$ and $x_d[n]$ are (2.215b)

$$X(e^{j\omega}) = \frac{1}{T} \sum_{k=-\infty}^{\infty} X_c\left(j\left(\frac{\omega}{T} - \frac{2\pi}{T}k\right)\right) \text{ and } X_d(e^{j\omega}) = \frac{1}{MT} \sum_{r=-\infty}^{\infty} X_c\left(j\left(\frac{\omega}{MT} - \frac{2\pi}{MT}r\right)\right). \quad (2.225)$$

Inserting $r=i+kM$, $-\infty < k < \infty$, $i=0, 1, \dots, M-1$ into $X_d(e^{j\omega})$ we get the dependence between $X_d(e^{j\omega})$ and $X(e^{j\omega})$

$$\begin{aligned} X_d(e^{j\omega}) &= \frac{1}{MT} \sum_{i+kM=-\infty}^{\infty} X_c\left(j\left(\frac{\omega}{MT} - \frac{2\pi}{MT}(i+kM)\right)\right) = \frac{1}{M} \sum_{i=0}^{M-1} \left[\frac{1}{T} \sum_{k=-\infty}^{\infty} X_c\left(j\left(\frac{\omega-2\pi i}{M} - \frac{2\pi}{T}k\right)\right) \right] = \\ &= \frac{1}{M} \sum_{i=0}^{M-1} X(e^{j\omega_M}), \quad \omega_M = \frac{\omega-2\pi i}{M} \end{aligned} \quad (2.226)$$

Fourier transform of downsampled signal $x_d[n]$ is composed of M copies of the periodic Fourier transform $X(e^{j\omega})$ frequency scaled, *stretched*, by M and shifted by integer multiplies of 2π . To avoid aliasing the bandwidth of $X(e^{j\omega})$ must be limited to $(2\pi/M)/2=\pi/M$ rad.

Operation of two times downsampling of lowpass signal is illustrated in Fig.2.59 in frequency domain. For $M=2$ $\Omega_{s2}=\Omega_{s1}/2$ and the Fourier transform of downsampled signal $x_d[n]$, from (2.226), is

$$X_d(e^{j\omega}) = \frac{1}{2}[X(e^{j\omega/2}) + X(e^{j(\omega-2\pi)/2})]. \quad (2.227)$$

Fig.2.59a shows the spectra scaled in the frequency in radians, and Fig.2.59b shows the spectra scaled in the frequency in radians per second with reference to sampling frequency. The spectrum of $x[n]$ occupies the whole bandwidth permissible by the sampling theorem (2.211). Reduced sampling frequency is $\Omega_{s2}=\Omega_{s1}/2$, and the sampling theorem must also be fulfilled for Ω_{s2} . For that reason signal $x[n]$ is first lowpass filtered with cutoff frequency $\pi/2$ rad (that is $\Omega_{s1}/2$ rad/s), and after that two times compressed (2.224).

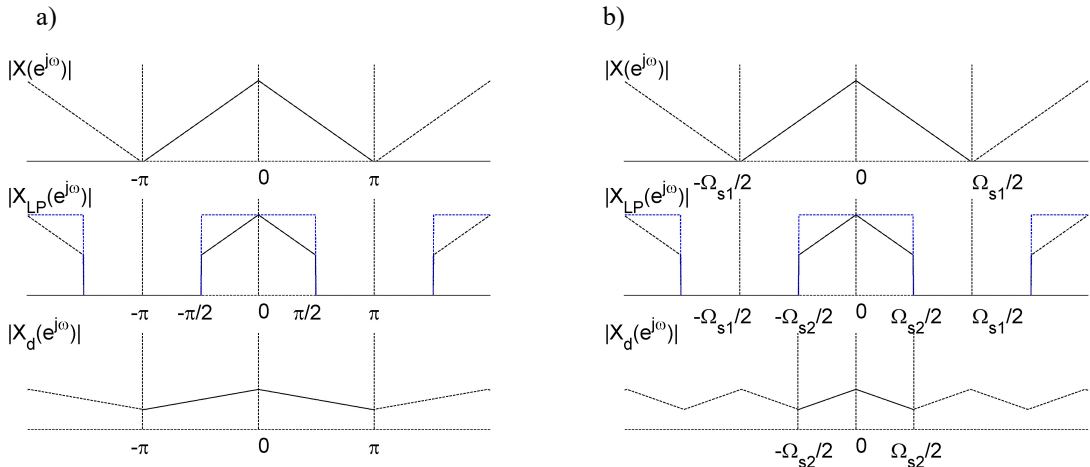


Fig.2.59 Two times downsampling of lowpass signal $x[n]$;
 $X(e^{j\omega})$ Fourier transform of $x[n]$,
 $X_{LP}(e^{j\omega})$ FT after lowpass filtering of $x[n]$,
 $X_d(e^{j\omega})$ FT of $x_d[n] = x[n2]$, i.e. after 2 times reduction of sampling frequency,
a) Interpretation for frequencies in radians,
b) Interpretation for frequencies in radians per second.

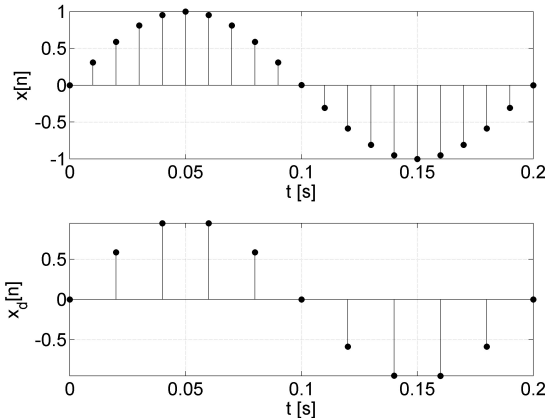


Fig.2.60 Two times downsampling of sinusoidal signal.

Fig. 2.60 illustrates two times downsampling of sinusoidal signal in the time domain. Downsampled signal $x_d[n]$ contains M times less samples than $x[n]$, but the duration of both signals in seconds is the same.

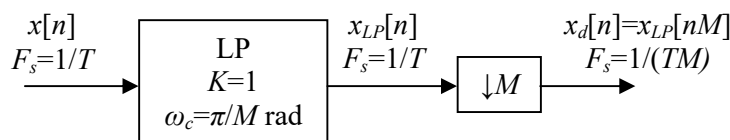


Fig.2.61 Downsampling system:
LP - discrete-time lowpass filter, ω_c - cutoff frequency, K - gain,
 $\downarrow M$ - compressor (2.224).

Fig. 2.61 depicts downsampling system. Downsampling system consists of lowpass anti-aliasing filter and compressor. Downsampling may be realized in several steps. For example, downsampling from $F_{s1}=96$ kHz do $F_{s2}=1$ kHz can be done in a single step with $M=96$, or in three steps with $M_1=8$, $M_2=6$, $M_3=2$. In the latter case computational complexity may be reduced.

Fig. 2.62 shows three times downsampling of the signal sampled with $F_s=100$ Hz that consists from the sum of sinusoidal signals with frequencies 5 Hz, 25 Hz and 45 Hz. Before compressing (2.224) the spectrum of the signal must be limited to $(100/3)/2 \approx 16.7$ Hz, which means that 25 Hz and 45 Hz components must be removed. If the spectrum is not limited then after compressing, aliases with frequencies $|100/3-25| = \pm 8.33$ Hz and $|100/3-45| = \pm 11.66$ Hz are observed in $X_d(e^{j\omega})$.

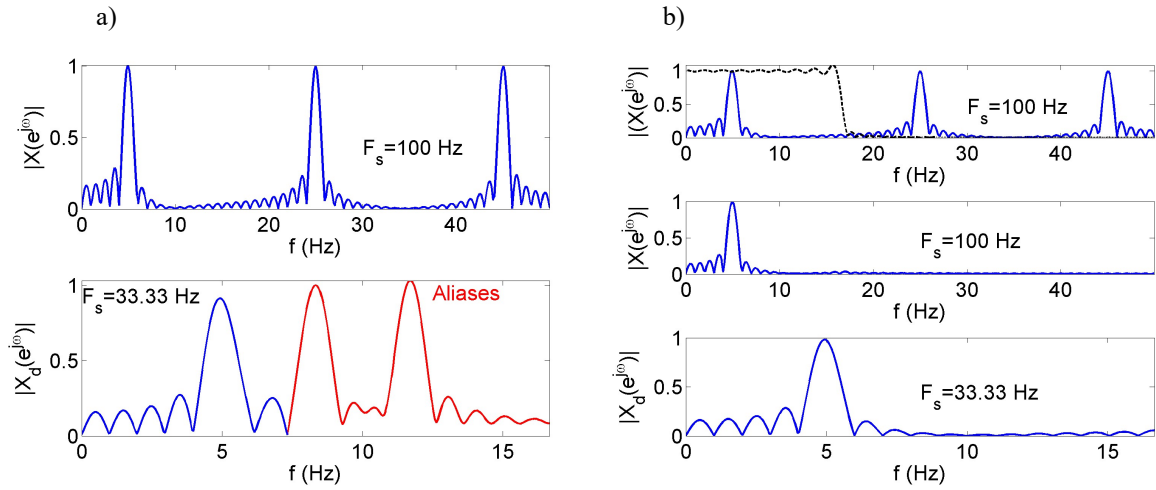


Fig.2.62 Three times downsampling example:
a) without LP anti-aliasing filter - incorrect result,
b) with LP anti-aliasing filter - correct result.

Increasing the sampling rate by integer factor L is done by interpolation of $x[n]$ values

$$x_i[n] = x[n/L] = x_c(nT/L), \quad n = 0, \pm L, \pm 2L, \dots \quad (2.228)$$

This operation is called *upsampling*, and $x_i[n]$ is upsampled or interpolated signal. Discrete-time upsampling system is shown in Fig. 2.63. Expander, denoted by $\uparrow L$, is defined as

$$x_e[n] = \begin{cases} x[n/L], & n = 0, \pm L, \pm 2L, \dots \\ 0, & \text{otherwise} \end{cases}, \quad (2.229a)$$

or equivalently

$$x_e[n] = \sum_{k=-\infty}^{\infty} x[k] \delta[n - kL]. \quad (2.229b)$$

The expander (2.229) inserts $L-1$ zeros in between successive samples of $x[n]$. Lowpass interpolating filter has cutoff frequency π/L rad and gain L .

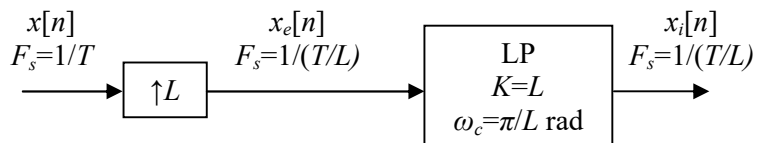


Fig.2.63 Upsampling system:
LP - discrete-time lowpass filter, ω_c - cutoff frequency, K - gain,
 $\uparrow L$ - expander.

The Fourier transform of expanded signal $x_e[n]$ is frequency-scaled, *squeezed*, version of the Fourier transform of $x[n]$

$$X_e(e^{j\omega}) = \sum_{n=-\infty}^{\infty} \left(\sum_{k=-\infty}^{\infty} x[k] \delta[n - kL] \right) e^{-j\omega n} = \sum_{k=-\infty}^{\infty} x[k] e^{-j\omega Lk} = X(e^{j\omega L}). \quad (2.230)$$

Operation of two times upsampling, i.e. $L=2$ and $X_e(e^{j\omega})=X(e^{j2\omega})$, of lowpass signal is illustrated in Fig.2.64 in frequency domain. Fig.2.64a shows the spectra scaled in the frequency in radians, and Fig.2.64b shows the spectra scaled in the frequency in radians per second with reference to sampling frequency. Lowpass interpolating filter preserves only the fragment of the spectrum similar to the spectrum of $x[n]$.

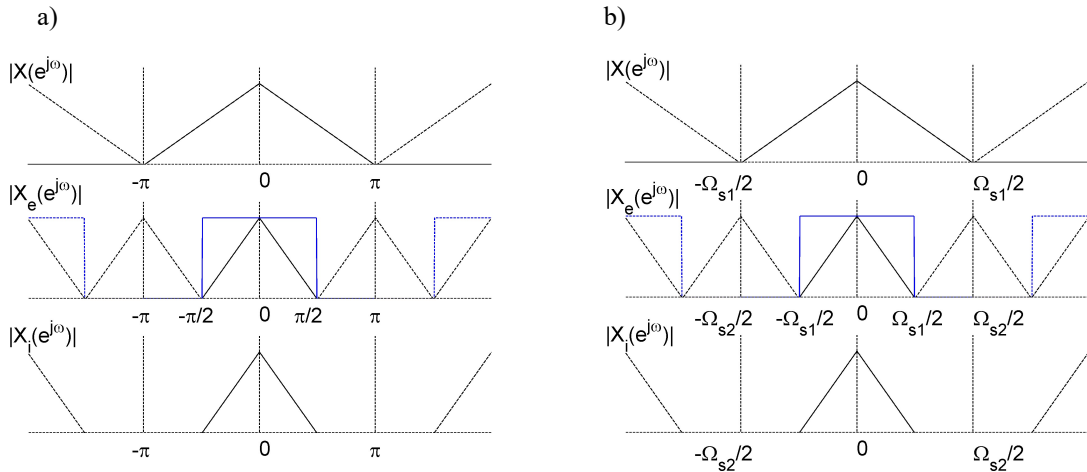


Fig.2.64 Two times upsampling of lowpass signal $x[n]$;

$X(e^{j\omega})$ Fourier transform of $x[n]$,

$X_e(e^{j\omega})$ FT of expanded signal $x_e[n]$,

$X_l(e^{j\omega})$ FT of upsampled (interpolated) signal $x_l[n]$,

a) Interpretation for frequencies in radians,

b) Interpretation for frequencies in radians per second.

Fig. 2.65 shows an example of three times upsampling of sinusoidal signal. First, the signal is expanded by inserting $L-1=2$ zeros between samples of $x[n]$, and next the values of new samples are interpolated by the impulse response of lowpass filter, that is by the function $\sin(x)/x$.

Fig.2.66 presents exemplary spectra of signals $x[n]$, $x_e[n]$, impulse response of interpolation filter $h[n]$, and upsampled signal $x_i[n]$ for three times upsampling.

Sampling rate can be changed by noninteger factor by successive upsampling and downsampling with integer factors as depicted in Fig. 2.67. Cascade connection of LP interpolating filter and LP anti-aliasing filter may be replaced by one LP filter designed on lower cutoff frequency and gain L . Sampling rate in the system shown in Fig. 2.67 is changed L/M times. For example, sampling frequency of audio signals may be changed from 44 kHz to 48 kHz by upsampling with $L=12$, and downsampling with $M=11$.

In Matlab sampling rate change by noninteger factor is implemented by a function `resample`.

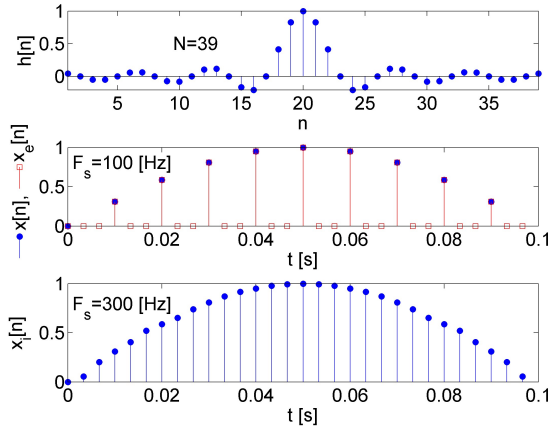


Fig.2.65 Three times upsampling of sinusoidal signal; from the top:
impulse response of lowpass interpolating filter, expanded signal, interpolated (upsampled) signal.

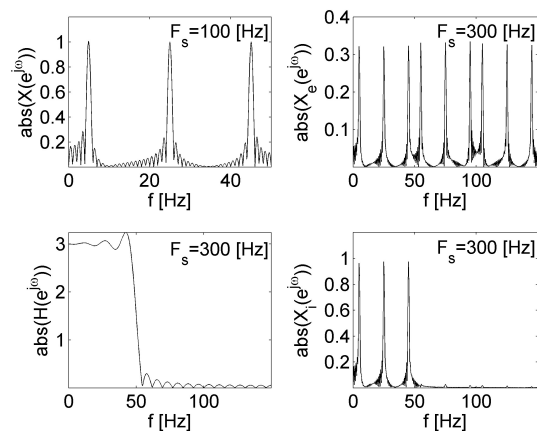


Fig.2.66 Three times upsampling of lowpass signal.

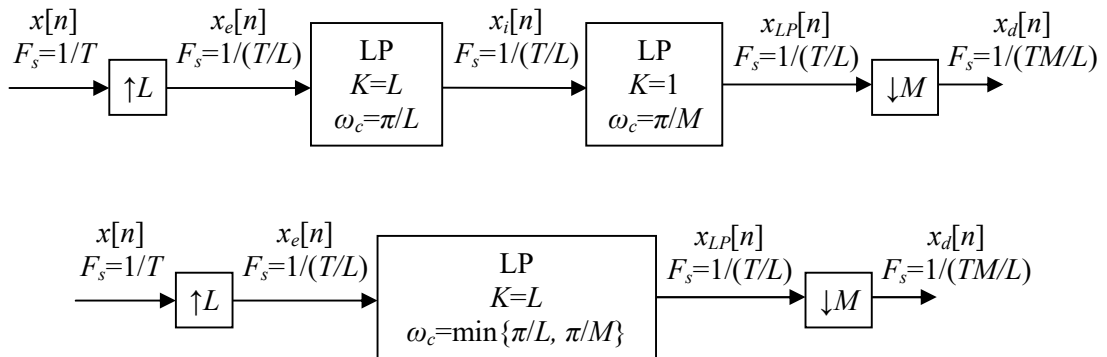


Fig.2.67 System for changing the sampling rate by noninteger factor, i.e. L/M times.

2.5.5 Multirate signal processing

Multirate signal processing refers to utilizing upsampling, downsampling, compressors and expanders to increase the efficiency of signal processing system.

Downsampling and upsampling identities

Downsampling and upsampling identities are shown in Fig. 2.68. $H(z^L)$ is a transform of expanded $h[n]$, i.e. $h[n]$ with $L-1$ zeros inserted between successive samples, and similarly $H(z^M)$ is a Fourier transform of $h[n]$ expanded by M .

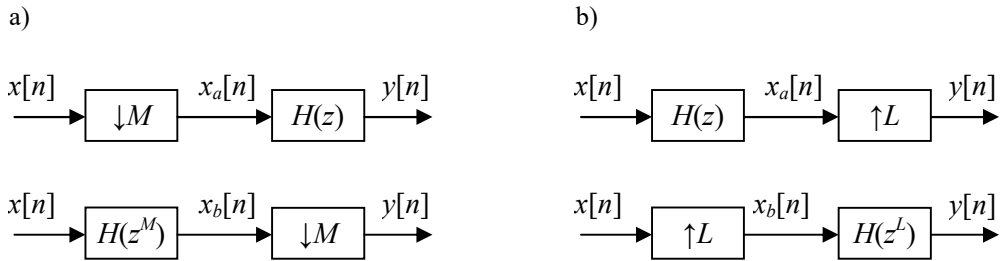


Fig.2.68 a) Downsampling identity,
b) Upsampling identity.

In case of *downsampling identity*, Fig. 2.68a, we have

$$X_b(e^{j\omega}) = H(e^{j\omega M})X(e^{j\omega}), \quad (2.231)$$

and the output, from (2.226), is

$$Y(e^{j\omega}) = \frac{1}{M} \sum_{i=0}^{M-1} X_b(e^{j\omega_M}), \quad \omega_M = \frac{\omega - 2\pi i}{M}. \quad (2.232)$$

Substituting (2.231) into (2.232) we get

$$Y(e^{j\omega}) = \frac{1}{M} \sum_{i=0}^{M-1} H(e^{j(\omega - 2\pi i)})X(e^{j\omega_M}), \quad \omega_M = \frac{\omega - 2\pi i}{M}. \quad (2.233)$$

Since $H(e^{j(\omega - 2\pi i)}) = H(e^{j\omega})$ (2.233) becomes

$$Y(e^{j\omega}) = H(e^{j\omega}) \frac{1}{M} \sum_{i=0}^{M-1} X(e^{j\omega_M}) = H(e^{j\omega})X_a(e^{j\omega}). \quad (2.234)$$

For the *upsampling identity*, Fig. 2.68b, we have

$$Y(e^{j\omega}) = X_a(e^{j\omega L}) = H(e^{j\omega L})X(e^{j\omega L}), \quad (2.235)$$

and because from (2.230) $X_b(e^{j\omega}) = X(e^{j\omega L})$

$$Y(e^{j\omega}) = H(e^{j\omega L})X_b(e^{j\omega}). \quad (2.236)$$

Polyphase decompositions

The polyphase decomposition of the sequence is obtained as a superposition of M subsequences, each consisting of every M th value of successively delayed versions of the sequence. Polyphase decomposition of an impulse response $h[n]$ is defined as

$$h_k[n] = h[nM + k], \quad (2.237)$$

where $k=0,1,2,\dots,M-1$, and $h_k[n]$ are called polyphase components, see Fig.2.68.

The original impulse response can be reconstructed from delayed polyphase components

$$h[n] = \sum_{k=0}^{M-1} h_k[n - k]. \quad (2.237a)$$

By neglecting zeros in polyphase components we define sequences $e_k[n]$

$$e_k[n] = h[nM + k] = h_k[nM] \quad (2.237b)$$

shown in Fig. 2.68.

Filter structure in polyphase representation is depicted in Fig. 2.69. $E_k(z^M)$ are Fourier transforms of extended by M polyphase components (2.237b). In z-Transform the filter transmittance is the sum of transmittances of all delayed polyphase components

$$H(z) = \sum_{k=0}^{M-1} E_k(z^M)z^{-k} \quad (2.238)$$

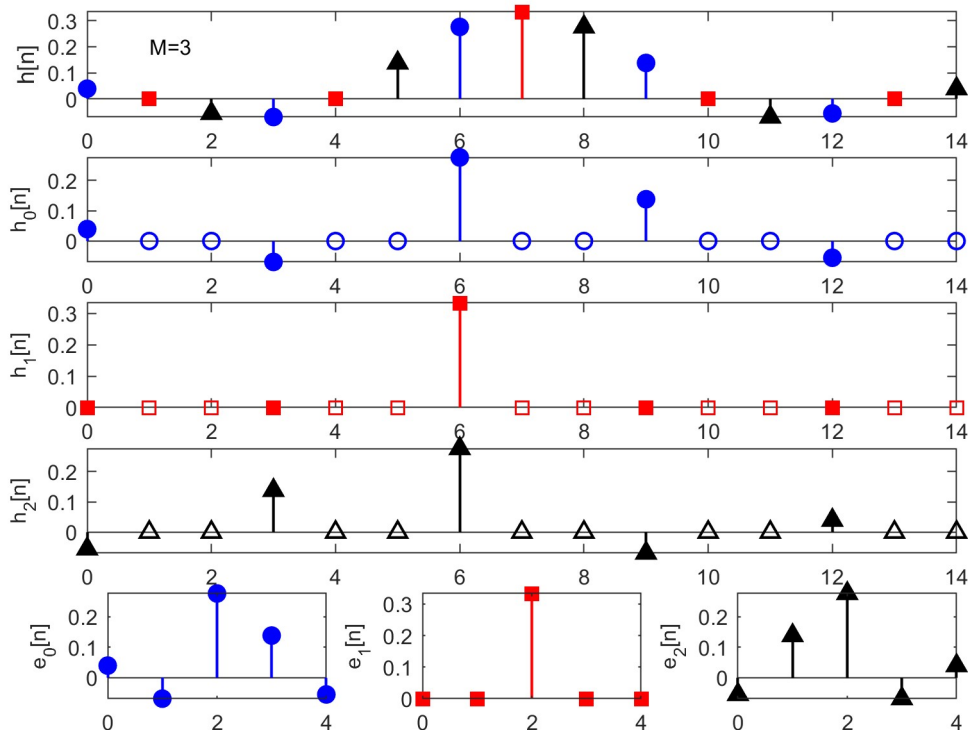


Fig.2.68 Exemplary impulse response $h[n]$ and its polyphase components $h_k[n]=h[nM+k]$ for $M=3$.

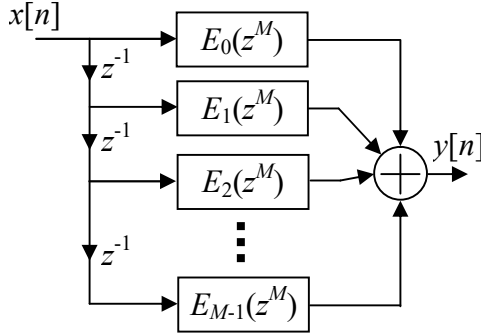


Fig.2.69 Polyphase representation of filter with impulse response $h[n]$.

The examples of application of polyphase decomposition are shown in Fig. 2.70 and Fig. 2.71 as realizations of downsampling and upsampling system.

In case of downsampling system shown in Fig.2.61 one output sample of the length N filter $h[n]$ requires N multiplications and $N-1$ additions in a single sampling period T . In case of polyphase implementation depicted in Fig.2.70b the length of filters is N/M and the rate of input data to polyphase filters is M times slower, thus polyphase implementation requires N/M multiplications and $(N/M-1)+(M-1)$ additions in a single sampling period MT .

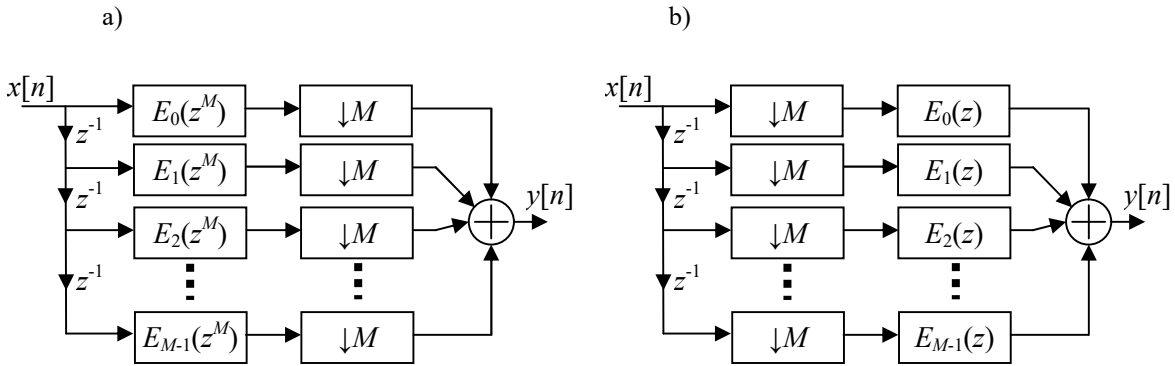


Fig.2.70 a) Polyphase representation of downsampling system from Fig.2.61,
b) Efficient downsampling system after applying downsampling identity Fig.2.68a.

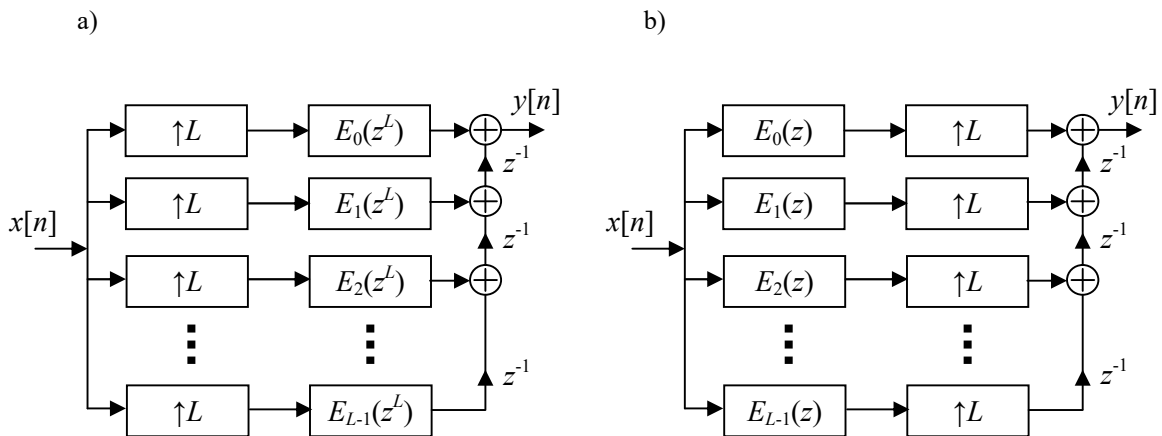


Fig.2.71 a) Polyphase representation of upsampling system from Fig.2.63,
b) Efficient downsampling system after applying upsampling identity Fig.2.68b.

2.5.6 Impulse invariance

Frequency response of continuous-time, lowpass LTI system $H_c(j\Omega)$

$$H_c(j\Omega) = 0, \quad |\Omega| \geq \frac{\Omega_s}{2} = \frac{\pi}{T} \quad (2.239)$$

may be realized by frequency response of discrete-time LTI system $H(e^{j\omega})$, i.e.

$$H(e^{j\omega}) = H_c\left(j\frac{\omega}{T}\right), \quad |\omega| < \pi \quad (2.240)$$

if

$$h[n] = Th_c(nT). \quad (2.241)$$

When $h[n]$, and $h_c(t)$ are related through (2.241), the discrete-time system is said to be an *impulse-invariant* version of the continuous-time system.

From (2.215b) for $h[n] = h_c(nT)$ we have

$$H(e^{j\omega}) = \frac{1}{T} \sum_{k=-\infty}^{\infty} H_c\left(j\left(\frac{\omega}{T} - \frac{2\pi}{T}k\right)\right), \quad (2.242)$$

and if (2.239) holds then one period of $H(e^{j\omega})$ equals to scaled $H_c(j\Omega)$

$$H(e^{j\omega}) = \frac{1}{T} H_c\left(j\frac{\omega}{T}\right), \quad |\omega| < \pi. \quad (2.243)$$

Moving scaling by T to time domain we get (2.241) and (2.240).

Example 2.14

Find discrete-time impulse invariant system of continuous-time system

$$H_c(s) = \frac{1}{s^2 + \sqrt{2}s + 1}. \quad (2.244)$$

First, we calculate impulse response of continuous-time system

$$h_c(t) = \sqrt{2} e^{-\frac{\sqrt{2}}{2}t} \sin\left(\frac{\sqrt{2}}{2}t\right). \quad (2.245)$$

Then, using (2.241) we get impulse response of discrete-time impulse invariant system

$$h[n] = Th_c(nT) = T\sqrt{2} e^{-\frac{\sqrt{2}}{2}nT} \sin\left(\frac{\sqrt{2}}{2}nT\right), \quad (2.246)$$

and finally the transmittance of discrete-time impulse invariant system

$$H(z) = \frac{z \left[T\sqrt{2} \sin\left(\frac{T\sqrt{2}}{2}\right) e^{-\frac{T\sqrt{2}}{2}} \right]}{z^2 - z \left[2 \cos\left(\frac{T\sqrt{2}}{2}\right) e^{-\frac{T\sqrt{2}}{2}} \right] + e^{-T\sqrt{2}}}. \quad (2.247)$$

Matlab digression

Inverse Laplace transform of (2.244) was computed by function `ilaplace`, and z-transform of (2.246) was computed by function `ztrans`. Both functions from Symbolic Math Toolbox.

Fig. 2.72 compares frequency response of continuous-time system (2.244) with two discrete-time impulse invariant systems (2.247) for sampling frequency $\Omega_s=15$ rad/s and $\Omega_s=100$ rad/s.

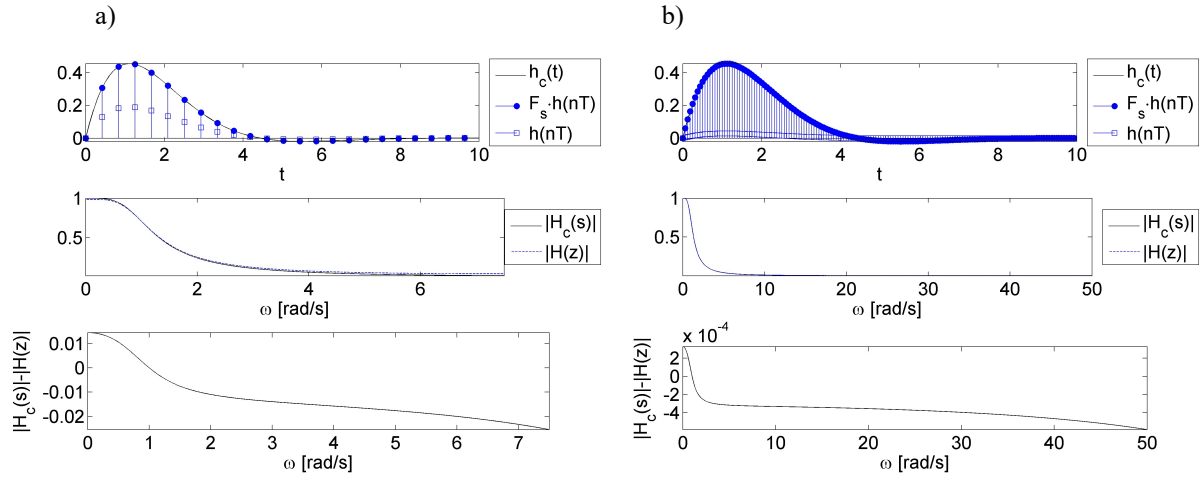


Fig.2.72 a) Comparison of impulse response and frequency response of continuous-time system

$$H_c(s) = \frac{1}{s^2 + \sqrt{2}s + 1} \text{ and two discrete-time impulse invariant systems,}$$

$$\text{a)} \Omega_s = 15 \frac{\text{rad}}{\text{s}} \rightarrow T = \frac{2\pi}{\Omega_s} = 0.4189 \text{ s}, H(z) = \frac{0.12858 z}{z^2 - 1.4225 z + 0.55301},$$

$$\text{b)} \Omega_s = 100 \frac{\text{rad}}{\text{s}} \rightarrow T = \frac{2\pi}{\Omega_s} = 0.0628 \text{ s}, H(z) = \frac{0.003775 z}{z^2 - 1.9112 z + 0.91498}.$$

2.6 Analysis of signals using DFT

DFT is often used for analysis of continuous-time signals in the signal processing system shown in Fig.1. In Fig.1 analyzed signal goes through the following processing stages:

- 1) Anti-aliasing filtering, sampling and quantization (in further discussion quantization is neglected) of continuous-time signal $x_c(t)$,
- 2) Windowing of discrete-time signal $x[n]$, i.e. $v[n]=w[n]x[n]$. As a result of time domain multiplication we observe integral convolution of the Fourier transforms of the signal $X(e^{j\omega})$ and the window $W(e^{j\omega})$

$$V(e^{j\omega}) = \frac{1}{2\pi} \int_{-\pi}^{\pi} X(e^{j\Theta}) W(e^{j(\omega-\Theta)}) d\Theta, \quad (2.248)$$

and not the spectrum of the signal itself. The convolution (2.248) will tend to smooth sharp peaks and discontinuities in $X(e^{j\omega})$. The spectrum of $X(e^{j\omega})$ is *smeared*.

- 3) Sampling the continuous spectrum $V(e^{j\omega})$ of discrete-time signal by DFT, i.e. computing $V(e^{j\omega})$ only for the set of frequencies $\omega=(2\pi/N)k$, $k=0,1,\dots,N-1$.

Processing stages 1-3 change the spectrum $X(j\Omega)$ of continuous-time input signal $x_c(t)$ as shown in Fig. 2.73. It is seen that the DFT spectrum in not exactly like $X(j\Omega)$.

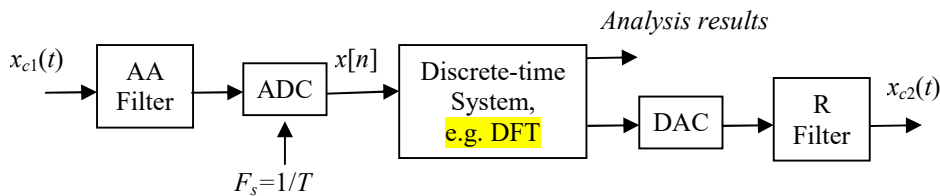


Fig. 1 Processing of continuous-time signals in discrete-time system. (repeated figure)

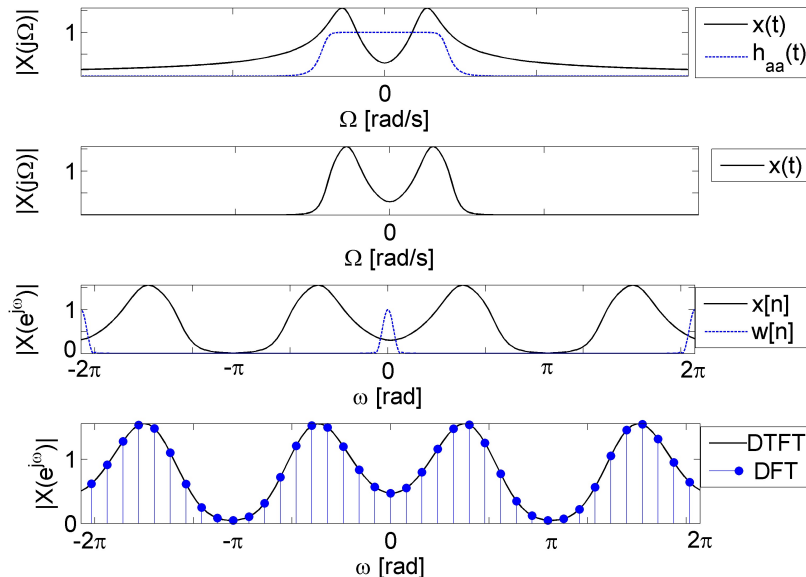


Fig.2.73 DFT analysis of continuous-time signal; from top to bottom:
the spectrum of continuous-time signal and magnitude response of anti-aliasing filter,
the spectrum of bandlimited continuous-time signal,
the spectrum of discrete-time signal and time window,
the spectrum of discrete-time windowed signal and DFT.

2.6.1 Analysis of sinusoidal signals

Consider the sum of two continuous-time, infinite length, sinusoidal signals

$$x_c(t) = A_0 \cos(\Omega_0 t + \phi_0) + A_1 \cos(\Omega_1 t + \phi_1), \quad -\infty < t < \infty. \quad (2.249)$$

After ideal sampling we have discrete-time representation

$$x[n] = A_0 \cos(\omega_0 n + \phi_0) + A_1 \cos(\omega_1 n + \phi_1), \quad \omega_0 = \Omega_0 T, \quad \omega_1 = \Omega_1 T, \quad -\infty < n < \infty, \quad (2.250)$$

where T is the sampling period.

Windowing is described by multiplication

$$v[n] = w[n]x[n] = A_0 w[n] \cos(\omega_0 n + \phi_0) + A_1 w[n] \cos(\omega_1 n + \phi_1). \quad (2.251)$$

By Euler equation sequence $v[n]$ is

$$v[n] = \frac{A_0}{2} w[n] e^{j\phi_0} e^{j\omega_0 n} + \frac{A_0}{2} w[n] e^{-j\phi_0} e^{-j\omega_0 n} + \frac{A_1}{2} w[n] e^{j\phi_1} e^{j\omega_1 n} + \frac{A_1}{2} w[n] e^{-j\phi_1} e^{-j\omega_1 n}. \quad (2.252)$$

By frequency shifting property (2.84) of DTFT $e^{j\omega_0 n} x[n] \rightarrow X(e^{j(\omega-\omega_0)})$ the DTFT of $v[n]$ is

$$V(e^{j\omega}) = \frac{A_0}{2} e^{j\phi_0} W(e^{j(\omega-\omega_0)}) + \frac{A_0}{2} e^{-j\phi_0} W(e^{j(\omega+\omega_0)}) + \frac{A_1}{2} e^{j\phi_1} W(e^{j(\omega-\omega_1)}) + \frac{A_1}{2} e^{-j\phi_1} W(e^{j(\omega+\omega_1)}). \quad (2.253)$$

According to (2.253) DTFT of windowed sinusoidal signal (2.251) consists of the DTFT of the window, replicated at frequencies $\pm\omega_0$ and $\pm\omega_1$ and scaled by the complex amplitudes of the individual complex exponentials that make up the signal, i.e. at frequencies $\pm\omega_0$ and $\pm\omega_1$ the scaled spectrum of the window is observed.

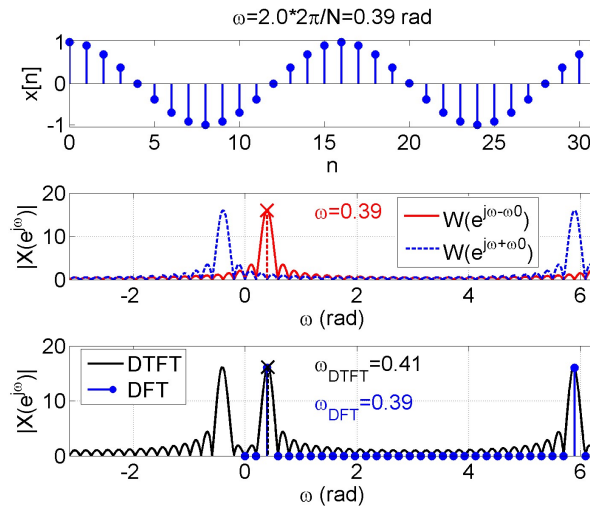


Fig.2.74 Synchronous sampling (2 periods); from top to bottom:
discrete-time sinusoidal signal,

the spectrum for negative and positive frequencies (2.253),

DTFT - spectral leakage shifts the maximum of mainlobe and DFT - two nonzero bins.

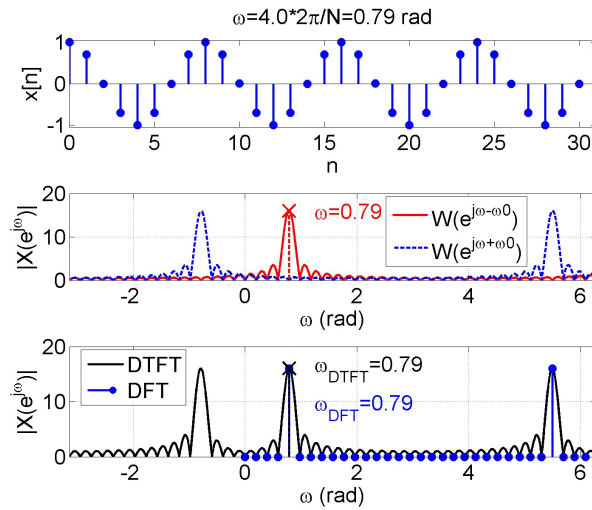


Fig.2.75 Synchronous sampling (4 periods); from top to bottom:
discrete-time sinusoidal signal,
the spectrum for negative and positive frequencies (2.253),
DTFT and DFT - two nonzero bins.

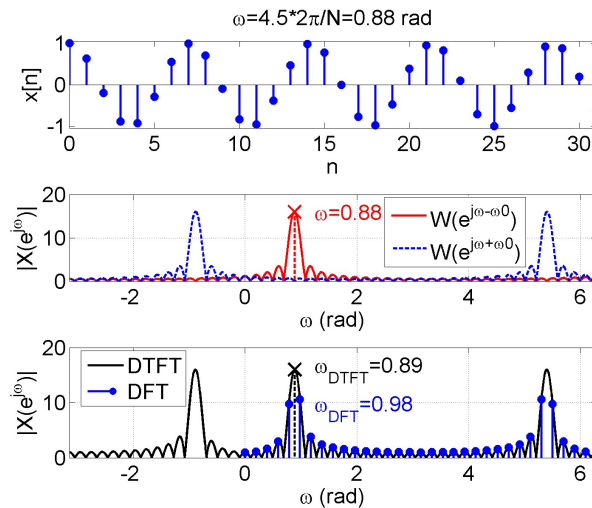


Fig.2.76 Nonsynchronous sampling (aperiodic signal); from top to bottom:
discrete-time sinusoidal signal,
the spectrum for negative and positive frequencies (2.253),
DTFT - spectral leakage shifts the maximum of mainlobe and DFT - all bins are nonzero, the maximum of the
mainlobe is not sampled.

Figs. 2.74-2.76 show the spectra of sinusoidal signal analyzed with rectangular window. The top subplots depict time signal $x[n]=\cos(\omega_0 n)$, middle subplots depict the spectrum for negative and positive frequencies (2.253), and the bottom subplots show DTFT and DFT of $x[n]$. The frequency of the signal is estimated as the frequency of the mainlobe magnitude maximum or the highest magnitude DFT bin. It is observed that the estimation is always correct in the middle subplot, it is correct for DFT if the signal is periodic (i.e. for synchronous sampling) and it may always be incorrect for DTFT.

As observed from (2.253) the spectrum of finite length sinusoidal signal consists of the spectrum for positive frequencies $\frac{A_0}{2} e^{j\phi_0} W(e^{j(\omega-\omega_0)})$ and the spectrum for negative frequencies $\frac{A_0}{2} e^{-j\phi_0} W(e^{j(\omega+\omega_0)})$. In both spectra the energy is not only concentrated in the mainlobe but also spills to the side-lobes. This phenomenon is called *spectral leakage*. By DTFT we compute the sum of both spectra from the signal samples, i.e.

$$V(e^{j\omega}) = \sum_{n=-\infty}^{\infty} A_0 w[n] \cos(\omega_0 n + \phi_0) e^{-j\omega n} = \frac{A_0}{2} e^{j\phi_0} W(e^{j(\omega-\omega_0)}) + \frac{A_0}{2} e^{-j\phi_0} W(e^{j(\omega+\omega_0)}). \quad (2.254)$$

The side-lobes of the spectrum for negative frequencies add, as complex numbers, to the mainlobe of the spectrum for positive frequencies and vice versa. Thus the maximum of the mainlobe may be shifted in frequency and magnitude causing incorrect estimation of signal's frequency as observed in Figs. 2.74-2.76 and amplitude. It is seen from (2.254) that the effect of spectral leakage depends also on the phase of sinusoidal signal.

Because of the spectral leakage the spectrum of a single sinusoidal signal disturbs itself. This disturbance is getting stronger when the mainlobes of the spectra for negative and positive frequencies are getting closer, i.e. the frequency of the signal in radians decreases. The disturbance made by leakage is stronger for the signal composed of the sum of sinusoids. In that case the side-lobes of sinusoidal components in the positive frequency spectrum disturb the mainlobes in the positive frequency spectrum, which is called *near leakage*, but also the side-lobes from negative frequency spectrum disturbs mainlobes in the positive frequency spectrum which is called *far leakage*. The influence of spectral leakage is reduced by using time windows with high attenuation of side-lobes. Windows previously described for designing FIR filters, i.e. cosine windows (2.165), self-convolution windows (2.172), Kaiser-Bessel window (2.175), are also well suited for DFT analysis. However when used for DFT analysis the window should be periodic, see Fig.2.42.

It is seen in Figs. 2.74-2.75 that for periodic sinusoidal signal the DFT samples zeros of the DTFT except of two nonzero frequency bins. For periodic signal DFT analysis is not affected by spectral leakage. However, if the signal is not periodic, i.e. the frequency is not integer multiply of $2\pi/N$ rad, then the DFT does not even sample the DTFT in signal's frequency ω_0 as depicted in Fig. 2.76. This leads to significant errors of frequency, amplitude and phase estimation.

Spectral resolution of DFT analysis is limited by the width of the mainlobe of the window and is defined as

$$\Delta F = \beta \frac{F_s}{N} \text{ Hz or } \Delta\omega = \beta \frac{2\pi}{N} \text{ rad}, \quad (2.255)$$

where β is the coefficient reflecting the bandwidth increase due to the particular window selected. The values of β for some popular windows are: rectangle $\beta=1$, triangle $\beta=1.33$, Hann $\beta=1.50$, Hamming $\beta=1.36$.

Fig. 2.77 illustrates the problem of spectral resolution for the sum of two sinusoidal signals. The difference between frequencies ω_1 , and ω_2 must be high enough to distinguish those two signals in the magnitude spectrum. In Fig. 2.78 it is shown that the spectral resolution increases when the observation interval, i.e. the number of samples, increases, however it is often not possible in practice to acquire longer observation.

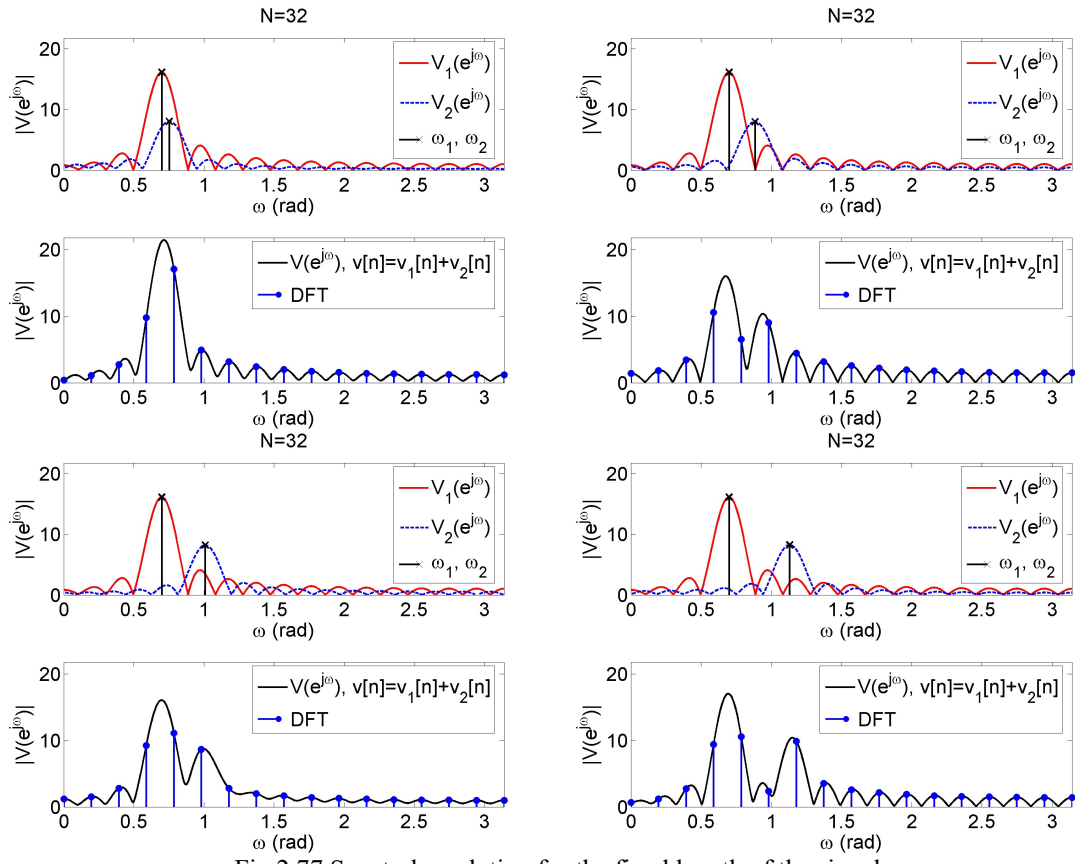


Fig.2.77 Spectral resolution for the fixed length of the signal
and increasing difference between frequencies of two sinusoidal signals.

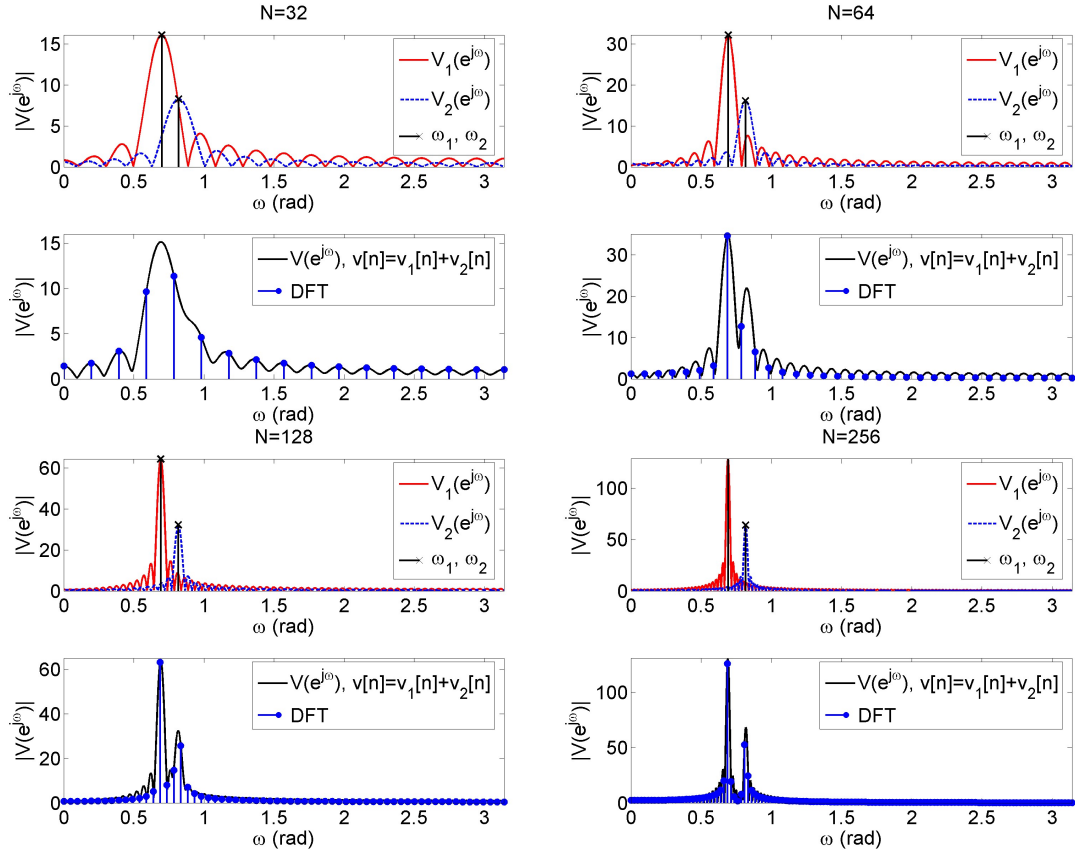


Fig.2.78 Spectral resolution for the fixed frequencies of two sinusoidal signals
and increasing length of the signal.

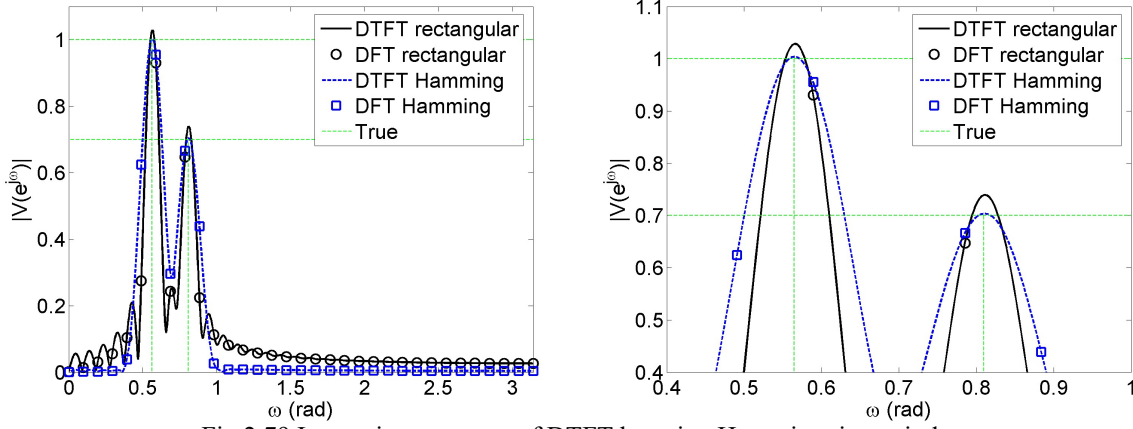


Fig. 2.79 Improving accuracy of DTFT by using Hamming time window.

Fig. 2.79 depicts the spectra of the sum of two sinusoids analyzed with rectangular and Hamming window. The true values of frequencies and amplitudes are marked by green lines. It is observed that accuracy of DTFT with Hamming window is better than accuracy of DTFT with rectangle window.

In summary:

- 1) In DFT/DTFT analysis signal is always windowed. If no specific window is used then the window is rectangular.
- 2) Rectangular window has the narrowest mainlobe, and thus the highest spectral resolution.
- 3) Rectangular window has the highest side-lobes (-13dB), and thus it is most susceptible to spectral leakage.
- 4) The width of the mainlobe decreases if the length of the window increases.
- 5) The amplitude of the side-lobes does not depend of signal length.

DFT samples DTFT. The sampling (frequency) step is $2\pi/N$ rad. By appending the vector of zero samples at the end of the signal frequency step can be decreased as depicted in Fig. 2.80.

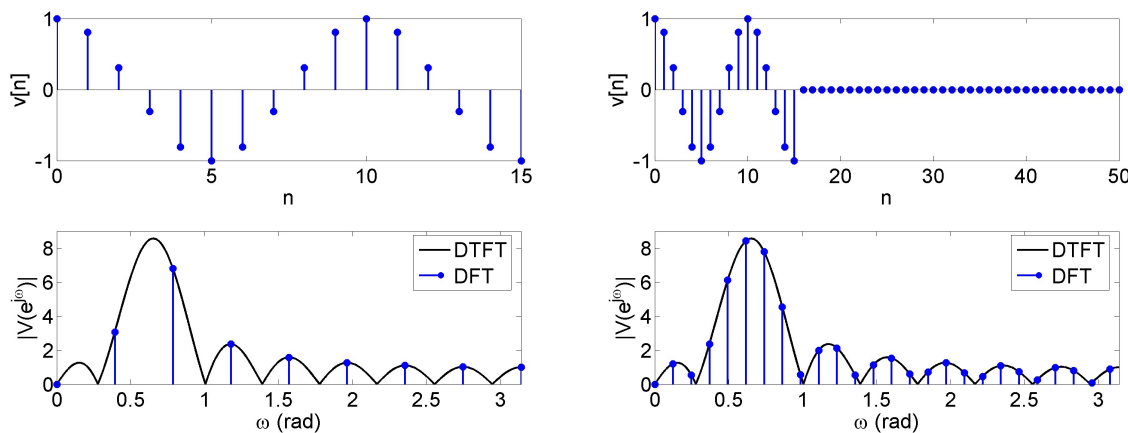


Fig. 2.80 Denser sampling of DTFT by appending zeros before computing DFT.

Matlab digression

fft(x,N) is the N -point FFT, padded with zeros if x has less than N points and truncated if it has more.

2.6.2 Time-dependent frequency analysis: the spectrogram

Short-Time Fourier Transform (STFT) is defined as

$$X[n, \lambda] = \sum_{m=-\infty}^{\infty} x[n+m]w[m]e^{-j\lambda m}, \quad (2.256)$$

where $w[n]$ is the time window. STFT is used in analysis of signals with varying spectra. Magnitude plot of $X[n, \lambda]$ is called *spectrogram*. According to (2.256) one dimensional signal $x[n]$ is represented as two dimensional function of discrete time n and continuous frequency λ . $X[n, \lambda]$ are DTFTs of fragments of $x[n]$ selected by window $w[n]$, the signal is shifted through the window that is in the fixed position.

By changing indexes in (2.256) with substitution $m' = n + m$ we get

$$X[n, \lambda] = \sum_{m'=-\infty}^{\infty} x[m']w[-(n-m')]e^{-j\lambda(n-m')}, \quad (2.257)$$

which is the convolution

$$X[n, \lambda] = x[n] * h_{\lambda}[n], \quad (2.258)$$

where

$$h_{\lambda}[n] = w[-n]e^{j\lambda n}. \quad (2.259)$$

From (2.258) it is seen that for fixed λ STFT $X[n, \lambda]$ is the output of LTI system with complex impulse response $h_{\lambda}[n]$ (2.259). From the frequency shifting property of DTFT (2.84) it is seen that DTFT of (2.259) is

$$H_{\lambda}(e^{j\omega}) = W(e^{j(\lambda-\omega)}). \quad (2.260)$$

Magnitude responses $H_{\lambda}(e^{j\omega})$ of exemplary window for $\lambda=0$ and $\lambda=1.6$ rad are depicted in Fig. 2.81.

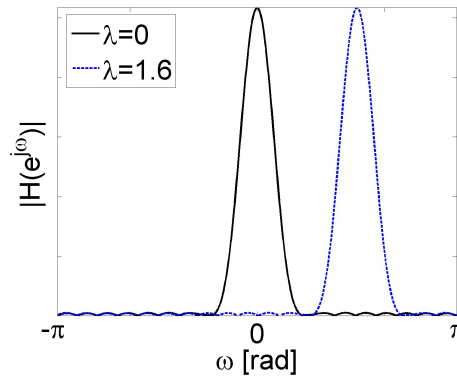


Fig.2.81 Fourier transforms of (2.259) for $\lambda=0$ and $\lambda=1.6$ rad.

In definition (2.256) the window is in fixed position and the signal is shifted through the window. Alternatively, STFT may be defined for the signal in fixed position and the window shifted along the signal

$$\check{X}[n, \lambda] = \sum_{m=-\infty}^{\infty} x[m]w[m-n]e^{-j\lambda m}. \quad (2.261)$$

The relation between two definitions is

$$\check{X}[n, \lambda] = e^{-j\lambda n} X[n, \lambda]. \quad (2.262)$$

In practice STFT is computed by DFT and is called *Short-Time Discrete Fourier Transform* (STDFT). The window length is L , i.e. $w[m]=0$ outside the interval $m=0,1,\dots,L-1$, and the length of the DFT is N , $N \geq L$. STDFT is

$$X[n,k] = X[n, \lambda = \frac{2\pi}{N} k] = \sum_{m=0}^{L-1} x[n+m]w[m]e^{-j\frac{2\pi}{N}mk}, \quad k = 0,1,\dots,N-1. \quad (2.263)$$

Similarly to (2.258) STDFT can be interpreted as a convolution

$$X[n,k] = x[n] * h_k[n], \quad k = 0,1,\dots,N-1, \quad (2.264)$$

where

$$h_k[n] = w[-n]e^{j\frac{2\pi}{N}nk}. \quad (2.265)$$

Equations (2.264-2.265) define the bank of N filters, with the k th filter having frequency response

$$H_k(e^{j\omega}) = W(e^{j(\omega_k - \omega)}), \quad \omega_k = \frac{2\pi}{N}k. \quad (2.266)$$

Filter bank representation of STDFT is depicted in Fig. 2.82a, and magnitude responses of exemplary filter banks are shown in Fig. 2.82b. Interpretation of $X[n, k]$ as an output of the filter bank is presented in Fig. 2.83.

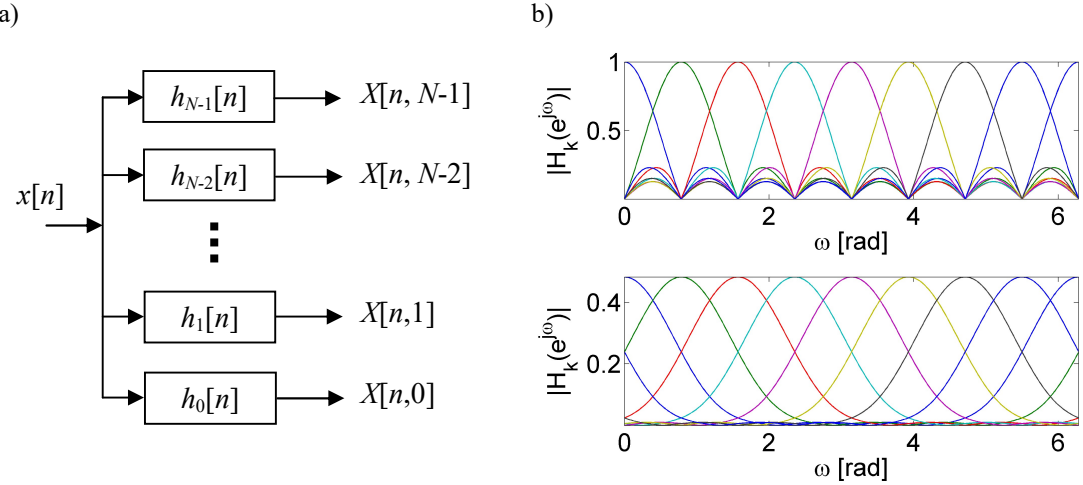


Fig.2.82 a) Filter bank representation of STDFT,
b) Magnitude response of STDFT filter bank for rectangular window (top),
and Hamming window (bottom) for $N=8$.

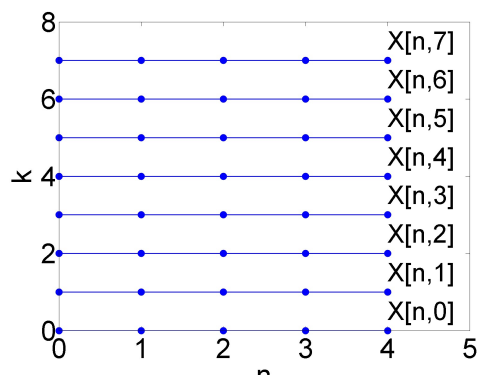


Fig.2.83 Interpretation of $X[n, k]$ as an output of the filter bank.

STDFT (2.263) may be sampled in the time axis n by the signal (or window) shifts R higher than one sample

$$X[rR, k] = \sum_{m=0}^{L-1} x[rR + m]w[m]e^{-j\frac{2\pi}{N}mk}. \quad (2.267)$$

where r is integer. The columns in sampled STDFT (2.267) matrix $X[rR, k]$ are DFTs computed from the signals fragments selected by the window $w[n]$ of length L shifted along the signal by R samples. Fig.2.83 shows two examples of $X[rR, k]$ sampling for $R=1$, and $R=2$.

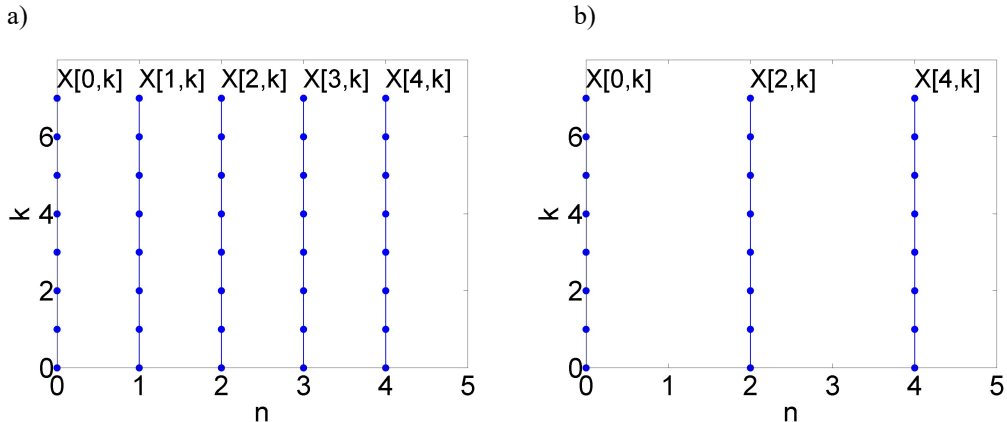


Fig.2.84 Examples of $X[n, k]$ sampling for $k=0,1,\dots,7$: a) $R=1$, b) $R=2$.

Spectrogram is used in analysis of nonstationary signals, i.e. the signals with parameters varying in time, e.g. sinusoidal signals with variable frequency, amplitude, and phase. Examples of nonstationary signals are: speech (or generally biomedical signals like ECG, EMG etc.), telecommunication signals, radar and sonar signals, etc.. However STDFT is calculated by DFT in a window of chosen length, and it is assumed that in this window analyzed signal is stationary. Short duration time window improves time resolution, but worsens frequency resolution. Long duration time window has poor time localization, but good frequency resolution, thus the length of the window is a compromise between time and frequency resolution of the spectrogram. By using windows with low side-lobes the effect of ringing is reduced in spectrogram but at the same time the frequency resolution is limited by the width of the mainlobe.

Example 2.15

Sinusoidal signal with amplitude modulation (AM) is defined as

$$x[n] = (1 + k_{AM} m[n]) \cos(\omega_0 n), \quad 0 < k_{AM} \leq 1. \quad (2.268)$$

[Fig. 2.85](#) shows spectrograms of AM signal (2.268) modulated by sinusoidal signal $m[n] = \cos(\omega_m n)$, $\omega_m \ll \omega_0$. It is observed that the frequency of AM signal is constant and the amplitude varies. Before DFT computations the signal with length $L=32$ was extended by appending the vector of zeros to the length $N_{FFT}=256$, see [Fig.2.80](#).

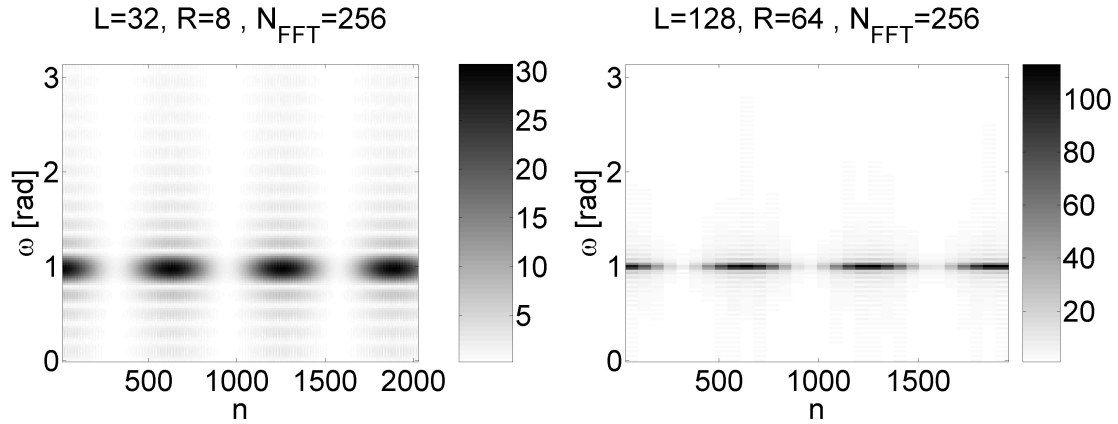


Fig.2.85 Spectrograms with rectangular window of sinusoidal AM modulation.

Example 2.16

Sinusoidal signal with frequency modulation (FM) having instantaneous frequency

$$\omega_{inst}[n] = \omega_0 - k_{FM} \sin(\omega_m n). \quad (2.269)$$

is defined as

$$x[n] = \cos(\omega_0 n + k_{FM} \cos(\omega_m n) / \omega_m). \quad (2.270)$$

Figs. 2.86-2.87 show spectrograms of FM signal (2.270) computed with rectangular window and Hamming window. It is observed that the frequency of FM signal varies and the amplitude is constant.

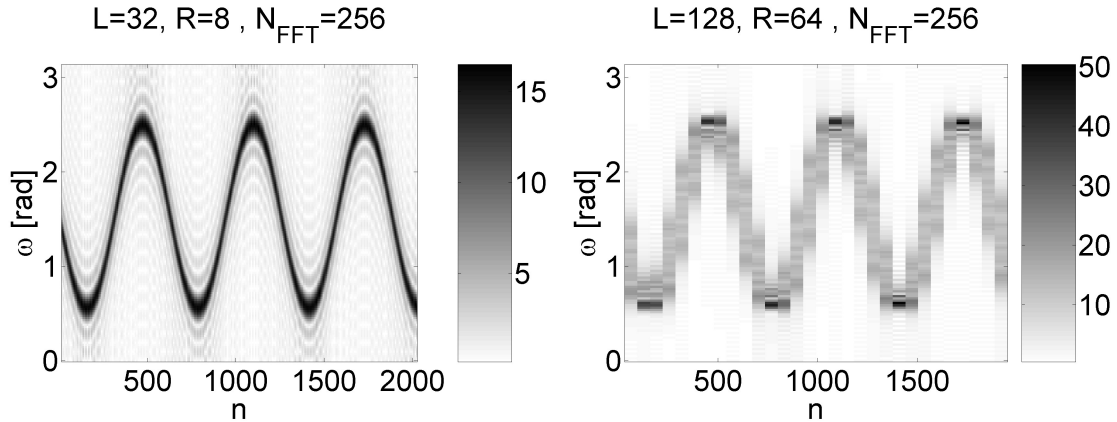


Fig.2.86 Spectrograms with rectangular window of sinusoidal FM modulation.

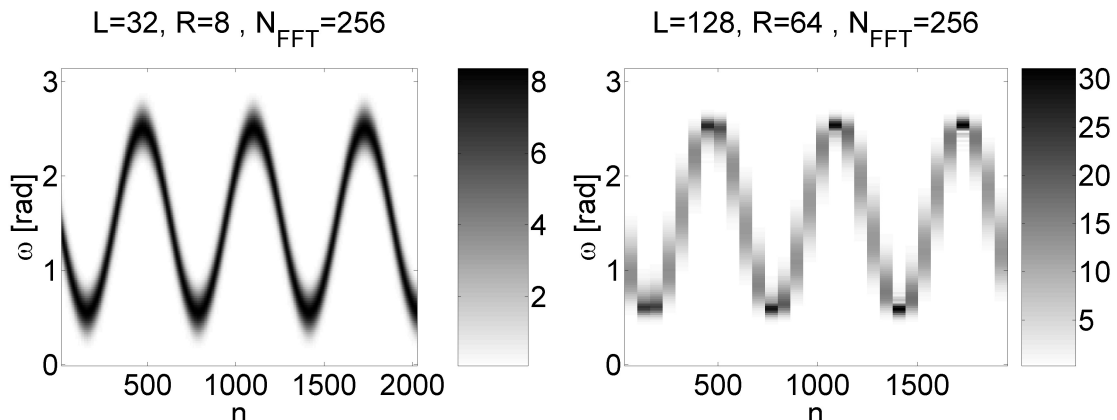


Fig.2.87 Spectrograms with Hamming window of sinusoidal FM modulation.

Example 2.17

[Fig. 2.88](#) shows exemplary speech signal, and [Figs. 2.89-2.90](#) depict its spectrograms computed with rectangular window in linear scale, and dB scale, i.e. $20\log_{10}|X[n, k]|$.

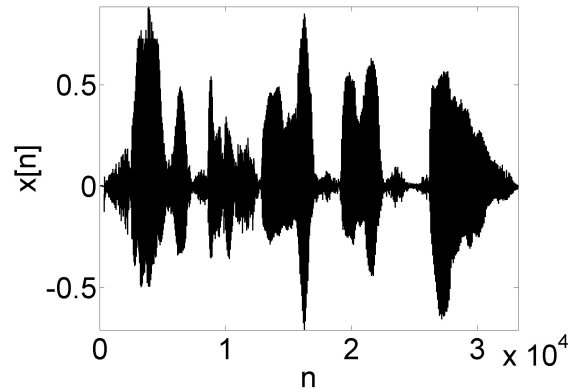


Fig.2.88 Exemplary speech signal; polish phrase 'książyc lśnił mocno noc całq' said by a women.

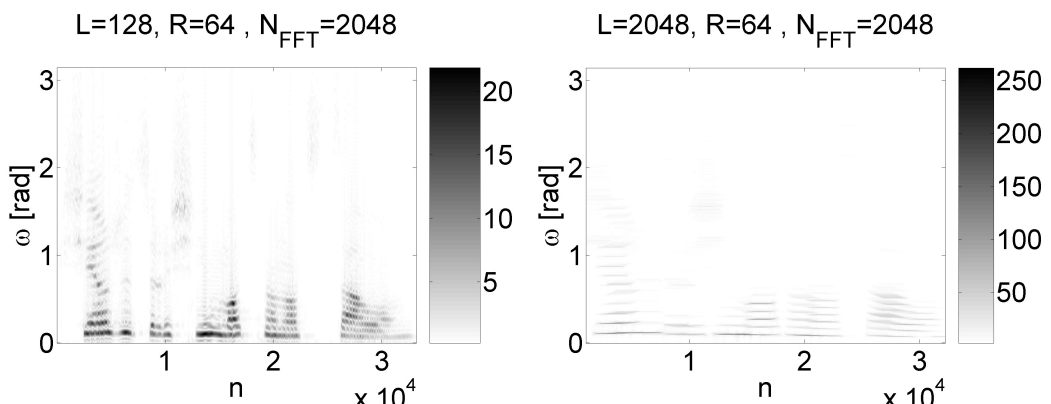


Fig.2.89 Spectrograms with rectangular window of the speech signal from [Fig.2.88](#).

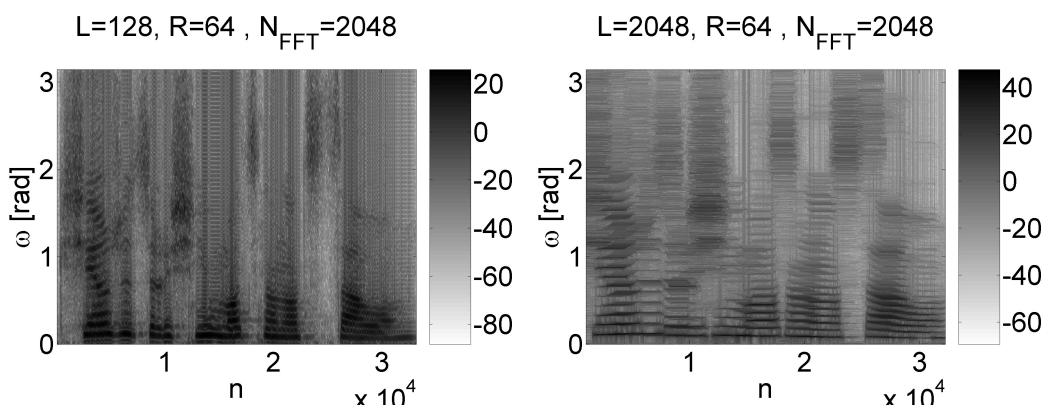


Fig.2.90 Spectrograms in dB with rectangular window of the speech signal from [Fig.2.88](#).

A.V. Oppenheim, R.W. Schafer, J.R. Buck, *Discrete-Time Signal Processing*, 2nd Ed., Prentice-Hall, 1999.
p.728 Time-dependent Fourier analysis of radar signals

2.6.3 Fourier analysis of stationary random signals: the periodogram

References

- [Britt93] C. Britton Rorabaugh, *Digital Filter Designer's Handbook: Featuring C Routines*, McGraw-Hill Education - Europe 1993.
- [Deli99] T. L. Deliyannis, Y. Sun, J. K. Fidler, *Continuous-Time Active Filter Design*, CRC Press LLC, 1999.
- [Harr78] F. J. Harris, "On the use of windows for harmonic analysis with the discrete Fourier transform," *Proc. IEEE*, Vol. 66, pp. 51-83, Jan. 1978.
- [Hay99] M. H. Hayes, *Schaum's Outline of Theory and Problems of Digital Signal Processing*, McGraw-Hill Companies, Inc. 1999.
- [Kay93] S. M. Kay, *Fundamentals of Statistical Signal Processing: Estimation Theory*, Prentice-Hall, 1993.
- [Lyons04] R. G. Lyons, *Understanding Digital Signal Processing*, Second Edition, Prentice-Hall, 2004.
- [Lyons99] Lyons R.G.: *Wprowadzenie do cyfrowego przetwarzania sygnałów*, WKŁ, Warszawa 1999.
- [MatFD] *Matlab Filter Design Toolbox*, available from www.mathworks.com.
- [MatIP] *Matlab Image Processing Toolbox*, available from www.mathworks.com.
- [MatSP] *Matlab Signal Processing Toolbox*, available from www.mathworks.com.
- [MatWT] *Matlab Wavelet Toolbox*, available from www.mathworks.com.
- [Moon99] T. K. Moon, W. C. Stirling, *Mathematical Methods and Algorithms for Signal Processing*, Prentice Hall 1999.
- [Oppen83] A. V. Oppenheim, A. S. Willsky, I. T. Young, *Signals and Systems*, Prentice-Hall, 1983.
- [Oppen99] A.V. Oppenheim, R.W. Schafer, J.R. Buck, *Discrete-Time Signal Processing*, 2nd Ed., Prentice-Hall, 1999.
- [Pap62] A. Papoulis, *The Fourier integral and its applications*, McGraw-Hill Book Company, Inc. 1962.
- [Phadke09] A. G. Phadke, J. S. Thorp, *Computer Relaying for Power Systems*, Second Edition, John Wiley & Sons Ltd, 2009.
- [Poll99] D.S.G. Pollock, *A Handbook of Time-Series Analysis, Signal Processing and Dynamics*, ACADEMIC PRESS, 1999.
- [Spe68] M. R. Speigel, *Mathematical Handbook of Formulas and Tables*. Schaum's Outline Series, McGraw-Hill, 1968.
- [Stein00] J. Y. Stein, *Digital Signal Processing: A Computer Science Perspective*, John Wiley & Sons, Inc. 2000.
- [Ziel05] T. P. Zieliński, *Cyfrowe przetwarzanie sygnałów. Od teorii do zastosowań*, WKŁ, Warszawa 2005, 2007, 2009.